NASA CR-112113

RELATIVE MOTION OF ORBITING SATELLITES

By J. B. Eades, Jr.

Prepared under Contract NAS1-10907 by
ANALYTICAL MECHANICS ASSOCIATES, INC.
(Report No. 72-27)

for

LANGLEY RESEARCH CENTER

ANALYTICAL MECHANICS ASSOCIATES, INC.
10210 GREENBELT ROAD
SEABROOK, MARYLAND 20801

FOREWORD

This report was prepared under NASA Contract NAS1-10907. The work was conducted under the direction of J. W. Drewry, Space Application and Technology Division, Langley Research Center.

The Analytical Mechanics Associates, Inc. program was conducted under the direction of Dr. J. B. Eades, Jr.

TABLE OF CONTENTS

Page

LIST OF FIGURES

List of Figures (cont)

List of Figures (cont)

List of Figures (cont)

LIST OF TABLES

SYMBOLS

a, b	Semi-major axis length, semi-minor axis length.
A, B	Constants (defined as used).
$\mathcal{C}_i$	Constants.
$\bar{e}_i$	Unit vectors in an i^{th} coordinate direction.
E	Specific (total) energy for a motion.
$\mathcal{E}$	Eccentric anomaly.
h, H	Specific moment of momentum, momentum ratio.
K_j	Constants.
m_j	Mass particles.
n	Mean motion.
P	Orbit parameter.
q	Special coordinate (as defined).
r_j, $\bar{r}_j$	Radius, radius vector.
s, ρ	Shell coordinates.
t	Time.
T_j	Specific thrust components.
V_j, $\bar{V}_j$	Speed, velocity (j^{th} components).
x, y, z	Cartesian coordinates.
α	Position angle (see eq. VII.12)
γ	Velocity elevation angle.
Δ	Determinant, dimensionless radius ratio.

$\delta\nu$	Dimensionless impulse ratio.
ϵ	Eccentricity.
φ	True anomaly.
θ	Position angle (see Fig. VII.1).
ψ	Position angle (reference orbit).
ι	Inclination angle (between orbital planes).
τ_k	Dimensionless thrust components.
ξ, η, ζ	Dimensionless cartesian coordinates.
λ, σ	Dimensionless shell coordinates.
$\omega, \bar{\omega}$	Angular speed, velocity.
μ	Gravitational parameter.

Subscripts

i, j, k	Indices.
T, I	Target, interceptor.
cr	Critical values (relating to a cusp).
M	Extreme values (for coordinates).
o, f	Initial value, final value.

Superscripts

$\dot{(\ )}$	Differentiation with respect to time.
$(\ )'$	Differentiation with respect to angle (φ).

RELATIVE MOTION OF ORBITING SATELLITES

By J. B. Eades, Jr.*

SUMMARY

The relative motion of orbiting bodies is concerned with describing the motion of one body, with respect to another, which is moving on an adjacent trajectory. The geometry for these problems differs distinctively from that representing an inertially referenced motion. Problems associated with intercept and rendezvous, and with the paths traced out by ejected particles are examples of situations of particular interest in the study of relative motions.

In this investigation the relative motion problem is analyzed, as a linearized case, first, and as a numerically determined solution, second, to provide a time history of the geometries representating the motion state. The displacement history and the hodographs for families of solutions are provided, analytically and graphically, to serve as an aid to understanding this problem area.

Linearized solution to relative motion problems of orbiting particles are presented for the impulsive and fixed thrust cases. Second order solutions are described to enhance the accuracy of prediction. A method has been developed to obtain accurate, numerical solutions to the intercept and rendezvous problem; and, special situations are examined.

A particular problem related to relative motions, where the motion traces develop a cusp, is examined in detail. This phenomenon is found to be dependent on a particular relationship between orbital eccentricity and the inclination between orbital planes. These conditions are determined; and, example situations are presented and discussed.

*Senior Analyst, Analytical Mechanics Associates, Inc.

RELATIVE MOTION OF ORBITING SATELLITES

INTRODUCTION

The information developed and discussed in this report is applicable to the study of relative motions between orbiting bodies in a space environment. The material contained herein is directed toward providing a better understanding of this problem area, and to the illustration of such motions by means of examples and discussions.

One of the basic guidelines followed throughout this investigation was to produce a document describing the geometry of relative motion situations. Also, to provide the analytical means for predicting the time history of the motion state. In meeting these requirements the investigation was designed so that this relative motion problem area was examined, first, as an analytical exercise and, second, as a numerical one. The reasoning behind this approach was to provide an easy-to-understand formulation of the phenomenon initially; and, second, to provide for a means of simulating relative motions on a more exact and accurate scale.

For the first approach the problems were studied in as simple a mathematical approach as possible; but with the essence of the physical situation being retained. To this end a linearization of the governing differential equations was made and the resulting expressions were manipulated to yield analytical results. In illustrating the use of these consequent expressions, example problems were selected, solved and discussed. For the second approach the examples were not restricted, mathematically, but were investigated as numerical exercises wherein more accurate simulations were provided. The results obtained here were analyzed, subsequently discussed, and illustrated as plots of the motion state and other quantities of interest.

The report, presented here, is composed of several sections--devoted to descriptions, discussions and examples - and of appendices, wherein the

mathematics used in the investigation is developed. In general, the foremost segments of the report describe the results acquired from this investigation. Here the example cases are studied and their consequences are noted. Much of this work is illustrated on graphs, figures, tables and by formulae produced to give a more complete description of the sample cases under investigation. In the appendices the more general mathematical developments are set down and summarized. It is from these segments of the report that the specializations, used in the front sections, are deduced.

As a quick summary and guide to the material presented herein the following comments are made: The first section discusses the more general aspects of the relative motion problem as it is described, analytically, from a linearized set of governing expressions. Here the problem considered is that of two orbiting particles, moving on adjacent paths about a common primary, under the influence of the gravitational attraction offered by the central mass. This problem is formulated with respect to a moving frame of reference, and is expressed in (both) cartesian and "shell" coordinates (see Fig. I.1 for a sketch depicting this). The mathematical developments for this section are to be found in Appendices A, B and C, at the rear of this document.

In the second section, this relative motion concept is examined by means of specific example cases. In particular, the two primary problem areas which were studied are related to the motion of masses ejected from an orbiting spacecraft; and, the relative motion of an intercept and rendezvous maneuver. In the next section a second order correction theory is presented and discussed. The purpose of this part of the study is to provide for an analytical means of bettering the predictations offered from the linear theory. An appendix is included, in the report, delineating the mathematical development for this (second order) method.

Next, an analytical approach for the relative motion of a thrusting-type particle is presented and discussed. Here, again, the mathematics is exercised

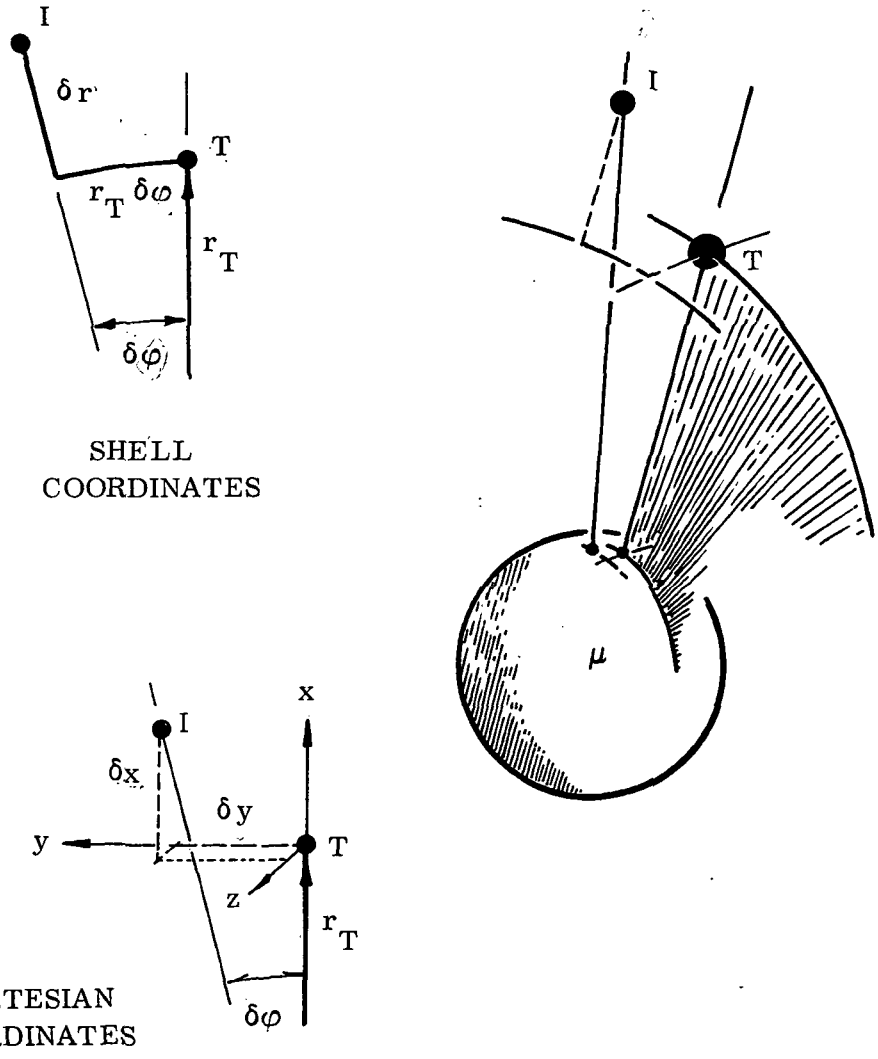

Fig. I.1. Sketch Depicting Two Particles (I, T) in Motion About a Primary μ. For convenience, in these relative motion examples, they will be referred to as the Target and the Interceptor. Shown here are the Cartesian and Shell Coordinates Used in Describing the Relative Motions.

by means of examples and representative cases. For clarity and understanding; these sample situations are illustrated, graphically, and by special formulations. Throughout this and the previous sections of this document, the mathematical formulae are (generally) expressed in a non-dimensional form. The reasoning behind this is to present a more universal representation; one not encumbered dimensionally, or seemingly restricted to a near-space environment. Of course, the reader should be ever cognizant of the restrictions and conditions imposed by those constraints introduced in the mathematical developments.

The last two sections in the report's main body are devoted to the description of "exact" solutions for relative motion situations. In the one case an exact intercept problem is discussed, while in the last section a deterministic relative motion problem is defined and illustrated. This last case illustrates a rather unusual phenomenon which can occur for the relative motion of nearby bodies. Specifically, it shows that traces of the motion may develop cusps if there is a properly related set of parameters defining the orbits. The particulars of this situation are fully described there and will not be mentioned, further, here.

The supporting mathematics for the last section of this report is contained in an appendix. In addition, the last appendix briefly describes a computer program which has been developed, and checked, to reproduce results for the various problem types described herein. In general this program will handle any and all of the cases described in the main body of the report, with the exception of the deterministic problem. This last example is handled separately, by a special computer routine, which is not described in the last appendix. The program mentioned there is sufficiently versatile to handle a rather large variety of relative situations - far more than what is indicated by the illustrations contained in the report's front sections. The imaginative and inventive investigator can find many other uses to which the program can be directed.

One comment regarding the references and bibliography of the report should be made. No attempt has been made here to include a full survey of the literature pertinent to this topic. Many references will not appear since they are included in the appropriate sections of those cited here. Finally, the investigators wish to apologize to those authors who may have been missed, and assure them that any such oversights were unintentional.

ANALYTIC SOLUTIONS FOR RELATIVE MOTION

II.1 A geometric interpretation for relative motions. - The linearized solutions describing the motion of one particle relative to another, when both move on adjacent orbits, have been obtained in Appendix A and Appendix B. For these developments the target, or reference body, was assumed to move along a circular orbit; however, the second particle, herein called the interceptor, was not constrained in this manner. Actually, the interceptor describes a closed figure in inertial space (generally, an ellipse); but, in order not to violate the ideas employed in the linearization, the state variables, relative to the target particle, have been assumed to be small. What is implied, then, is that the dimensionless variables introduced in the Appendixes -- ξ, η, ζ; ξ', η', ζ', as well as λ, σ; λ', σ' -- are all considerably smaller than unity, in magnitude.

The two appendices mentioned above describe the interceptor's relative motion from a set of linearized differential equations, written in cartesian coordinates (Appendix A), and in shell coordinates (Appendix B). From an examination of the several expressions (see eqs. (A.33, A.34, and B.22)) one can see the marked similarity which these equations display. At least in form, then, these two resultants represent a same figure of geometry insofar as the described, planar, relative motion is concerned.

For conciseness and, to a degree, for completeness the following discussions will be made primarily in terms of cartesian coordinates. Also, for convenience, the descriptions will be discussed in terms of the dimensionless variables (eqs. A.33) and (A.34)); however, when necessary the dimensional variables can be brought out simply by invoking the transformations noted in eq. (A.32), Appendix A.

Since the ζ (or z) state components are uncoupled from the ξ, η (or x, y) quantities, it is convenient to discuss a relative motion as either an "in-plane" or an "out-of-plane" problem. The in-plane motion will require

only the ξ, η coordinates to locate the interceptor as it moves in the plane of the target vehicle. Alternately, the out-of-plane case can be discussed in terms of the (ξ, ζ) and/or (η, ζ) coordinates, additionally, depending on the physical situation to be described.

It should be mentioned that these relative position coordinates have the following meaning:

> The coordinate ξ (or x) is measured in the radial direction; it is positive away from the target vehicle; the +y (or $+\eta$) component is measured "forward" of the target, in the plane of motion; lastly, the ζ (or z) component completes a right hand orthogonal frame of reference, it is directed normal to the target's orbital plane and is positive valued in agreement with the right hand rule for vectors.

A word description of the shell coordinates will be given subsequently.

II.2.1 The in-plane motion: For this case the relative motion is described from the ξ, η expressions found in eqs. (A.33) and (A.34).

It is seen that these expressions contain both constants and cyclic terms; and, in addition, the η-expression has a secular component. If this secular term is disregarded, for the moment, then it is evident that the resulting expressions define a motion which, geometrically, is an ellipse. This figure is, then, indicative of how the interceptor moves relative to the target. It should be noted also that the ellipse has a fixed eccentricity; it is not centered at the target, generally; and, when the secular term is included, the ellipse moves, or "meanders", continually in the η-direction.

Translated into motions referred to fixed space axes, it should be apparent that the interceptor moves along a central field ellipse as the target flies along its prescribed circular path in the same space.

Also, from a study of these relative motion state equations, it is noted that the interceptor's period of motion is the same as that for the target. This condition is compatible with the ideas imposed in the linearization procedure; consequently, it is supposed, a priori, that the relative state components are "small" quantities. The idea, here, of small displacements necessarily constrain the applicability of the linearized solutions, especially in regard to the contribution made by the secular term to the motion.

II.2.2 The relative motion ellipse: As mentioned above, the relative motion ellipse is not centered at the target vehicle. The geometric center is off-set from the coordinate origin according to the size of the constant terms in these expressions; thus, the geometric origin of this trajectory figure is positioned at (ξ_c, η_c), where

$$\xi_c = 2\,(\eta'_o + 2\xi_o), \tag{II.1a}$$

and

$$\eta_c = (\eta_o - 2\xi'_o). \tag{II.1b}$$

The secular term in the η-expression serves to describe the "meandering", or "drifting", of this relative motion figure. Since this parameter has the form of a dimensionless speed, it will be referred to as the "η-drift" quantity; it is defined as;

$$\eta_{(\text{drift})} \equiv -3\,(\eta'_o + 2\xi_o). \tag{II.2}$$

It should be recognized that this term is directly related to the parameter ξ_c defined above. It is also evident that the drift (for a positive initial displacement) would carry the relative motion ellipse aft of the target; thus, there is an ever

increasing separation between the geometric center of the relative motion figure and the target vehicle (the coordinate origin). In this regard the motion of the interceptor could be described, generally, as a meandering ellipse which carries the interceptor further and further away from the target.

To illustrate that the relative motion figure is an ellipse, examine eqs. (A.33a) with the secular term neglected. Denoting the amplitude from these expressions as K_2; i.e, letting

$$K_2 \equiv \sqrt{(\xi'_o)^2 + (3\xi_o + 2\eta'_o)^2} \quad , \tag{II.3}$$

then the (two) displacement expressions can be recast as:

$$\frac{\xi - \xi_c}{K_2} = \cos(\varphi_T + K_3) \tag{II.4a}$$

and

$$\frac{\eta - \eta_c}{(-2K_2)} = \sin(\varphi_T + K_3); \tag{II.4b}$$

which, when squared and added together yield

$$\left(\frac{\xi - \xi_c}{K_2}\right)^2 + \left(\frac{\eta - \eta_c}{2K_2}\right)^2 = 1. \tag{II.5}$$

Needless to say this describes the ellipse in cartesian form; it has a minor-to-major axis ratio of 1:2; and, it has a fixed eccentricity (independent of the initial values), which is

$$\epsilon = \frac{\sqrt{3}}{2} . \tag{II.6}$$

To illustrate some of the geometry for this figure, the sketch, shown below, depicts the various properties just discussed,

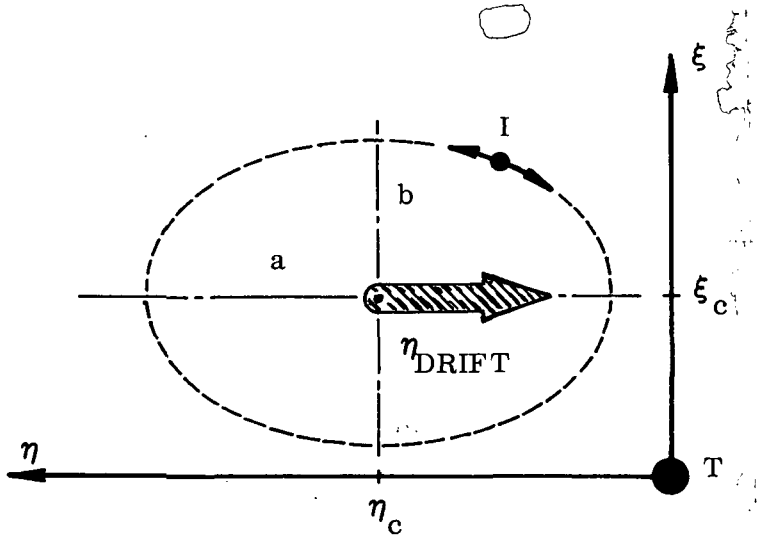

a = major length (=$2K_2$)

b = minor length (=K_2)

ξ_c, η_c are the geometric center's coordinates (see eqs. II.1)

T, I designate the Target (coordinate origin) and Interceptor particles, respectively.

Fig. II.1 A sketch depicting the instantaneous relative motion ellipse for the interceptor (I) moving about the target (T). The interceptor's motion is determined by its initial values; however, the basic geometry shown here is a "drifting ellipse"* centered away from T, with the motion of I having a cyclic part, with period equal to that of T. Only the in-plane case is depicted here.

II.2.3 A special case (no drift): Assume, for a moment, that the relative motion ellipse has no drift in the η-direction. To satisfy this condition it is required that,

$$\eta_o' = 2\xi_o \,. \tag{II.7}$$

As a consequence of this the interceptor's motion becomes fixed in the target-centered relative motion frame of reference.

In addition to the "drift" vanishing, this same condition has an influence on the location of the geometric center for the relative motion figure. That is, according to eq. (II.1a), $\xi_c = 0$ and, therefore, the relative motion figure will be centered at $(0, \eta_c)$. Furthermore, aside from relocating the geometric

*A more precise geometric description of the full figure, would be to refer to it as a "prolate cycloid".

center, it is evident that this requirement affects the amplitude of the motion. That is, now,

$$K_2 = \sqrt{(\xi'_o)^2 + (\xi_o)^2} \quad ; \tag{II.8}$$

however, the diminished figure has not had its minor-to-major axes ratio altered; and, it has the same eccentricity as before.

II.2.4 A very special case: For this very special case, suppose that in addition to the restrictions above another condition is imposed on the variables. In this regard, suppose that

$$\eta_o = 2\xi'_o \, . \tag{II.9}$$

For this case it is seen that the relative motion figure is centered, now, at the target (i.e., $\xi_c = \eta_c \equiv 0$)! This added constraint does not alter the shape of the relative motion ellipse, nor does it affect the eccentricity of the figure.

Another quantity which is influenced by setting the drift to zero is the phase angle (K_3), noted in eqs. (II.4). When the drift vanishes, K_3 reduces to

$$K_3 = \tan^{-1}\left[\frac{-\xi'_o}{+\xi_o}\right] . \tag{II.10}$$

(Note the similarity, in form, between this value of K_3 and that for K_6; see eqs. (A.34a)).

For the case presently under investigation, a manipulation of the expressions for ξ, η shows that the in-plane coordinate equations reduce to a set of simpler equations; that is, from eqs. (A.33b),

$$\xi = \xi_o \cos\varphi_T + \xi'_o \sin\varphi_T \, , \tag{II.11a}$$

and

$$\eta = \eta_o \cos\varphi_T + \eta'_o \sin\varphi_T \, . \tag{II.11b}$$

Of course, in these expressions the initial state variables must satisfy the stated constraints, i.e., $\eta'_o = -2\xi_o$, and $\eta_o = 2\xi'_o$.

Incidentally, as an alternate definition, the coordinate expressions may also be written as (see eqs. (A.33a)),

$$\xi = \sqrt{(\xi'_o)^2 + (\xi_o)^2} \quad \cos(\varphi_T + K_3), \tag{II.12a}$$

and

$$\eta = -2\sqrt{(\xi'_o)^2 + (\xi_o)^2} \sin(\varphi_T + K_3), \tag{II.12b}$$

with K_3 defined as noted above.

These last equations describe the relative motion as an ellipse, which is, now, centered at T (the target). The figure has a major-to-minor axis ratio of 2:1, and an eccentricity, $\epsilon = \sqrt{3}/2$. (Note that this geometric figure has no meandering associated with the interceptor's relative motion; the interceptor has a bounded region, about the target, in which it is presumed to move).

These rather simple but illustrative cases, mentioned in the preceding paragraphs, have been included here to aid one in visualizing what geometry the analytic coordinate equations describe for the interceptor's motion, in general. It should be equally evident that many other relative motion situations could be described; but, that these would be given in rather specific terms according to the specialization imposed on the various coordinate equations. As a matter of fact, subsequent sections of this document will deal with various other situations which are of interest to space flight operations.

II.3 The relative motion hodograph. - Before leaving this discussion, some comments should be made regarding the hodograph for this relative motion problem. One should recall that a hodograph is constructed by mapping a motion onto appropriate "velocity" planes. In essence, then, the situation discussed

above, in terms of displacements, could equally well be described in terms of the corresponding speed components (ξ', η').

From an inspection of eqs. (A.34), Appendix A, it is apparent that the geometric figure described on the (ξ', η') plane is also an ellipse; one with its geometric center displaced from the target, as an origin for the graph. As was the case for the previous discussion, this figure has a fixed eccentricity and a major-to-minor axis ratio of 2:1.

As a matter of interest the geometric center of this ellipse is located at (ξ'_c, η'_c) wherein,

$$\xi'_c = 0,$$

and

$$\eta'_c = -3(\eta'_o + 2\xi_o). \tag{II.13}$$

Interestingly, the condition of no "drift" -- described for the displacement ellipse -- would cause the center of the hodograph ellipse to be shifted to the origin (see eqs. (II.1)). This is a situation of natural consequence! Evidently, then, the offset of the hodograph is directly associated with the "drift" phenomenon found for the displacement relations.

Of necessity the complete hodograph -- like the overall displacement representation-- is a three dimensional geometry which becomes rather complicated, in form, if all coordinate components are considered simultaneously. Rather than go into a lengthy description of this at this time, such will be deferred until later when the more specific details can be examined.

II.4 Comments. - One word of caution should be injected at this point. The expressions described and discussed above were obtained from the "linearized" differential equations of motion. Intuitively one knows that these equations are limited in predictability, from both a mathematical and physical point of view.

Unfortunately it is quite difficult to state, a priori, the extent of these limitations; and to relate the exact nature of how far actual cases may depart from the linearized predictions. On the other hand, these "linearized solutions" have, at least, afforded one an insight into the relative motion problem; also, they do provide one with the knowledge of what to expect in the large. The caution which is given here is that the reader should not view these equations as an end unto themselves, but should always regard them as "estimates and trends" of the actions which are to be found from more rigorous studies. Contrary to this, it should not be taken as fact that the descriptions given here will not be, at certain times and situations, rather close to the actual results. As a matter of fact there will be some instances where "good indications" are obtained from the linear theory; some of these will be demonstrated in subsequent sections of this report.

II.5 Study cases from the relative motion equations. - Many problems in celestial mechanics, which deal with two or more bodies in motion, could benefit from a study of their relative motions. Actually, the two-body problem is, to a large degree, one such situation. Certainly a study of the intercept and rendezvous problem, for one vehicle with another, is a most meaningful case for study in relative motion. In fact there are a fair number of simulations which could fit into this category of flight mechanics problems. In order to illustrate the use and utility of the relative motion results described herein, several problem types will be considered and investigated later.

To a large extent the several case studies to be undertaken in the following sections will fall into one or both of the following two broad categories:

1. The intercept and rendezvous of two vehicles which are in orbit about a primary.

2. The motion of an object ejected from an orbiting spacecraft.

Within these rather loose classifications one will find problem variations, and related situations presented; these are expected to enhance the knowledge previously gathered from other case studies.

II.6 The relative motion problem in shell coordinates. - In Appendix B, a solution to the linearized relative motion problem is presented in shell coordinates. Since these coordinates describe the motion only in the plane of the target particle, the results are directly analogous to the in-plane solution described in cartesian form. For purposes of clarity, the shell coordinates may be described as follows:

> The displacements (ρ, s) define a relative position as; a difference in radii (ρ), and an arc length (s) at a fixed radius, r_T. The coordinate, ρ, is positive if $r_I > r_T$ while s is positive-valued when the interceptor is ahead of the target.

In order to continue the analogy between developments, these state variables are again described in both dimensional and dimensionless form. The normalizing quantities introduced here are the same as those used previously; that is, the displacements are normalized by r_T while the speeds are ratioed to the circular speed ($r_T \dot{\varphi}_T$). Likewise, the independent variable is (again) shifted from "t" to "φ_T" by means of the relationship, $\varphi_T = \dot{\varphi}_T t$.

The transformations relating the dimensional to the non-dimensional variables are found in eqs. (B.10). However, it should be noted that these transforms are identical in format for both the cartesian and shell coordinate schemes.

II.7. The relative motion ellipse: In order to describe the relative motion in terms of a geometric figure, one should consider the expressions given in eqs. (B.22), of Appendix B. There the dimensionless state variables are described in an equation form which is identical to those obtained in Appendix A, for the in-plane case. In this regard it is evident that the geometry described earlier,

for the cartesian representations, would suffice for the present case. For this reason it would be redundant to repeat these descriptions, except to note that the coordinates have a somewhat different meaning, physically, in the two representations.

It is probable that some minor differences might be found in results acquired from the use of these two representations, in a given problem; however, these differences should be quite small. Also, it should be remembered that the analyses are acquired from linearized equations, and that the applicability of these, in either and both cases, is limited to the region "near" to the target itself.

In view of the fact that the figure of geometry, describing the relative motion problem in cartesian coordinates, for both the trajectory and the hodograph, was an ellipse then it is apparent that the same figures would be found here. Since the two representations lead to identical equation forms, then it is evident that no new information is to be gained from an examination of these expressions, when compared to the others. Of course, had the equations evolved into new and/or different forms, then one might expect to acquire added knowledge of this problem.

As a matter of interest it will be demonstrated, subsequently, that the differential equations, expressed in shell coordinates, can be manipulated into a form allowing for an immediate first integral of the motion. This situation will be studied in a following section.

II.8 Comments. - It has been ascertained that the basic format of the relative motion problem, acquired from the linearized differential equations of motion, is identical for both the shell and cartesian coordinates. Consequently, the major portions of the following work will be described and discussed in terms of cartesian representations. This is done, primarily, for consistency and conciseness of notation. Also, this will alleviate the reader from having to retain a large number of notational quantities in his memory.

II.9 A modified solution in shell coordinates. - Solutions to the relative motion problem, as derived in Appendix A and Appendix B, were obtained from a set of linearized governing differential equations (see, for example, eqs. (B.15)). These solutions evolved from a consideration of only first order terms, in the coordinates and their derivatives, within these governing differential expressions.

A close examination of the general differential equations (such as eqs. (B.13)) will confirm the fact that some improvement to the linearized solution could be had simply by manipulating these expressions, analytically, prior to their expansion and integration.

As a consequence the procedure which will be followed below is one aimed at the development of a solution type which might lead to improved accuracy compared to the purely "linearized" solutions previously discussed.

II.10 Solution to the differential equations. - In order to achieve the ends desired here, one may begin with the dimensionless governing equations developed in Appendix B; these expressions are

$$\sigma'' = - \frac{2\lambda' (1+\sigma')}{(1+\lambda)} \quad , \tag{II.14a}$$

and

$$\lambda'' = (1+\lambda)(1+\sigma')^2 - (1+\lambda)^{-2} . \tag{II.14b}$$

For convenience and manipulation purposes, the procedure which follows will be described in dimensionless shell coordinates; hence the solution will be applicable to the planar relative motion problem. The third positional degree of freedom is suppressed in this analysis.

It should be evident that the first of the above expressions is separable; consequently it leads directly to a first integral; namely,

$$\ell n\ (1+\sigma')\ (1+\lambda)^2 = \ell n\ \mathcal{C}, \tag{II.15a}$$

with $\ell n\ \mathcal{C}$ serving as a constant of integration. Alternately, this result may be expressed as

$$\mathcal{C} = (1+\sigma')\ (1+\lambda)^2; \tag{II.15b}$$

this indicates a rather significant relationship between the variables (λ, σ'). For purposes of comparison, this expression is analogous to eq. (B.16), obtained from the linearized expansions developed in Appendix B.

The second expression in eq. (II.14) also has a first integral, one which is readily obtained after multiplying through the expression with the derivative λ'; and, after substitution for σ' from eq. (II.15b). Thus, after carrying out these operations, one finds that the equivalent differential equation is

$$\frac{1}{2}\left[\left(\lambda'\right)^2\right]' = -\left[\frac{\mathcal{C}^2}{2}\ (1+\lambda)^{-2}\right]' + \left[(1+\lambda)^{-1}\right]', \tag{II.16}$$

wherein the $(\sim)'$ signifies differentiation, as before.

Necessarily, the form of this last result suggests the following first integral:

$$\frac{(\lambda')^2}{2} + \frac{\mathcal{C}^2}{2(1+\lambda)^2} - \frac{1}{1+\lambda} = \mathcal{C}_2. \tag{II.17}$$

Here $\mathcal{C}_2$ is a (second) constant of integration which will be identified subsequently.

Unfortunately, eqs. (II.16) and (II.17) do not lend themselves to a second integration due to the nonlinearity which is present. In order to continue with the analytic solution, from these first integrals, it will be necessary to reduce the complexity of the integrands. However, before continuing with these evaluations it would be informative to consider another analytic formulation, one which

is in line with the more usual procedures followed in astrodynamics.

II.11 The dimensionless momentum and energy equations. - Recalling that two-body, central field problems are characterized as having constant specific angular momentum and total energy; then, for the formulations assumed here, one should naturally look for similar relations in this case.

In this connection the scalar moments of momenta for the two particle vehicles, relative to the attracting center, may be defined as follows:

For the two vehicles;

$$h_j = r_j^2 \dot{\varphi}_j; \text{ where } j = I, T. \tag{II.18a}$$

Making use of the coordinate relations, eqs. (B.7), the momentum expression for the interceptor is;

$$h_I = r_T^2 \left(1+\frac{\rho}{r_T}\right)^2 \left(1+\frac{\dot{s}}{r_T\dot{\varphi}_T}\right) \dot{\varphi}_T. \tag{II.18b}$$

After manipulating this expression, and incorporating the transformations from eqs. (B.10) and (B.12), it can be shown that

$$\frac{h_I}{h_T} \equiv H = (1+\lambda)^2 (1+\sigma'), \tag{II.18c}$$

where H represents the ratio of these specific angular momenta.

Apparently, then, the first integral--obtained in eq. (II.15)--is precisely equivalent to this momentum ratio. Actually, this should be expected in view of the manner by which the specific moment of momentum expressions are usually obtained. Therefore, the constant in equation (II.15) has been defined.

Next, consider the specific energy expressions for the two particles (I and T). Since the interceptor is not constrained in the same manner as particle T, then its specific energy equation is written as,

$$E_I = \frac{V_I^2}{2} - \frac{\mu}{r_I} = \frac{\dot{r}_I^2 + (r_I \dot{\varphi}_I)^2}{2} - \frac{\mu}{r_I} \quad . \tag{II.19a}$$

With the target (T) assigned to fly a circular path about the attracting primary, its specific energy is conveniently given as:

$$E_T = -\frac{\mu}{2r_T} = \frac{-V_T^2}{2} = -\frac{(r_T \dot{\varphi}_T)^2}{2} \quad . \tag{II.19b}$$

Now, if the dimensionless coordinates, and the transformations developed in Appendix B, (eqs. (B.7, B.8, B.10 and B.12)) are introduced into eq. (II.19a) above, it can be shown that,

$$E_I = \frac{(r_T \dot{\varphi}_T)^2}{2} \left[\left(\lambda'\right)^2 + (1+\lambda)^2 (1+\sigma')^2 \right] - \frac{\mu}{r_T} (1+\lambda)^{-1}. \tag{II.19c}$$

Next, recalling that $\mu/r_T \equiv V_T^2$ (here) then it follows that eq. (II.19c) can be recast as,

$$\frac{E_I}{-E_T} = \left[\left(\lambda'\right)^2 + (1+\lambda)^2 (1+\sigma')^2 \right] - 2 (1+\lambda)^{-1}. \tag{II.20a}$$

If a substitution for the quantity $(1+\sigma')$ is made, from eq. (II.18c), then eq. (II.20a) is rewritten as

$$\frac{E_I}{-E_T} = (\lambda')^2 + \frac{\mathcal{C}^2}{(1+\lambda)^2} - \frac{2}{(1+\lambda)} \, . \tag{II.20b}$$

Now, comparing eqs. (II.20b) and (II.17) it is seen that the integration constant, $\mathcal{C}_2$, in the latter expression, can be identified with the energy ratio, $E_I/-E_T$.

Once again, here is a result which should not be considered as unexpected since the procedure followed in obtaining the first integral, eq. (II.17), parallels the manipulations usually employed in determining an energy equation for central field motions.

II.12 Determining the position coordinates (λ, σ). - Moving on toward a solution to the relative motion problem, the necessary second integrals for the motion must be obtained. Continuing then, with a substitution of eq. (II.18c), into the second of eqs. (II.14), one finds that,

$$\lambda'' = \frac{H^2-(1+\lambda)}{(1+\lambda)^3} . \qquad \text{(II.21)}$$

This equation is to be integrated if one is to obtain an expression for the coordinate λ as a function of the (present) independent variable, φ_T. Unfortunately this equation cannot be integrated directly, in closed form; hence, for analytical purposes an expansion of the denominator is proposed (this assumes that $\lambda \ll 1.0$). After expanding and regrouping terms one finds that, through third order in λ,

$$\lambda'' = (H^2-1) - (3H^2-2)\,\lambda + 3(2H^2-1)\,\lambda^2 - 2(5H^2-2)\,\lambda^3 + 0(\lambda^4). \qquad \text{(II.22)}$$

(This equation is equivalent to the expansion given as the second of eqs. (B.14), Appendix B). As in the previous case, an analytic expression is acquired after the linearized eq. (II.22) has been truncated, at terms of $0(\lambda)$; and, that reduced (linear) differential equation has been integrated. That is, after the truncation,

$$\lambda'' + (3H^2-2)\,\lambda \cong H^2 - 1, \qquad \text{(II.23)}$$

one finds a solution in the following form:

$$\lambda \cong \frac{B^2}{A^2} + C_3 \cos(A\varphi_T) + \mathcal{C}_4 \sin(A\varphi_T), \tag{II.24}$$

wherein $\mathcal{C}_3$ and $\mathcal{C}_4$ are constants of integration. In this resultant the other constants (A and B) are defined by;

$$A^2 = 3H^2 - 2, \tag{II.25a}$$

and

$$B^2 = H^2 - 1, \tag{II.25b}$$

from eq. (II.22). These last numbers are obviously related to the dimensionless momentum factor (H), noted in eq. (II.18c). Normally it is expected that H will be close to unity; thus A^2 is also close to unity while B^2 is small.

A differentiation of eq. (II.24) leads, next, to the dimensionless "speed" quantity (λ'); that is

$$\lambda' \cong A\left[-\mathcal{C}_3 \sin(A\varphi_T) + \mathcal{C}_4 \cos(A\varphi_T)\right]. \tag{II.26}$$

This relation will aid in the evaluation of the integration constants, which must be consistent with the initial conditions for the problem.

Continuing with the solution: In order to describe the coordinate, σ, one could return to eq. (II.14a), incorporate eq. (II.24) and integrate for this dimensionless variable. As a consequence of these operations it is easily shown that

$$\sigma \cong \mathcal{C}_5 + \left[\frac{H}{A}\left(1-2\,\frac{B^2}{A^2}\right) - \frac{1}{A}\right]A\varphi_T - 2H\left[\frac{\mathcal{C}_1}{A}\sin(A\varphi_T) - \frac{\mathcal{C}_2}{A}\cos(A\varphi_T)\right], \tag{II.27}$$

wherein $\mathcal{C}_5$ is the constant of integration obtained in this step. An appropriate substitution for λ' has been included, here, from eq. (II.26).

It is informative to note that this last state variable is a more complicated expression than its counterpart (λ). That is, a comparison of eqs. (II.24) and (II.27) will indicate that σ involves constants and cyclic components (as does the coordinate λ); however, in addition to these one sees that σ involves a secular term which was not apparent in the evaluation for λ.

Also, it should be mentioned that the results obtained here have an argument, for the cyclic elements, which is $A\varphi_T$ rather than φ_T alone (this is compared with corresponding expressions in Appendix B). Consequently, the argument here is proportional to the momentum factor (H) through the constant "A". In fairness to the mathematical procedures followed in this development, the difference in arguments ($A\varphi_T$ and φ_T) is rather small, generally, since A is approximately unity for close proximity orbits. In addition, it should be recalled that φ_T is <u>not</u> measured from a pericenter but is the angular displacement of the target from its initial position; that is, the position prescribed at $t = 0$, for "T".

II.13 <u>Evaluation of Constants</u>. - The several constants of integration noted in eqs. (II.24) through (II.27) will be described in terms of the initial conditions for the problem. Therefore, assuming general initial values; such as, at $t = 0$ (i.e., $\varphi_T = 0$):

$$\lambda = \lambda_o ; \quad \lambda' = \lambda'_o ; \quad \sigma = \sigma_o ; \tag{II.28}$$

then the constants $\mathcal{C}_i$ ($i = 3, 4, 5$) may be determined in the usual manner.

Incorporating the constants into the solution equations mentioned above, it is easily shown that these expressions take on the following forms:

$$\lambda = \left(\frac{A^2-1}{3A^2} \right)\left[1-\cos\left(A\varphi_T\right)\right] + \lambda_o \cos\left(A\varphi_T\right) + \frac{\lambda'_o}{A} \sin\left(A\varphi_T\right) ; \qquad \text{(II. 29a)}$$

$$\lambda' = \lambda'_o \cos\left(A\varphi_T\right) - A\left[\lambda_o - \left(\frac{A^2-1}{3A^2}\right)\right] \sin\left(A\varphi_T\right) ; \qquad \text{(II. 29b)}$$

and $$\sigma = \sigma_o + \left[\left(\frac{A^2+2}{3A^2}\right)^{3/2} - \frac{1}{A}\right] A\varphi_T + 2\sqrt{\frac{A^2+2}{3A^2}} \left(\frac{\lambda'-\lambda'_o}{3A^2}\right) ; \qquad \text{(II. 29c)}$$

while, from eq. (III. 5c)

$$\sigma' = \sqrt{\frac{A^2+2}{3A^2}} * \frac{A}{(1+\lambda)^2} - 1. \qquad \text{(II. 29d)}$$

These equations describe the state of motion for the interceptor, relative to the target, at any time (t); or, as noted previously, at any displacement angle, $\varphi_T = \dot{\varphi}_T t$. These expressions show that the state variables are coupled; hence, the displacements, etc. are not obtained independently. Also, recalling that A, $B \propto H$, then the dynamical constants for the system are actually proportional to powers of H, the specific momentum ratio for the complete system. Hence, in theory, H (thus A^2, B^2) can be described from initial values; and, the time (or position) history of the state quantities can be mapped, subsequently. From these several, general expressions the motion of the interceptor relative to the target is described in a rather straightforward manner.

II. 14 Line of sight formulations. - As an adjunct to the descriptions of the state trajectories, a formulation for the line-of-sight angles has been prepared. This development is found in Appendix C.

In the Appendix, the line-of-sight angles are described for in-plane motions using the two-coordinate representation; cartesian and shell coordinates. For

these formulations the angular position of the target particle, relative to the interceptor (I), is denoted as $\measuredangle$ LOS; and the angle locating the interceptor from the target, is designated as $\measuredangle$ los.

In the description of these angles, the relative position coordinates are given in dimensional and dimensionless form so that computation could be made without conversion of quantities.

For a graphical description of these angles, and their relationship to the coordinates, one should consult the sketches found in the appendix. The extension to a three-dimensional case is rather straightforward, but somewhat involved in manipulation. That formulation is not included here; it could be obtained but not without some labor being involved.

II.15 Comments. - This completes a description of the basic analytical developments for the relative motion problem. To this point, the linearized and modified solutions, in two-coordinate representations, have been obtained. A geometric description of the state variable traces has been ascertained, and a line-of-sight formulation developed. In the following sections of this report, example case studies will be made; these will illustrate the results thus far obtained and will provide some added knowledge of the general problem area. Also, in subsequent developments, formulations will be carried out to describe methods which will lead to greater accuracy and prediction capabilities for certain elements of the relative motion problem.

In the next chapter (III), a study of some representative examples will be undertaken, as the first step toward applying the results described in this section.

RELATIVE MOTION PROBLEMS

III.1 Applications using the relative motion equations. - In the next few sections use will be made of the analytical results described in the foregoing paragraphs. In particular, to illustrate the nature of the trajectories traced out on the representative (state) planes for the motion, specific problem types will be examined.

As a first study, the relative motion equations will be utilized as a means of defining the paths traced out by particles launched from the target (T). In view of the constraints placed on those results, by having developed the expressions from a set of linearized differential equations, it must be presumed that these ejected particles remain in the vicinity of the parent particle. Otherwise, it is known that the predictability of the state expressions is degraded, and the mathematical results are meaningful only to the extent that they indicate trends in the motion.

As a second example to be studied, the problem of intercept-and-rendezvous, by means of velocity impulses, will be examined. Again, the linearized state equations will be used to formulate the methodology, with the understanding that in the following sections an improved solution will be determined.

III.2 The motion of ejected objects. - A category of problem studies, relevant to the relative motion problem, considers the path of objects which are ejected from (say) the target vehicle. In some respects this might be viewed as a reverse intercept situation since the motions to be described originate at the coordinate origin and their time history will, in general, carry them away from the target spacecraft.

Because of their movement in space these particles may have motions which are cyclic in the vicinity of the spacecraft; or, they may be carried, continually, away from the launch point by a combination of cyclic and secular displacement terms. From a practical point of view these cases could represent what happens when relatively small objects are ejected from space vehicles, in orbit; or, these expressions may serve to describe the motion which an astronaut

might experience after he pushes away from his parent vehicle. Without the presence of physical constraints, it should be evident that some objects could become "lost" in space simply due to the manner in which they are "pushed" away, or ejected from the parent particle.

III.3 Equations of motion. - The mathematical expressions used to examine these case studies are the same equations which one would employ in the investigation of any relative motion problem. Due to the assumed smallness of amplitudes it will not be necessary to utilize a highly accurate mathematical model, initially. As a matter of fact it has been determined that with small initial values, etc., the linearized solutions are quite adequate. Therefore, the state of motion can be described by either eqs. (A.29), (A.30)--or eqs. (A.33), (A.34)--from Appendix A; or by eqs. (B.22) from Appendix B.

To be consistent in the following representations, dimensionless variables will be used; the appropriate relative motion equations are set down below. One should recall that in the cartesian system of coordinates all three dimensional variables are described, while the shell coordinates are representative of planar displacements only. Thus, as an example of the state equations:

(a) for cartesian coordinates (see Appendix A):

$$\xi = 2(2\xi_o + \eta'_o) + \left(\sqrt{(\xi'_o)^2 + (3\xi_o + 2\eta'_o)^2}\right) \cos(\varphi_T + K_3) ,$$

$$\eta = \eta_o - 2\xi'_o - 3(2\xi_o + \eta'_o)\,\varphi_T - 2\left(\sqrt{(\xi'_o)^2 + (3\xi_o + 2\eta'_o)^2}\right) \sin(\varphi_T + K_3),$$

$$\zeta = \left(\sqrt{\zeta_o^2 + (\zeta'_o)^2}\right) \cos(\varphi_T + K_6),$$

$$\xi' = -\left(\sqrt{(\xi'_o)^2 + (3\xi_o + 2\eta'_o)^2}\right) \sin(\varphi_T + K_3),$$

$$\eta' = \eta'_o - 2\left[(2\eta'_o + 3\xi_o) + \left(\sqrt{(\xi'_o)^2 + (3\xi_o + 2\eta'_o)^2}\right) \cos(\varphi_T + K_3)\right],$$

and

$$\zeta' = -\left(\sqrt{\zeta_o^2 + (\zeta'_o)^2}\right) \sin(\varphi_T + K_6); \tag{III.1}$$

wherein

$$K_3 = \tan^{-1}\left[\frac{-\xi'_o}{-(2\eta'_o + 3\xi_o)}\right], \text{ and } K_6 = \tan^{-1}\left[\frac{-\zeta'_o}{\zeta_o}\right].$$

In a similar fashion, a set of representative equations are:

(b) for shell coordinates (see Appendix B):

$$\lambda = \lambda_o + \lambda'_o \sin\varphi_T + (3\lambda_o + 2\sigma'_o)(1-\cos\varphi_T),$$

$$\sigma = \sigma_o + \sigma'_o \varphi_T - 2\left[\lambda'_o(1-\cos\varphi_T) + (3\lambda_o + 2\sigma'_o)(\varphi_T - \sin\varphi_T)\right],$$

$$\lambda' = \lambda'_o \cos\varphi_T + (3\lambda_o + 2\sigma'_o)\sin\varphi_T,$$

and $$\sigma' = \sigma'_o - 2\left[\lambda'_o \sin\varphi_T + (3\lambda_o + 2\sigma'_o)(1-\cos\varphi_T)\right]. \tag{III.2}$$

The cartesian coordinates $(\xi, \eta, \zeta; \xi', \eta', \zeta')$ correspond to the (x, y, z) relative motion frame of reference shown in Appendix A. The shell coordinates $(\lambda, \sigma; \lambda', \sigma')$ relate to the displacements (ρ, s) introduced in Appendix B.

For studies involving in-plane situations the coordinates which would be applicable are the (ξ, η) and/or the (λ, σ) variables. To view motions occurring out-of-plane of the target, the coordinates of interest would be either

(ξ, ζ), or (η, ζ), depending on the case to be examined.

III.4 Representative examples.

Example I: As a first example, consider the relative motion of an object which is impulsively propelled (radially) away from the target. The initial values applicable to this situation will be (in cartesian variables):

$$\xi_o = \eta_o = \eta'_o = 0; \quad \xi'_o \neq 0;$$

the ζ coordinate is not needed here.

The reduced equations describing this state of motion are, from eqs. (III.1):

$$\xi = \xi'_o \sin \varphi_T,$$

$$\eta = -2\xi'_o (1-\cos \varphi_T),$$

$$\xi' = \xi'_o \cos \varphi_T,$$

$$\eta' = -2\xi'_o \sin \varphi_T; \qquad \text{(III.3)}$$

since

$$K_3 = \tan^{-1}\left(\frac{-\xi'_o}{0}\right) \equiv \mp \pi/2,$$

depending on whether $\xi'_o \lesseqgtr 0$.

An inspection of these equations indicates that the geometric figure representing the motion, on the (ξ, η) plane, is an ellipse. The figure has its center displaced along the η axis (by an amount $-2\xi'_o$); and, has a major-to-minor axis ratio of 2:1 (hence the eccentricity = $\sqrt{3}/2$). To illustrate the statements above, mathematically, eqs. (III.3) may be manipulated to yield the following expression for the graph of the motion:

$$\left(\frac{\xi}{\xi'_o}\right)^2 + \left(\frac{\eta + 2\xi'_o}{2\xi'_o}\right)^2 = 1. \qquad \text{(III.4)}$$

The expression clearly defines the ellipse described in the preceding paragraph.

Fig. III.1 shows a plot of the displacements for; (1) a positive ξ'_o (Case I)*, and (2) for a negative value of ξ'_o (Case II)*. At points along the path there are tics to indicate the relative position of the ejected particle for appropriate values of φ_T (as noted).

Interestingly, when the particle is projected radially outward (with $\xi'_o > 0$) it follows a path which takes it aft of the spacecraft (T), but returns it to the target once each orbital period ($\varphi_T = 2\pi$). (For identification, directions are indicated on the figure corresponding to $\xi'_o \lesseqgtr 0$).

A projection downward ($\xi'_o < 0$) reverses the figure of motion, giving the object a path which carries it down and forward of the target vehicle over the first half of the orbit; and, upward and back to the target during the last half of the motion. Heuristically one can visualize these "looping figures" as ellipses in inertial space; figures which would suggest a return to the point of origin at the end of each orbital circuit.

The geometry describing the relationship which exists between the speed components (the hodograph) can be seen on Fig. III.1. However, the specific case shown corresponds to $\xi'_o > 0$.** This figure is also an ellipse (note the equations), but one which is centered at the coordinate origin ($\xi'_c = \eta'_c = 0$). Like the motion of the ejected particle, this figure also has a 2:1 ratio for the axes, and an eccentricity = $\sqrt{3}/2$.

---

* Here, and in all subsequent cases illustrated, the non-dimensional initial speeds are set at unity. This is done to retain perspective between case studies, and for ease in manipulation. Certainly a unit, non-dimensional impulse is not physically compatible with the constraints on the problem; but it is mathematically convenient.

**When $\xi'_o < 0$ the hodograph is unaltered; but, the originating point is shifted, on the curve, from $(+\xi'_o, 0)$ to $(-\xi'_o, 0)$.

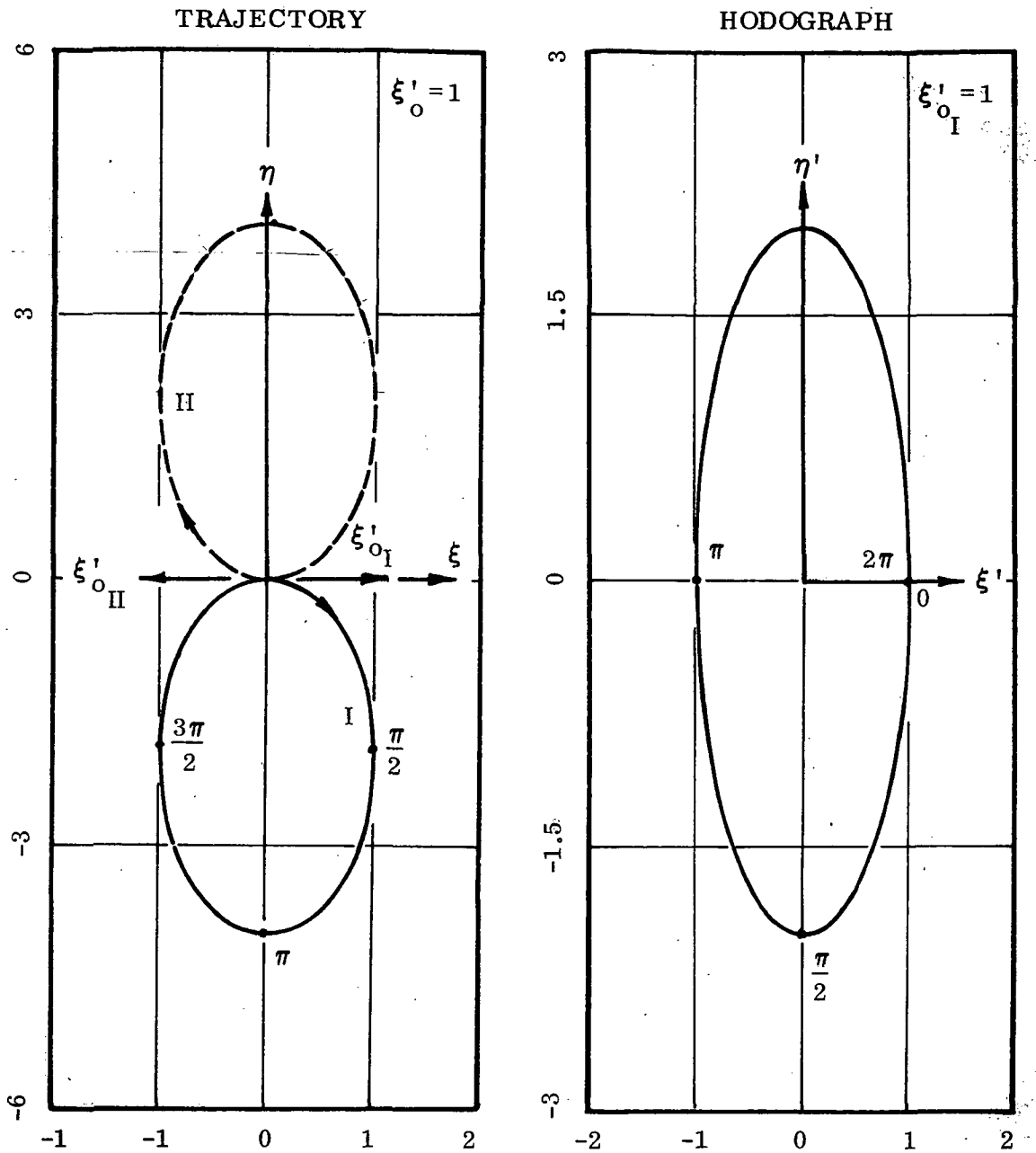

Fig. III.1. Relative Motion Traces, TRAJECTORY and HODOGRAPH, due to an Impulse (ξ'_o) Applied to Particle I at the Position of T. The Trajectory is shown for both $\pm \xi'_o$.

Again, from eqs. (III.3) one can ascertain that the equation of the hodograph is:

$$\left(\frac{\xi'}{\xi'_o}\right)^2 + \left(\frac{\eta'}{2\xi'_o}\right)^2 = 1, \tag{III.5}$$

describing the ellipse indicated above.

This example is the simplest non-trivial case considered for in-plane motion; yet it is typical of the rather unsuspected nature of events which can occur in relative motion studies.

Example II: The second example considers an in-plane motion also, but differs from the previous case in that this time the particle is projected forward of the target vehicle, in the direction of motion. Initial values for this study are:

$$\xi_o = \eta_o = \xi'_o = 0; \quad \eta'_o \neq 0;$$

(the ζ-components are not required).

The state equations for the motion are deduced from the governing expressions, eqs. (III.1), and are easily reduced to:

$$\xi_o = 2\eta'_o\,(1-\cos\varphi_T),$$

$$\eta = -3\eta'_o\,(\varphi_T - \frac{4}{3}\sin\varphi_T),$$

$$\xi' = 2\eta'_o \sin\varphi_T,$$

and

$$\eta' = -3\eta'_o\,(1 - \frac{4}{3}\cos\varphi_T), \tag{III.6}$$

since $K_3 = \tan^{-1}\left(\frac{0}{-2\eta'_o}\right) = \left\{\begin{matrix}\pi \\ 0\end{matrix}\right\}$, depending on the sign of η'_o.

A study of these expressions shows that the (ξ, η) motion describes an ellipse (basically); but one with a "meandering" origin (that is, one with a general motion in the η-direction). Also, one notes that the character of the displacements is cyclic, of period = 2π; thus the motion is repetitive. A plot of the trajectory (for $\eta'_o > 0$) is depicted on Fig. III.2; the graph shows that (here) $\xi \geq 0$ (always) while η is initially positive, but generally appears as an incrementing negative displacement. As before, to obtain some idea of the orientation and scale for the track, tics* have been used to indicate variations of the motion, over one period, for the maneuver.

Mathematically, eqs. (III.6) can be used to obtain an equation for this figure of the motion. It is easy to show this is:

$$\left(\frac{\xi - 2\eta'_o}{2\eta'_o}\right)^2 + \left(\frac{\eta + 3\eta'_o \varphi_T}{4\eta'_o}\right) = 1. \qquad \text{(III.7)}$$

In the equation, the term $\eta_c \equiv -3\eta'_o \varphi_T$ would indicate that the η-displacement of the origin is secular, in nature; this is, indeed, indicative of the "meandering" mentioned above. Probably as a more correct definition of the displacement curve, it would be proper to call it a prolate cycloid.

The hodograph of this motion is shown on the figure, but for the case of $\eta'_o > 0$. As might be expected this figure is also an ellipse; however, it has an origin which is shifted away from the geometric center, and is stationary on the plane. Note that this shift is 3 units of the speed scale, in the $+\eta'$-direction, corresponding to the secular influence found in the solution equations. As before, the axes of the ellipse are in a 2:1 ratio, hence the eccentricity = $\sqrt{3}/2$; and, the motion direction, about the figure (for $\eta'_o > 0$), is as indicated on this graph.

Using the speed relations, eqs. (III.6), one can show that the equation for the hodograph is:

* With each tic is an indication of the appropriate displacement, φ_T.

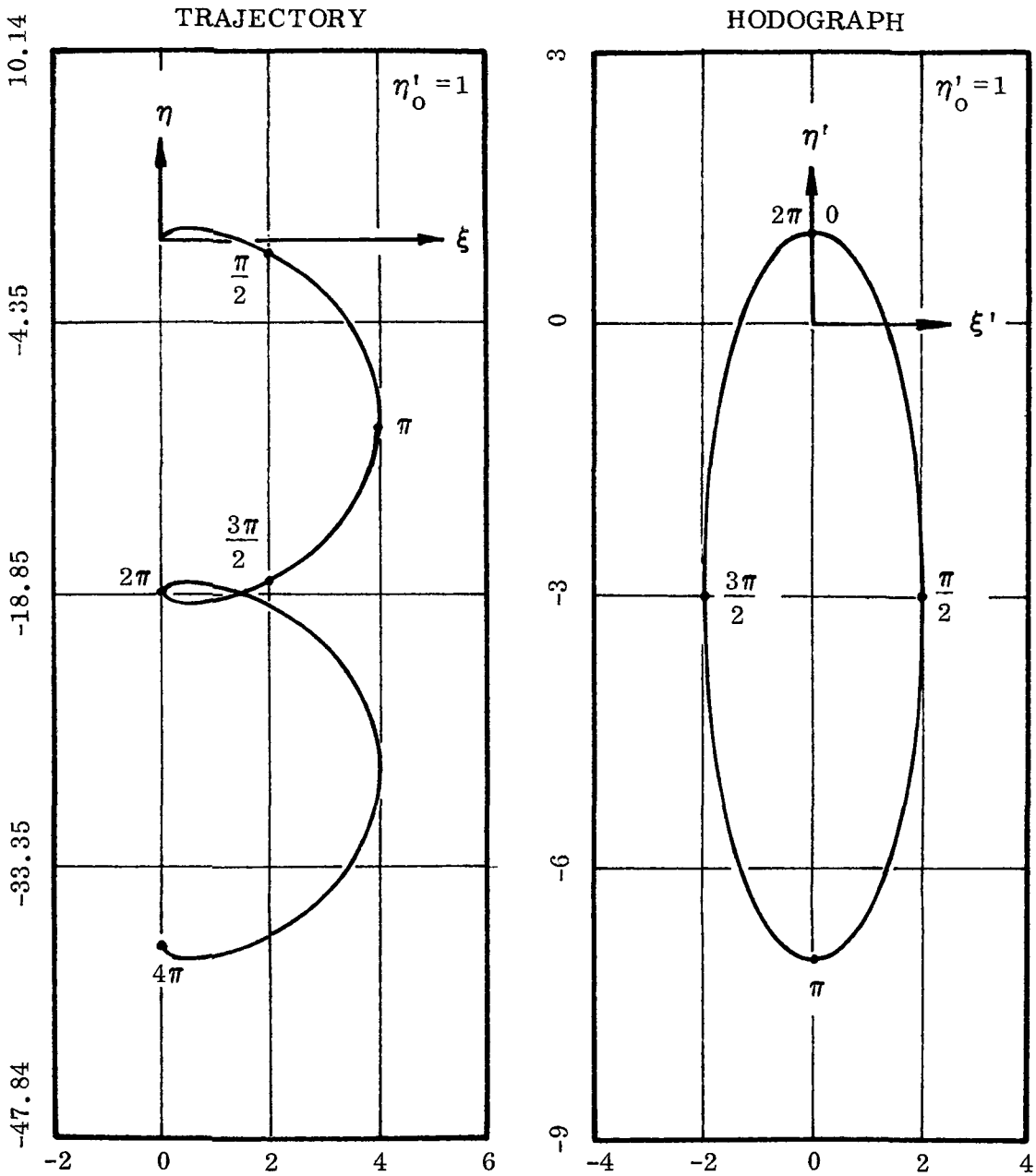

Fig. III.2. Relative Motion Traces, for I, due to an Impulse (η_o') Applied at the Position of T.

$$\left(\frac{\xi'}{2\eta'_o}\right)^2 + \left(\frac{\eta' + 3\eta'_o}{4\eta'_o}\right)^2 = 1. \qquad \text{(III. 8)}$$

The unusual nature of this motion is due to the fact that the input ($\eta'_o > 0$) produces an overall loss in displacement. As time progresses the ejected particle becomes increasingly further separated from the spacecraft; hence a "return to the target" becomes more difficult as time goes by.

A close inspection of this motion will show that near t=0 the launched particle moves, first, ahead of the target then it rises (with ξ, $\eta > 0$); and, finally, it moves aft into the region where $\xi > 0$, $\eta < 0$! (Note that the sign of η changes at $\varphi_T = \frac{4}{3} \sin \varphi_T$).

Example III: Logically the next case study should consider a particle being launched with an impulse having both ξ'_o and η'_o components. One would expect that the resulting motion should show influences from both of the previous cases, with weighting being given to the components according to the magnitude and sign of the inputs (ξ'_o, η'_o).

For identification, the equations describing this state of motion are:

$$\xi = \xi'_o \sin \varphi_T + 2\eta'_o (1-\cos \varphi_T),$$

$$\eta = \eta'_o \varphi_T - 2\left[\xi'_o (1-\cos \varphi_T) + 2\eta'_o (\varphi_T - \sin \varphi_T)\right],$$

$$\xi' = \xi'_o \cos \varphi_T + 2\eta'_o \sin \varphi_T ,$$

and

$$\eta' = \eta'_o - 2\left[\xi'_o \sin \varphi_T + 2\eta'_o (1-\cos \varphi_T)\right]; \qquad \text{(III. 9)}$$

wherein the prescribed initial values are: $\xi_o = \eta_o = 0$; $\xi'_o \neq 0$, $\eta'_o \neq 0$ (as before, the ζ variables are not needed).

In order to specifically describe the path followed by the particle, for these conditions, the initial values $(\xi'_o = \eta'_o) > 0$ are selected* and a trajectory computed and plotted. The geometry corresponding to this case is presented below on Fig. III.3. As one might expect the motion appears to be quite like that for the previous case where $\xi'_o = 0$, $\eta'_o > 0$. However, a noticeable difference occurs here; that is, initially, the particle moves away from the parent vehicle in a definite outward fashion, climbing into the region where $\xi, \eta > 0$, crossing through $\eta = 0$ and then falling aft of the target vehicle. Near the terminus of each cycle of the motion one finds that $\xi < 0$ (a situation not encountered in the earlier case), and that the loop in the trajectory figure is not symmetric about a line (η = constant) passing through the point corresponding to $\varphi_T = 2\pi$. This pecularity can be traced to the initial value, $\xi'_o \neq 0$. If one would rewrite the displacement equations it would become apparent that the trajectory trace could be described as a figure closely akin to a prolate cycloid.

The hodograph for this motion is found to be an ellipse, similar in appearance to those obtained earlier; and, having the same basic characteristics noted there (shape, relative size and eccentricity). Once again the coordinate origin is shifted away from the geometric center of the figure; but, the points corresponding to various values of φ_T are displaced in comparison to the earlier case; see Example II, where $(\xi'_o = 0, \quad \eta'_o > 0)$.

Mathematically, the state equations can be made to yield the following equation for the hodograph:

$$\left(\frac{\xi'}{\sqrt{\xi'^2_o + 4\eta'^2_o}}\right)^2 + \left(\frac{\eta' + 3\eta'_o}{2\sqrt{\xi'^2_o + 4\eta'^2_o}}\right) = 1. \qquad \text{(III.10)}$$

On the hodograph, and the displacement figure, corresponding velocity vectors are noted to illustrate the correlation between the two figures. Remembering that the velocity vector has the direction of the displacement tangent, then

*Again, for convenience and clarity the initial impulse values used in the example are set at unity.

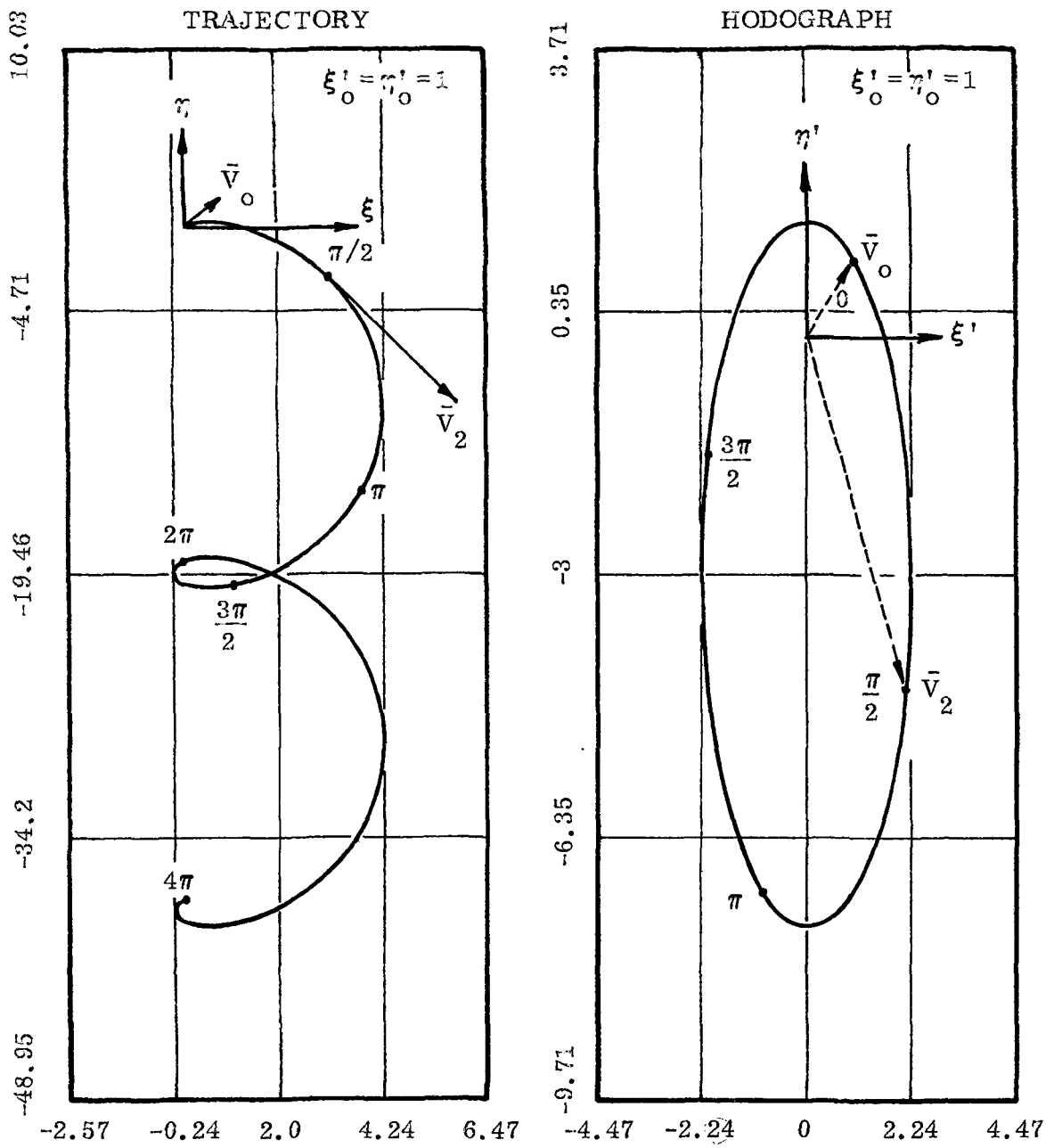

Fig. III.3. Relative Motion Traces due to an Impulse having Components ξ'_o, η'_o. Representative Velocity Vectors (at $\varphi_T = 0,\ \pi/2$) are Shown to Illustrate Correlation between the Trajectory and Hodograph Planes.

the hodograph has an obvious utility in describing the state of the relative motion. A simultaneous study of both figures will indicate magnitudes and locations of maxima and minima of state conditions. These figures are useful in describing the conditions needed to effect proper changes in state, at some desired position; and can be helpful in defining operational aspects of flight maneuvers.

As a means of ascertaining the accuracy of the predictions afforded by these linearized solutions, a numerical integration for this case was carried out; and, the numbers obtained have been compared to the analytic answers. Using as initial inputs, $\xi'_o = \eta'_o = 10^{-4}$, a fourth order Runge-Kutta integrator provided results which indicated that the agreement between cases is more than close.

Example IV: This next case is the first of two situations which will consider an out-of-plane motion, due to an initial speed component, ζ'_o. This first study has the following initial values:

$$\xi_o = \eta_o = \zeta_o = \eta'_o = 0,$$

$$\xi'_o = \zeta'_o = 1. \text{ (but positive).}$$

The "reduced" state equations, shown below, indicate that the motion is a modification of that described in Example I, earlier. The complete motion is defined from:

$$\xi = \xi'_o \sin \varphi_T,$$

$$\eta = -2 \left[\xi'_o (1-\cos \varphi_T) \right],$$

$$\zeta = \zeta'_o \sin \varphi_T ,$$

$$\xi' = \xi'_o \cos \varphi_T ,$$

$$\eta' = -2\xi'_o \sin \varphi_T \ ,$$

and

$$\zeta' = \zeta'_o \cos \varphi_T \ . \qquad \text{(III.11)}$$

In this case the relative motion trajectory has a full three-dimensional geometry. The in-plane figure is the ellipse from Example I, while the motion in the ξ, ζ plane (a plane viewed from behind the target) is a line, passing through the origin, having a positive slope (see Fig. III.4a). Necessarily with ξ'_o, $\zeta'_o > 0$ the displacements are at first, positive--then negative, and symmetric in aspect.

An equation, describing this motion trace,easily obtained from eqs. (III.11); is,

$$\xi = \frac{\xi'_o}{\zeta'_o} \zeta_o \ . \qquad \text{(III.12)}$$

The motion, as viewed on the η, ζ plane (shown as if seen from above the target spacecraft) is an ellipse, also. (See Fig. III.4b). The ellipse, for the initial values chosen, has an axis ratio of 2:1; and has the origin of coordinates located at a terminus of the major axis. As noted in the displacement expressions, the coordinates are cyclic in their variations, and have a period matching that of the target vehicle.

For this figure, the equation obtained from eqs. (III.11) is:

$$\left(\frac{\eta + 2\xi'_o}{2\xi'_o}\right) + \left(\frac{\zeta_o}{\zeta'_o}\right)^2 = 1. \qquad \text{(III.13a)}$$

This is a 2:1 ellipse only when the impulse has components of equal magnitude. One should recall that these figures are obtained using unit-valued impulses.

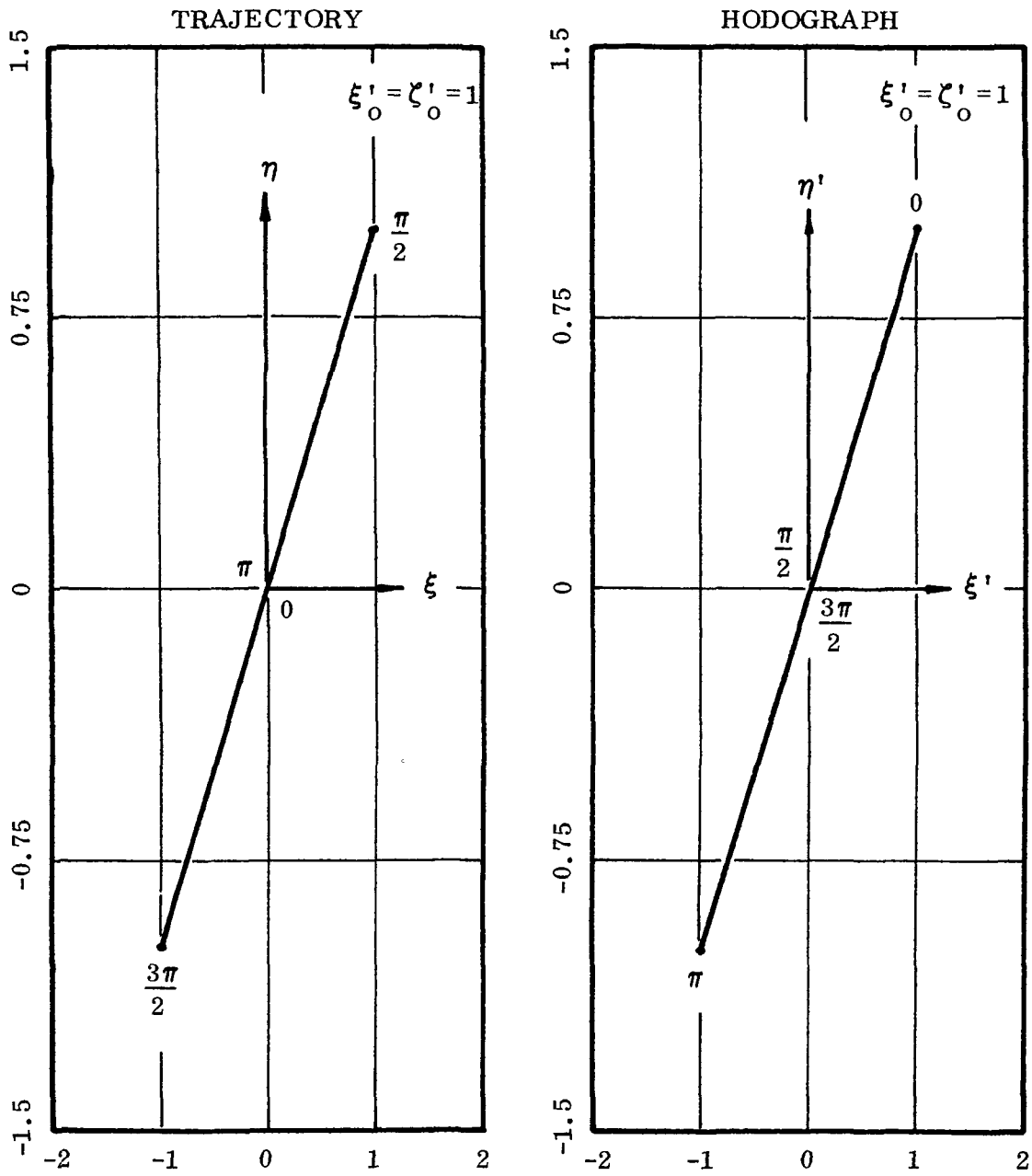

Fig. III.4a. Relative Motion Traces due to an Impulse having Components ξ'_o, ζ'_o. These figures Describe In-Plane Motions of I with respect to T.

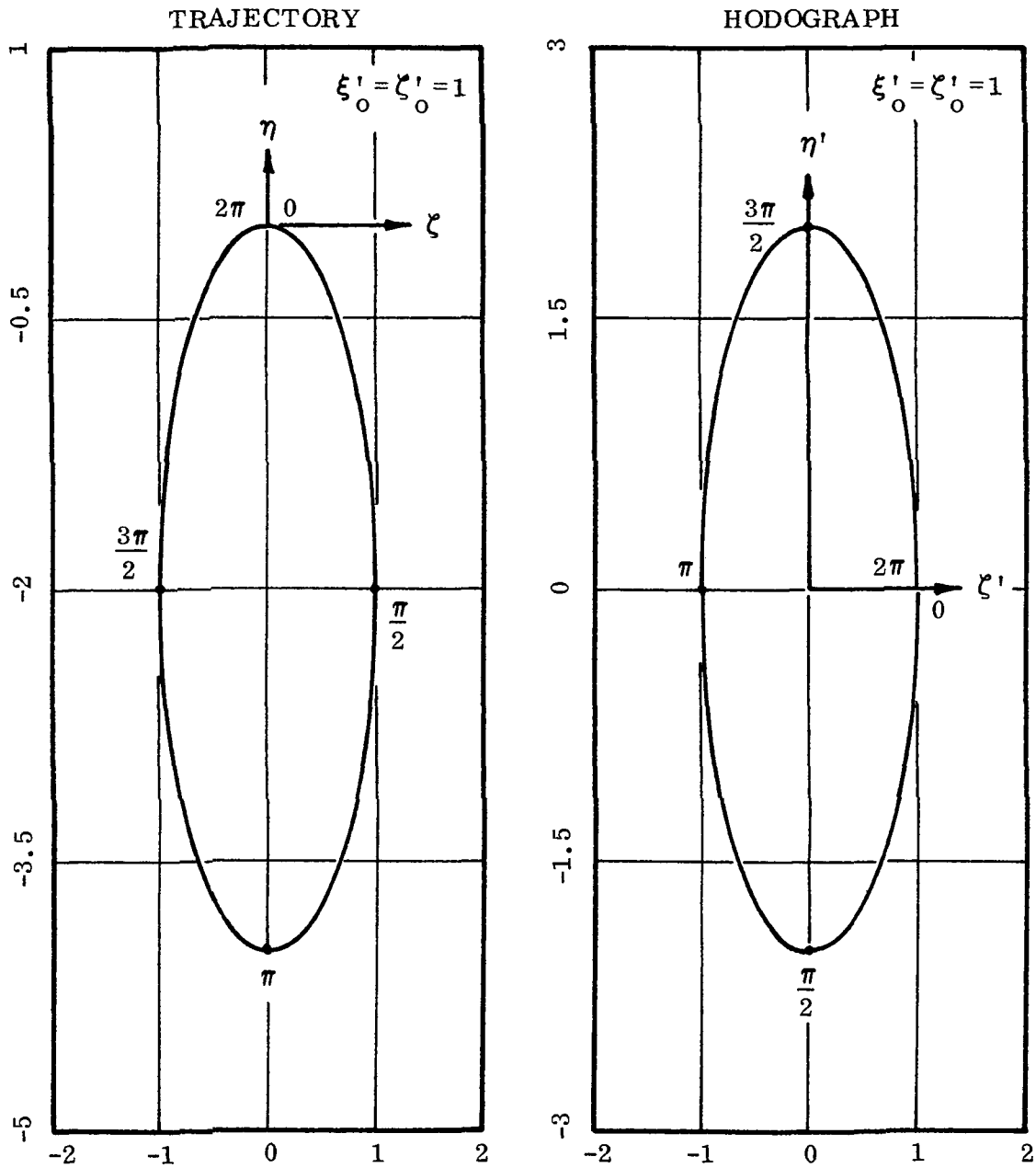

Fig. III.4b. Out-of-Plane Relative Motion Traces due to an Impulse with Components ξ'_o, ζ'_o.

The hodograph (planes) for this case are: (1) the same as shown on Fig. III.1; and, (2) the pair of geometries plotted on Fig. III.4. It is somewhat incidental that the hodograph figures are quite similar to the displacements on all three planes. A distinct difference, however, is that the geometric centers of these ellipses do not coincide with the origins for the displacements. A comparison of the two sets of graphs will best illustrate these differences.

For purposes of continuity, the hodograph equations are listed below. These describe the two figures on Fig. (III.4), where the plots were made using unit, unscaled impulse quantities (ξ'_o, ζ'_o):

$$\xi' = \frac{\xi'_o}{\zeta'_o}\,\zeta' ,$$

and

$$\left(\frac{\eta'}{2\xi'_o}\right)^2 + \left(\frac{\zeta'}{\zeta'_o}\right)^2 = 1. \qquad \text{(III.13b)}$$

Example V: The last case to be studied here has the following initial values:

$$\xi_o = \eta_o = \zeta_o = \xi'_o = 0;$$

$$(\eta'_o = \zeta'_o) > 0.$$

The expressions which describe the state variable are deduced to be:

$$\xi = 2\eta'_o\,(1-\cos\varphi_T),$$

$$\eta = -3\eta'_o\,(\varphi_T - \frac{4}{3}\sin\varphi_T),$$

$$\zeta = \zeta'_o \sin\varphi_T ,$$

$$\xi' = 2\eta'_o \sin\varphi_T ,$$

$$\eta' = -3\eta'_o \left(1 - \frac{4}{3} \cos \varphi_T\right),$$

and

$$\zeta' = \zeta'_o \cos \varphi_T. \qquad \text{(III. 14)}$$

The similarity here, to the situation shown for Example II is noted; for conciseness, that phase of the motion will not be discussed again at this time. Instead, the motion traced on the (ξ, ζ) and (η, ζ) planes will be noted and commented upon; also, the associated hodographs--corresponding to these planes--will be mentioned.

The (ξ, ζ) displacements describe an ellipse*, characterized as before; this is readily seen from Fig. (III. 5a).

In much the same manner as noted earlier, the inclusion of an η'_o input produces rather unpredictable results (due to the presence of secular terms); the trace of the motion on the (η, ζ) plane is to be found on (Fig. III. 5b). Here one notes that when $\eta'_o > 0$ the particle commences to move ahead of the target vehicle; however, it ultimately falls behind the target and continues to move away from it. The obvious side-to-side motion, due to ζ'_o, is also apparent from this graph.

The mathematical expressions describing the trace figures are:

(a) the ellipse,

$$\left(\frac{\xi - 2\eta'_o}{2\eta'_o}\right) + \left(\frac{\zeta}{\zeta'_o}\right)^2 = 1;$$

and (b) the S-shaped curve,

$$\frac{\eta}{3\eta'_o} = \frac{4}{3}\left(\frac{\zeta}{\zeta'_o}\right) - \varphi_T. \qquad \text{(III. 15)}$$

*Note that here the initial impulse levels have been set at unity, simultaneously.

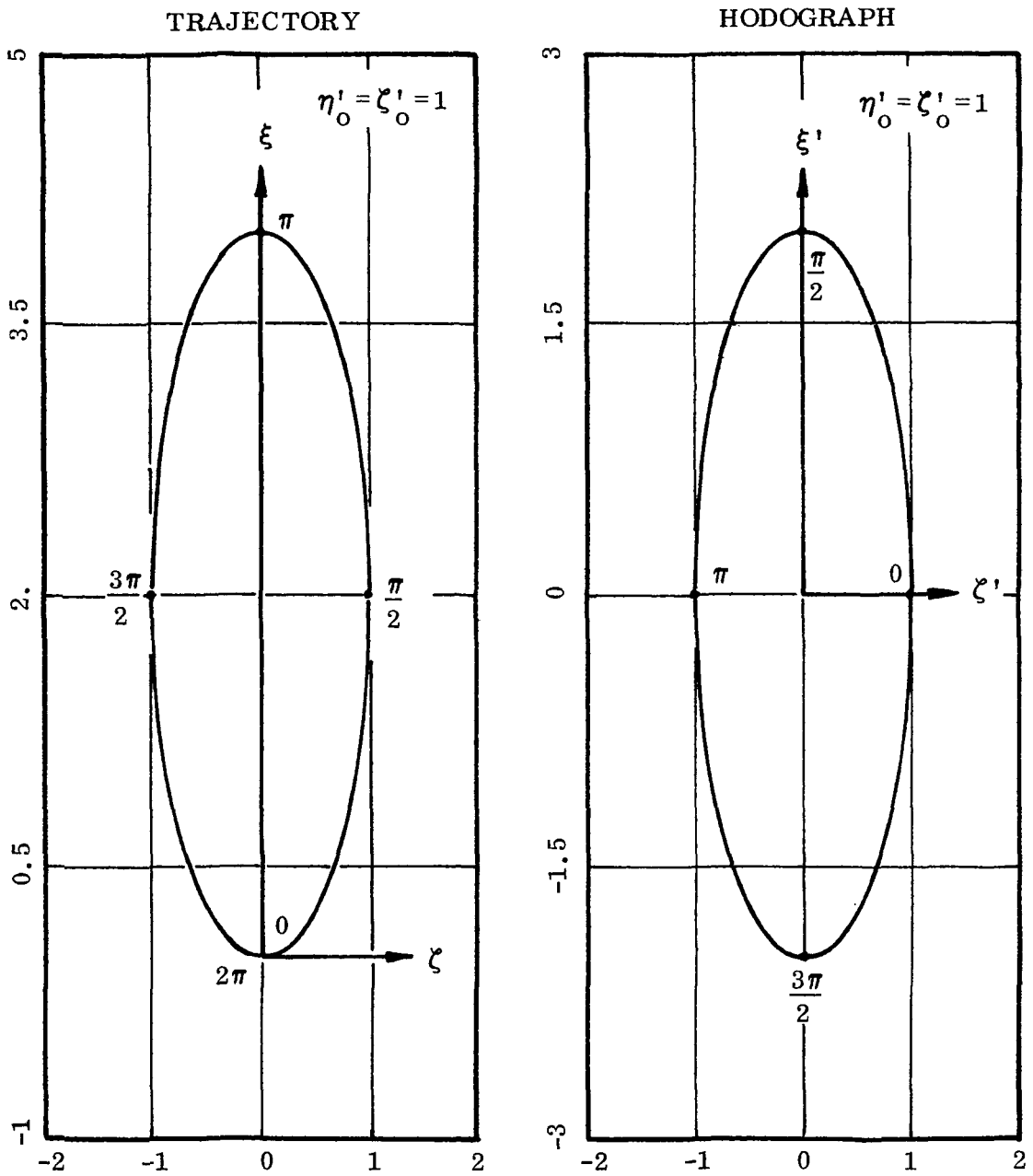

Fig. III.5a. In-Plane Motion Traces, for Particle I, due to an Impulse with Components η'_o, ζ'_o.

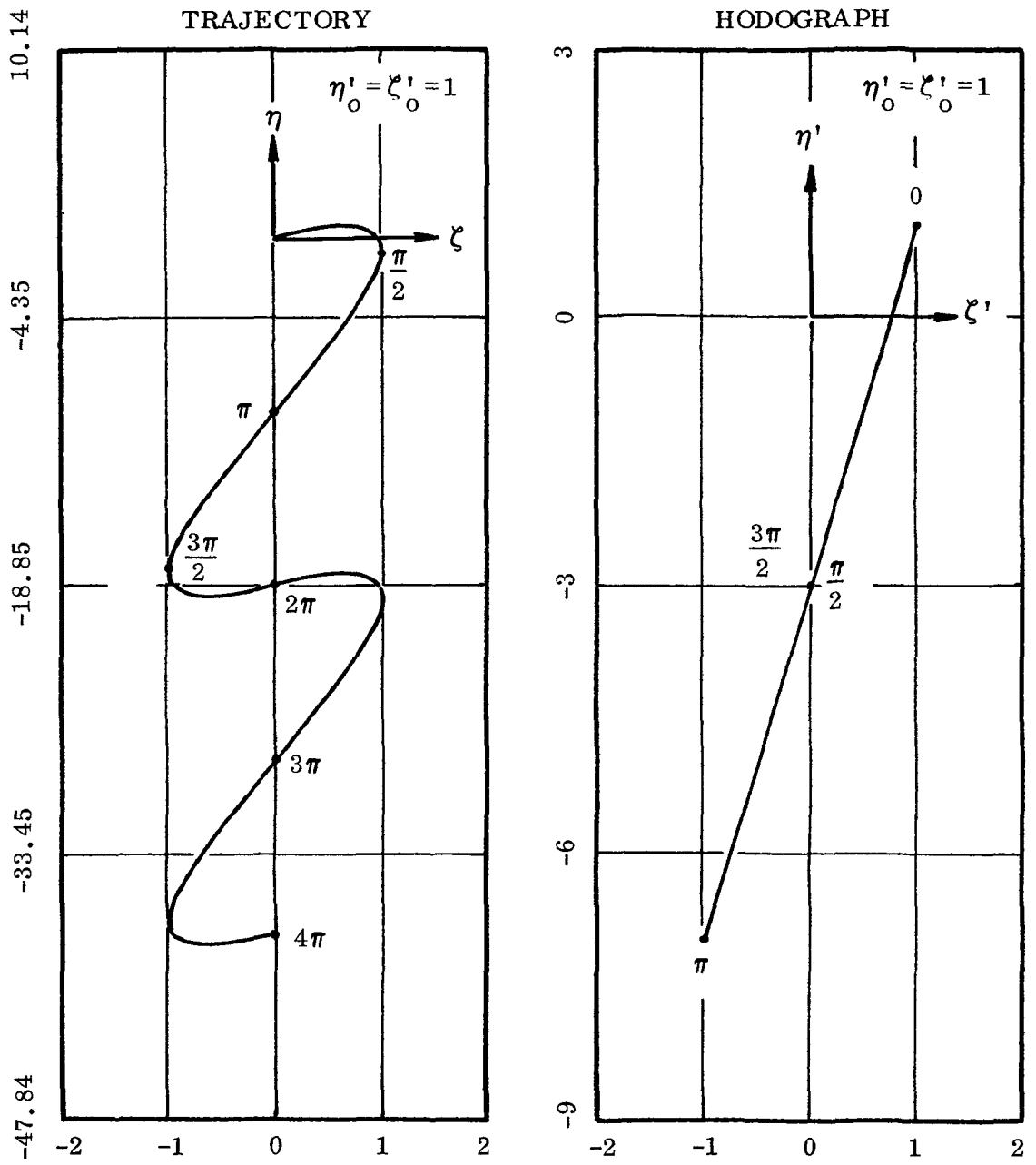

Fig. III.5b. Out-of-Plane Traces, for Particle I, due to Impulse with Components η'_o, ζ'_o Applied at T.

If one considers the three trace planes together, it is evident that the complete geometry of this relative motion is described by a curve traced onto the surface of an elliptic cylinder whose axis parallels the η-direction. This would be a somewhat difficult result to gather, a priori; thus, the value of these planar motion representations.

The hodographs corresponding to the planes of motion are shown, with the trajectories, on the figures. Here the characteristic elliptic figure is found, in the one case; however, the η', ζ' figure is determined to be a straight line crossing the η' axis aft of the origin. In view of past discussions these geometries should be self explanatory and, consequently, do not require further comment here.

To complete the analytical descriptions for the representative planes, the hodograph equations are included below:

(a) The (ξ', η') trace is the ellipse,

$$\left(\frac{\xi'}{2\eta'_o}\right)^2 + \left(\frac{\eta' + 3\eta'_o}{4\eta'_o}\right)^2 = 1; \tag{III.16a}$$

while (b) that one traced onto the (ξ', ζ') plane is,

$$\left(\frac{\xi'}{2\eta'_o}\right)^2 + \left(\frac{\zeta'}{\zeta'_o}\right)^2 = 1 \tag{III.16b}$$

(an ellipse with its center at the coordinate origin);

and (c) the line representing the (η', ζ') trajectory:

$$\eta' + 3\eta'_o = \left(\frac{4\eta'_o}{\zeta'_o}\right) \zeta . \tag{III.16c}$$

Example VI: To illustrate another use of the relative motion equations, in conjunction with the ejected particles problem, consider the following example.

Suppose Example I is modified in the following manner:

> Let the problem begin as before, but assume that a second impulse is applied at some preselected position on the trajectory. In particular, let this impulse occur when the ejected particle has moved to the $\varphi_T = 3\pi/2$ position. At this location, suppose the impulse is applied so that the relative velocity is nulled completely; and, from there the particle moves along its new trajectory unimpeded.

From Example I, it is seen that the particle is at the position ($\xi = 1$, $\eta = -2$) when $\varphi_T = 3\pi/2$. From the hodograph it is evident that the applied impulse (to null the relative velocity here) is $\left[-(\xi', \eta')_{\varphi_T = 3\pi/2} \equiv -(\xi' = -1)\right]$.

Now, the initial state of the particle, as it moves onto its new trajectory is:

$$\xi_o = -1, \ \eta_o = -2, \ \zeta_o = 0;$$

$$\xi'_o = 0, \ \eta'_o = 0, \ \zeta'_o = 0.$$

The appropriate equations, defining the new trajectories will be:

$$\xi = 4\xi_o \left(1 - \frac{3}{4} \cos \varphi_T\right),$$

$$\eta = \eta_o - 6\xi_o (\varphi_T - \sin \varphi_T);$$

$$\xi' = 3\xi_o \sin \varphi_T,$$

$$\eta' = -6\xi_o (1-\cos \varphi_T) ;$$

and the initial value of $\varphi_T \left(\equiv \varphi_{T_o} \right) = 0$, for compatibility in the variables. If this solution is graphed (for one period of motion), the result is as shown on Fig. III.6.

It should be evident that the new displacement trajectory is a cycloid; and, that the hodograph is the ellipse:

$$\left(\frac{\xi'}{3\xi_o}\right)^2 + \left(\frac{\eta' - 6\xi_o}{6\xi_o}\right)^2 = 1.$$

It is apparent that the new figure no longer reaches the radial distance for the target, and that the interceptor's track, in inertial space, lies within the circular orbit of the target. (i.e., $\xi < 0$, for all φ_T).

III.5 Comments. - The five cases investigated in the above paragraphs serve to illustrate the nature of the relative motions produced by impulses applied to an object being ejected from a parent vehicle which is moving along a prescribed circular orbit in space. Needless to say, variations of these figures could be produced simply by imposing other initial values; or, by constructing more complex space flight maneuvers.

Figure III.7 is included here to illustrate, schematically, some possible uses and interpretations one might give to the motion studies in the foregoing examples. On this sketch several illustrations are made to indicate means of achieving nearby orbits, from a parent vehicle (T).

On the upper portion of this figure a particle may be sent from T to A by (say) an application of the impulse represented in Example I. If the impulse would be reversed, then position A' might be achieved. A particle could be sent

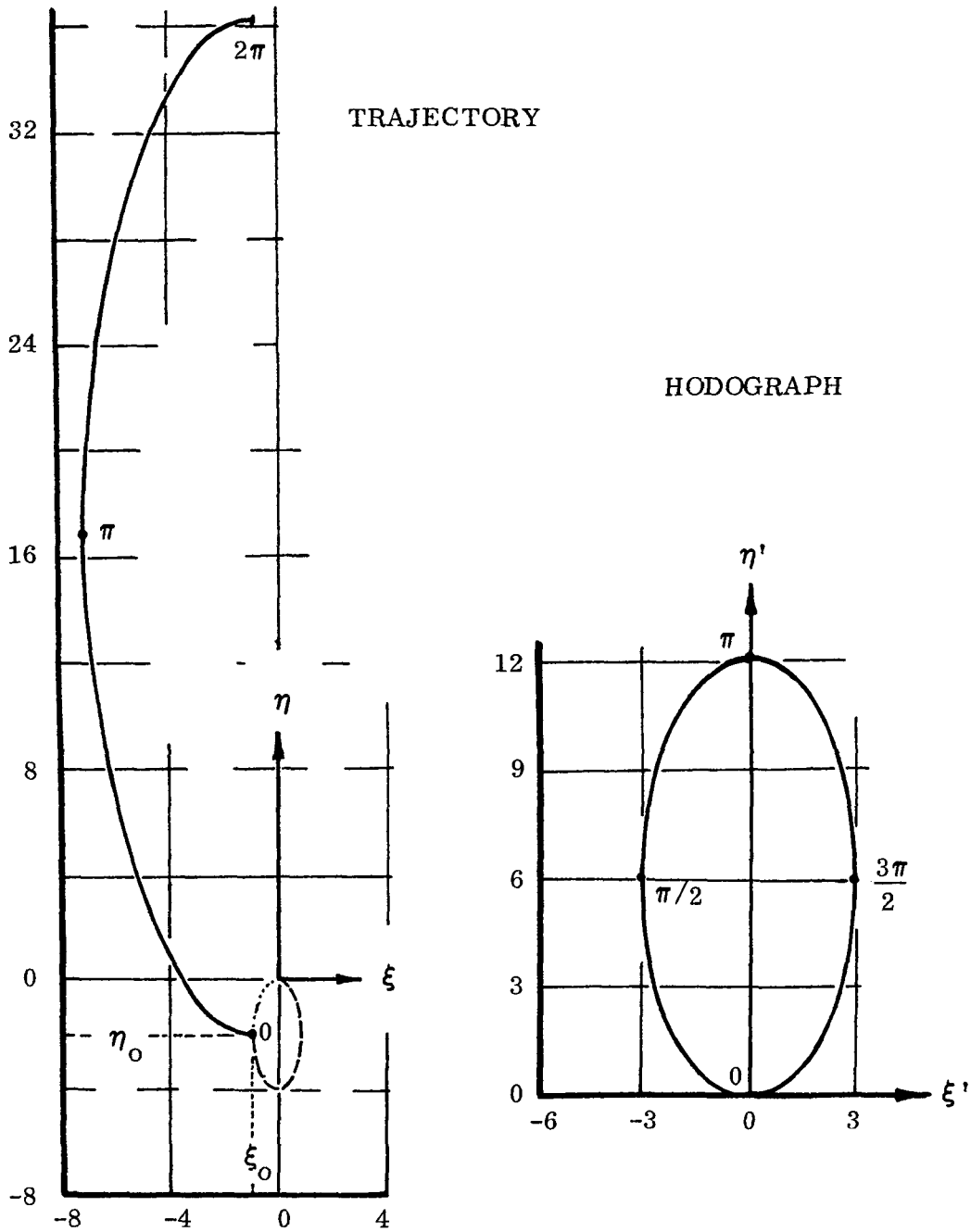

Fig. III.6. Relative Motion due to an Impulse Applied at a Position Away from the Origin, T. Motion originates at (ξ_o, η_o) with relative speed of zero magnitude.

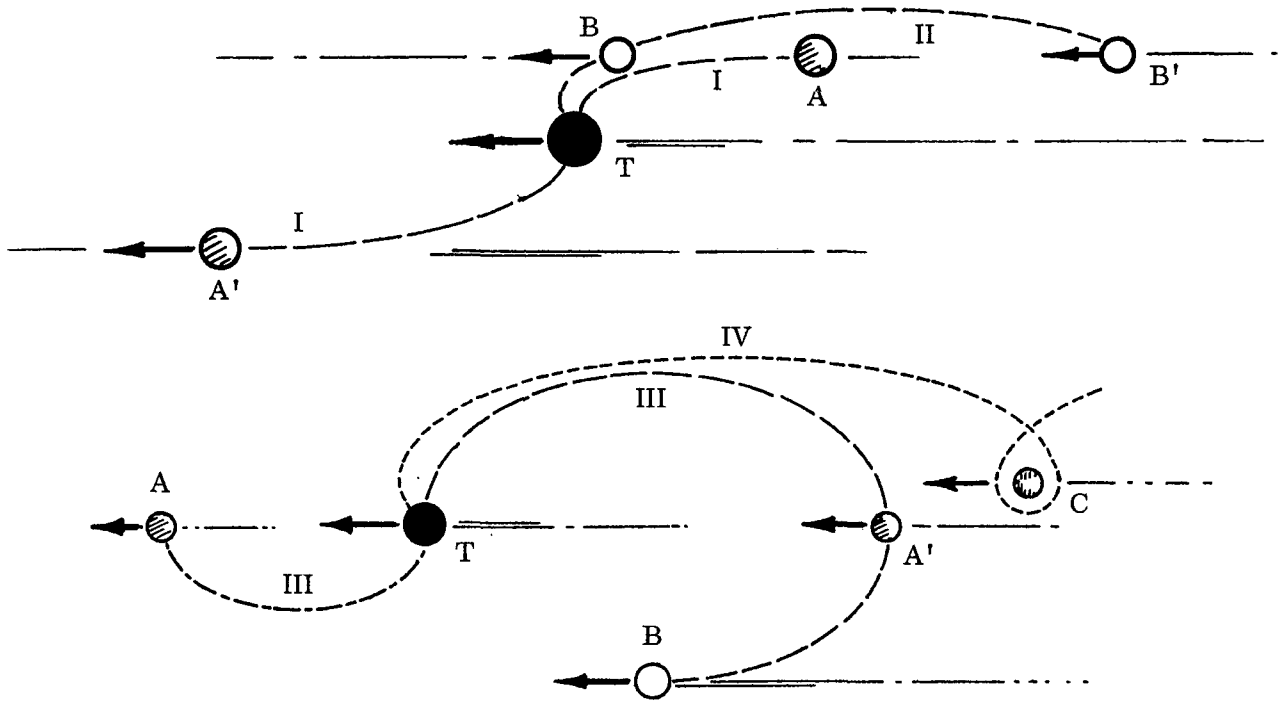

Fig. III.7. Sketch Showing Several Possible Transfers for Impulses Applied, at T, to Particle I.

to position B and/or B' by use of the impulse described in Example II. Obviously, other schemes and applications could just as easily be visualized.

On the lower part of this figure the illustrations depict a means of reaching positions ahead (A) and behind (A') the target; or transfer to achieve a lower orbital position (B) with a particle. These cases are indicative of the applications noted in Examples I and II, respectively. The trace, noted as IV, is an application of the impulse described in Example III. Here, a "messenger particle" is launched from $\bar{T}$ to interrogate a particle at $\bar{C}$ on an adjacent orbit.

This figure is intended to demonstrate that the geometries described in the various examples of this section are indeed indicative of operational modes one might consider useful in future space flight operations.

Before leaving this section it should be mentioned that several of the example cases noted here have been checked for accuracy of prediction by comparing the analytic answers with numerical evaluations. It was found that so long as the initial speeds were constrained to levels of the order of 10^{-3} to 10^{-4} (in dimensionless units), the displacements shown here compared very well with the numerical results, for a cycle of the orbital motions. These verifications serve, quite remarkably, to enhance the value of such analytic developments since those which have been obtained here were acquired from a linearization applied to the governing differential equations.

One interesting observation made from studying the figures describing the ejected particle motions, is that the solutions predict both closed and open geometries. It is apparent that closed displacement trajectories result so long as the initial impulse is applied orthogonal to the target's flight path direction. When this condition is not met, such as the application of an impulse η_o', then the trace figures are "open". Of course, this conclusion is easily verified from a consideration of the state equations (for instance, see eqs. (A.33), Appendix A).

There one sees that the secular term involves the parameters (ξ_o, η'_o), hence the nulling of these components would result in only constant and cyclic quantities as descriptors of the motion. It should be apparent that, in general, both parameters, or an appropriate combination of them, must be nulled if the displacement geometries are to be closed figures.

III.6 Intercept and rendezvous. - The problem referred to here as "intercept and rendezvous" begins with two particles in orbit about an attracting primary mass point. Generally, the interceptor will be flying on an orbit which places it in close proximity to the target vehicle; which, in turn, is in motion along a slightly different path in space.

At some selected instant in time an impulsive "action" will be initiated which alters the path of the interceptor so that, subsequently, the particle overtakes and comes into contact with the target. This flight operation, of bringing the two vehicles to the same point, in space, at the time, (t*), is referred to as the intercept maneuver.

Rendezvous, on the other hand, occurs at the termination of the intercept phase; it is associated with an impulsive "action" undertaken to assure "soft-contact" between the two particles. Hence, at rendezvous the two vehicles meet in space with their relative displacements and speeds reduced to zero simultaneously. Thus, the final state of the relative motion is described by a null vector for the system.

In order to provide a problem which will be amenable to analytic manipulations the various "actions" which are to be undertaken in the performance of an intercept and rendezvous operation will be velocity impulses. Thus, the relative speed components undergo instantaneous changes; hence the vehicles are placed onto new--and slightly altered--flight paths, while the path segments are continuous ballistic arcs; continuous, except for those instants when the impulses are applied.

III.7 Coordinate representations. - In this report various sets of relative motion equations have been described. Two of these are derived from "linearized" differential equations of motion; while in other instances the solutions are less dependent on the linearization. Even though the basic concepts of intercept and rendezvous will be consistent, there are some minor differences which will warrant documenting these various schemes. Therefore, in the following developments all of these methods will be discussed.

III.8.1 The intercept and rendezvous maneuver.

(a) Cartesian coordinates: The analytic expressions which relate to this problem, per se, have been developed in Appendix A; there they are presented in dimensional (x, y, z; $\dot{x}$, $\dot{y}$, $\dot{z}$) and dimensionless (ξ, η, ζ; ξ', η', ζ') form. For convenience, the procedures to be outlined here will refer specifically to the dimensionless coordinates; however, the corresponding dimensional expressions will be referenced throughout by noting appropriate equations in square brackets.

To facilitate the development which follows, the pertinent expressions from Appendix A are noted below.

(a) The coordinates describing relative positions (from eq. (A.33))*, are:

$$\xi = \xi_o + (3\xi_o + 2\eta'_o)(1-\cos\varphi_T) + \xi'_o \sin\varphi_T ,$$

$$\eta = \eta_o - 3(2\xi_o + \eta'_o)\varphi_T - 2\xi'_o(1-\cos\varphi_T) + 2(3\xi_o + 2\eta'_o)\sin\varphi_T ,$$

and

$$\zeta = \zeta_o \cos\varphi_T + \zeta'_o \sin\varphi_T . \qquad \text{(III.17)}$$

These expressions locate I with respect to T when the two vehicles are circulating about a common primary; and, where mutual attractions between the vehicles are neglected.

*Historically, these equations are found in the literature developed from the so-called Euler-Hill differential equations. Also, these same results in dimensional form were found in Art. 26-5, in "Space Technology", edited by H. Seifert, (Wiley, 1959).

(The corresponding dimensional expressions are given as [eqs. (A.29b)]).

(b) The relative speed relations, corresponding to the displacements, are (from eqs. (A.34)):

$$\xi' = \xi'_o \cos \varphi_T + (3\xi_o + 2\eta'_o) \sin \varphi_T ,$$

$$\eta' = \eta'_o - 2[(3\xi_o + 2\eta'_o)(1-\cos \varphi_T) + \xi'_o \sin \varphi_T] ,$$

and $$\zeta' = \zeta'_o \cos \varphi_T - \zeta_o \sin \varphi_T , \qquad \text{(III.18)}$$

(and, the corresponding dimensional relations are found in [eqs. (A.30b)]).

The above equations describe the speed of I with respect to T as the two bodies move about the primary. For these expressions one should recognize that the argument of the trigonometric, and related angular rate, terms could be replaced according to $\varphi_T \equiv \dot{\varphi}_T t$ (here); this is consistent with the constancy of the rate term, $\dot{\varphi}_T$.

These equations describe, fully, the relative state of the motion for one orbiting body with respect to the other; but, they are for the case of a second body moving on a prescribed circular path. Beginning at the initial time, $t = t_o$, a complete time history of a motion can be ascertained from these relations--insofar as linear theory is capable of predicting such.

III.8.2 Conditions for intercept. - Suppose that at some time t^* an intercept between the two particles is desired. Assuming that at the initial position (x_o, y_o, z_o) the interceptor has been given proper initial speeds $(\dot{x}_o^*, \dot{y}_o^*, \dot{z}_o^*)$; then at $t = t^*$ it is apparent that eqs. (A.33b) would produce a set of zeros for their terminal values. That is; with proper initial values, at the prescribed time, $t = t^*$, eqs. (A.33b) become:

$$\xi \equiv 0 = \xi_o + (3\xi_o + 2\eta'_o{}^*)\ (1-\cos \varphi_T{}^*) + \xi'_o{}^* \sin \varphi_T{}^*,$$

$$\eta \equiv 0 = \eta_o - 3(2\xi_o + \eta'_o{}^*)\ \varphi_T{}^* - 2\xi'_o{}^*\ (1-\cos \varphi_T{}^*) + 2(3\xi_o + 2\eta'_o{}^*) \sin \varphi_T{}^*,$$

and $$\zeta \equiv 0 = \zeta_o \cos \varphi_T{}^* + \zeta'_o{}^* \sin \varphi_T{}^* \ . \qquad \text{(III. 19)}$$

(A similar condition could be written in terms of the dimensional expressions, from [eqs. (A.29b)]). In reference to the angle of transfer, φ_T, the intercept would occur at $\varphi_T \equiv \varphi_T{}^*$ since, $\varphi_T{}^* \equiv \dot{\varphi}_T t^*$.

By the very nature of eqs. (III. 19) one can consider these expressions as a description of the speed components necessary to achieve intercept, at the time, t*, from a known initial position $(\xi_o,\ \eta_o,\ \zeta_o)$. Thus, solving for the quantities $(\xi'_o{}^*,\ \eta'_o{}^*,\ \zeta'_o{}^*)$ it can be shown that:

$$\xi'_o{}^* = \frac{\xi_o\ (3\varphi_T{}^* \cos \varphi_T{}^* - 4 \sin \varphi_T{}^*) + 2\eta_o\ (1-\cos \varphi_T{}^*)}{8\ (1-\cos \varphi_T{}^*) - 3\varphi_T{}^* \sin \varphi_T{}^*}\ ,$$

$$\eta'_o{}^* = -\ 2\xi_o + \frac{2\xi_o\ (1-\cos \varphi_T\ ) - \eta_o \sin \varphi_T{}^*}{8\ (1-\cos \varphi_T) - 3\varphi_T{}^* \sin \varphi_T{}^*}\ ,$$

and $$\zeta'_o{}^* = -\ \zeta_o \cos \varphi_T{}^*. \qquad \text{(III. 20)}$$

(For reference purposes the corresponding dimensional speeds, necessary to guarantee intercept, are:

$$\frac{\dot{x}_o{}^*}{\dot{\varphi}_T} = \frac{x_o\ (3\dot{\varphi}_T t^* \cos \dot{\varphi}_T t^* - 4 \sin \varphi_T t^*) + 2y_o\ (1-\cos \dot{\varphi}_T t^*)}{8\ (1-\cos \dot{\varphi}_T t^*) - 3\dot{\varphi}_T t^* \sin \dot{\varphi}_T t^*}\ ,$$

$$\frac{\dot{y}_o^*}{\dot{\varphi}_T} = -2x_o + \frac{2x_o\,(1-\cos\dot{\varphi}_T t^*) - y_o \sin\varphi_T^*}{8\,(1-\cos\dot{\varphi}_T t^*) - 3\dot{\varphi}_T t^* \sin\dot{\varphi}_T t^*}\ ,$$

and $$\frac{\dot{z}_o^*}{\dot{\varphi}_T} = -z_o \cos\varphi_T^*\ . \qquad \text{(III. 21)}$$

In retrospect, calculating the speed components required to achieve intercept, using eqs. (III. 21) above, requires a preselected value for the time-to-intercept (t*)--measured from the initial point (x_o, y_o, z_o), where (arbitrary) $t \equiv 0$. Needless to say it would be fortuitous indeed if the interceptor would just happen to have these particular speeds initially. Normally one would expect that some impulsive action would be required to achieve the intercept.

It is visualized that these velocity changes might be provided by means of thrusters (in a real situation); but, at any rate, once these speeds are acquired by the intercepting vehicle, at the prescribed initial point, then intercept will be expected to occur at the selected time, t*. During the ballistic coasting phase (from $t = 0$ to $t = t^*$) the target vehicle would move over a range angle φ_T^* along its circular orbit; while the interceptor moves through a range angle, φ_I^*, to a point of intercept.

There are two limiting cases which should be mentioned here in regard to eqs. (III. 20) [or, eqs. (III. 21)]. First, from a physical point of view, one would surmise that as t* becomes small, values of the intercept speed $(\sim')^*$ should increase without limit, generally. An inspection of the defining expressions would indicate that this is indeed the case.

Secondly, the denominator in eqs. (III. 20) has a singularity at $\varphi_T^* = 2\pi$ (or, when t* = the period of the motion for the target particle, T). Recognizing this fact, it is evident that one should not attempt to describe intercepts corresponding to this condition. Actually, it is not likely that the linear results will be

very accurate for such an extended time lapse. In most cases it is expected that these (linearized) expressions should not be used for transfers beyond (say) half an orbit. Generally speaking, the accuracy of these equations, beyond this level, is degraded to the extent that only quantitative information is produced; also, it is likely that near to $\varphi_T^* = 2\pi$ even the quantitative levels would not be indicative of the real motion.

III. 8. 3 Time history of the intercept maneuver. - Once the time to intercept (t^*) has been selected, and the speeds to achieve intercept have been determined, then a time history of the state of motion--from $t = 0$ to $t = t^*$--can be ascertained. If a plot of the interceptor's track is desired--plotted as relative displacements (ξ, η, ζ), or as the relative motion hodograph (ξ', η', ζ')--then the information needed for such graphs can be obtained from eqs. (III. 19), (III. 20) [or correspondingly, from eqs. (A. 29b), (A. 30b)]. However, for this maneuver the values of $\xi_o'^*, \eta_o'^*, \zeta_o'^*$ $[\dot{x}_o^*, \dot{y}_o^*, \dot{z}_o^*]$ must replace $\xi_o', \eta_o', \zeta_o'$ $[\dot{x}_o, \dot{y}_o, \dot{z}_o]$ in the state prediction equations. As a check on the results obtained in this operation, one should recall that at $t = t^*$ $(\varphi_T = \varphi_T^*)$ the ξ, η, ζ $[x, y, z]$ coordinates should vanish; this would indicate that the intercept has occured. On the other hand, the values of ξ', η', ζ' $[\dot{x}, \dot{y}, \dot{z}]$ do not vanish, necessarily, at intercept. In general these terminal quantities are different from zero, and represent the requirement to be satisfied by the rendezvous aspect of the maneuver; an action to occur at the terminal point itself.

The expressions which define the relative motion are noted to have a same period as the target particle; hence, the idea of small displacements for the interceptor is borne out.

III. 8. 4 The impulse schedule, for intercept and rendezvous. - In the paragraphs above, a method for determining the velocity components needed to effect an intercept was described. As noted there, these speeds are generally not the same as those which the interceptor would have at its initial position in space. As a

consequence of this requirement it is apparent that an action must be taken, by the interceptor, if the maneuver is to occur as desired. That is, a velocity change (relative and/or inertial) must be provided at the initial point; and, specifically, this change must occur so that the intercept will occur at the time prescribed, (in the time $\Delta t \equiv t^* - t_o$).

Presume, for instance, that the interceptor has some known initial velocity $\bar{V}_o$ ($\equiv \frac{d\bar{r}}{dt}$ at $t = 0$); then after determining the required initial velocity $\bar{V}_o{}^*$, a ballistic intercept should occur. Accordingly, the change in (relative) velocity which must be given to the interceptor, at the initial point, is,

$$\delta \bar{V}_o = \bar{V}_o{}^* - \bar{V}_o .$$

It has been stated earlier that all such "actions" will be treated herein as velocity impulses. In this context, then, the dimensionless impulse magnitude needed to bring about the intercept is:

$$\delta \nu_o \equiv \frac{\delta V_o}{V_T} = \sqrt{(\xi'_o{}^* - \xi'_o)^2 + (\eta'_o{}^* - \eta'_o)^2 + (\zeta'_o{}^* - \zeta'_o)^2} \quad . \tag{III.22}$$

At the termination of the maneuver, when the two vehicles are in very close proximity, it is expected that they will have a non-zero relative velocity. Since, at rendezvous, one desires to have the final contact occur at zero velocity, then the "action" which must occur there is one to nullify the terminal relative velocity. Thus, the final impulse which must be applied to the interceptor is

$$\delta \bar{V}_f = - \bar{V}(t^*); \tag{III.23}$$

necessarily this has a magnitude of

$$\delta \nu_f \equiv \frac{\delta V_f}{V_T} = \sqrt{(-\xi')^2 + (-\eta')^2 + (-\zeta')^2} \quad , \tag{III.24}$$

in dimensionless values, obtained at $t = t^*$. In this last expression the velocity components are those obtained from eqs. (III.18) [or eqs. (A.30b)] when t is set to t^* (or $\varphi_T = \varphi_T{}^*$); and, where the initial speed components were the $(\sim')^*$ quantities. (That is, the arbitrary relative initial velocity has been replaced by the corresponding, required intercept value; e.g., $\bar{V}_o \equiv \bar{V}_o{}^*$).

(b) Shell coordinates: The intercept problem, when expressed in shell coordinates is of the same format as that outlined above (in cartesian coordinates) with the obvious exception that the coordinates and the motion equations are altered, accordingly. Due to the sameness which is observed here, only a brief outline of the procedure to be followed will be presented here.

In order to provide discussion variations, the operational procedure which will be described next will be in terms of appropriate dimensionless quantities.

The principal results, needed to satisfy this problem situation, are those noted by eqs. (B.22) in Appendix B; the set (B.22a) being the displacement relations, while the set (B.22b) is the corresponding "speed" expressions.

III.8.5 Conditions necessary for intercept. - With the intercept assumed to occur at a position $\varphi_T \equiv \varphi_T{}^*$ (corresponding to $t = t^*$), then eqs. (B.22a) are rewritten with the initial speeds replaced by the $(\sim')_o{}^*$ quantities--and φ_T specifically set to $\varphi_T{}^*$. Since these are the conditions which produce the intercept; then the relative displacements vanish, at $\varphi_T{}^*$, and the resulting expressions solved to yield the speeds required for intercept, as before.

In this regard, these initial speeds are found to be:

$$\lambda_o{}'^* = \frac{\lambda_o\,(3\varphi_T{}^* \cos\varphi_T{}^* - 4\sin\varphi_T{}^*) + 2\sigma_o\,(1-\cos\varphi_T{}^*)}{8\,(1-\cos\varphi_T{}^*) - 3\varphi_T{}^*\sin\varphi_T{}^*}\ ,$$

and $$\sigma_o'^* = -2\lambda_o + \frac{2\lambda_o\,(1-\cos\varphi_T^*) - \sigma_o \sin\varphi_T^*}{8\,(1-\cos\varphi_T^*) - 3\varphi_T^* \sin\varphi_T^*} \quad . \tag{III.25}$$

Only two speed components appear, here, since this maneuver is constrained to the target's plane of motion.

In passing, it is interesting to compare these results with those found for the problem expressed in cartesian quantities (see eqs. (III.21)). The marked similarity, which is found to exist, should not be wholly unexpected since the procedures followed in both cases were the same, in principle. The implications are that since the linearization procedures are similar then a change in coordinate system has little, if any, influence on the format of the outcome.

III.8.6 Time history of the intercept. - In order to plot the variations in speed and displacement, experienced by the interceptor during its flight along the collision ballistic arc, one can employ eqs. (B.22) using, as initial values, the quantities $(\lambda_o, \sigma_o; \lambda_o'^*, \sigma_o'^*)$ and setting the transfer angle (thus the time) to $\varphi_T = \varphi_T^*$. A graphing of these traces would serve to illustrate how the final ballistic phase of the intercept maneuver occurs.

III.8.7 The impulse schedule. - Once more, assuming that the initial and final relative velocity changes are provided by impulses, then the required values for these--occurring at $t=0$ $(\varphi_T = 0)$ and at $t = t^*$ $(\varphi_T = \varphi_T^*)$--can be ascertained. For a vehicle having known (or given) initial speeds, $(\sim')_o$; and having determined the values necessary for intercept, $\left((\sim')_o\right)$, then the initial (dimensionless) impulse magnitude is

$$\delta\nu_o \left(\equiv \frac{\delta V_o}{\dot{r}_T \dot{\varphi}_T} \right) = \sqrt{(\lambda_o' - \lambda_o')^2 + (\sigma_o'^* - \sigma_o')^2} \quad . \tag{III.26}$$

In describing the final (or rendezvous) impulse one needs to know the interceptor's speed when it reaches the target vehicle; i.e., the speed at $t = t^*$ (i.e., $\varphi_T = \varphi_T{}^*$). These are the speeds to be nullified, thereby insuring a final contact at zero relative velocity. In order to define these terminal speeds one evaluates eqs. (B.22b), using $\varphi_T{}^*$ in place of φ_T, and replacing the initial speeds, $(\sim')_o$, with the intercept values, $\left((\sim')_o\right)$. Consequently, the final impulse, to be applied, is:

$$\delta\nu_f \left(\equiv \frac{\delta V_f}{\dot{r}_T \dot{\varphi}_T} \right) = \sqrt{\lambda' (\varphi_T{}^*)^2 + \sigma' (\varphi_T{}^*)^2} \quad . \tag{III.27}$$

Equations (III.26) and (III.27) describe the impulse schedule needed to provide;(1) the intercept and, (2) the rendezvous for the two point-mass vehicles. In order to give proper physical dimensions to these quantities, the dimensionless parameters should be multiplied by the (constant ratioing) scalar, $(r_T \dot{\varphi}_T)$.

III.9 Problem variations.

(a) Intercept, including a mid-course correction: The problem which has been described and discussed in the foregoing sections was predicated on the concepts of an ideal situation. For a more realistic case, the likelihood of matching the necessary initial speeds, and actually bringing about the intercept and rendezvous with a single pair of impulses, is unlikely. In fact it is more reasonable to assume that a re-evaluation of the entire situation (and possibly another impulsive action) would have to be made at some point along the intercept track in order to successfully complete the intercept and rendezvous maneuver, even within the accuracy of the linearized solution's predictions.

As a means of illustrating these ideas, a word example--which is, itself, somewhat academic--will be used to illustrate a procedure which is suggested for this study. This proposed operation could include one, or more, "mid-course" velocity corrections.

Assume for the moment that a required impulse has been determined and applied; however, presume that the thruster has produced a slightly incorrect acceleration, and that intercept (per se) will not quite occur. Once it has been ascertained that an inaccuracy is apparent, in connection with the maneuver, then a new impulse must be determined, and applied, so that the intercept does occur. In essence, then, the second impulse would be, effectively, a "mid-course correction"; one which does guarantee an ultimate success for the intended maneuver.

Needless to say, there is a distinct possibility that more than one mid-course correction may have to be applied; however, it should be recognized that such a case would be simply an extension of the basic ideas just outlined.

After any mid-course correction has been determined, there will be a whole new set of state conditions which come into play. These are (effectively) the "new initial values" required for the intercept problem. In principle, then, the mid-course values become new initial values, and the resulting problem will have to be solved in the same manner as the ideal case; that dealt with in the foregoing sections.

(b) The power-limited intercept: In the discussions offered above, no consideration has been given to possible constraints which might be placed on the case studies.

From a practical point of view the size of an impulse, needed to accomplish intercept, could easily be beyond the capabilities of a spacecraft's propulsion system. Should this be the case, then it would become necessary to bring about an intercept by, possibly, one or the other of the following schemes; or by some other scheme, entirely.

Consider the following operation: On finding that the required impulse is larger than that which the interceptor can provide, it could be that a waiting period would have to be initiated. A subsequent impulse would be delayed until

the intercept requirement is within the capabilities of the spacecraft. This situation suggests a continual re-evaluation of the intercept requirements, and the application of an impulse (say) just as soon as the vehicle is able to provide that needed. Obviously, it is presupposed that the required impulse will, ultimately, fall within the capability of the interceptor.

Rather than undertake the maneuver, as indicated immediately above, a second possibility exists. Here the procedure would be to go ahead with the flight operation, by (say) applying an impulse, then making (mid-course) correction(s) later in order to complete the intended maneuver. This would be an undertaking to be employed in lieu of the waiting scheme suggested above.

A necessary adjunct to solving any of these problem types would be a high-speed computer. The computational device is essential in view of the impracticality of making the necessary calculations manually.

III.10 Systems evaluations. - Having developed these methods for predicting and describing the intercept and rendezvous problem, the schemes should be tested in order to ascertain their accuracy and to determine their limitations. The essentials to be looked for, in any case, would be how well the methods predict the required impulses and how close the computed intercept can be described by any particular scheme. It is known, a priori, that errors will be incurred, when these ideas are compared with numerically integrated situations; what is not known is how large the subsequent errors might be. Likely there will be differences in the error magnitudes depending on what initial positions are chosen, and on which of the computational schemes one employs.

In order to gain a better insight into the predictability and accuracy of these various methods, various examples should be studied in order to gather this information.

III.11 The small arc intercept approximation. - In the terminal phase of the intercept maneuver the separation distance between vehicles is sufficiently small, nominally, that linearized solutions suffice for prediction purposes. In a like manner, if the intercept is to occur in a short time period (i.e., within a small arc of displacement) then the linearized results must surely hold. The question which logically arises next is whether or not an even less complicated formulation might suffice. Or, in other words, could one obtain useful approximations from, say, the linearized solutions themselves.

To this end, then, a development is described below which leads to an approximation of the "linearized" interceptor impulse requirement. That is, eqs. (III.21) are reduced for a small arc transfer approximation. For this reduction the equations are manipulated to obtain simpler expressions; the method of approach is to expand the various terms in eqs. (III.21) and retain only first order terms representing the transfer angle. These results are listed as follows: Approximation for the impulsive intercept requirement,

(a) in dimensional cartesian variables:

$$\dot{x}_o^* = -\frac{x_o}{t^*} + y_o \dot{\varphi}_T ,$$

$$\dot{y}_o^* = -\frac{y_o}{t^*} - x_o \dot{\varphi}_T ,$$

$$\dot{z}_o^* = -\frac{z_o}{t^*} + z_o \frac{\dot{\varphi}_T^2 t^*}{3} ; \qquad \text{(III.28)}$$

which can be expressed by the equivalent vector expression;

$$\bar{V}_o^* = -\frac{\bar{r}_{r_o}}{t^*} - \bar{\omega} \times \bar{r}_{r_o} + \left(\frac{\bar{\omega} \cdot \bar{r}_{r_o}}{3} \right) \bar{\omega} t^* . \qquad \text{(III.29)}$$

(b) in dimensionless cartesian variables;

$$\xi_o'^* = -\frac{\xi_o}{t^*} + \eta_o ,$$

$$\eta_o'^* = -\frac{\eta_o}{t^*} - \xi_o ,$$

$$\zeta_o'^* = -\frac{\zeta_o}{t^*} + \frac{\zeta_o \varphi_T^*}{3} . \qquad \text{(III. 30)}$$

As for the previous developments, the $(\sim)_o^*$ quantities represent the impulse values required for intercept; $(\sim)_o$ terms are the initial values; and t^* is the time set for the maneuver. In the vector expression the angular velocity $(\bar{\omega})$ is $\bar{\omega} \equiv \dot{\varphi}_T \bar{e}_z$, with $\bar{e}_z$ being the unit vector orthogonal to the target's plane of motion.

In order to assess the validity and accuracy of this approximation, several cases were studied and the approximate results compared with the corresponding numerical evaluations. These comparisons are noted in the following tabulations.

In the table, the eccentricity (ϵ) refers to the interceptor's track; (x_o, y_o) represent the initial relative displacement (as does $\bar{r}_{r_o}$); and φ_T refers to the arc of displacement. The $(\Delta\dot{x}_o^*, \Delta\dot{y}_o^*)$ refer to the difference, in value, between the numerical and approximate results; and, the % error refers to the same differences.

It is interesting to note that this approximation provides excellent results for arcs up to 5^o, for paths with eccentricities in excess of 1/10, for the in-plane maneuver; however, it is expected that this would not produce sizeable changes in the three-dimensional results.

By all appearances it seems that this approximation could be utilized for accurate predictions in the terminal intercept operation.

TABLE III.1

SMALL ARC APPROXIMATION

Initial Values			Calculation Results				Transfer Values		
ecc.	x_o	y_o	$\Delta\dot{x}_o^*$	error	$\Delta\dot{y}_o^*$	error	t*	$\Delta\varphi_T$	r_{r_o}
****	M	M	M/S	%	M/S	%	Sec.	(^{o}, (rad))	(km.)
.002	8.333	-238.75	$-1.22*10^{-4}$	.023	$-3.353*10^{-3}$	.046	$31\frac{1}{3}$	2^o, (.04)	.2414
.002	52.048	-594.361	$-2.134*10^{-3}$	.154	$-1.9202*10^{-2}$	.26	$75\frac{1}{3}$	5^o, (.09)	.5955
.002	207.801	-1170.739	$-1.707*10^{-2}$	.64	$-7.62*10^{-2}$	1.07	$156\frac{3}{4}$	10^o, (.17)	1.1909
.005	-21.031	599.847	$+3.048*10^{-4}$	.025	$7.62*10^{-3}$	.041	$31\frac{1}{2}$	2^o, (.04)	.5955
.005	-131.247	1493.523	$+5.182*10^{-3}$	.16	$4.877*10^{-2}$	.26	$78\frac{2}{3}$	5^o, (.09)	1.497
.005	-523.952	2941.326	$+4.267*10^{-2}$	.64	$1.938*10^{-1}$	1.08	$159\frac{1}{2}$	10^o, (.17)	2.993
.04	8382.017	2729.489	$-2.316*10^{-1}$	.08	$3.322*10^{-2}$	.035	$31\frac{3}{4}$	2^o, (.04)	8.851
.04	20646.3	7935.179	-1.372	.54	$2.134*10^{-1}$	.17	$79\frac{1}{2}$	5^o, (.09)	22.128
.04	40162.67	19492.304	-5.364	2.3	$9.144*10^{-1}$	.55	$159\frac{1}{2}$	10^o, (.18)	44.659

TABLE III.1 (concluded)

SMALL ARC APPROXIMATION

Initial Values			Calculation Results				Transfer Values		
ecc.	x_o	y_o	$\Delta\dot{x}_o^*$	error	$\Delta\dot{y}_o^*$	error	t*	$\Delta\varphi_T$	r_{r_o}
****	M	M	M/S	%	M/S	%	sec.	(^{o}, (rad))	(km.)
0.1	21656.39	7017.42	$-5.791*10^{-1}$	.08	$9.144*10^{-2}$	.035	$32\frac{1}{3}$	2^o, (.04)	22.692
0.1	53481.53	20536.86	-3.688	.57	$5.486*10^{-1}$	.18	$80\frac{1}{2}$	5^o, (.09)	57.293
0.1	104430.48	50968.76	-14.204	2.4	2.377	.55	$163\frac{1}{2}$	10^o, (.17)	116.195
0.2	45871.58	14737.41	-1.25	.09	$2.012*10^{-1}$	.04	$33\frac{1}{3}$	2^o, (.04)	48.28
0.2	113821.08	43656.9	-8.23	.62	1.219	.18	84	5^o, (.09)	121.99
0.2	223806.86	110414.33	-39.014	3.2	1.219	.13	171	11^o, (.19)	249.45

LINEAR THEORY, SECOND ORDER CORRECTION

IV.1 Introduction. - In general, the basic mathematical tools used to solve relative motion problems are results from linearized theory. These analytical expressions have been used to predict the state of a relative motion; to describe the motion in geometric form; and, to provide a basis for guidance and control formulations, among other uses.

In previous sections of this report these equations have been manipulated for special purposes, such as describing intercept and rendezvous estimations, for both long and short time durations, as well as other studies. Throughout, in these various utilizations, the restrictions due to the linearization have been a constraining factor. Constraining in the sense that limited (though not in every case, predictable) accuracy has been the consequence of this simplification.

In this section, a formulation is described which, in part, reduces the effects of this constraint. Here, a second order correction to the linear theory is provided; this is a correction which enhances the accuracy of the analytical results and extends its range of applicability.

IV.2 Second order formulation. - An evaluation of these second order corrections has been carried out in Appendix E. There the method of approach was described, and the resulting analytical expressions were set down. It would be redundant to do more than note the procedure and list the basic results in this section. Consequently, the statements in the following paragraphs will summarize the material in that appendix, and, will note some general aspects of test examples which have been studied.

The differential equations describing the relative motion were given in Appendix A, symbolically, as eq. (A.5). The reduction of that general formula came about through an expansion of the gravity term; and in that appendix only first order quantities, in the dependent variables, were retained. Carrying this same procedure to second order, the differential equations (in dimensionless

variables), are those given as eqs. (E.6), Appendix E.

In order to obtain a system of equations which could be solved readily, the dependent variables were presumed to be expressible as a series of ordered quantities. Each succeeding factor in the sum to be of higher order than the preceding one. Also, the multiplicity of factors was assumed to constitute terms of corresponding order of magnitude. In this regard, a product of two first-order terms was presumed to form a factor of second order, and so on.

When governing equations were separated, according to order of magnitude, it was apparent that the linearized solutions (from first order quantities) became the driving functions for the set of second order equations. Consequently, one achieves a scheme suggesting a simple method (in concept) for acquiring higher order solutions. Equations (E.9) display the system of expressions which were solved to form the second order corrections.

Since the linearized results (see eq. (E.10)) included general initial values, the second order terms were set to zero, initially. Subsequently, a second order solution was formed as the sum of a first order solution plus the second order correction; this is indicated in Section E.7, Appendix E. In general, the second order corrections are composed of constants, secular terms and harmonic quantities. The coefficients of the variants (here) are made up of constants (initial term); while the harmonic functions have single and double frequency (this is in contrast to the linear solutions where all such terms had the same periodicity).

It should be recalled that the linearized solution had no coupling between the in-plane and normal (out-of-plane) components. As a consequence these two parts of the solution were acquired independently. For the second order corrections a coupling between solution parts was found to exist. However, this occurred through the driving functions rather than through the kinematic or dynamic parts of the expressions. This circumstance allowed the in- and out-of-plane solutions to be handled separately, also. In addition to this, it is seen that if one selects the

initial conditions appropriately, it is possible to keep some separability in the second order solution. (A study of the coefficients will point to the proper selection which would produce this result). A consequence of these conditions is that (as suspected) the second order solution is not "complete", hence, the analytic results thus far acquired will, at best, only improve the accuracy and predictability for a given problem. Ultimately this solution will diverge in somewhat the same manner as did the linearized one.

IV.3 Second order correction formulae. - The formulas obtained as the second order corrections are given as eqs. (E.31, E.32), Appendix E. These dimensionless quantities are listed below, for reference and convenience:

(a) dimensionless cartesian coordinates (displacements);

$$\xi_2 = K_6 + (K_7 + K_8\varphi_T)\varphi_T + (\mathcal{C}_5 + K_9\varphi_T)\sin\varphi_T + (\mathcal{C}_6 + K_{10}\varphi_T)\cos\varphi_T + K_{11}\sin 2\varphi_T + K_{12}\cos 2\varphi_T ,$$

$$\eta_2 = K_{\eta\eta} + K_{13}\varphi_T + (K_{14} + K_{18}\varphi_T)\sin\varphi_T + (K_{15} + K_{19}\varphi_T)\cos\varphi_T + K_{16}\sin 2\varphi_T + K_{17}\cos 2\varphi_T,$$

$$\zeta_2 = K_1 + (\mathcal{C}_3 + K_4\varphi_T)\sin\varphi_T + (\mathcal{C}_4 + K_5\varphi_T)\cos\varphi_T + K_2\sin 2\varphi_T + K_3\cos 2\varphi_T; \qquad \text{(IV.1)}$$

(b) dimensionless cartesian speed components;

$$\xi_2' = K_7 + 2K_8\varphi_T + (K_9 - \mathcal{C}_6 - K_{10}\varphi_T)\sin\varphi_T + (K_{10} + \mathcal{C}_5 + K_9\varphi_T)\cos\varphi_T + 2(K_{11}\cos 2\varphi_T - K_{12}\sin 2\varphi_T) ,$$

$$\eta_2' = K_{13} + (K_{18} - K_{15} - K_{19}\,\varphi_T)\sin\varphi_T + (K_{14} + K_{19} + K_{18}\,\varphi_T)\cos\varphi_T$$

$$+ 2(K_{16}\cos 2\varphi_T - K_{17}\sin 2\varphi_T),$$

and

$$\zeta_2' = (K_4 - \mathcal{C}_4 - K_5\,\varphi_T)\sin\varphi_T + (K_5 + \mathcal{C}_3 + K_4\,\varphi_T)\cos\varphi_T + 2(K_2\cos 2\varphi_T$$

$$- K_3\sin 2\varphi_T)\,. \qquad \text{(IV.2)}$$

The various constants displayed in the expressions above are listed below in a more compact form than that shown in Appendix E. Suitable substitutions should verify the compatibility between sets. (In this listing all $(\sim)_o$ quantities are initial values; and, $A \equiv 3\xi_o + 2\eta_o'$, $B \equiv 2\xi_o + \eta_o'$).

$$K_1 = \frac{3}{2}(\xi_o'\,\zeta_o' - \zeta_o A)\,, \qquad K_2 = \frac{1}{2}(\zeta_o' A - \zeta_o\,\xi_o')\,, \qquad K_3 = \frac{1}{2}(\zeta_o A + \xi_o'\zeta_o')\,,$$

$$K_4 = 3\zeta_o B\,, \qquad K_5 = -3\zeta_o' B\,,$$

$$K_6 = 3\left\{\xi_o A + \eta_o' B + \frac{1}{2}\left[\xi_o^2 + \eta_o^2 - \xi_o'^2 + \frac{1}{2}(\zeta_o^2 + \zeta_o'^2)\right]\right\}\,, \quad K_7 = 3(\eta_o - 2\xi_o')\,B\,,$$

$$K_8 = -\frac{9}{2}B^2, \qquad K_9 = 3AB\,, \qquad K_{10} = 3\xi_o' B\,,$$

$$K_{11} = -(\xi_o' A + \frac{1}{2}\zeta_o\zeta_o')\,, \qquad K_{12} = \frac{1}{2}\left[A^2 - \xi_o'^2 - \frac{1}{2}(\zeta_o^2 - \zeta_o'^2)\right]\,,$$

$$K_{13} = -3\left[AB + \frac{1}{2}(\xi_o'^2 - \xi_o^2 + \zeta_o^2 + \zeta_o'^2) + \eta_o(\eta_o - \xi_o')\right]\,,$$

$$K_{14} = 2\left[A^2 + B^2 + 2\xi_o(\xi_o + \eta_o')\right] + 3\eta_o(\eta_o - \xi_o') + 2\xi_o'^2 + \zeta_o^2 + 2\zeta_o'^2\,,$$

$$K_{15} = \xi_o' A + 3\xi_o (\xi_o' - \eta_o') + 2\zeta_o \zeta_o' , \qquad K_{16} = \frac{1}{2} K_{12} + \frac{3}{8} (\zeta_o^2 - \zeta_o'^2) ,$$

$$K_{17} = -\frac{1}{2} (K_{11} + \frac{3}{2} \zeta_o \zeta_o') , \qquad K_{18} = 3\xi_o' B \ (=K_{10}), \qquad K_{19} = -3AB \ (=-K_9),$$

$$K_{\eta\eta} = -(K_{10} - K_{17} + \frac{1}{2} K_{15}), \qquad \phi_3 = \zeta_o' (B + \xi_o) + \xi_o' \zeta_o ,$$

$$\phi_4 = \zeta_o A - 2\xi_o' \zeta_o', \qquad \phi_5 = -(K_7 + K_{10} + 2K_{11}) \quad \phi_6 = -(K_6 + K_{12}). \qquad \text{(IV.3)}$$

(here, as before, the $(\sim)'$ terms represent derivatives with respect to the position angle, φ_T).

When dimensional quantities are desired, from the second order solutions, the procedure is the same as that noted previously. That is, if the transforms (see eqs. (A.31), (A.32), Appendix A) are applied, the desired dimensional quantities are obtained.

It is quite evident that the rather complicated format of these second order correction terms makes it difficult to describe a general geometric figure for these expressions. For this reason, no attempt will be made to do so at this time. Necessarily, these correction equations are of little value alone; they must be added to the linearized result in order to provide meaningful information. Though it is not immediately apparent, from viewing the equations above, the values which they yield (in an example) are small, initially. They do not contribute much to the solution until the problem has moved significantly from the initial state. Many of the terms are oscillatory in makeup, with single or double frequency; the secular parts of the solution are largely coupled with harmonics so that their contributions to the results are not simply described.

The constants noted here (K_j, $\mathcal{C}_i$) are <u>all</u> dependent on the initial state; hence, any solution (here) is markedly influenced by initial conditions.* This fact has been demonstrated, by examples, wherein it was found that not all initial values provided like degrees of accuracies as the solutions progressed. Some combinations of initial values produced "better answers" than others; and not all second order answers were as predictable as the linear results in some (near-to-the-origin) regions of the solution. (These statements are based on differences between the analytic predictions and numerical evaluations.)

Due to the labor involved in computing the terms needed in an evaluation of the second order solutions, a computer program has been developed to perform the required calculations. This program can compute the linear and second order solutions, simultaneously and separately; hence, the capability of comparing these solution types for a variety of inputs.

IV.4 <u>Comments.</u> - The analysis discussed in the foregoing discussions allows one to perform many of the more general relative motion calculations with the assurance of greater accuracy and predictability. As a basic guide, the second order solutions will normally maintain accuracy to within a few percent for as much as two orbital periods ($\varphi_T \cong 4\pi$). Beyond this range the state predictions become degraded even though the trends are maintained for a longer interval in the primary variable. (This is in contrast to the loss suffered by linear results in approximately half an orbit). It is difficult to be more explicit concerning accuracy and applicability, at this time, due to the variety of initial value conditioned problems which could be studied under the second order solutions formulation.

Rather than become involved in the labor of extending this method, for increased accuracy and predictability, it has become evident that the numerical approach would be a more useful extension. For this reason the analytical methods have not been pursued beyond the present level of effort in this report.

*Necessarily these constants involve quadratics in the initial state variables.

RELATIVE MOTION FOR A THRUSTING PARTICLE

V.1 Relative motion for a thrusting vehicle. - In this section a study of the relative motion for a thrusting vehicle, represented by a mass particle, is undertaken. In the investigation, the bodies are assumed to maneuver so that one particle has its motion referred to the reference particle moving on a circular orbit. The pertinent mathematical developments for this problem are found in Appendix D.

For mathematical tractability the thrust is assumed to have a fixed magnitude, hence the problem can be linearized and, consequently, it has an analytical solution. The resulting relative motion state equations are examined, here, as several example types; each of these is described and discussed.

V.2.1 General motion equations. - In Appendix D, where expressions for the state variables were obtained, the various equations are presented in both dimensional (x, y, z, $\dot{x}$, $\dot{y}$, $\dot{z}$) and dimensionless (ξ, η, ζ, ξ', η', ζ') form. The purpose of this is to provide the reader with a choice of expressions, for his use, when investigating various problem types. Of course, the dimensionless expressions have a more general utility in that they are easier to visualize, and to apply, for a variety of physical situations. This does not imply that the dimensional equations are more restricted - compared to the dimensionless ones - rather, that the dimensional ones are more cumbersome in notation. It should be borne in mind that both sets of equations are constrained, in applicability, by the linearization which has been imposed. As a consequence, this analysis should provide "good" results in the near neighborhood of the origin, with divergence to be expected as one moves into regions more removed from that reference point.

With these various constraints placed on the formulation, one is able to obtain analytic expressions for the state of the motion. The results, listed below, are markedly akin to those developed in Appendix A (where the thrust terms were deleted). Here, the equations are expressed in terms of the independent

variable ($\dot{\varphi}_T t$) and constants (initial values plus the specific thrust magnitudes). It should be noted that the present solution has been obtained as an initial value problem. It has been subjected to a linearization of the differential equations of motion, and to the other restrictions noted above. For a more comprehensive discussion of the constraints and the methodology employed, here, the reader should consult the various appendices.

The state equations which are listed below include both forms (dimensional and dimensionless) for comparison purposes. The two types will be presented together; however, in some instances discussions will point to one type, then another. This approach does not imply any particular significance; actually both equation forms are identical, they differ only by the constants introduced in the non-dimensionalization.

V.2.2 Dimensional forms. - The dimensional equations of state for the relative motion of a thrusting particle, obtained in Appendix D, are;

(a) for the displacements;

$$x = x_o + \frac{\dot{x}_o}{\dot{\varphi}_T}(\dot{\varphi}_T t) - \left[A\,(\dot{\varphi}_T t - \sin \dot{\varphi}_T t) + B\,(1-\cos \dot{\varphi}_T t)\right],$$

$$y = y_o + \left[\frac{\dot{y}_o}{\dot{\varphi}_T} - \frac{3}{2}\,\frac{T_y}{\dot{\varphi}_T^{\,2}}\,(\dot{\varphi}_T t)\right]\dot{\varphi}_T t + 2\left[B\,(\dot{\varphi}_T t - \sin \dot{\varphi}_T t) - A\,(1-\cos \dot{\varphi}_T t)\right],$$

and $$z = z_o \cos \dot{\varphi}_T t + \frac{\dot{z}_o}{\dot{\varphi}_T} \sin \dot{\varphi}_T t + \frac{T_z}{\dot{\varphi}_T^{\,2}}\,(1-\cos \dot{\varphi}_T t);$$

(b) for the relative speeds;

$$\frac{\dot{x}}{\dot{\varphi}_T} = \frac{\dot{x}_o}{\dot{\varphi}_T} - \left[A\,(1-\cos \dot{\varphi}_T t) + B \sin \dot{\varphi}_T t\right],$$

$$\frac{\dot{y}}{\dot{\varphi}_T} = \frac{\dot{y}_o}{\dot{\varphi}_T} - \left(2\,\frac{\dot{x}_o}{\dot{\varphi}_T} - \frac{T_y}{\dot{\varphi}_T^{\,2}}\right)\dot{\varphi}_T t + 2\left[B\,(1-\cos\dot{\varphi}_T t) + A\,(\dot{\varphi}_T - \sin\dot{\varphi}_T t)\right],$$

and $$\frac{\dot{z}}{\dot{\varphi}_T} = \frac{\dot{z}_o}{\dot{\varphi}_T}\cos\dot{\varphi}_T t + \left(\frac{T_z}{\dot{\varphi}_T^{\,2}} - z_o\right)\sin\dot{\varphi}_T t\ ;$$

wherein

$$A \equiv \left(\frac{\dot{x}_o}{\dot{\varphi}_T} - 2\,\frac{T_y}{\dot{\varphi}_T^{\,2}}\right), \text{ and } B \equiv -\left(3x_o + 2\,\frac{\dot{y}_o}{\dot{\varphi}_T} + \frac{T_x}{\dot{\varphi}_T^{\,2}}\right).$$

Here, the $(\sim)_o$ quantities are initial values, and the $T_j \left(=\frac{F_j}{m_I}, (j = x, y, z)\right)$ are the specific thrust components.

V.2.3 Dimensionless forms. - The corresponding dimensionless expressions, similar to the above equations, are:

(a) for the displacement coordinates:

$$\xi = \xi_o + \xi'_o\,\varphi_T - \left[A_o\,(\varphi_T - \sin\varphi_T) + B_o\,(1-\cos\varphi_T)\right],$$

$$\eta = \eta_o + (\eta'_o - \tfrac{3}{2}\,\tau_\eta\varphi_T)\,\varphi_T + 2\left[B_o\,(\varphi_T - \sin\varphi_T) - A_o\,(1-\cos\varphi_T)\right],$$

and $$\zeta = \zeta_o\cos\varphi_T + \zeta'_o\sin\varphi_T + \tau_\zeta\,(1-\cos\varphi_T)\ ;$$

(b) for the speed components:

$$\xi' = \xi'_o - \left[A_o\,(1-\cos\varphi_T) + B_o\sin\varphi_T\right],$$

$$\eta' = \eta'_o - (2\xi'_o - \tau_\eta)\,\varphi_T + 2\left[B_o\,(1-\cos\varphi_T) + A_o\,(\varphi_T - \sin\varphi_T)\right],$$

and $\zeta' = \zeta'_o \cos \varphi_T + (\tau_\zeta - \zeta_o) \sin \varphi_T$;

wherein

$$A_o \equiv (\xi'_o - 2\tau_\eta), \quad B_o \equiv -(3\xi_o + 2\eta'_o + \tau_\xi).$$

In these last expressions the independent variable (φ_T), and the dimensionless dependent variables $(\xi, \eta, \zeta; \xi', \eta', \zeta')$ are defined by:

$$\varphi_T \equiv \dot{\varphi}_T t; \quad \xi \equiv \frac{x}{r_T}, \quad \eta \equiv \frac{y}{r_T}, \quad \zeta \equiv \frac{z}{r_T}; \quad \xi' \equiv \frac{d\left(\frac{x}{r_T}\right)}{\dot{\varphi}_T\, dt} = \frac{d}{d\varphi_T}\left(\frac{x}{r_T}\right), \text{ etc.}$$

Here, r_T, $\dot{\varphi}_T$ are constants for the circular orbit of m_T. In a similar manner the dimensionless thrust parameters are defined by,

$$\tau_j \equiv \frac{T_j}{r_T \dot{\varphi}_T^2}, \quad (j = \xi, \eta, \zeta).$$

These notations are explained in Appendices A and D.

V.3 Application. - Using the equations above, one can predict the relative state of motion for the particle, m_I, as it moves in the vicinity of m_T under the added influence of a fixed thrust. Of course the predictability, here, is understood to mean, 'in a linear sense'. As noted earlier, these stated results may be used to obtain relative motion traces in either (or both) the displacement or velocity spaces. Also, these quantities may be used, directly, to acquire range and range-rate data for a thrusting particle.

It should be apparent that these expressions have applicability to a variety of examples. For instance, using the τ_η component, only, in the ξ, η, and ξ', η' expressions, one could simulate the "influences" of atmospheric drag on a "maneuvering particle". Also, since τ_ξ is in the radial direction, it could be

introduced to simulate the effect of radiation pressure, as a driving force, for (say) a solar-sailing vehicle. Needless to say other simulation could be devised by an imaginative reader.

In the following paragraphs some specific applications of the above results will be noted and commented upon. Generally, these selections have been somewhat arbitrary; however, they have been singled out for the particular purpose to which they are applied.

V.4.1 The intercept problem for constant thrusting action. - As a first example to be considered, here, the problem of intercept, with fixed thrusting, will be examined. The conditions which govern the intercept are similar to those noted previously; that is, the thrusting particle (m_I) is attempting to reach the reference particle (m_T) in a specified time $(t = t^*)$. In this regard the problem here is akin to the impulsive intercept studied earlier; and, in particular, the requirements for intercept are the same as noted there.

In order to ascertain the "level of thrust" needed to achieve the intercept, one may view the situation as follows:

In a time, t^*, the two particles are to have their separation distance reduced to zero. This requirement is influenced by the initial state $(x, y, z; \dot{x}, \dot{y}, \dot{z})_o$ and the (yet to be determined) thrust level(s), T_j. In the next paragraph a scheme to determine the needed thrust will be explained.

V.4.2 The required thrust. - It should be apparent that for a given state of motion the thrust can be ascertained by setting the relative displacements to zero, at the intercept time (t^*), and solving for the unknown (T_j) parameters.

This mathematical operation has been carried out in Appendix D, consequently, it will not be repeated here. For convenience, however, the required "thrust components to provide intercept" are noted below.

(a) Dimensional form (see eqs. (D.14)):

$$\frac{T^*_x}{(\dot{\varphi}_T)^2}\,\Delta = x_o\left[24\,(\dot{\varphi}_T t^*)\sin\dot{\varphi}_T t^* - 3(\dot{\varphi}_T t^*)^2\,(2+\frac{3}{2}\cos\dot{\varphi}_T t^*) - 28(1-\cos\dot{\varphi}_T t^*)\right]$$

$$+ 2y_o\left[\dot{\varphi}_T t^* - \sin\dot{\varphi}_T t^*\right] + \frac{\dot{x}_o}{\dot{\varphi}_T}\left[\frac{3}{2}\,(\dot{\varphi}_T t^*) - 4(1-\cos\dot{\varphi}_T t^*)\right](\dot{\varphi}_T t^*)$$

$$+\frac{\dot{y}_o}{\dot{\varphi}_T}\left[14\,(\dot{\varphi}_T t^*)\sin\dot{\varphi}_T t^* - 3(\dot{\varphi}_T t^*)^2\,(1+\cos\dot{\varphi}_T t^*) - 16(1-\cos\dot{\varphi}_T t^*)\right],$$

$$\frac{T^*_y}{(\dot{\varphi}_T)^2}\,\Delta = \left[\left(4\,\frac{\dot{x}_o}{\dot{\varphi}_T} - \frac{\dot{y}_o}{\dot{\varphi}_T}\,(\dot{\varphi}_T t^*) - y_o\right)(1-\cos\dot{\varphi}_T t^*)\right] - 2\left[x_o\,(\dot{\varphi}_T t^* - \sin\dot{\varphi}_T t)\right.$$

$$\left. + \frac{\dot{x}_o}{\dot{\varphi}_T}\,(\dot{\varphi}_T t^*)\sin\dot{\varphi}_T t^*\right],$$

and

$$\frac{T^*_z}{(\dot{\varphi}_T)^2} = -\frac{\frac{\dot{z}_o}{\dot{\varphi}_T}\sin\dot{\varphi}_T t^* + z_o\cos\dot{\varphi}_T t^*}{1-\cos\dot{\varphi}_T t^*}\;; \qquad \text{(V.1)}$$

with,

$$\Delta = 8\left[1-\cos\dot{\varphi}_T t^* - (\dot{\varphi}_T t^*)\sin\dot{\varphi}_T t^*\right] + \frac{(\dot{\varphi}_T t^*)^2}{2}\left[5+3\cos\dot{\varphi}_T t^*\right].$$

(b) Dimensionless forms (see eqs. (D.15)):

$$\tau^*_\xi \Delta = \xi_o \left[24\varphi^*_T \sin\varphi^*_T - 3(\varphi^*_T)^2 (2 + \frac{3}{2}\cos\varphi^*_T) - 28(1-\cos\varphi^*_T)\right]$$

$$+ 2\eta_o\left[\varphi^*_T - \sin\varphi^*_T\right] + (\xi'_o)\left[\frac{3}{2}\varphi^*_T \sin\varphi^*_T - 4(1-\cos\varphi^*_T)\right]\varphi^*_T$$

$$+ (\eta'_o)\left[14\,\varphi^*_T \sin\varphi^*_T - 3(\varphi^*_T)^2 (1+\cos\varphi^*_T) - 16\,(1-\cos\varphi^*_T)\right],$$

$$\tau^*_\eta \Delta = \left[(4\xi'_o - \eta'_o\varphi^*_T - \eta_o)(1-\cos\varphi^*_T)\right] - 2\left[\xi_o\,(\varphi^*_T - \sin\varphi^*_T) + \xi'_o\varphi^*_T \sin\varphi^*_T\right],$$

and

$$\tau^*_\zeta = -\frac{\zeta'_o \sin\varphi^*_T + \zeta_o \cos\varphi^*_T}{1-\cos\varphi^*_T}\,; \qquad \text{(V.2)}$$

with

$$\Delta = 8\left[1-\cos\varphi^*_T - \varphi^*_T \sin\varphi^*_T\right] + \frac{(\varphi^*_T)^2}{2}\left[5 + 3\cos\varphi^*_T\right].$$

V.4.3 State predictions. - Having determined the thrust magnitudes needed for an intercept, a trace of the motion's state can be obtained, for the intercept track, from the initial point to the contact position.

In order to predict the displacements during this maneuver, one can apply the expressions for (say) (ξ, η, ζ) - (see eqs. (D.10) wherein the τ_j values are replaced by the τ^*_j parameters determined above. Similarly, the speeds along the intercept path are obtained using eqs. (D.10b), for the time (or position) range, 0 to t*, (corresponding to a displacement φ^*_T)).

These predictions should give $\xi = \eta = \zeta = 0$, at intercept; however, the corresponding values for ξ', η', ζ' are not zero, there, generally. Of course, the applicability of these results to a "real case" is restricted due to the linearization used in obtaining the analytical results. Unfortunately, there is no real,

quick means of determining the errors in these predictions since the scheme used here has required the displacements to vanish, as an a priori condition. If one is to ascertain the level of error in this analysis, it would be necessary to (say) numerically integrate the problem, for intercept, using identical inputs, and determine the "miss distance" which occurs. Of course, a "true solution" to the intercept may be had by iteratively correcting the thrusts (τ_j^*). It should be mentioned that one such scheme has been employed in this work to provide the "true" values of τ_j^* needed to produce an intercept; this will be commented upon subsequently.

V.5.1 Ejected particles, with thrusting. - The next example of a thrusting particle to be discussed, is concerned with the prediction and description of motion for particles "ejected" from m_T.

Assuming that the powered bodies move away from the parent particle under no (added) influence other than thrust, then the corresponding (dimensionless) state expressions are, from eqs. (D.10):

(a) Displacements:

$$\xi = 2\tau_\eta (\varphi_T - \sin\varphi_T) + \tau_\xi (1-\cos\varphi_T),$$

$$\eta = 4\tau_\eta (1-\cos\varphi_T - \frac{3}{4}\varphi_T^2) - 2\tau_\xi (\varphi_T - \sin\varphi_T),$$

and

$$\zeta = \tau_\zeta (1-\cos\varphi_T); \qquad \text{(V.3a)}$$

(b) Speeds:

$$\xi' = 2\tau_\eta (1-\cos\varphi_T) + \tau_\xi \sin\varphi_T ,$$

$$\eta' = -2\left[2\tau_\eta (\frac{3}{4}\varphi_T - \sin\varphi_T) + \tau_\xi (1-\cos\varphi_T)\right],$$

and

$$\zeta' = \tau_\zeta \sin\varphi_T . \qquad \text{(V.3b)}$$

From these results it is evident that the τ_ζ-thrust component does not influence motion in the (ξ, η)-plane, and vice versa. (This is, of course, a consequence of the linearization introduced in the analytical development). Also, one should note that the in-plane (ξ, η) motions are subjected to trigonometric and secular variations - produced by the thrusting action. As an aid to a better understanding of these trace geometries, several typical cases will be described (below). Also, the traces are included here to clarify the word descriptions.

Due to the composition of the expressions, above, it is trivial to consider cases wherein $\tau_\xi = \tau_\eta = 0$, $\tau_\zeta \neq 0$; consequently, the τ_ζ influence on the motion will be discussed in combination with one (or both) of the other components, only.

The typical cases, mentioned above, are discussed in the following paragraphs.

V.5.2 In-plane motion, for $\tau_\xi \neq 0$. - For this case the displacements are obtained from the coordinate relations:

$$\xi = \tau_\xi (1-\cos \varphi_T),$$

$$\eta = 2\tau_\xi (\sin \varphi_T - \varphi_T) \; ; \tag{V.4a}$$

while the hodograph for this motion is described by:

$$\xi' = \tau_\xi \sin \varphi_T \; ,$$

$$\eta' = -\, 2\tau_\xi (1-\cos \varphi_T). \tag{V.4b}$$

Neglecting, for the moment, the secular part of eqs. (V.4a) it is apparent that the (ξ, η) trace is a (one-to-two) ellipse, described by,

$$\left(\frac{\xi - \tau_\xi}{\tau_\xi}\right)^2 + \left(\frac{\eta}{2\tau_\xi}\right)^2 = 1. \qquad \text{(V.5a)}$$

The figure has a displaced origin located at $((\xi, \eta)_c = (\tau_\xi, 0))$. The effect produced by the secular term is such that the ellipse has a continual "drift" in the η-direction*. The drift rate (here) is: $|\eta|_{drift} = 2|\tau_\xi|$. It should be evident that the thrusting particle has its motion confined to that region "outside" of the m_T-particle's circle, touching the circle once each orbit, if $\tau_\xi > 0$. The particle moves from outside to inside the target's circle, if $\tau_\xi < 0$; also, the drift is "ahead" of m_T (in this case).

The figure traced on the hodograph plane is an ellipse, whose axes have a one-to-two ratio; but, whose center is displaced to $((\xi', \eta')_c = (0, -2\tau_\xi))$. The parametric expression for this (non-drifting) ellipse is:

$$\left(\frac{\xi'}{\tau_\xi}\right)^2 + \left(\frac{\eta' + 2\tau_\xi}{2\tau_\xi}\right)^2 = 1. \qquad \text{(V.5b)}$$

(Typical traces, on the two representative planes, for an unscaled τ_ξ (=1.0) are shown on Fig. V.1. The direction of traverse on the hodograph would be reversed if sgn (τ_ξ) was changed).

V.5.3 In-plane motion, for $\tau_\eta \neq 0$. - When τ_η is the only thrust component allowed, the motion traces are obtained from an appropriately reduced set of equations; reduced from eqs. (V.3).

Neglecting the secular terms, again, it can be seen that, basically, the displacement trace geometry is a one-to-two ellipse, centered not at the origin. Also, this ellipse is drifting in both the ξ- and η-directions. Specifically, the drift rate, in ξ, is a fixed value $(\sim\tau_\eta)$; but the figure is moving due to an acceleration in the η-direction. This leads to a trace which has, for $\tau_\eta > 0$, an "outward" drift coupled with an incrementing displacement aft of m_T. The trace appears as an oscillation superposed onto an almost parabolic figure.

*The trace on the displacement plane, for unscaled τ_j values (i.e. $\tau_\xi = 1$), produces a cycloid. This figure can be generated by the moving ellipse if the drift rate is correct.

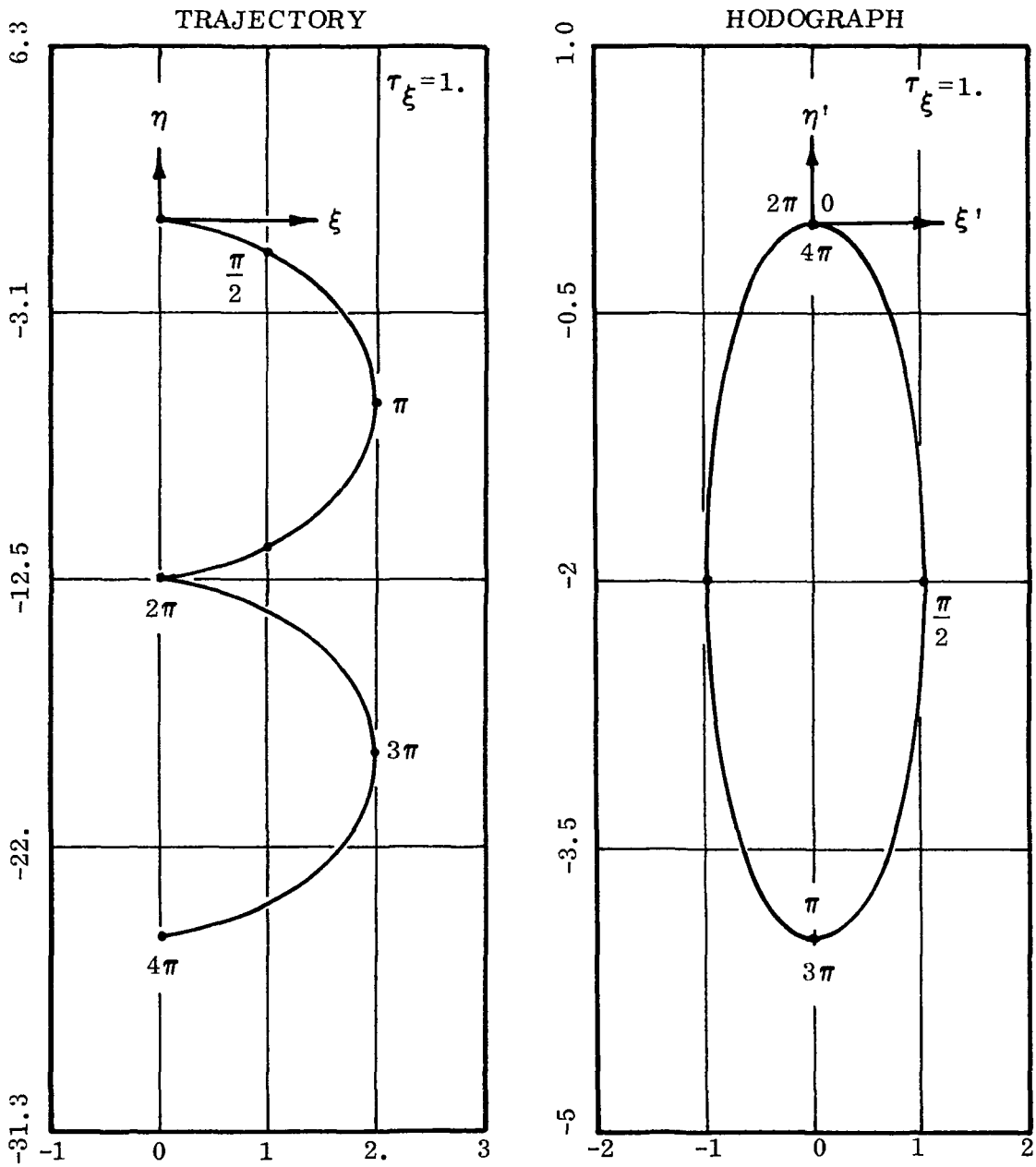

Fig. V.1. Relative Motion Traces, TRAJECTORY and HODOGRAPH, for a Particle (I) due to Constant Thrusting Action, (τ_ξ). Motions Originate at Particle T, with Initial Values (ξ, η, $\zeta = 0$; ξ', η', $\zeta' = 0$).

The hodograph, for this motion, can be visualized as a drifting ellipse, having a one-to-two ratio of axes, and a displaced origin*. A parametric expression for the ellipse is given by,

$$\left(\frac{\xi'-2\tau_\eta}{2\tau_\eta}\right)^2 + \left(\frac{\eta'}{4\tau_\eta}\right)^2 = 1. \qquad \text{(V.6)}$$

For this trace, $\xi' > 0$ if $\tau_\eta > 0$, while η' may begin as a positive value, but rapidly becomes negative. (Typical traces for an unscaled τ_η (=1) are found on Fig. V.2).

Before leaving this example case it would be worth while to point out that this case, and the preceding one, constitute a basis for in-plane powered motion. A combination of thrusts (τ_ξ, τ_η) would necessarily lead to a combination of geometries descriptive of the motions. In the next section, the combined thrust case is described.

V.5.4 <u>In-plane motion, for $\tau_\xi \neq 0$, $\tau_\eta \neq 0$.</u> - The displacement and hodograph traces, here, are produced by combining both of the foregoing cases. Geometrically the composite diagrams are quite similar, in shape, to those obtained in the problem immediately above.

For the situation here the displacement trace has secular terms which imply a moving, basic geometric figure. If the secular parts are ignored, it is found that this basic trace is an ellipse (axes in a one-to-two ratio) with the origin drifting in the ξ-direction and accelerating along η.

The parametric equation for the ellipse is,

$$\frac{(\xi-\tau_\xi)^2}{(\tau_\xi^2+4\tau_\eta^2)} + \frac{(\eta-4\tau_\eta)^2}{4(\tau_\xi^2+4\tau_\eta^2)} = 1; \qquad \text{(V.7a)}$$

*The "drifting ellipse" is more properly described as a prolate cycloid traced onto the (ξ', η')-plane.

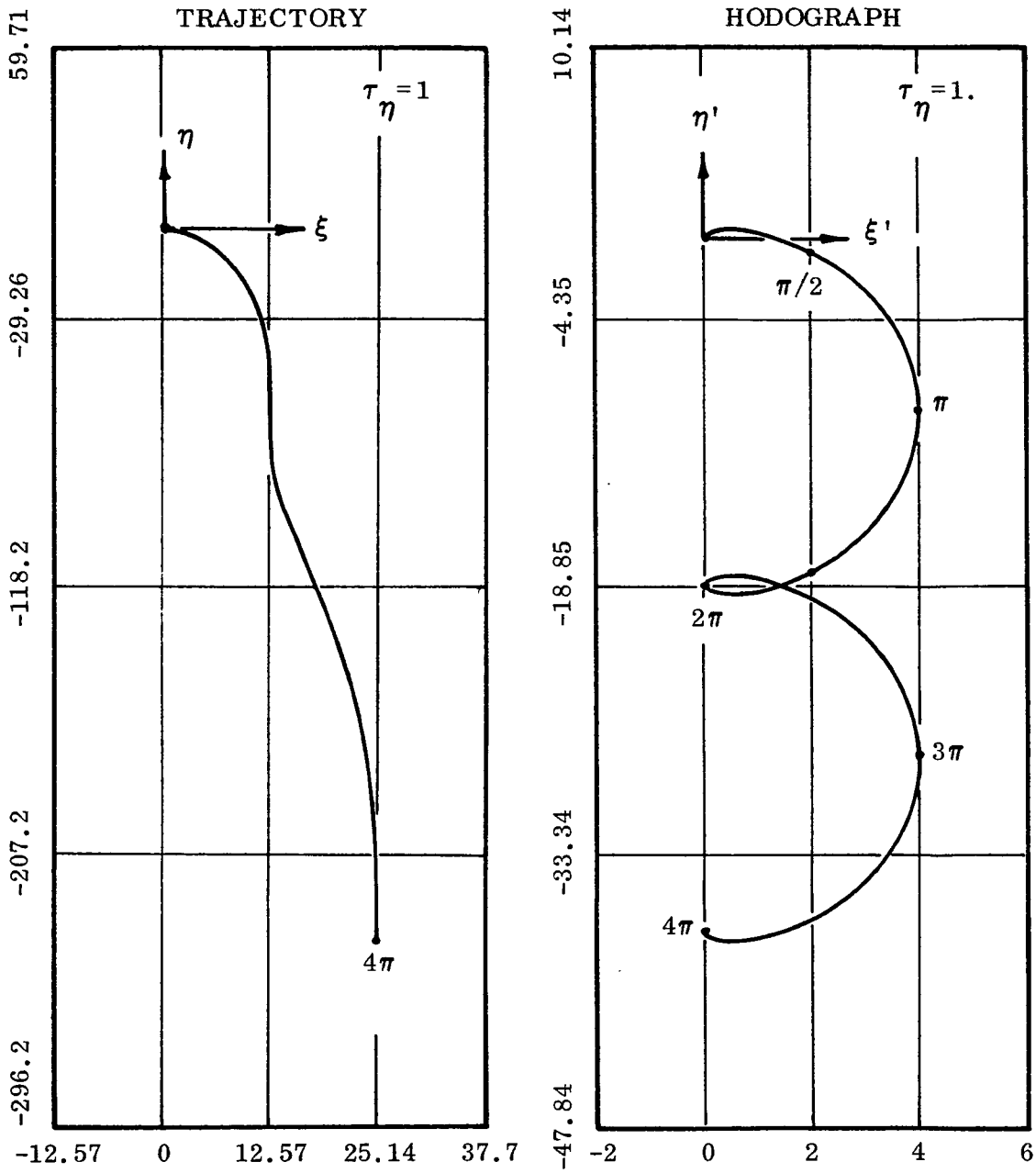

Fig. V.2. Relative Motion Traces, for Particle I, due to Constant Thrusting Action (τ_η). Motion originates at T, with Initial Values (ξ, η, $\zeta = 0$; ξ', η', $\zeta' = 0$).

while the "drifting" of this figure is described by: $|\xi|_{drift} = 2|\tau_\eta|$, and $|\eta|_{drift} = 6|\tau_\eta|$.

The hodograph for this case is also a drifting ellipse, appearing to be much like the one in the previous section. One exception is that this figure is skewed, compared to the other; with a two-axes offset for the center. The drift for this figure is again in the η-direction, at a rate $|\eta'|_{drift} = 3|\tau_\eta|$. The parametric expression, describing the ellipse*, is:

$$\frac{(\xi' - 2\tau_\eta)^2}{4\tau_\eta^2 + \tau_\xi^2} + \frac{(\eta' + 2\tau_\xi)^2}{4(4\tau_\eta^2 + \tau_\xi^2)} = 1. \qquad \text{(V.7b)}$$

Graphs showing the form of these traces are found on Fig. V.3; the thrusts used to develop these plots were set at unity (an unscaled value), hence the figures are representative of the results, only.

V.5.5 <u>In-and-out-of-plane motions, for $\tau_\xi = \tau_\zeta = 1.0$.</u> - The next figures describe the effect produced by one in-plane and one out-of-plane thrust component. Since the in-plane state variables are coupled, the consequences of this action will produce a full three-dimensional representation for the motion.

It is evident that because of the uncoupled nature of the present linearized results, the in-plane (ξ, η) trace would be identical to that described in Section V.5.2; consequently, those in-plane traces are not repeated here. Instead, the descriptions here will be concerned with the other two out-of-plane representations.

Examining the expressions for displacement and speed it is seen that both of these traces are straight lines, described by;

$$\frac{\xi}{\tau_\xi} = \frac{\zeta}{\tau_\zeta}, \text{ and } \frac{\xi'}{\tau_\xi} = \frac{\zeta'}{\tau_\zeta}. \qquad \text{(V.8a)}$$

*The "moving ellipse" is actually a prolate cycloid - this describes the trace on the (ξ', η')-plane.

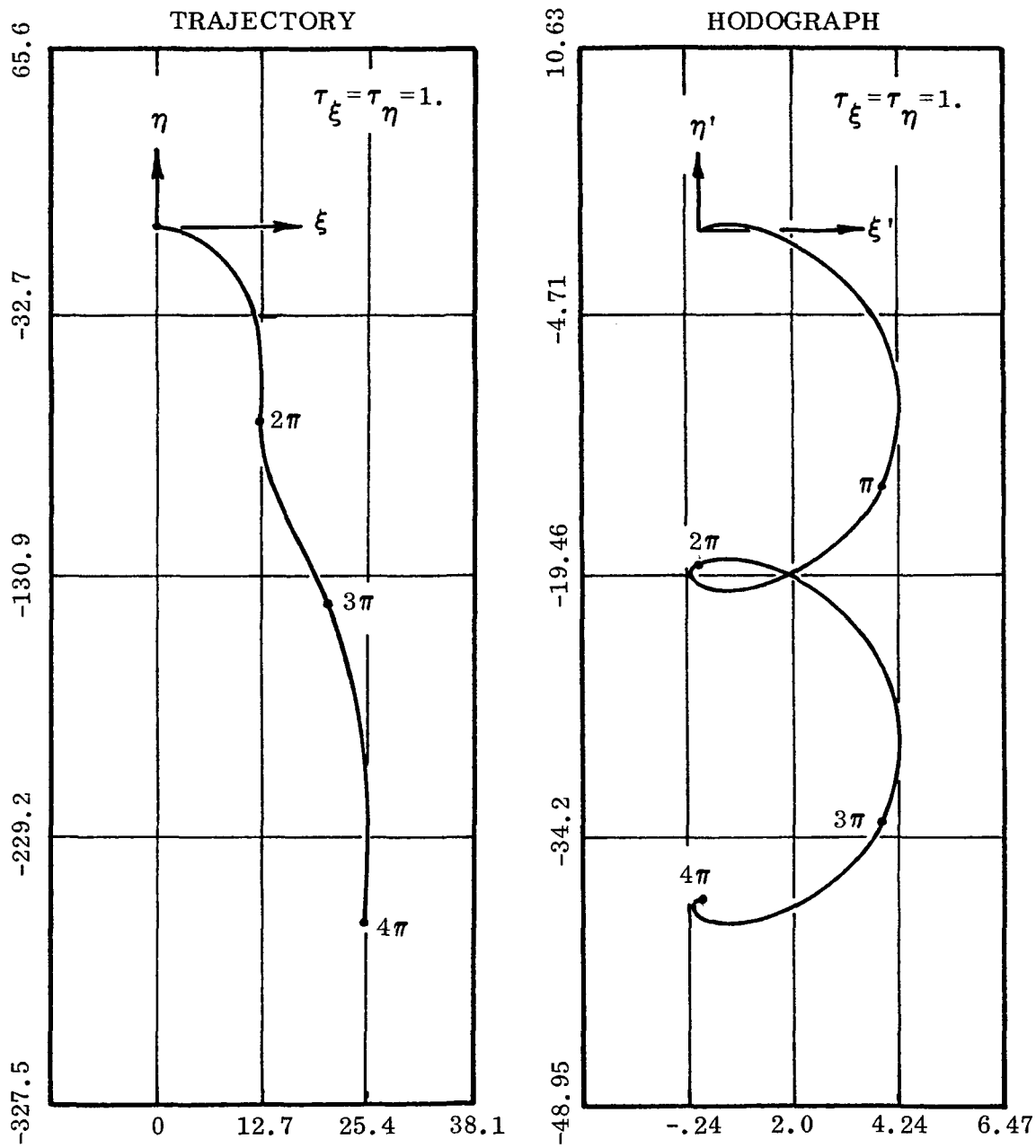

Fig. V.3. Relative Motion Traces, for Particle I, due to Constant Thrusting Action (τ_ξ, τ_η). Motion originates at T with Zero Initial Values.

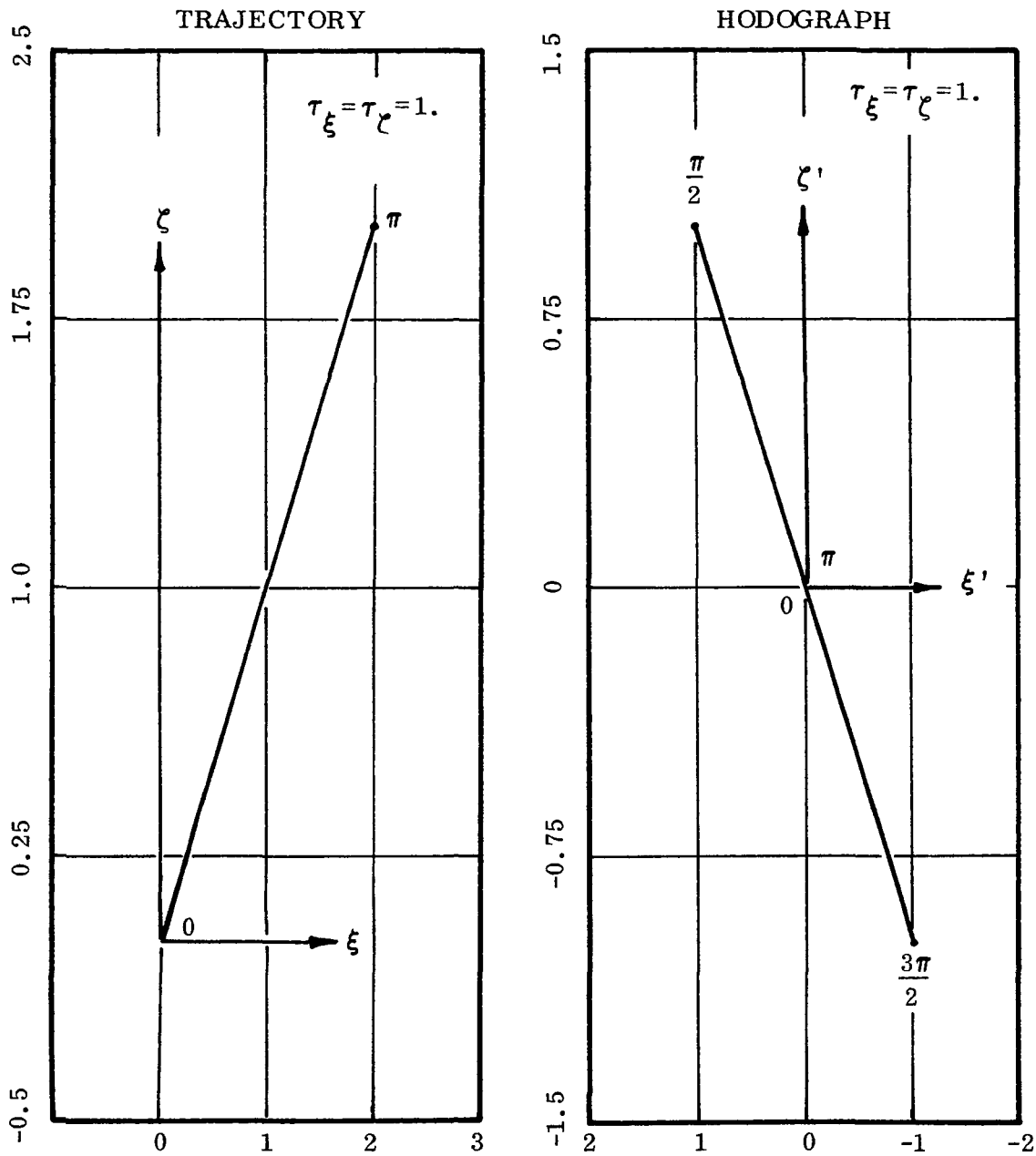

Fig. V.4. Out-of-Plane Motion Traces due to Constant Thrusting Action (τ_ξ, τ_ζ). Motion originates with Zero Initial State Values.

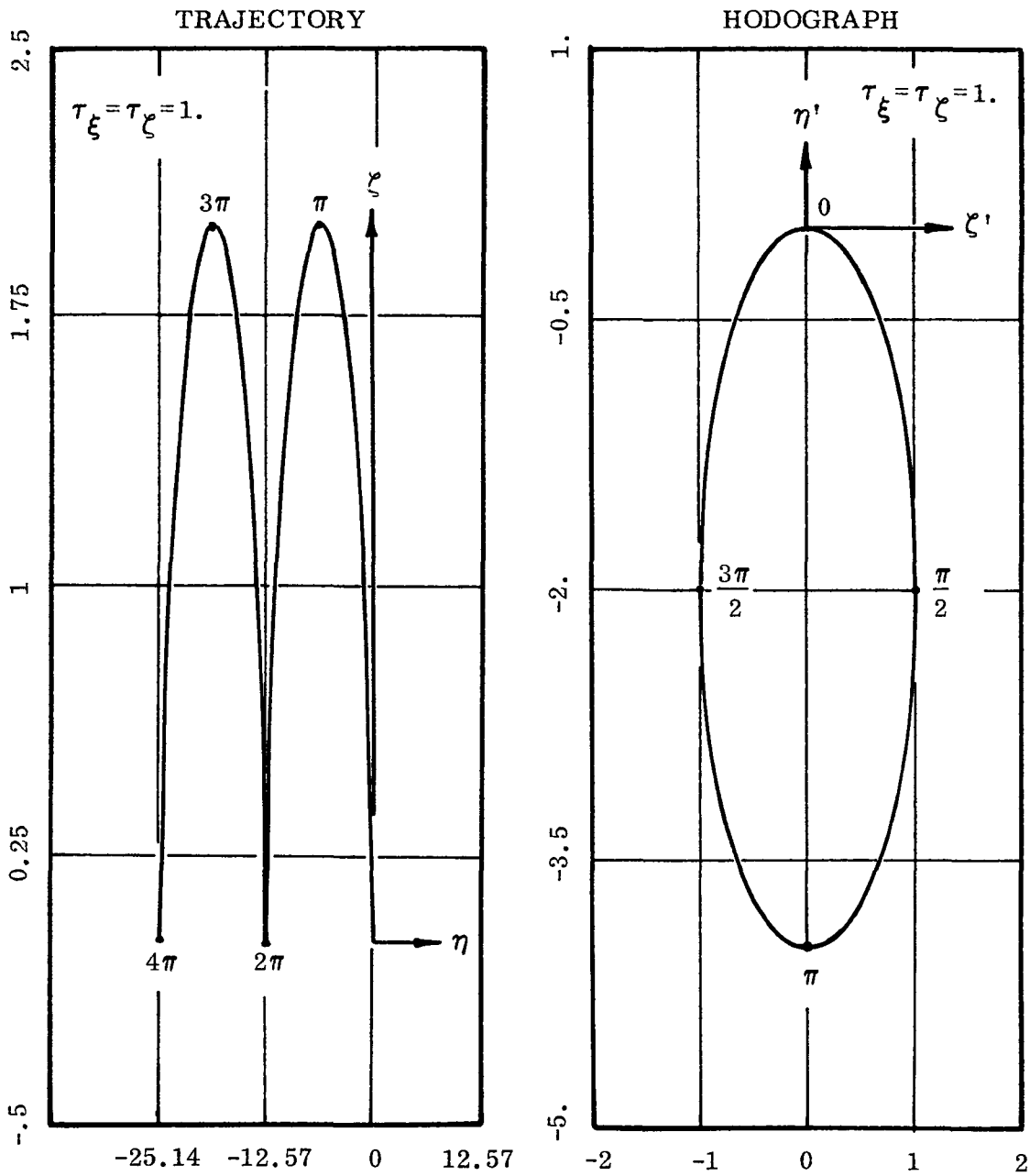

Fig. V.4. (concluded). Motion on the (ξ, ζ) and (ξ', ζ') planes.

The hodograph corresponding to the above displacement trace is also a moving figure - one which has motion in an η'-direction. If the secular term is neglected then the trace is a "line", described by:

$$\frac{\eta'}{4\tau_\eta} = \frac{\zeta'}{\tau_\zeta} \quad . \tag{V.9b}$$

The effect of the drift here is to move this line, continually, in a fixed direction.

Typical traces, for unscaled τ_j values, are shown on Fig. V.5. A study of these plots will provide a better understanding of the developed motion on each of the plane types.

For traces produced on the (ξ, ζ)- and (ξ', ζ')-planes it is apparent that: (a) the displacement trace is a moving ellipse (moving in the ξ-direction)- or, for unscaled τ_j, the figure is a cycloid. (b) Correspondingly, the figure describing the hodograph is an ellipse whose general equation is:

$$\left(\frac{\xi' - 2\tau_\eta}{2\tau_\eta}\right)^2 + \left(\frac{\zeta'}{\tau_\zeta}\right)^2 = 1. \tag{V.9c}$$

This ellipse, for unscaled thrust quantities, has a two-to-one axis ratio, and a displaced origin of coordinates.

As noted for an earlier case, the plots depicting the (ξ, η) and (ξ', η') traces are not reproduced here since these would be identical to the corresponding figures depicting the motion provided by $\tau_\eta = 1$.

The last case study to be described here will consider motions produced by a full unscaled thrusting action. This will be the subject of the next section.

V.5.7 Full motion, for $\tau_\xi = \tau_\eta = \tau_\zeta = 1$. - Under this action the motion is actually a combination of the previous cases, and could be described by a conglomerate addition of coordinates (throughout). Because of this combination it would be advisable to study the traces on Figs. V.6, carefully.

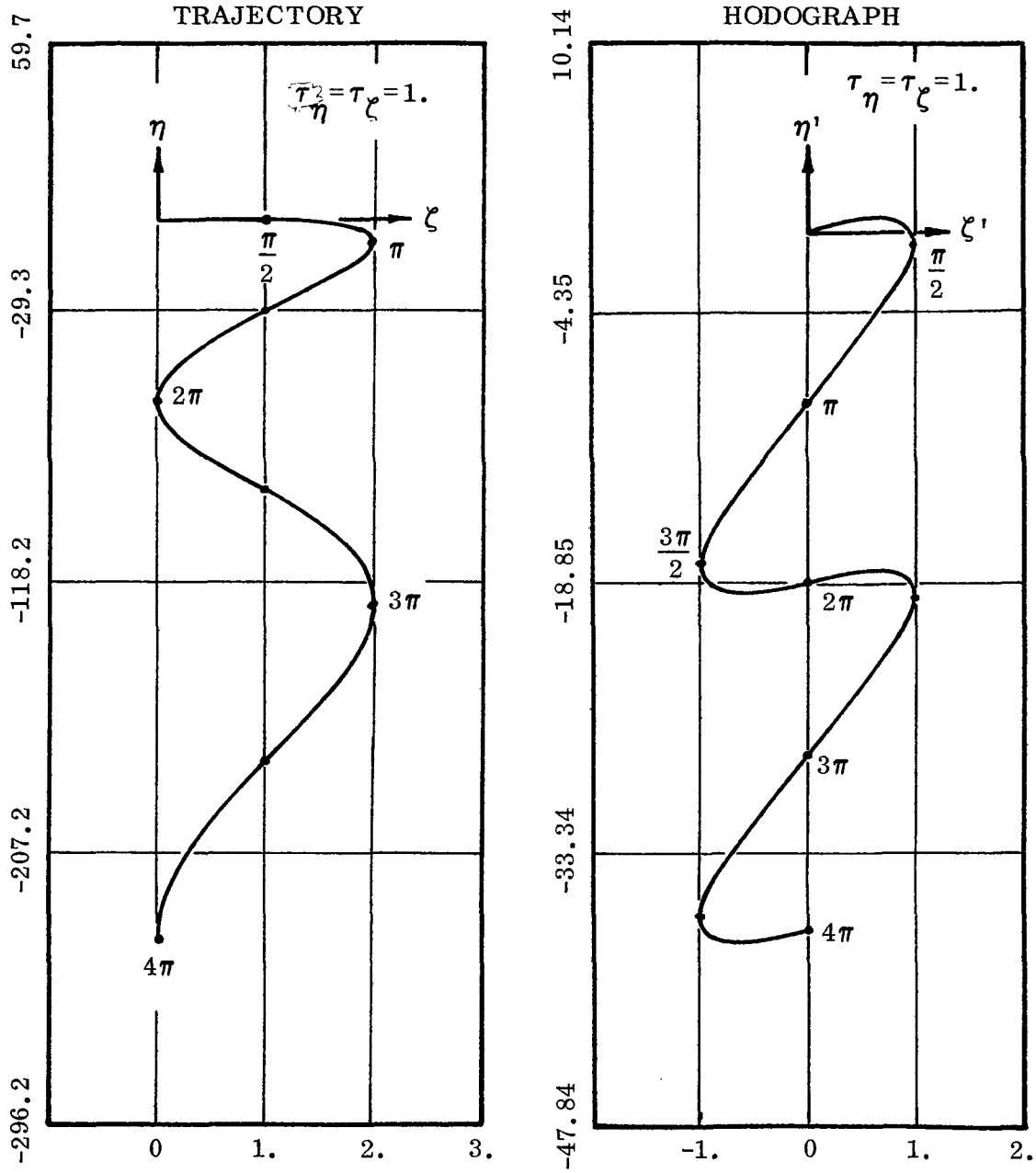

Fig. V.5. Out-of-Plane Relative Motion Traces due to Constant Thrusting Action (τ_η, τ_ζ). Motion originates with Zero Initial State.

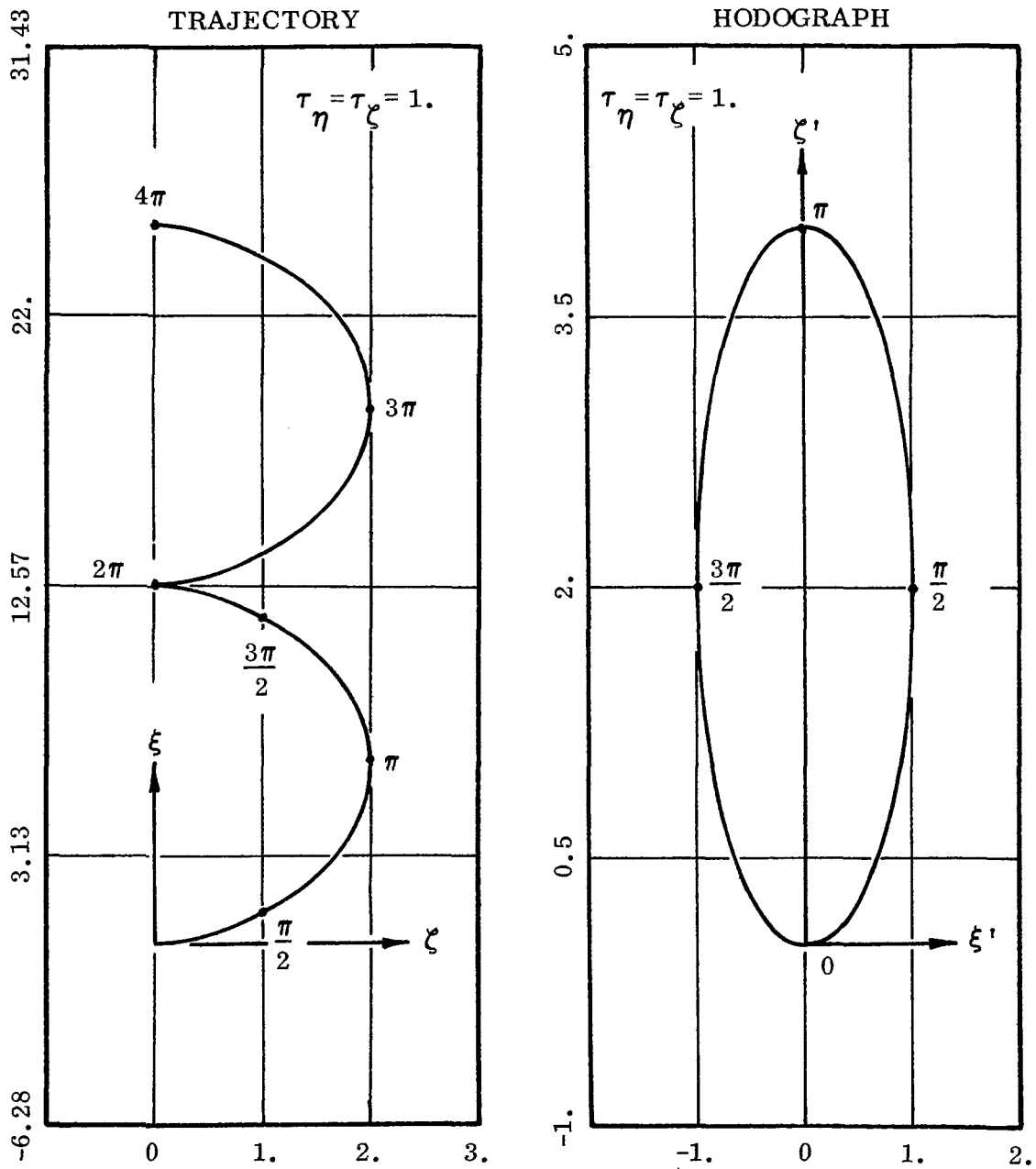

Fig. V.5. (concluded). Relative Motion Traces on (ξ, ζ) and (ξ', ζ') planes.

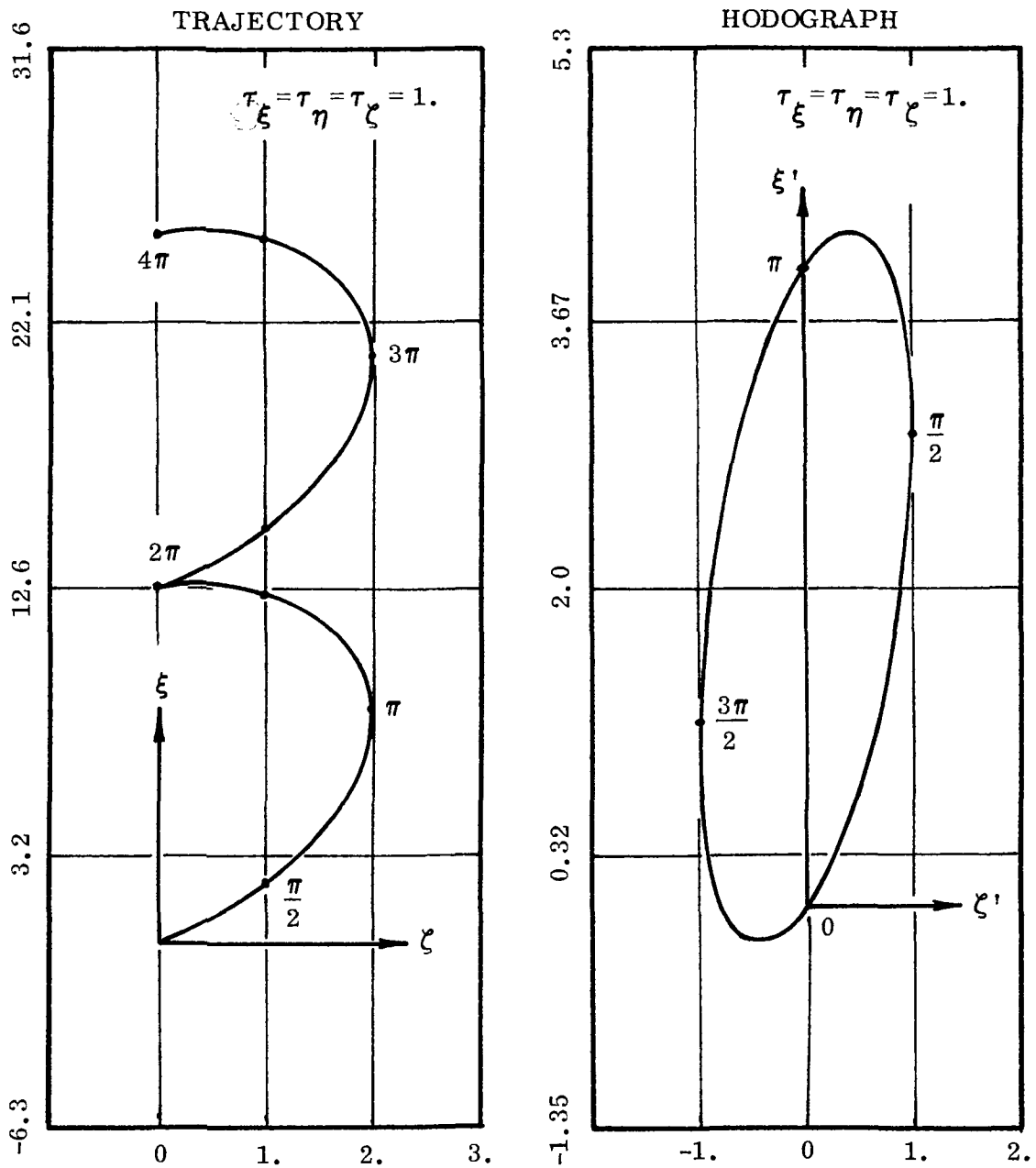

Fig. V.6. Relative Motion Traces for Constant Thrusting Action (τ_ξ, τ_η, τ_ζ). Initial Values: (ξ, η, $\zeta = 0$; ξ', η', $\zeta' = 0$).

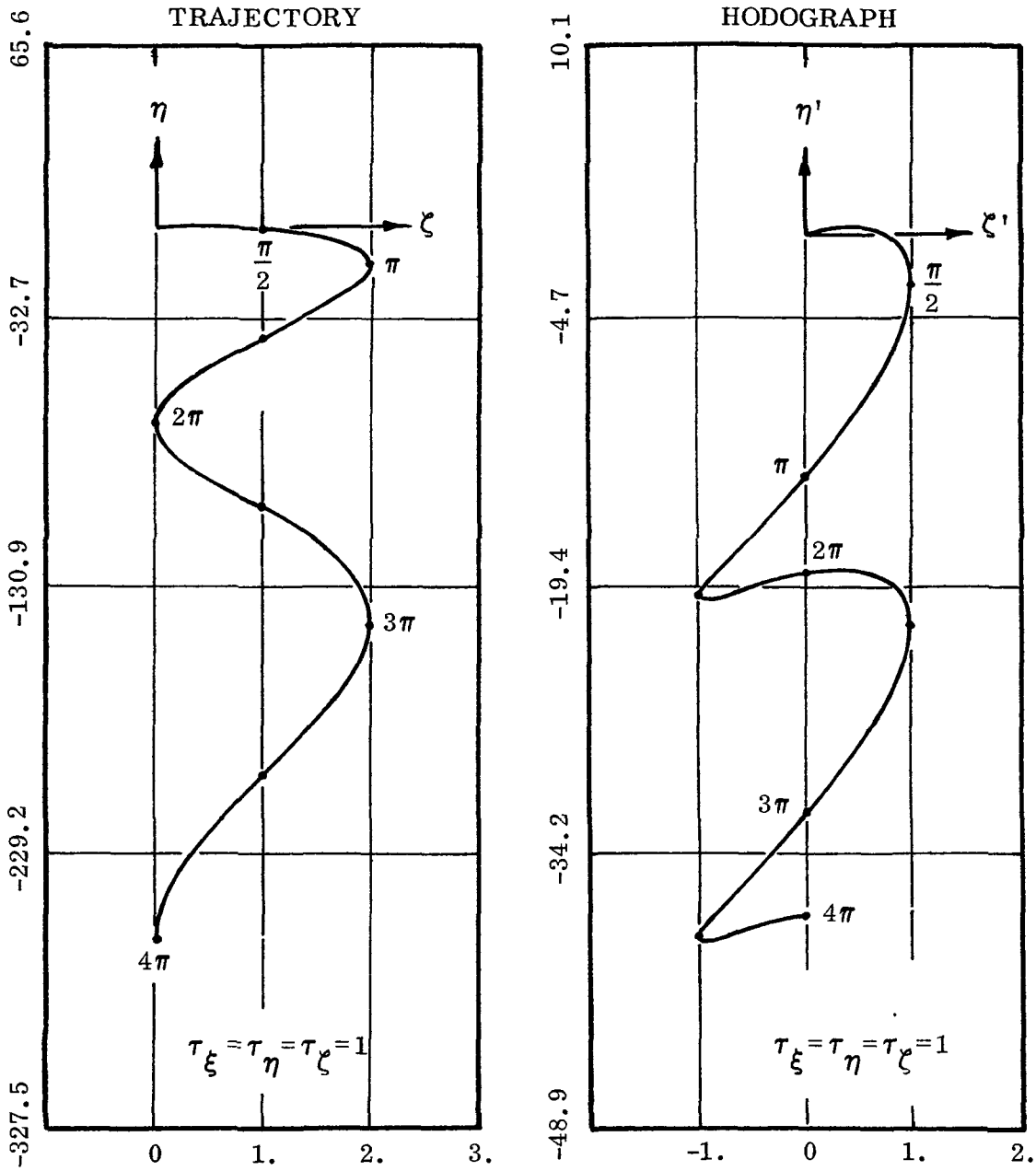

Fig. V.6. (concluded). Motion Traces on (η, ζ) and (η', ζ') planes.

For unscaled thrusts (τ_j) the displacement trace produces a skewed cycloid on the (ξ, ζ)-plane. The skewing is represented by a cyclic variance in the ξ-component. A parametric representation of the trace can be obtained as;

$$\xi = \frac{\tau_\xi}{\tau_\zeta}\,\zeta + 2\tau_\eta\,(1-\cos\varphi_T). \tag{V.10}$$

The hodograph for this case is described by an ellipse on the (ξ', ζ')-plane; but, the ellipse has a slant major axis; the inclination of this slant major axis, with respect to the ξ'-axis, can be described by:

$$\tan\beta \equiv \frac{\zeta'\,(\xi'\,\max)}{\xi'_{\max}} = \frac{\tau_\zeta\tau_\xi}{2\tau_\eta\sqrt{4\tau_\eta^2+\tau_\xi^2}+(4\tau_\eta^2+\tau_\xi^2)}\,. \tag{V.11}$$

For unscaled τ_j quantities the hodograph is a two-to-one ellipse whose center is shifted from the geometric center and (as noted) has its major axis skewed relative to the coordinate axes.

The displacement trace on the (η, ζ)-plane is noted to be geometrically similar to the (corresponding) trace developed for $\tau_\eta = \tau_\zeta$ (=1) earlier. The hodograph, corresponding to this displacement trace is much like that for the earlier case (where $\tau_\eta = \tau_\zeta$), but has a skewed aspect. Thus the present hodograph appears as a skewed version of the earlier trace.

V.6 Comments. - The developments described in this section are obviously an extension of the work presented in Section III. The difference between the two sections is added thrusting capability included herein. Since the aim here, as elsewhere, was to provide analytical expressions for the relative motion, this was facilitated by including a constant thrust component to each linearized, component differential equation.

The examples cited in the section were markedly similar to those in Section III; actually the case studies were identical in concept.

It was found that for the "ejected particles" problem the relative motion traces were significantly changed because of the thrusting. Also, it was found - though not specifically illustrated here - that thrust makes a difference in the intercept problem. However, the effect on intercept does not appear as significantly as for the "ejected particles" cases studied.

It should be mentioned that the examples in this section (and others) may be reproduced by the computer program developed for the investigation. The ejected particles examples and the intercept problem can be detailed by this program. Also, the capability of reproducing the results, by means of plots, showing variations for the state variables, is incorporated into the program; and, can be implemented as a called-for output.

The material presented in the next section is a logical extension and follow-on to this one. There, the intercept of one vehicle with another will be described; but, without the constraint of linearization. In this regard the work outlined there represents an "exact" solution to that situation. Also, the methodology is extended so that the relative motion between two particles, both on eccentric paths, is described. The illustrative example, detailed there, is of this type.

AN EXACT SOLUTION FOR INTERCEPT

VI.1 Introduction. - The problem of intercept, described in Sections III and V herein, was expressed in an analytical form obtained from the linearized solutions developed in Appendices A and D, respectively. In view of the limitations imposed by the simplification of the governing differential equations, those results, generally, suffered a loss in accuracy and predictability. In order to overcome these deficiencies, the problem must be solved in a manner which would eliminate these error sources from the formulation.

A method is described in this section of the report which does solve the problem so that the resulting solution is exact. That is, the solution does not "lose accuracy" as the calculations proceed away from the region of the origin; however, the method itself is not analytic, rather it is a numerical evaluation for the problem.

VI.2.1 The intercept formulation. - The end conditions for this problem are precisely those noted before, in Sections III and V. The requirement for intercept is met by properly adjusting the initial speeds, and/or thrust, so that the relative displacement vanishes at the preselected orbital position or time. To this extent the problem here, and that described earlier, are identical. The difference in the methods arises primarily in properly defining the physical condition(s) which guarantee the intercept at the time desired. Of course, in order to obtain an "exact solution" a numerical integration of the relative motion equations is needed, after a properly defined impulse schedule (for ballistic arcs), or thrusting level (for powered arcs), has been ascertained.

The crux of the problem, now, is to determine this set of impulses, or thrust components, which will achieve the intercept. A procedure, adopted here, to determine these inputs is one which utilizes the linear results as first estimates. Subsequently these estimates are refined, by an iterative technique, until a suitable solution to the problem is obtained. That is, the iterator corrects

the input until the terminal condition for intercept is achieved. (Needless to say, the application of this method is by means of a computer program incorporating the iterator* and a numerical integrator to solve the problem.)

A description of the methodology employed in this approach is given in the next few paragraphs.

VI. 2. 2 Solution for the intercept problem. - In principle the problem which is solved here is the same as that described earlier, except that now the linearization is not undertaken. As before, the governing equations describe a relative motion but with terminal conditions of intercept imposed on them. For compatibility, this problem and the previous ones are identical in formulation; i.e., two bodies are considered, without mutual interaction; and, with one body (the target) assumed to have a circular orbit about the attracting primary. The intercept is to occur at a preselected time; the maneuvering particle flies along either a ballistic, or powered, arc depending on the operational mode selected. In concept, the powered mode assumes a "small" thrust level so that mass depletion of the interceptor is of no consequence.

After the iterator has determined a set of impulse, or thrust, values an integrated solution for the problem is obtained as a time history of the state variables. For convenience these data will be listed, or used to plot graphs depicting the interceptor's relative motion**. The usual graphical outputs appear as displacement plots, and hodographs, for the interceptor. Again, for consistency and convenience, the manipulated equations, internal to the computer program, are in dimensionless form.

The program accepts dimensional inputs and produces dimensional output quantities with internal manipulations carried out otherwise.

---

*Horsewood, J. L., et al: HILTOP, Heliocentric Interplanetary Low Thrust Trajectory Optimization Program; AMA Report No. 71-38, Contract NAS5-11364, November 1971; pgs. 42-48; Analytical Mechanics Associates, Inc., Seabrook, Md.

**A brief description of the program is included herein as Appendix H.

For descriptive purposes the system of integrated equations is listed below. These are set down in dimensionless form using the notations in Appendices A and D; they describe the interceptor's motion with respect to the target. For impulsive intercept the thrust terms are (necessarily) deleted; and, in all cases, the inputs include an initial state and the time to intercept.

A general statement of this formulation is given by eq. (A.5), Appendix A. In order to obtain proper expressions, eqs. (A.1) are modified to include the specific thrust, and eq. (A.14), the kinematic description of acceleration, is used to complete the mathematical statement. In scalar form, specialized for m_T on a circular orbit and m_I the maneuvering particle, it can be shown that these equations become:

$$\xi'' = 2\eta' + (1+\xi) - \frac{(1+\xi)}{\Delta^3} + \tau_\xi ,$$

$$\eta'' = -2\xi' + \eta - \frac{\eta}{\Delta^3} + \tau_\eta ,$$

and

$$\zeta'' = -\frac{\zeta}{\Delta^3} + \tau_\zeta ; \qquad \text{(VI.1)}$$

wherein $\Delta^3 \equiv [(1+\xi)^2 + \eta^2 + \zeta^2]^{3/2}$, and $\tau_j = \dfrac{T_j}{r_T \dot{\varphi}_T^{\,2}}$. As before, $(\sim)'$ signifies differentiation with respect to the angle, φ_T $(\equiv \dot{\varphi}_T t)$.

These equations will describe an intercept when the inputs include a proper set of thrust and/or impulse components (as determined using the iterator). Without these special inputs (i.e., for arbitrary input data), the program computes a relative motion trajectory for the interceptor incident to these inputs.

Consequently, with the iterator-integrator program module the intercept problem can be solved, as an exact solution, not subject to the constraints

imposed by a linearization of the governing differential equations. One restriction which still exists here is that of assuming the target's trajectory is a circle. Of course this was done, initially, so that the numerical solution would be consistent with the analytical one. For many case studies it would be desirable to remove this constraint, but to do so without disrupting, too severely, the logic used for the intercept maneuver. A method of approach for this situation will be described below.

VI.2.3 Intercept on eccentric trajectories. - As an extension to the method outlined above, the circular orbit constraint can be removed so that both particles travel eccentric paths. The concept and implication of this idea is simple; this maneuver can be viewed as nothing more than two simultaneous solutions of the previous problem. When these two cases are treated as a relative motion problem, themselves, then the resulting output defines an intercept maneuver involving eccentric trajectories throughout.

If the problem considers an impulsive intercept, then the iterator treats both bodies as maneuvering particles. Of course it is not required that this be the case, actually; the investigator may use one set of output data as an "input" for the target vehicle thereby causing any maneuvering to be imposed onto the remaining vehicle. However, under any operational concept, the initial inputs are similar to those described earlier for the simpler intercept. Here a "fictitious" target is presumed, for each particle of interest, with the intercept designed to occur at this reference (imaginary) particle.

The sketch below illustrates, schematically, the geometry of this situation and leads to the formulation described there.

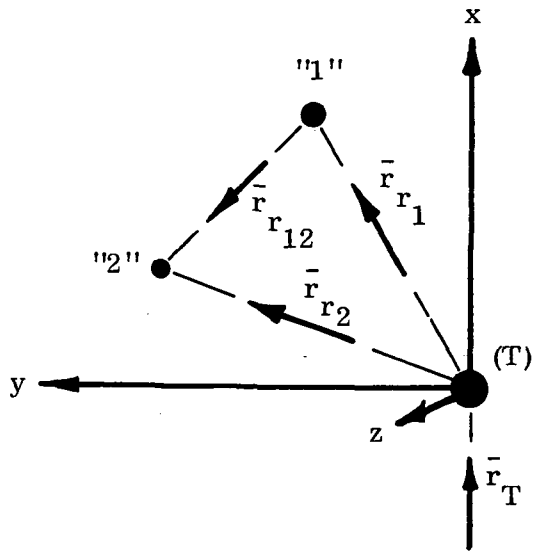

Particles ("1" and "2") are those of interest here; T is the (fictitious) relative motion origin - this is analogous to the "target" particle described elsewhere. For this scheme the intercept occurs (between "1" and "2") at the orbit of T; thus there are two intercept problems to be solved simultaneously; one, between T and "1", the other between T and "2".

From the sketch, it is seen that,

$$\bar{r}_{r_2} = \bar{r}_{r_1} + \bar{r}_{r_{12}} ;$$

or

$$\bar{r}_{r_{12}} = \bar{r}_{r_2} - \bar{r}_{r_1} ,$$

hence

$$\dot{\bar{r}}_{r_{12}} = \dot{\bar{r}}_{r_2} - \dot{\bar{r}}_{r_1} ; \qquad \text{(VI.2)}$$

these describe the relative motion state for m_I with respect to m_T, as desired.* In concept, the intercept problem between these particles is solved; and, for both trajectories having arbitrary eccentricity. These expressions may be formed from the output of the iterator-integrator module described earlier. To this extent the problem is solved compatible with the governing expressions given as eqs. (VI.1).

Even though the discussions above relate to the impulsive intercept, a similar method can be described for the thrusting interceptor. Because of the rather obvious similarity which exists for the two situations, the thrusting intercept problem will not be discussed in any detail here.

*Here m_I and m_T are the particles ("1" and "2") above.

VI.3.1 An example. - As a means of aiding the discussions above, and to clarify the problem described there, a sample situation will be examined. Also, from information provided in the output, other data of consequence can be developed and commented upon.

In this example the intercept is to occur by impulse. The two particles (I and T) are located by the following initial values:

Target	Interceptor
$x_o \equiv -979$ km	$x_o = -1749$ km
$y_o \equiv -850$ km	$y_o = -834$ km
$\dot{x}_o \equiv 0 = \dot{y}_o$	$\dot{x}_o \equiv 0 = \dot{y}_o$

(Note that this intercept problem is planar).

The fictitious target (or origin of reference) has an assumed orbit of 6860 km; hence it travels at approximately 7.632 km/sec. It is desired to have the intercept occur at t = 3872.6 sec (an arbitrary selected time). The corresponding displacement angle for the imaginary target is $\varphi_T \cong 246.8^o$ (determined from t).

The first estimate of the initial speeds, for an intercept, comes from the linear solution (see eqs. III.20, or III.21). The subsequently iterated ("exact") values are determined from the computer module (these are dependent on the initial state and time to intercept); both sets are listed below for comparison.

	Target	Interceptor
From Linear Theory:	$\dot{x}_o^* \cong -47.3$ m/s	$\dot{x}_o^* \cong +7.62$ m/s
	$\dot{y}_o^* \cong 2002.0$ m/s	$\dot{y}_o^* \cong +3616.0$ m/s
Exact (Iterator) Values:	$\dot{x}_o^* \cong +81.5$ m/s	$\dot{x}_o^* \cong +177.3$ m/s
	$\dot{y}_o^* \cong +1982.0$ m/s	$\dot{y}_o^* \cong +3851.0$ m/s
Error, at intercept, due to Linear Theory inputs:	$s_f = 165.1$ km	$s_f = 4250.0$ km
Eccentricity of Intercept Trajectory:	0.10	0.20
Terminal State (Exact Solution):	$x_f \cong 0$, $y_f \cong 0$	$x_f \cong 0$, $y_f \cong 0$
	$\dot{x}_f \cong -679.0$ m/s	$\dot{x}_f \cong -1393$ m/s
	$\dot{y}_f \cong -193$ m/s	$\dot{y}_f \cong -391.6$ m/s

(Note: the quantities listed above are referred to the fictitious target as an origin for the relative coordinates).

Traces of the relative motion state, for the two particles (I and T), referred to the fictitious (origin) particles, are shown on Fig. VI.1. The coordinates for these graphs are in dimensionless variables; the initial point(s) for these traces are denoted as, IP.

From the figures it is evident that the target (T) moves inside the interceptor's (I) track on both the displacement and hodograph planes. On each figure trace there are "tics" which depict equal time (angle) increments during the maneuver. (For reference, the tics denote $\Delta t \cong 276.6$ sec (or, $\Delta\varphi_T \cong 17.63^o$)).

Also, each graph has a dashed line inscribed, between traces, to correlate a position on the various plots. It should be recognized that on Figs. VI.1 the fictitious target assumes the origin position (0, 0); hence these traces are descriptive of the two relative motions (for the m_I and m_T of the problem).

Figures VI.2 are indicative of the relative motion for the interceptor (m_I) with respect to the (true) target (m_T). In this regard the origin (0, 0) is occupied by m_T, and the trace outlines the relative motion for m_I. As before the initial position (for m_I) is noted as IP, while the dashed line on each plot corresponds to the one inscribed on Figs. VI.1; also, the graph's coordinates are dimensionless variables.

The state variables for m_I with respect to m_T are, from the figures, as follows:

At t = 0 (Initial state): $\xi_o \cong -0.112$, $\xi_o'^* \cong +0.0125$; $\eta_o \cong 0.003$, $\eta_o'^* = +0.245$.

At $t = t_f$ (Intercept): $\xi_f \cong 0$, $\xi_f' \cong -.0939$; $\eta_f \cong 0$, $\eta_f' \cong -0.026$.

On Fig. VI.2a the dashed line would serve to define the "look-angle" of the target (at O) from the interceptor! The corresponding line is seen on Fig. VI.1a.

VI.3.2 Range and range-rate. - Valuable information regarding the maneuver can be obtained from these relative motion traces. Among the more important items are range and range-rate data, depicting how this operation progresses. Recognizing that range is the length of the relative position vector, $|\bar{r}_r|$, then it follows that range-rate is symbolically given by $|\dot{\bar{r}}_r|$. These data are obviously represented on Figs. VI.2.

For instance, the range of m_I, at any time during intercept, is the length of that line connecting the origin (0, 0) to a specified point on the curve. Also, a

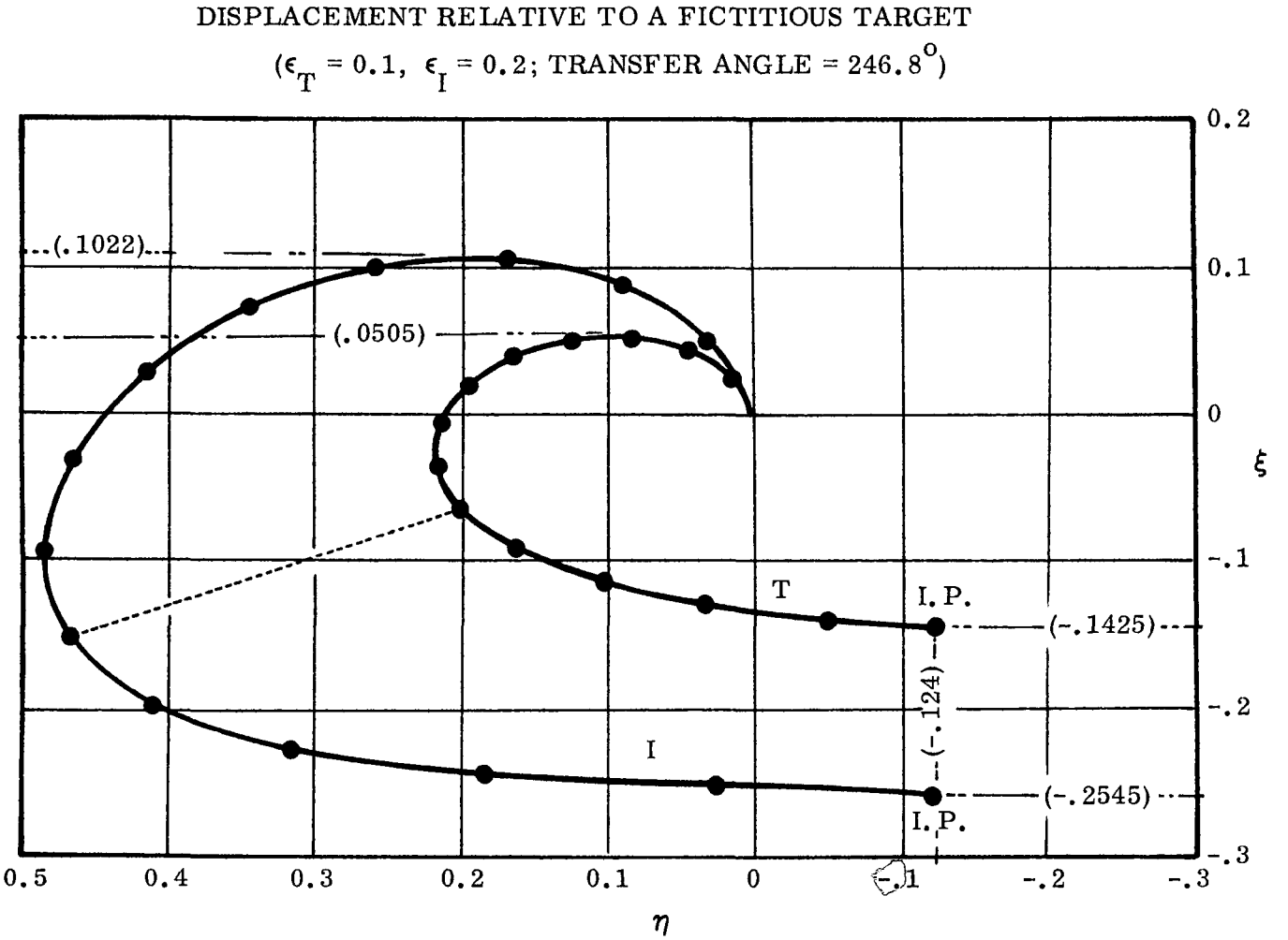

Fig. VI.1. In-Plane Trajectory Traces for Motion of I and T, Relative to an Origin on a Circular Orbit, for the "Exact" Intercept Problem. Both Particles (I, T) Move on Arbitrary, Closed Eccentric Paths About μ.

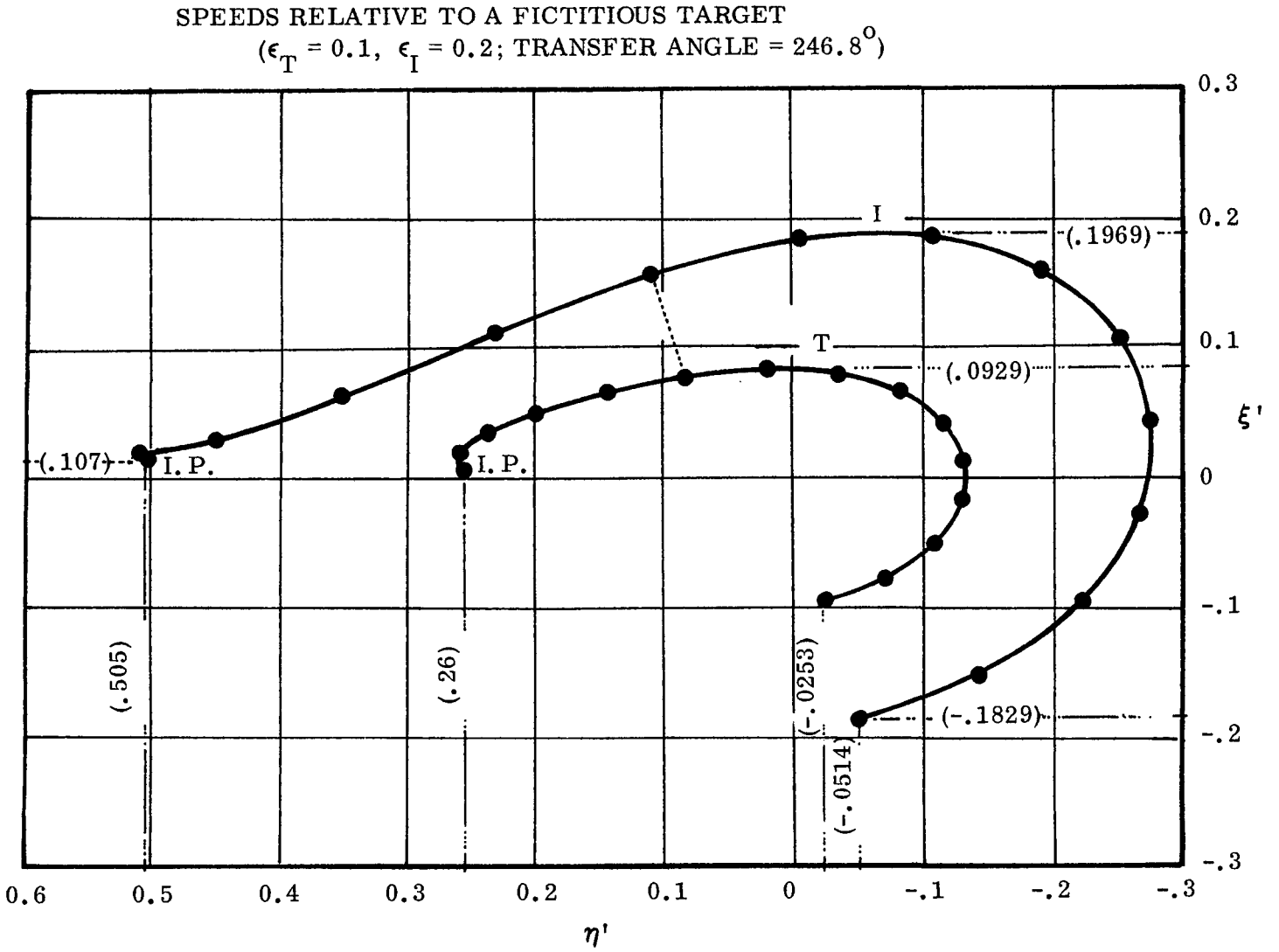

Fig. VI.1. (concluded). In-Plane Hodographs for the "Exact" Intercept Problem.

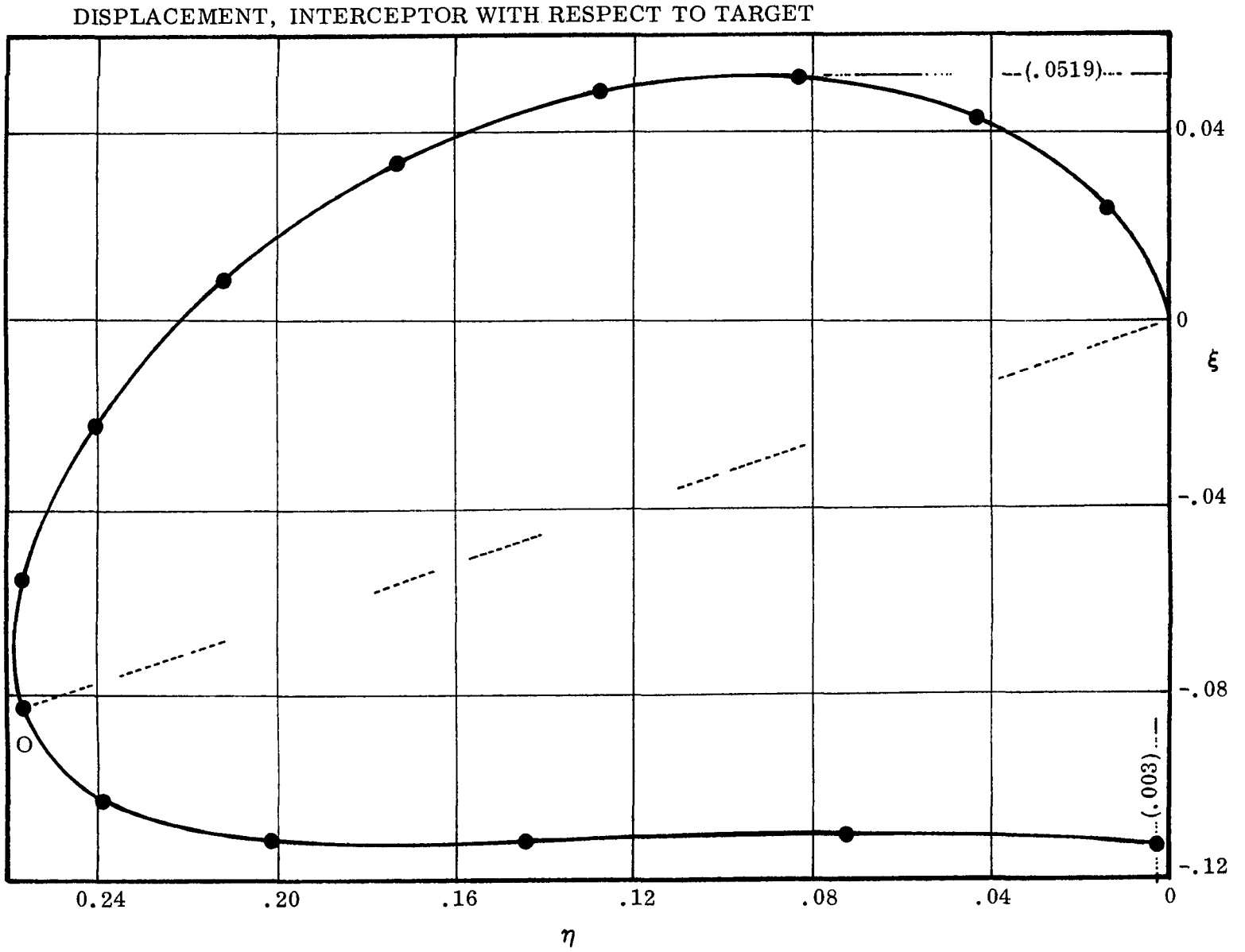

Fig. VI.2. Trajectory of I, with respect to T, for the "Exact" Intercept Problem.

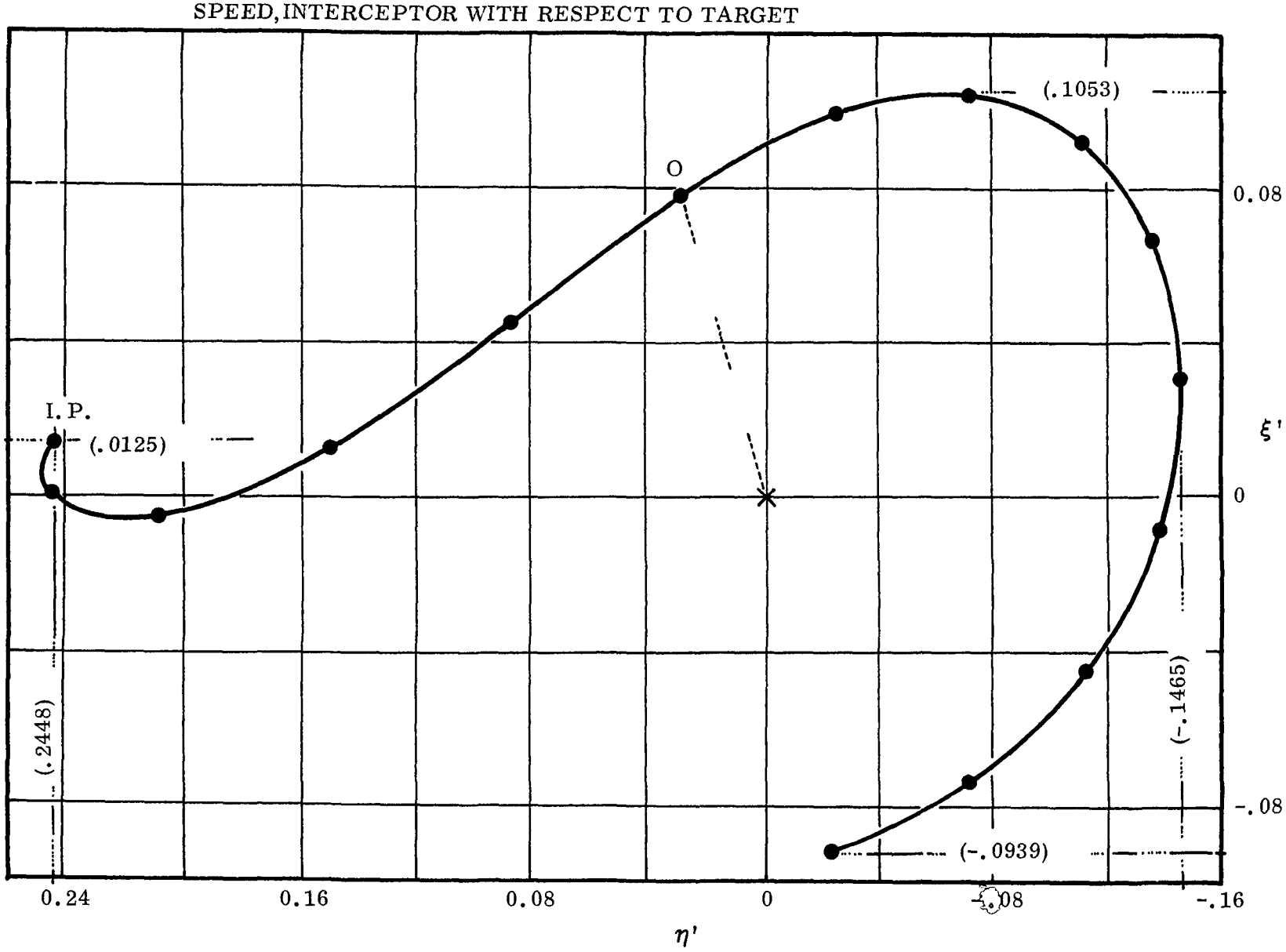

Fig. VI.2. (concluded). Relative Motion Hodograph, for I, in the "Exact" Intercept Problem.

time history of the "range" is inferred from this relative displacement trace (see Fig. VI.2a). Thus, by means of concentric circles, centered at the origin, one is able to ascertain this variation. It should be apparent that the range increases (with time) until the particle is in the vicinity of that point where the dashed line cuts the trace. There the range is a maximum; and, from that point on to the intercept the range decreases monotonically.

Range-rate is acquired from Fig. VI.2b; here one sees that this quantity increases, reaches a maximum (just after leaving IP) and falls to its least value (near the "O" symbol). Next, the range-rate increases to a local maximum, falls to a local minimum, and rises slightly to the terminal point. Here, also, a clear description of this variation can be had by constructing (appropriate) concentric circles centered at the origin (0, 0). Needless to say, the variation of range-rate is a more complicated phenomenon than the time history of the range, for this example.

VI.4 Comments. - In this portion of this report a method has been described which allows one to obtain an "exact" solution to the intercept problem; and, extends the methodology to provide for intercept involving general, closed eccentric paths.

The example described here depicts an intercept produced by an impulse. The same general ideas, as noted here, apply to the thrusting particle intercept operations. For conciseness, and to avoid redundancy, no such similar (thrusting) example has been included here.

A DETERMINISTIC RELATIVE MOTION SOLUTION

VII.1 Introduction. - In the following paragraphs a relative motion for two particles on adjacent orbits, about the same primary, will be studied subject to the condition that both motions have the same period. Here, the geometric properties of the relative displacement and velocity traces, on a proper set of representative planes, will be investigated. In this regard a complete state of the motion can be obtained; and, consequently the range and range-rate variations, over one or more orbits, are defined.

From an examination of the results obtained here, it has been found that cusps appear on some of the motion traces provided that a proper relationship is impressed on the eccentricity and inclination. For this part of the investigation one particle is assumed to move on a circular path while the second one travels along an ellipse. The conditions necessary for cusps to appear are derived, and typical traces, with and without this geometric anomaly, are displayed and examined.

Since these descriptions will be based on results developed in Appendix F, wherein a linearization of the defining equations was not employed, then this formulation is mathematically deterministic. As a consequence the traces presented here are true representations of the relative motion; 'true' in the sense that the earlier approximations have been circumvented.

VII.2 Example of a particular relative motion. - The example which is proposed for investigation, next, will utilize the formulation developed in Appendix F; and will be used to show an unusual geometric property which was found in this relative motion problem.

This example considers the special case wherein m_2 is detached from m_1 at the nodal position, but released so that the two resulting planes are inclined to one another. Necessarily, at the nodal axis, the two orbital radii are equal ($r_2 = r_1$); however, the true anomalies are not equal, here, in general.

In illustrating the unusual geometric traces which have been found, the two orbits are assumed to have a same period of motion. In addition, it is presumed that the orbit for m_1 is circular (hence r_1 = a constant), while that for m_2 is an ellipse.

VII.3 Description of the orbits, and their parameters. - In line with these assumptions, then, at the line of nodes it is apparent that

$$r_2 = r_1 = a_2,$$

where a_2 is the semi-major axis length for the orbit of m_2.

Next, using the conic equation it is seen that this initial position can be defined as,

$$\cos \varphi_{2_o} = - \epsilon_2; \tag{VII.1}$$

and, consequently, $\sin \varphi_{2_o} = \sqrt{1-\epsilon_2^2}$. Making use of eq. (F.15), Appendix F, and the above result, the circular functions for path 2 are,

$$\cos \varphi_2 = \cos (\varphi_{2_o} + \theta) = - \left[\epsilon_2 \cos \theta + \sqrt{1-\epsilon_2^2} \sin \theta \right],$$

and

$$\sin \varphi_2 = \sqrt{1-\epsilon_2^2} \cos \theta - \epsilon_2 \sin \theta. \tag{VII.2}$$

The conic expressions describing these orbits may be recast in terms of the conditions imposed above; consequently,

(a) for m_1: $r_1 = r_c$ (a constant);

and, (b) for m_2 (since $a_2 = r_c$) :

thus,
$$r_2 = \frac{r_c (1-\epsilon_2^2)}{1-\epsilon_2 (\epsilon_2 \cos\theta + \sqrt{1-\epsilon_2^2} \sin\theta} , \qquad \text{(VII. 3)}$$

(see Fig. VII.1 for a geometric representation of this problem).

In a like manner the speed components at representative points along each trajectory are described as follows;

(a) *for* m_1:

$$V_{r_1} = 0, \; V_{\varphi_1} = V_c \left(\equiv \sqrt{\mu / r_c} \right) ; \; V_1 = V_c ; \qquad \text{(VII. 4a)}$$

and, (b) for m_2:

$$V_{r_2} = \frac{\mu}{h_2} \epsilon_2 \left[\sqrt{1-\epsilon_2^2} \cos\theta - \epsilon_2 \sin\theta \right] = \dot{r}_2 ,$$

$$V_{\varphi_2} = \frac{\mu}{h_2} \left[1-\epsilon_2 (\epsilon_2 \cos\theta + \sqrt{1-\epsilon_2^2} \sin\theta) \right] = (r_2 \dot{\varphi}_2) . \qquad \text{(VII. 4b)}$$

Combining these, it is found that the speed for the second particle is:

$$V_2 = \frac{\mu}{h_2} \left\{ 1 + \epsilon_2^2 (1-2\cos\theta) - 2\epsilon_2 \sqrt{1-\epsilon_2^2} \sin\theta \right\}^{\frac{1}{2}} . \qquad \text{(VII. 4c)*}$$

As an aid to relating these two orbital motions one should note, in particular, the descriptive quantities listed below:

(A) The specific energy for the orbiting particles:

$$E_1 = -\frac{V_c^2}{2} , \text{ and } E_2 = \frac{V_2^2}{2} - \frac{\mu}{r_2} = -\frac{\mu}{2a_2} , \qquad \text{(VII. 5a)}$$

which, when evaluated at $r_2 = r_c$ (the nodal line) leads directly to,

$$E_2 = -\frac{V_c^2}{2} \text{ (since } r_c = a_2). \qquad \text{(VII. 5b)}$$

*Subscripts, $(\sim)_1$ and $(\sim)_2$, signify the separate orbits; h is the specific angular momentum for an orbit; ϵ is the eccentricity; φ is the true anomaly.

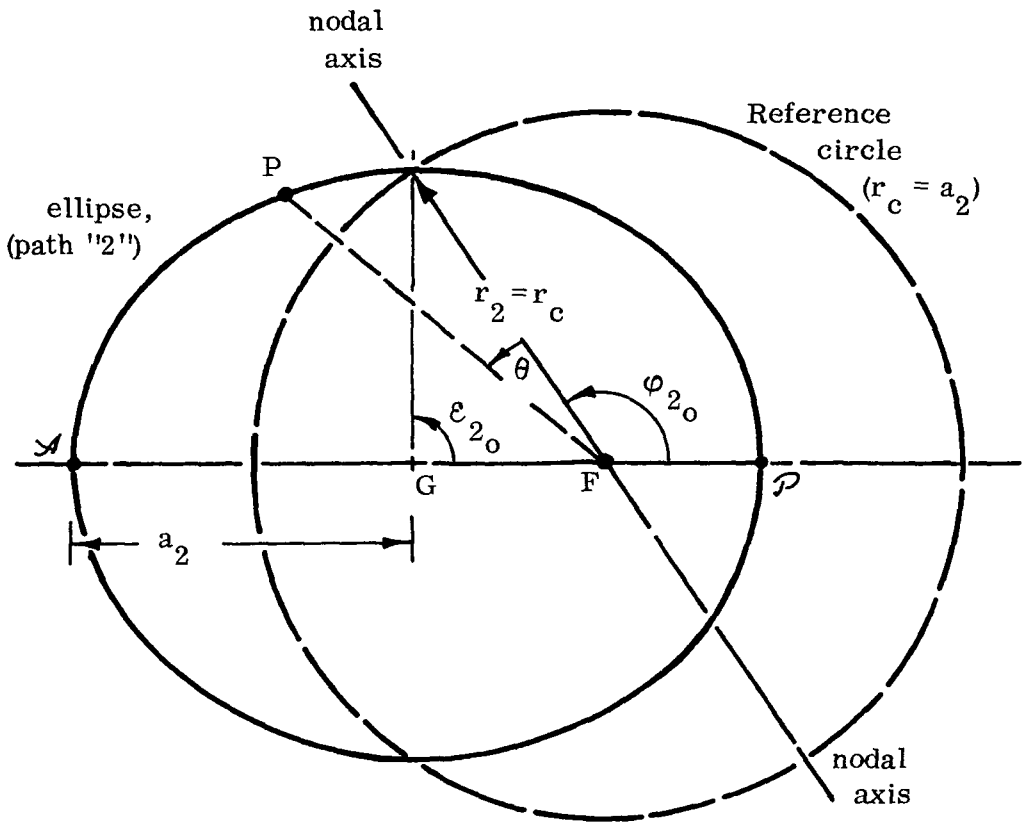

P is a general position
θ is the position angle, measured from nodal axis
$\mathcal{A}$ = apocenter
$\mathcal{P}$ = pericenter

F locates the primary focus

G is the geometric center, ellipse

Fig. VII.1. Geometry for the Deterministic Relative Motion Problem.

Hence, from the energy expressions,

$$V_{2_o}^2 = V_c^2 \quad . \tag{VII.5c}$$

(B) The specific moment of momentum for each orbit is:

$$h_1 = r_c V_c, \text{ and } h_2 = r_2 V_{\varphi_2}; \tag{VII.6a}$$

or, using the last eqs. (VII.4b), and recognizing that $\theta = 0$ at the nodal line, then

$$h_2 = \frac{\mu}{V_c} \sqrt{1-\epsilon_2^2} = r_c V_c \sqrt{1-\epsilon_2^2} \quad ; \tag{VII.6b}$$

leading to,

$$h_2 = h_1 \sqrt{1-\epsilon_2^2} \quad . \tag{VII.6c}$$

(C) The eccentricity anomaly for these orbits is obtained from the general relationship,

$$\tan \frac{\mathcal{E}}{2} = \sqrt{\frac{1-\epsilon}{1+\epsilon}} \tan \frac{\varphi}{2} \quad . \tag{VII.7a}$$

When this is applied at the nodal point one finds that;

$$\text{(a) for } (m_1): \quad \mathcal{E}_{1_o} = \varphi_{1_o} \quad ; \tag{VII.7b}$$

and

$$\text{(b) for } (m_2): \quad \mathcal{E}_{2_o} = \pi/2. \tag{VII.7c}$$

(D) Kepler's equation ($(n_j t = \mathcal{E}_j - \epsilon_j \sin \mathcal{E}_j)$; $(j = 1, 2)$) for these orbits reduces to;

(a) for m_1: $n_1 t = \mathcal{E}_1 = \varphi_1$;

and (b) for m_2: $n_2 t = \mathcal{E}_2 - \epsilon_2 \sin \mathcal{E}_2$, (VII. 8a)

where each of the mean motions (n_j) is,

$$n_j = \sqrt{\frac{\mu}{a_j^3}} \quad , \quad (r_c = a_1 = a_2) \; ; \tag{VII. 8b}$$

hence, the n_j are constants for this example. In particular n_j reduces to

$$n = \sqrt{\frac{\mu}{r_c^3}} = \dot{\varphi}_1 \; . \tag{VII. 8c}$$

VII. 4 Geometric considerations. - Since the trajectories are presumed to be a circle (for m_1) and an ellipse (for m_2), then the geometry of the starting point is of particular interest. (See Fig. (VII. 2) for this representation).

According to eq. (VII. 7c) the eccentric anomaly locating the starting point ("O") is $\mathcal{E}_{2_o} = \frac{\pi}{2}$. However, from eqs. (VII. 7b) and (VII. 8c),

$$\mathcal{E}_{1_o} = \varphi_{1_o} = \dot{\varphi}_1 \; t_o = n t_o \; , \tag{VII. 9a}$$

wherein t_o is the time required to reach point "O" from pericenter. Next, using eqs. (VII. 8a) and (VII. 7c) it is apparent that

$$\varphi_{1_o} = \frac{\pi}{2} - \epsilon_2 \; . \tag{VII. 9b}$$

This last expression states that the initial eccentric anomaly for orbit 1 is ϵ radians <u>less</u> than that of orbit 2. Consequently m_1 must move only $\frac{\pi}{2} - \epsilon$ radians along its path, to reach the initial point, while m_2 must move $\frac{\pi}{2}$

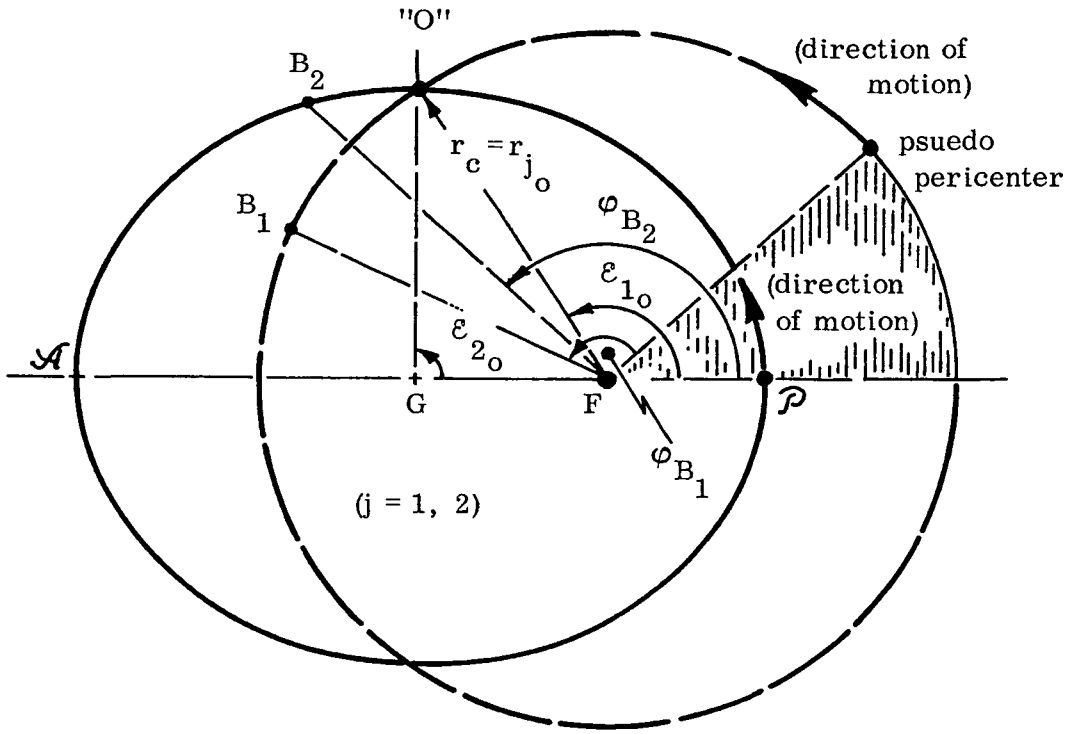

At initial point ("O"): $\varepsilon_{2_o} = \frac{\pi}{2}$, $\varepsilon_{1_o} = (\frac{\pi}{2} - \epsilon_2)$

Points B_j are representative positions beyond "O", (j = 1, 2)

Fig. VII.2. Orbit Geometry for the Study Example Case.

radians, from pericenter, to reach "O" in the same time, t_o.

One explanation of this is the following: The speed on path 1 is constant while that on path 2 varies. Then, near pericenter (2) the local speed $V_2 > V_c$ (local). (Actually, the speed on this path decreases from its value at pericenter to V_c (local) at "O"). Consequently m_2 moves over a larger angle in a given time than does m_1. Hence, there must be a "pseudo-pericenter"* (for path 1) which is located ϵ radians closer to "O" than the pericenter for path 2.

Now, making use of this idea, it is apparent that the increments in eccentric anomaly, locating points "B" on Fig. VII.2, beyond the initial point "O", are described by:

(a) for m_1:

$$\delta \mathcal{E}_1 \equiv (\mathcal{E}_{1_B} - \mathcal{E}_{1_o}) = \varphi_{1_B} - \varphi_{1_o} = \dot{\varphi}_1 (t_B - t_o) = \dot{\varphi}_1 \, \delta t; \qquad \text{(VII.10a)}$$

and, (b) for m_2:

$$\delta \mathcal{E}_2 \equiv (\mathcal{E}_{2_B} - \mathcal{E}_{2_o}) = 2 \left\{ \tan^{-1} \left[\sqrt{\frac{1-\epsilon_2}{1+\epsilon_2}} \left(\frac{\sqrt{1-\epsilon_2^2} \cos\theta - \epsilon_2 \sin\theta}{1-(\epsilon_2 \cos\theta - \sqrt{1-\epsilon_2^2} \sin\theta)} \right) \right] \right\} - \frac{\pi}{2}. \qquad \text{(VII.10b)}$$

To determine $\delta \mathcal{E}_1$ it is necessary to define the time increment, δt; this may be done in the following manner.

Since the time to reach "O", from pericenter "2", is

$$t_o = \frac{1}{n} \left(\mathcal{E}_{2_o} - \epsilon_2 \sin \mathcal{E}_{2_o} \right) = \frac{1}{n} \left(\frac{\pi}{2} - \epsilon_2 \right),$$

(see eqs. (VII.8a), (VII.7c)) then the time needed to reach a general point "B_2" from "O", is

*The "pseudo-pericenter" is nothing more than an "originating point" for path 1; this is where m_1 must start its motion in order to reach "O" at time t_o.

$$\delta t = t_B - t_o = \frac{1}{n}\left\{2\tan^{-1}\left[\sqrt{\frac{1-\epsilon_2}{1+\epsilon_2}}\left(\frac{\sqrt{1-\epsilon_2^2}\cos\theta - \epsilon_2\sin\theta}{1-(\epsilon_2\cos\theta + \sqrt{1-\epsilon_2^2}\sin\theta)}\right)\right]\right.$$

$$\left. + \frac{\epsilon_2\sqrt{1-\epsilon_2^2}\,(\epsilon_2\sin\theta - \sqrt{1-\epsilon_2^2}\cos\theta)}{1-\epsilon_2\,(\epsilon_2\cos\theta + \sqrt{1-\epsilon_2^2}\sin\theta)} - \left(\frac{\pi}{2} - \epsilon_2\right)\right\}, \qquad \text{(VII.11a)}$$

(this is the time increment, δt, in eq. (VII.10b).

Alternately, (see eq. (VII.10a)) the increment in transfer angle, $\delta\varphi_1$, from "O" to "B_1", is

$$\delta\varphi_1 = n\,\delta t. \qquad \text{(VII.11b)}$$

Eqs. (VII.10) and (VII.11) aid in defining the relative position of m_2, with respect to m_1, after m_2 has been placed on its orbit at the initial point "O". In the next section the relative position and velocity components are described for this example.

VII.5 Relative position and speed components. - The relative position for m_2 is defined by eqs. (F.5) in Appendix F. However, in utilizing those expressions, here, one should recognize that $r_1 = r_c$ while r_2 is obtained from eq. (VII.3), above. Also, for this problem the angle, ψ, in eqs. (F.5),is replaced by the quantity, $\delta\varphi_1$, eq. (VII.11b).

Next, taking account of eq. (VII.3), the relative position coordinates may be recast (in dimensionless form) as;

$$\xi \equiv \frac{x}{r_c} = \frac{(1-\epsilon_2^2)\,[\cos\theta\cos\alpha + \sin\theta\cos\iota\sin\alpha]}{1-\epsilon_2\,(\epsilon_2\cos\theta + \sqrt{1-\epsilon_2^2}\sin\theta)} - 1, \qquad \text{(VII.12a)}$$

$$\eta \equiv \frac{y}{r_c} = \frac{(1-\epsilon_2^2)[\sin\theta\cos\iota\cos\alpha - \cos\theta\sin\alpha]}{1-\epsilon_2(\epsilon_2\cos\theta + \sqrt{1-\epsilon_2^2}\sin\theta)}, \tag{VII.12b}$$

and

$$\zeta \equiv \frac{z}{r_c} = \frac{(1-\epsilon_2^2)\sin\theta\sin\iota}{1-\epsilon_2(\epsilon_2\cos\theta + \sqrt{1-\epsilon_2^2}\sin\theta)}, \tag{VII.12c}$$

wherein α has replaced $\delta\varphi_1$ for convenience of notation.

In these expressions α is a determinable function of θ and the eccentricity (ϵ) according to eq. (VII.11b).

Now, to obtain expressions for the relative speeds, using eqs. (F.13), Appendix F, it is necessary to take into account eqs. (VII.4) and (VII.6), and the definition, $V_c^2 \equiv \mu/r_1$. Making the required substitutions, and simplifying, it is found that (as dimensionless quantities) the speeds are;

$$\xi' \equiv \frac{\dot{x}}{V_c} = \frac{[\epsilon_2\sqrt{1-\epsilon_2^2} - \sin\theta]\cos\alpha + [\cos\theta - \epsilon_2^2]\cos\iota\sin\alpha}{\sqrt{1-\epsilon_2^2}}$$

$$+ \frac{(1-\epsilon_2^2)[\sin\theta\cos\iota\cos\alpha - \cos\theta\sin\alpha]}{1-\epsilon_2(\epsilon_2\cos\theta + \sqrt{1-\epsilon_2^2}\sin\theta)}, \tag{VII.13a}$$

$$\eta' \equiv \frac{\dot{y}}{V_c} = \frac{[\sin\theta - \epsilon_2\sqrt{1-\epsilon_2^2}]\sin\alpha + [\cos\theta - \epsilon_2^2]\cos\iota\cos\alpha}{\sqrt{1-\epsilon_2^2}}$$

$$- \frac{(1-\epsilon_2^2)[\cos\theta\cos\alpha + \sin\theta\cos\iota\sin\alpha]}{1-\epsilon_2(\epsilon_2\cos\theta + \sqrt{1-\epsilon_2^2}\sin\theta)}, \tag{VII.13b}$$

and

$$\zeta' \equiv \frac{\dot{z}}{V_c} = \frac{(\cos\theta - \epsilon_2^{\,2})\sin\iota}{\sqrt{1-\epsilon_2^{\,2}}} \quad . \tag{VII.13c}$$

Here, eqs. (VII.12) and (VII.13) define the relative position and speed of m_2 with respect to m_1. Note that from these expressions, for a given path (ϵ_2) and inclination (ι), the state variables are strongly dependent on θ - the position for m_2 measured from "O". Of course, the "size" of the reference orbit is also important here; this is evident by the implicit and explicit presence of r_1 $(=r_c)$.

VII.6 Path for the relative motion. - After having determined the state variables for this example, the expressions were found to produce an unusual geometry on some of the relative motion traces. Specifically, it has been found that marked changes in the displacement curves, for different sets of parameters describing path 2, can occur. In particular, the planar traces develop cusps for a proper set of parameters $(\epsilon_2,\ \iota)$.

To determine the relationship required between these parameters, leading to a cusp, the trace found on the $(\eta,\ \zeta)$-plane is considered, first.

When a cusp occurs the speed components η' and ζ' vanish, simultaneously; consequently, one finds that the conditions necessary for this are:

(1) $\cos\theta = \epsilon_2^{\,2}$,

and (2) $\iota = \cos^{-1}\left[\dfrac{(\sqrt{1-\epsilon_2^{\,2}} - \epsilon_2)^2}{\sqrt{1-\epsilon_2^{\,2}}} - \dfrac{\epsilon_2^{\,2}}{\sqrt{1-\epsilon_2^{\,4}}}\ \dfrac{\cos\alpha}{\sin\alpha}\right]$, (VII.14)

from eqs. (VII.13).

Now, using the first condition, above, the expression for α $(\equiv (\alpha)_{cr})^*$ becomes;

$^*(\alpha)_{cr}$ is the "critical" value; or, that value of α at which the cusp occurs.

$$(\alpha)_{cr} = 2\tan^{-1}\left\{\frac{\epsilon_2(\epsilon_2 - \sqrt{1-\epsilon_2^2})}{(1+\epsilon_2)(1-\sqrt{1+\epsilon_2^2}) + \epsilon_2^2}\right\} + \frac{\epsilon_2^2}{\sqrt{1+\epsilon_2^2}} - \left(\frac{\pi}{2} - \epsilon_2\right). \qquad \text{(VII.15)}$$

This expression and the second of eqs. (VII.14) depend on eccentricity alone; hence the relationship between (ι, ϵ_2) is explicitly defined. What this implies is that for a given eccentricity there is a unique inclination at which cusps may appear on the (η, ζ)-plane.

Analogous to the case above there are similar conditions defining cusps on the traces for the (ξ, ζ)-plane. These conditions, found from eqs. (VII.13) also, are:

(1) $\cos\theta = \epsilon_2^2$,

and

$$(2)\quad \iota = \cos^{-1}\left\{\frac{(\epsilon_2 - \sqrt{1+\epsilon_2^2})^2}{\sqrt{1-\epsilon_2^2}} + \frac{\epsilon_2^2}{\sqrt{1-\epsilon_2^4}}\,\frac{\sin\alpha}{\cos\alpha}\right\}. \qquad \text{(VII.16)}$$

Again, the value of $(\alpha)_{cr}$, implied by eq. (VII.16), is acquired from eq. (VII.15). The difference between these two situations is found in the argument of the arc-cosine term. As a consequence, cusps on the planes of the motion occur at different inclinations (ι), for a same eccentricity.

In order to show the variation of ι, with ϵ_2, a program was written to evaluate eqs. (VII.14), (VII.15) and (VII.16). Results from these calculations are found on Figs. VII.3.

Figs. (VII.3) show how ι must vary with eccentricity (ϵ_2), in order that cusps occur on the (η, ζ)- and (ξ, ζ)-planes, respectively. These graphs have a geometric similarity; however, the eccentricity range is larger for the graph describing cusps on the (ξ, ζ)-plane. Also, the maximum inclination at which cusps may occur, is largest for the traces on the (ξ, ζ)-plane. It is

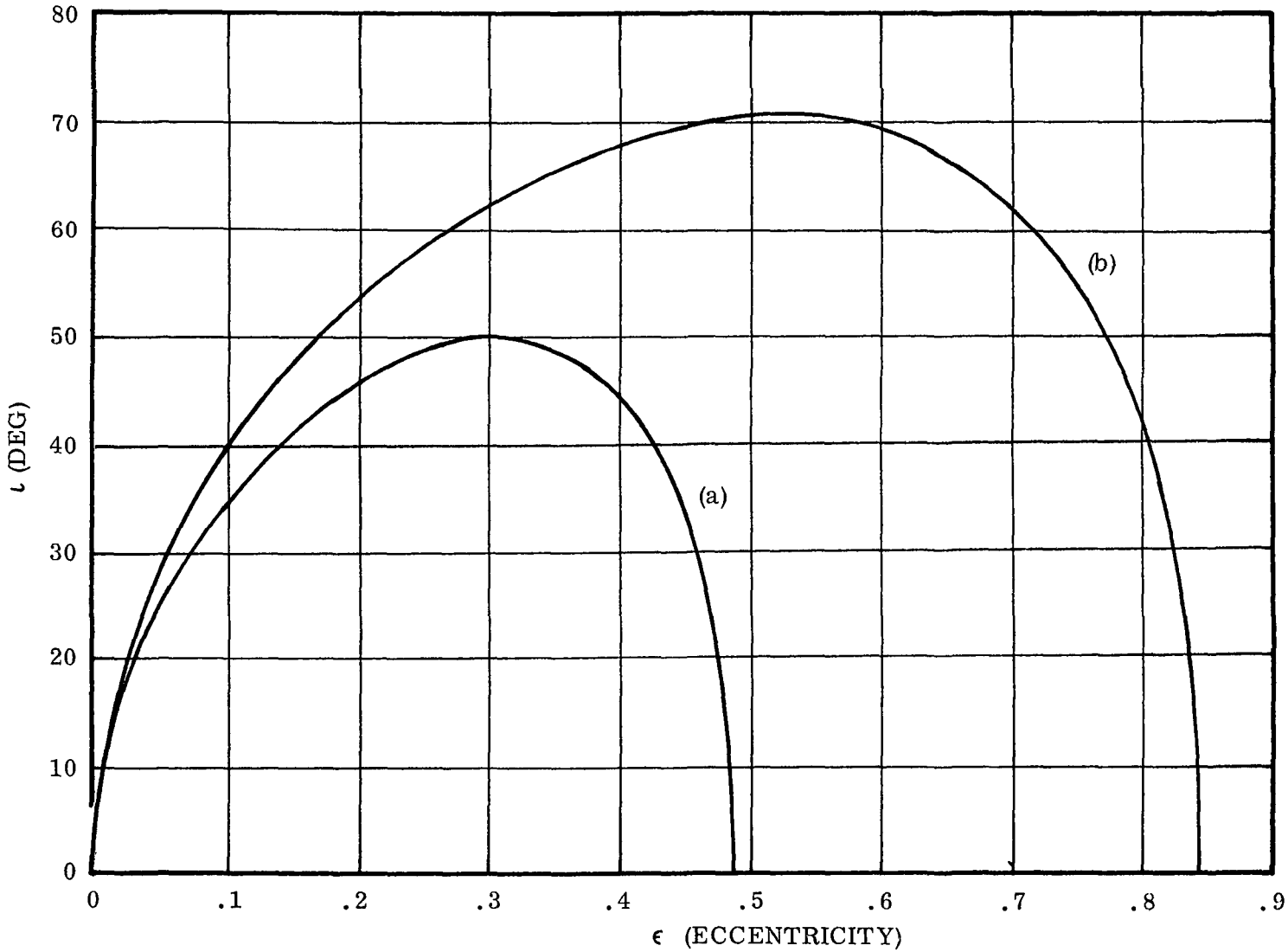

Fig. VII.3. Mapping of Inclination versus Eccentricity at which Cusps occur on Motion Traces. Curve (a) refers to the (η, ζ) plane; curve (b) to the (ξ, ζ) plane.

apparent, now, that cusps may occur, but only for a limited range of eccentricity (see the figures). Also, it is seen that the critical inclination changes most rapidly at the extremes of the eccentricity range; and, for a very small eccentricity cusps may occur on both planes at nearly the same inclination.

Fig. VII.4 delineates the critical values for θ and α as functions of the eccentricity. These are the special position angles at which cusps occur.

The angle θ_{cr} is seen to decrease with increasing eccentricity (beginning at $\theta_{cr} = \pi/2$), while the value of α_{cr} increases almost linearly with the eccentricity. For small eccentricity, θ_{cr} remains close to $\pi/2$, while α_{cr} increases markedly! No particular significance is attributed to these variations other than the fact that the cusps move "along" the planar traces, while the line of nodes is retrograde, as the eccentricity increases.

VII.7.1 Traces on the planes of motion. - Fig. VII.5 shows, in schematic, projections of a given "relative motion" on the three representative coordinate planes. In addition to this one can construct plots for the speed components, which are similar to the displacement traces but which represent the relative motion in an appropriate velocity-space.

In order to clarify several interesting aspects of this investigation, a series of plots has been prepared. These begin with a simplest case (Fig. VII.6), where a circular orbit relative motion ($\epsilon_2 = 0$) is described. Next is a series of traces (Fig. VII.7) for a slightly eccentric orbit, showing a progression in inclination through that for a cusp; and, finally, on (Fig. VII.8), plots for an inclination of $\pi/2$ are presented.

In the next several paragraphs these graphs will be discussed, with several salient points being noted.

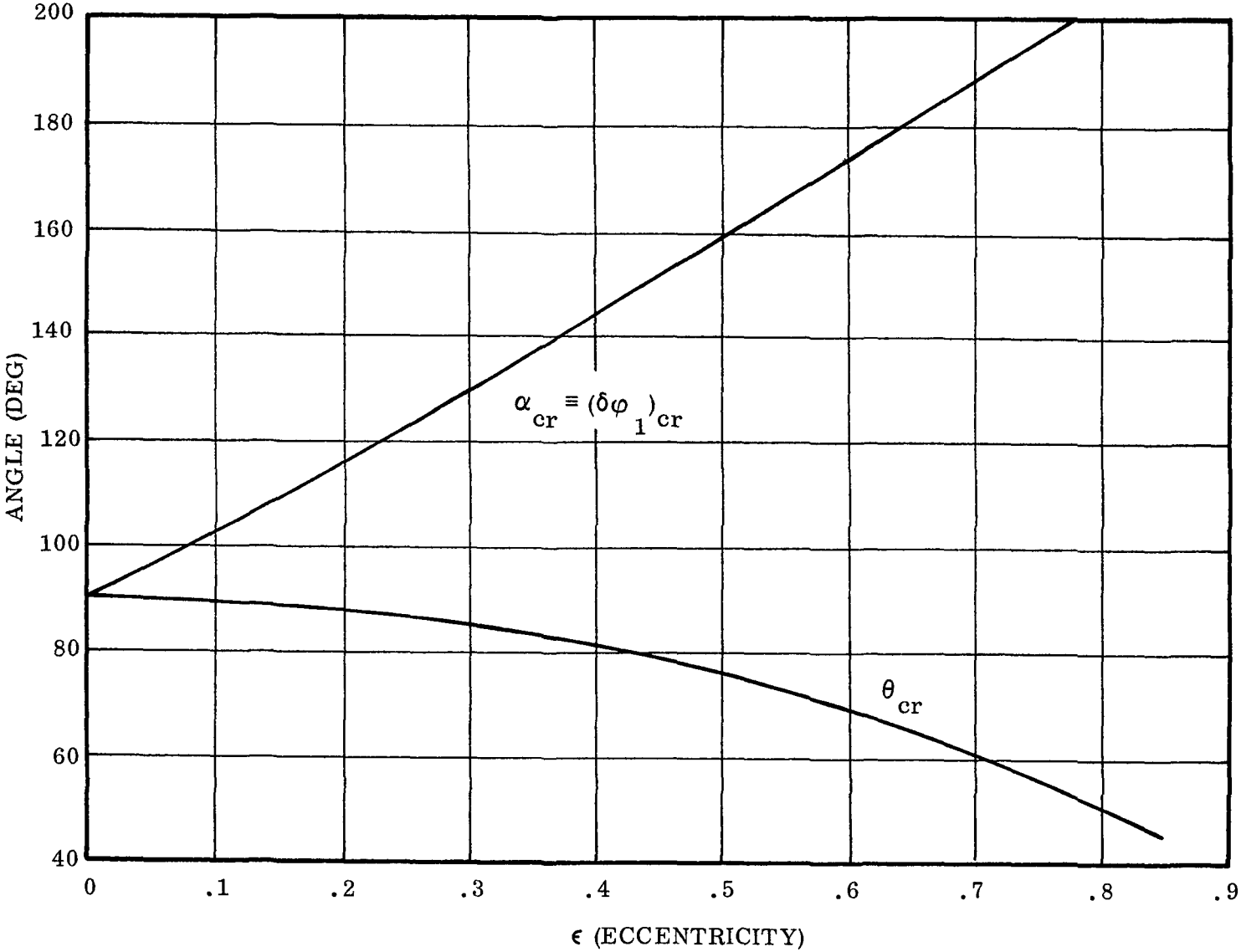

Fig. VII.4. Mapping of the Position Angles (α, θ), at which Cusps occur, versus Eccentricity.

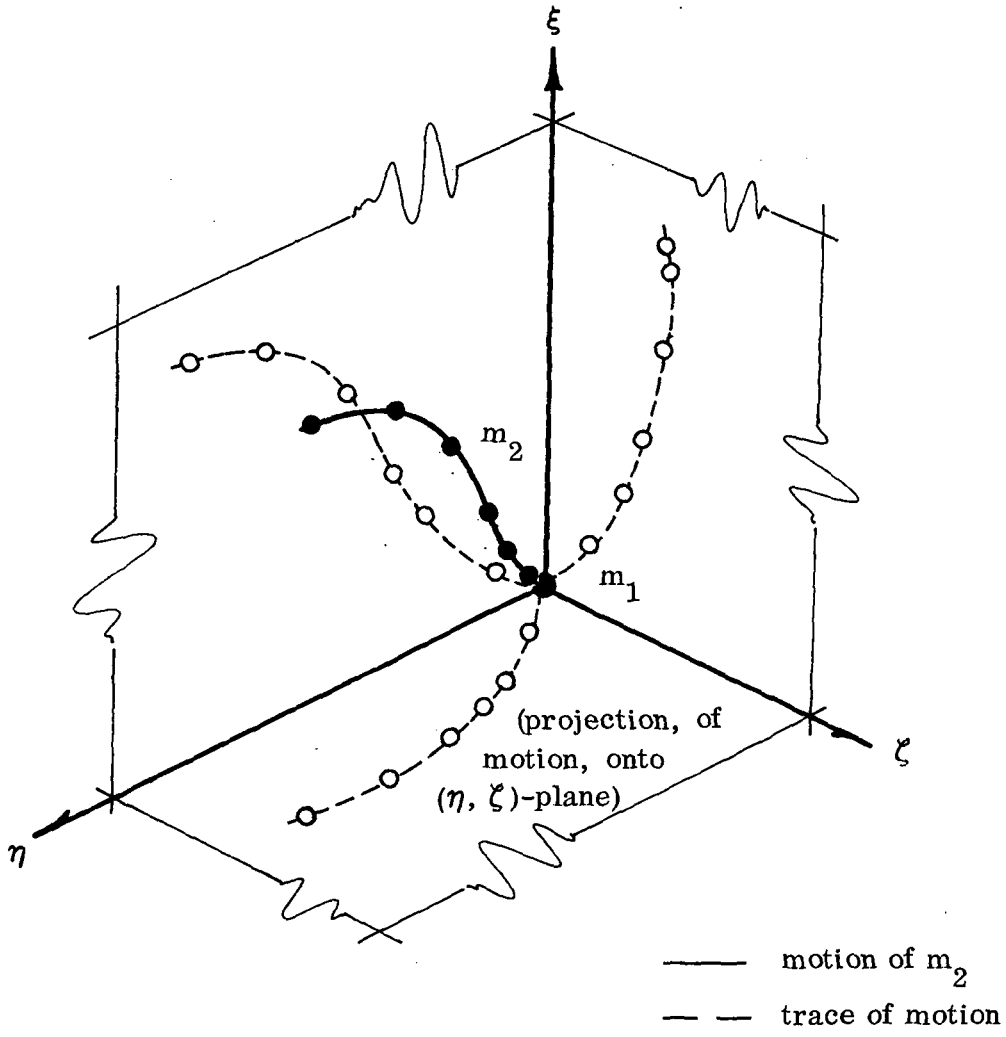

Fig. VII.5. Sketch depicting planar traces for a general three-space motion. Shown is a relative motion for m_2 with respect to m_1.

VII.7.2 Circular orbits for m_1 and m_2. - The simplest case for this relative motion problem occurs when both particles have circular orbits. Here, the critical inclination (for cusps) is zero degrees (see Fig. VII.3) while θ_{cr} and α_{cr} are both $\pi/2$ (see Fig. VII.4).

Traces for this case are found on Fig. VII.6; there the relative motion state for all inclinations, up to and including $\pi/2$, is inferred. That is, all non-zero inclinations are represented by geometrically similar curves -- the only difference between cases would be a change in scale.

Fig. VII.6a shows the motion traces onto the (ξ, η)-plane, in dimensionless, normalized (ξ, η) variables.* These traces will be circles on a properly scaled figure; however, each circular trace has a period which is half of the (m_1) orbital period. It should be apparent that the circles increase in size with increasing "ι". The view, on Fig. VII.6a, is indicative of the motion as seen from the $+\zeta$-axis position.

Fig. VII.6b describes the motion as it is projected onto the (η, ζ)-plane. The trace here is a view as seen from "above"; or, from the $+\xi$-axis. This figure has a period equal to that of the reference orbit; hence one "figure 8" is obtained for each complete orbit of m_1.

The trace for the (ξ, ζ)-plane is found on Fig. VII.6c. There the motion trace is as it would be seen from "behind" m_1. This is a trace from "IP" to the lower left extremity, back through "IP" to the right extremal, and thence to the "IP" again. All of this movement occuring in a time equal to the period of m_1.

The corresponding relative motion hodographs** are seen on these same figures. Because of the similarity to the displacement traces, the various hodographs are presented as noted in the captions. Dimensionless scales, initial points, (IP)', and directions of motion are as indicated on the plots. The periodicity of these graphs match that of the displacements for each geometrical figure type.

*On the graphs initial points are designated by (IP); coordinates of this point are, necessarily, (0, 0). On the hodographs a cross ("X") denotes the origin (0, 0). The arrows indicate the progression of motion on these figures.

**The hodographs are scaled in dimensionless values. The normalizing quantity, used here, is the speed of the reference particle (m_1); i.e., $V_1 = V_c$.

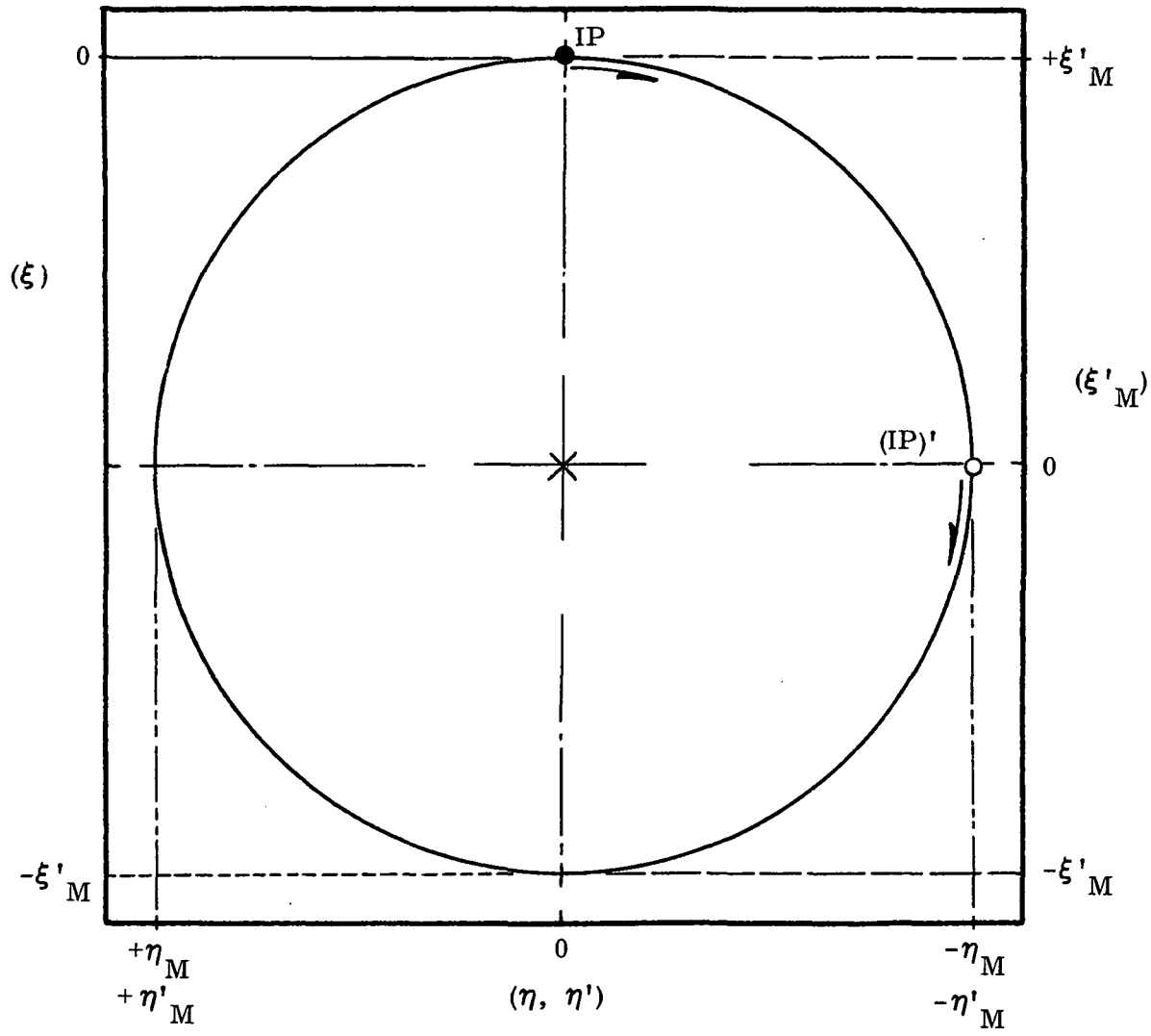

Fig. VII.6a. Relative Motion Traces, on the (ξ, η) and (ξ', η') planes, for m_2, when Both Particles move on Circular Orbits. Trace equations are: $(\xi + (1-\cos \iota)/2)^2 + \eta^2 = ((1-\cos \iota)/2)^2$; $\xi'^2 + \eta'^2 = (1-\cos \iota)^2$ Extremals are: $\xi_M = 1-\cos \iota$, $\eta_M = (1-\cos \iota)/2$; $\xi'_M = 1-\cos \iota = \eta'_M$. These circles have a period which is half the orbit period.

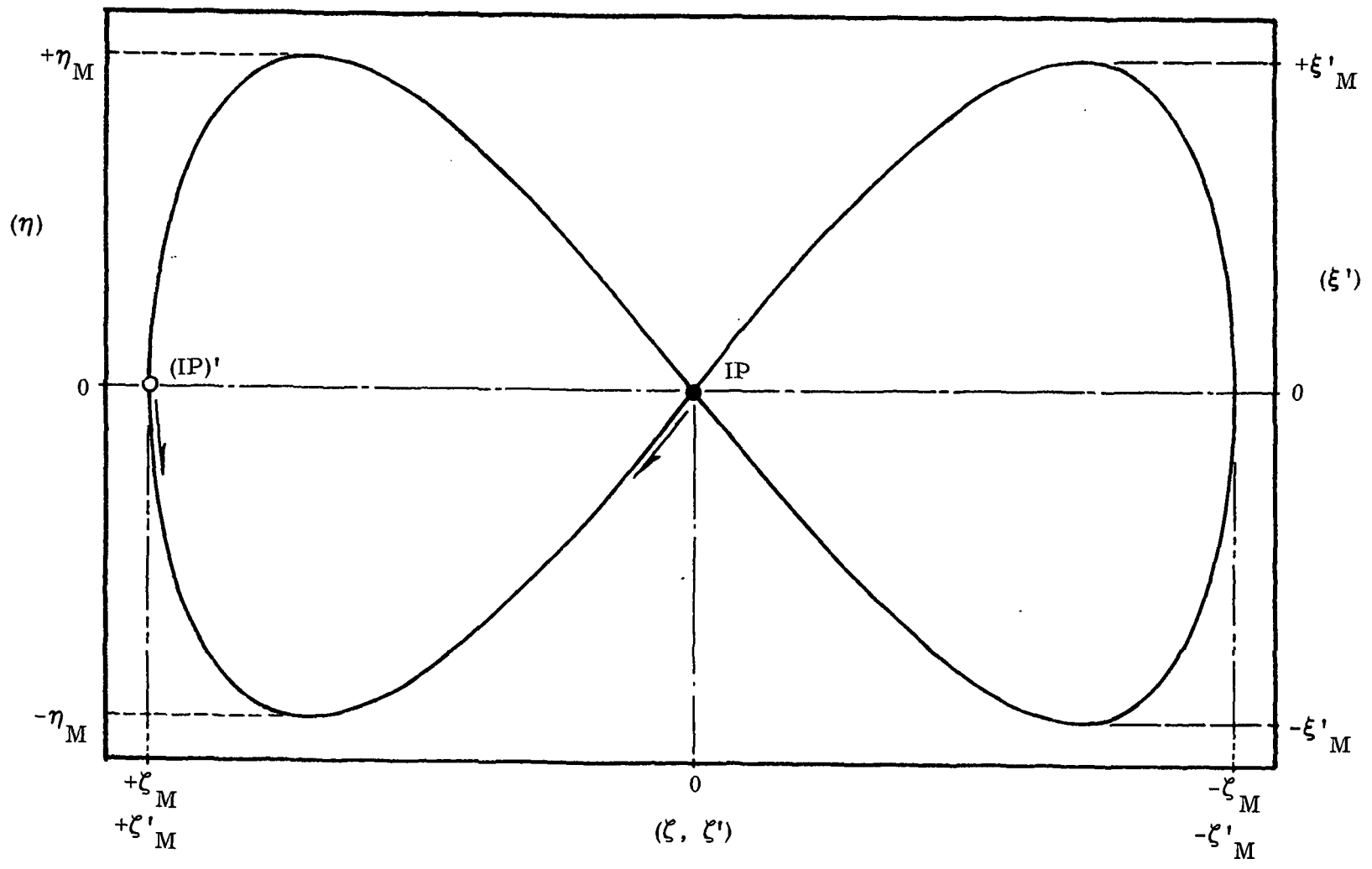

Fig. VII.6b. Motion Traces on the (η, ζ) and (ξ', ζ') planes for Both Particles on Circular Orbits. The traces are lemniscates: $\eta \sin \iota = \zeta\,(1-\cos \iota) \cos \theta$; $\xi' \sin \iota = -2\zeta'\,(1-\cos \iota) \sin \theta$. Extremals for these curves are: $\eta'_M = (1-\cos \iota)/2$, $\zeta_M = \sin \iota$; $\xi'_M = (1-\cos \iota)$, $\zeta'_M = \sin \iota$.

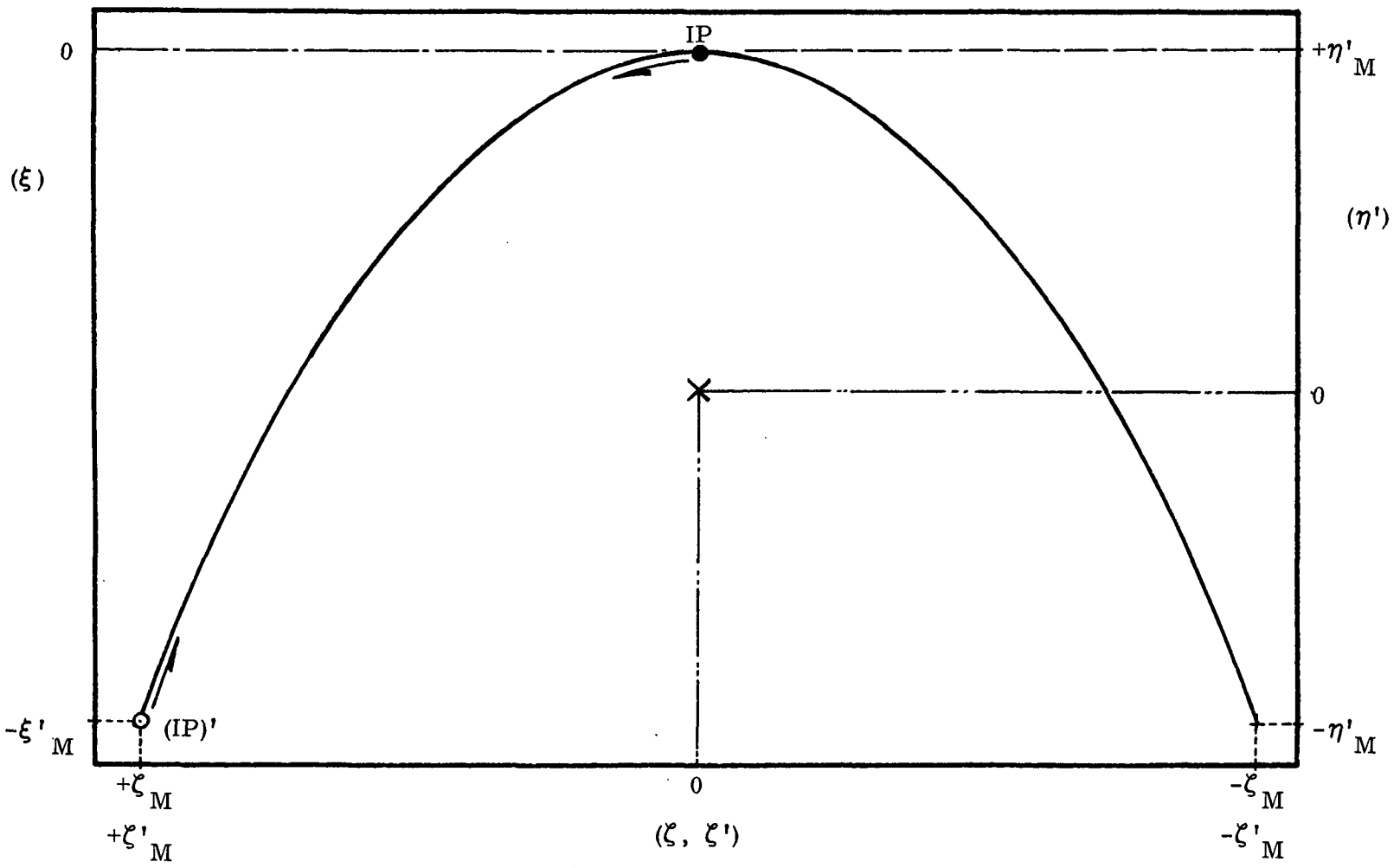

Fig. VII.6c. Traces on the (ξ, ζ) and (η', ζ') planes for Both Particles Moving along Circular Paths. The parabolas are defined by: $\xi = -\zeta^2 (1-\cos \iota)/\sin^2 \iota$, and $\eta' (1+\cos \iota) = \sin^2 \iota - 2\zeta'^2$. Extremals for the traces are: $\xi_M = (1-\cos \iota) = \eta'_M$, $\zeta_M = \sin \iota = \zeta'_M$.

Looking, for a moment, at the (ξ', ζ') hodograph (Fig. VII.6b), it is apparent that a cusp can occur on the (ξ, ζ)-plane since this curve passes through the origin of the graph. Of course this geometry is seen on the displacement figure.

(It should be noted that in this analysis "ι" is a bounded parameter. This restriction is made since, for $\iota > \pi/2$, the trace(s) would infer retrograde motions -- a condition not considered here).

VII.7.3 The evolution of a cusp. - Fig. VII.7 shows a motion trace with a "cusp", in addition to traces for orbits having inclinations less than and greater than the critical value (for the prescribed eccentricity).

Specifically, these plots shown here are for $\epsilon_2 = 0.1$,* and for inclinations, $\iota \cong 24.38^{\circ}$ (below the critical); $\iota \cong 34.38^{\circ}$ (the critical value); and, $\iota \cong 44.38^{\circ}$ (an inclination above the critical). On these plots the scales are incremented so that the curves show an undistorted geometric shape for the traces.

On Fig. VII.7a, the "bean-shaped" curve is typical of subcritical traces. Next is the critical case with what appears to be a cusp; and, finally, there is a trace with a "loop" which is typical of above-critical inclinations.

It should be apparent that the smooth (pre-critical) trace degenerates to "almost a cusp"; and, finally, the trace folds over itself forming a "loop" indicating a local reversal in the direction of the relative motion.

The true cusp, for this eccentricity, is found on Fig. VII.7b. There the smooth (pre-critical) curve develops into a cusp; and, finally forms a "loop" at the super-inclination. The direction of motion, for a full excursion on each plot, is noted on the figure.

For comparison, Fig. VII.7b should be reviewed along with Fig. VII.6b; this will illustrate the influence of eccentricity (and/or inclination) on this re-

*This choice of eccentricity was arbitrary.

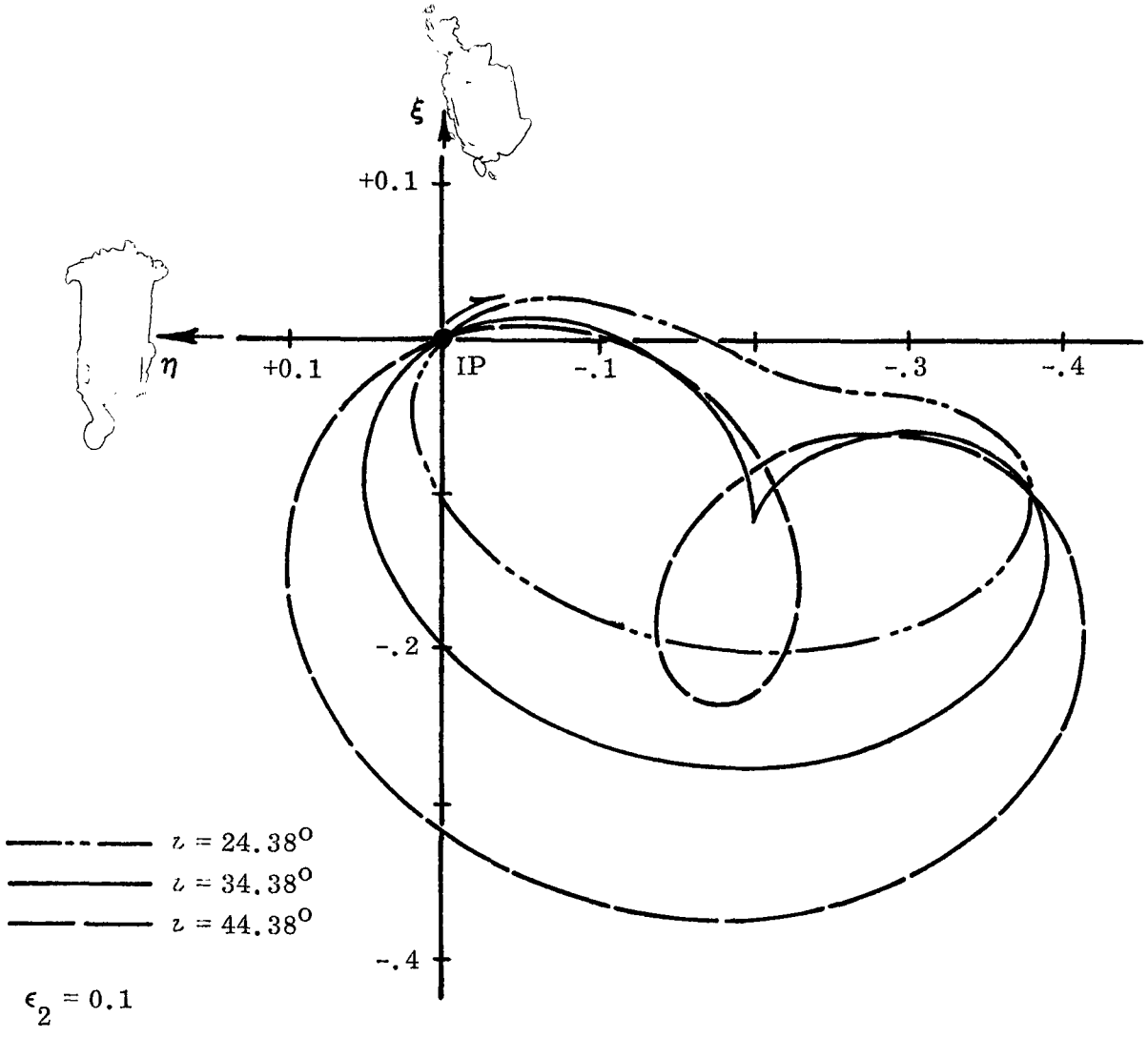

Fig. VII.7a. Traces of Relative Motion describing the evolution of a Cusp. Motion projected onto the (ξ, η)-plane for below, critical and super-critical inclinations.

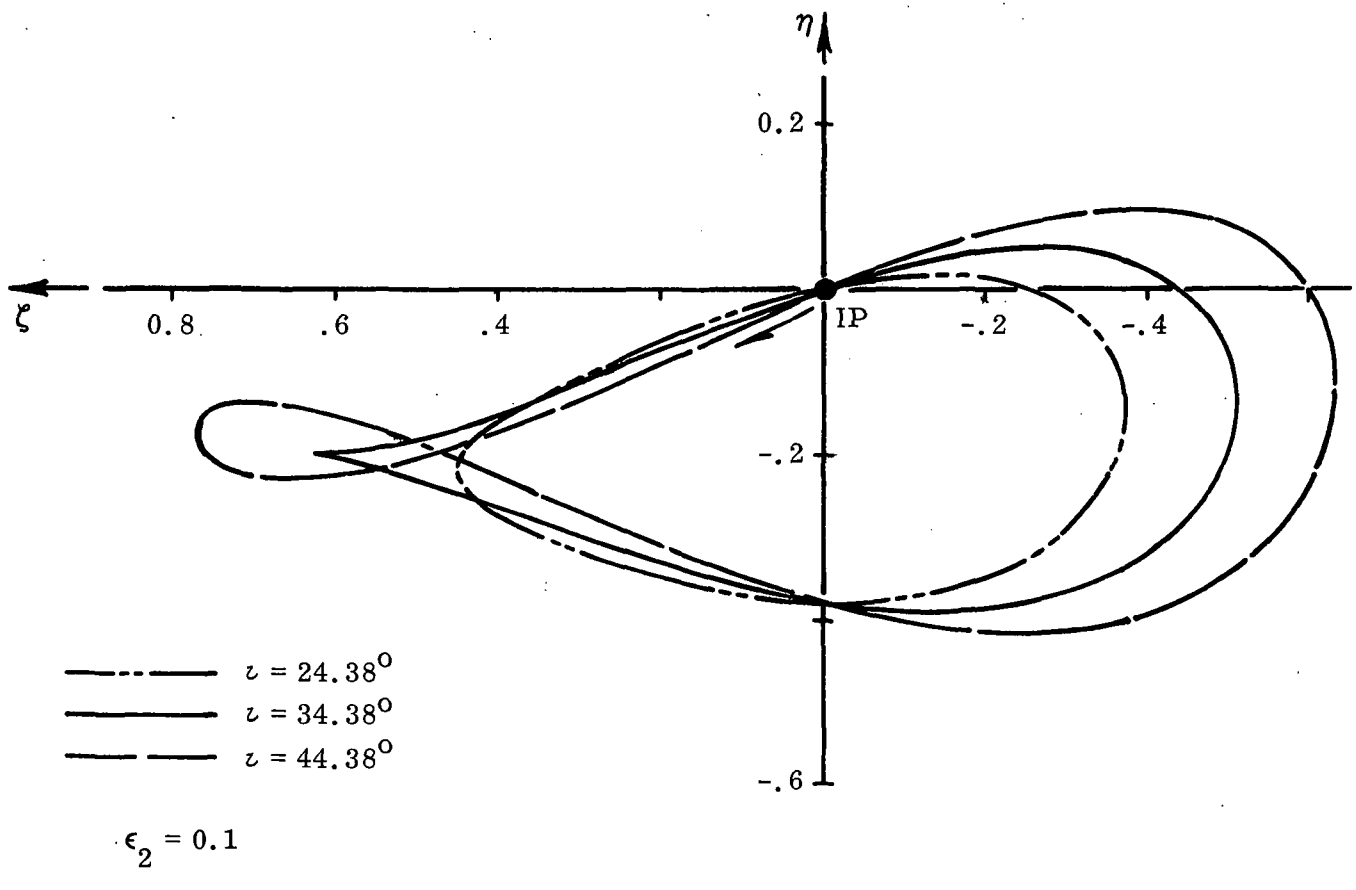

Fig. VII.7b. Motion Traces on the (η, ζ)-plane for a Cusp, occuring at $\iota = 34.38^{\circ}$ ($\epsilon_2 = 0.1$). Shown are projection at, below, and above the critical inclination.

lative motion.

Fig. VII.7c is analogous to Fig. VII.6c; but, here, the trend toward the cusp is fully evident. Also, the "loop" formed at the post-critical inclination, is quite apparent. (All of these traces are for one orbital period, only.)

The hodographs, Figs. VII.7d, VII.7e, are akin to the plots for the circular case ($\epsilon_2 = 0$), shown on Figs. VII.6. In the present instance one can detect the cusp from the (η', ζ') curves since one graph passes through the origin. For all of the remaining hodograph traces this condition is not found; hence the cusp is typical to the (η, ζ)-plane, alone.

VII.7.4 The extreme inclination of an eccentric orbit. - On Figs. (VII.8a) through (VII.8f) the relative motion traces for an extreme inclination ($\iota = \pi/2$), at eccentricity, $\epsilon_2 = 0.1$, are found.

If these graphs are compared with Figs. (VII.6), one sees that they tend toward the former case. Obviously the symmetry of Figs. (VII.6) is absent, here, because of the orbit's eccentricity; needless to say, this asymmetry would necessarily increase with increasing eccentricity. As in the circular orbit case, here one plane exhibits a double "loop", with each "loop" of the trace having a period roughly equal to half of that for the reference circular orbit.

From an inspection of the hodographs, it is evident that no cusps are predicted since none of the plots pass through the origin.

VII.7.5 Range and range-rate information. - In order to illustrate how range and range-rate information may be influenced by the presence of a cusp, a set of curves has been prepared. These graphs were obtained from the calculations made for Section VII.7.3, above (for the critical inclination); and are designated here as Fig. VII.9. Note that these data are presented in dimensionless (or, normalized) form, and are plotted against position angle, referred to the m_1 orbit.

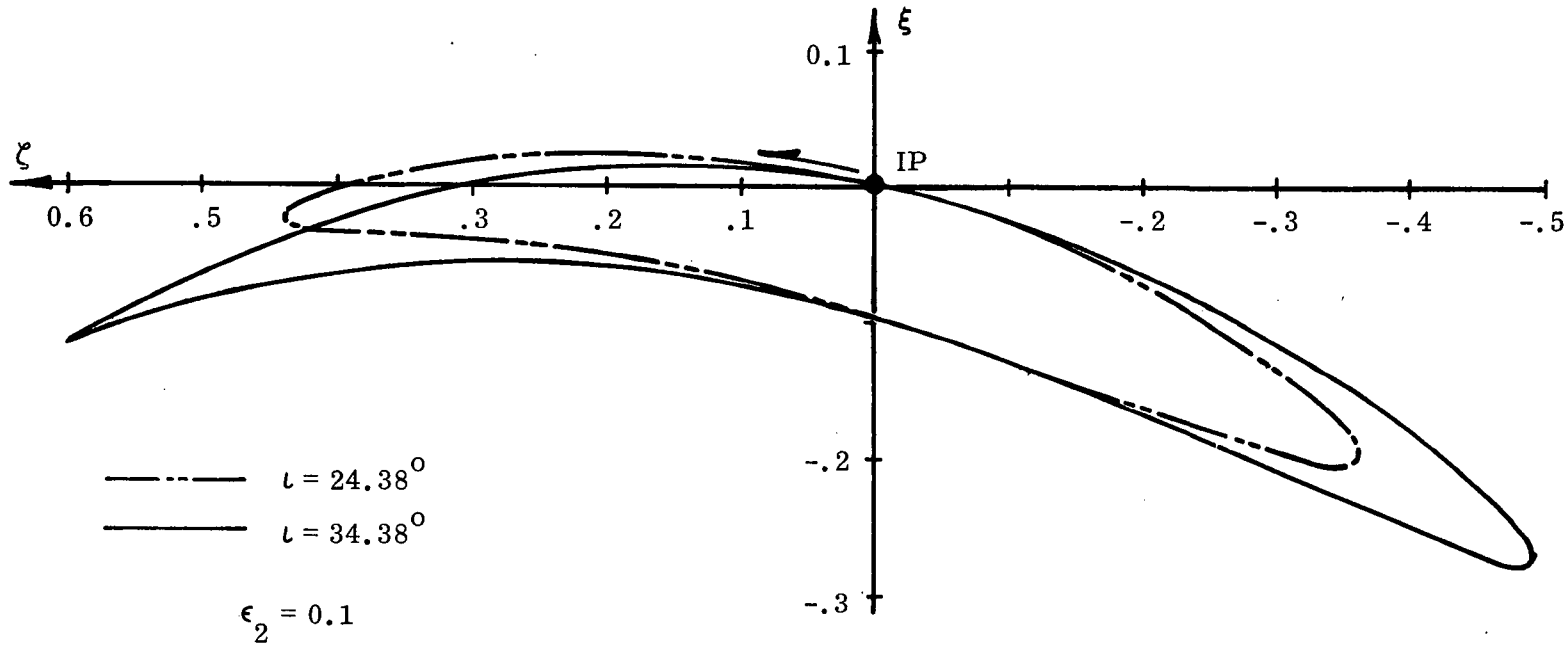

Fig. VII.7c. Projections of a Relative Motion, onto the (ξ, ζ)-plane, for Cusp occuring at $\iota_{cr} = 34.38^{\circ}$.

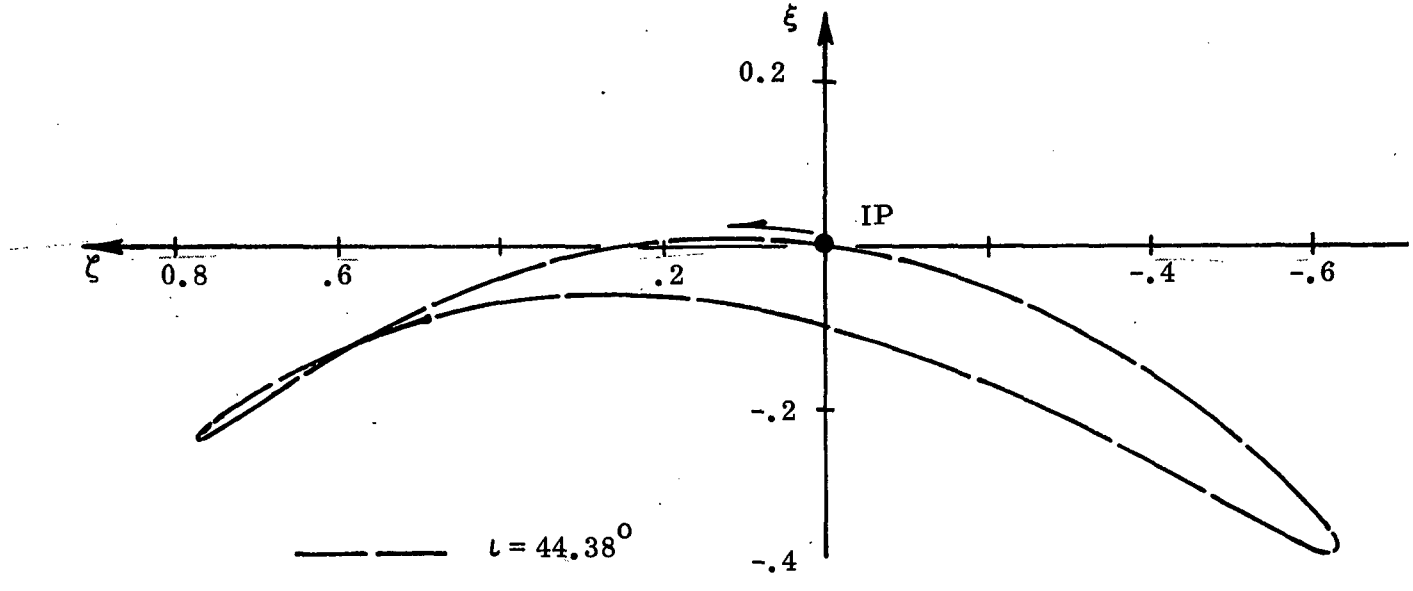

Fig. VII.7c. (concluded)

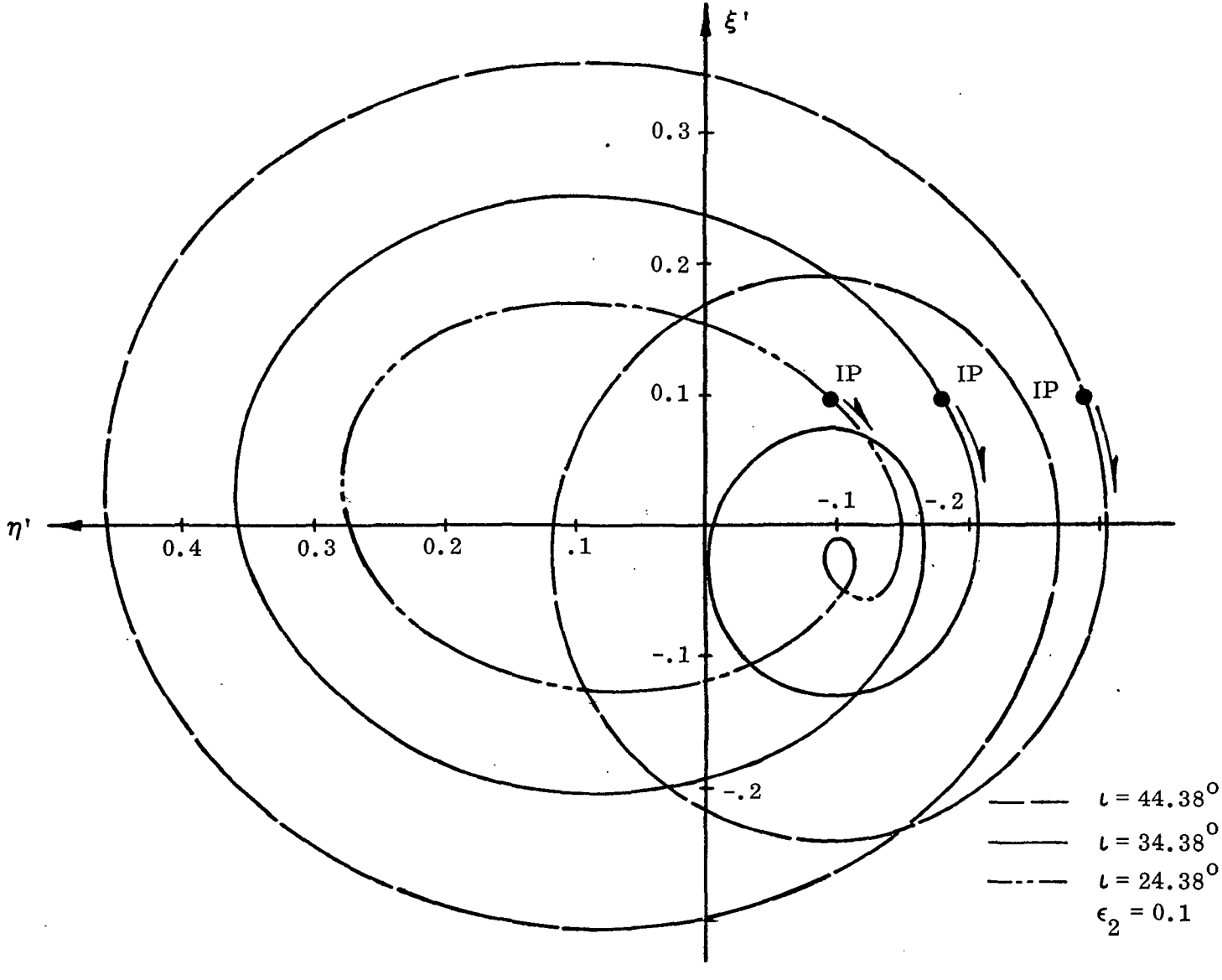

Fig. VII.7d. Hodograph Traces for the Development of a Cusp on the (η, ζ)-plane.

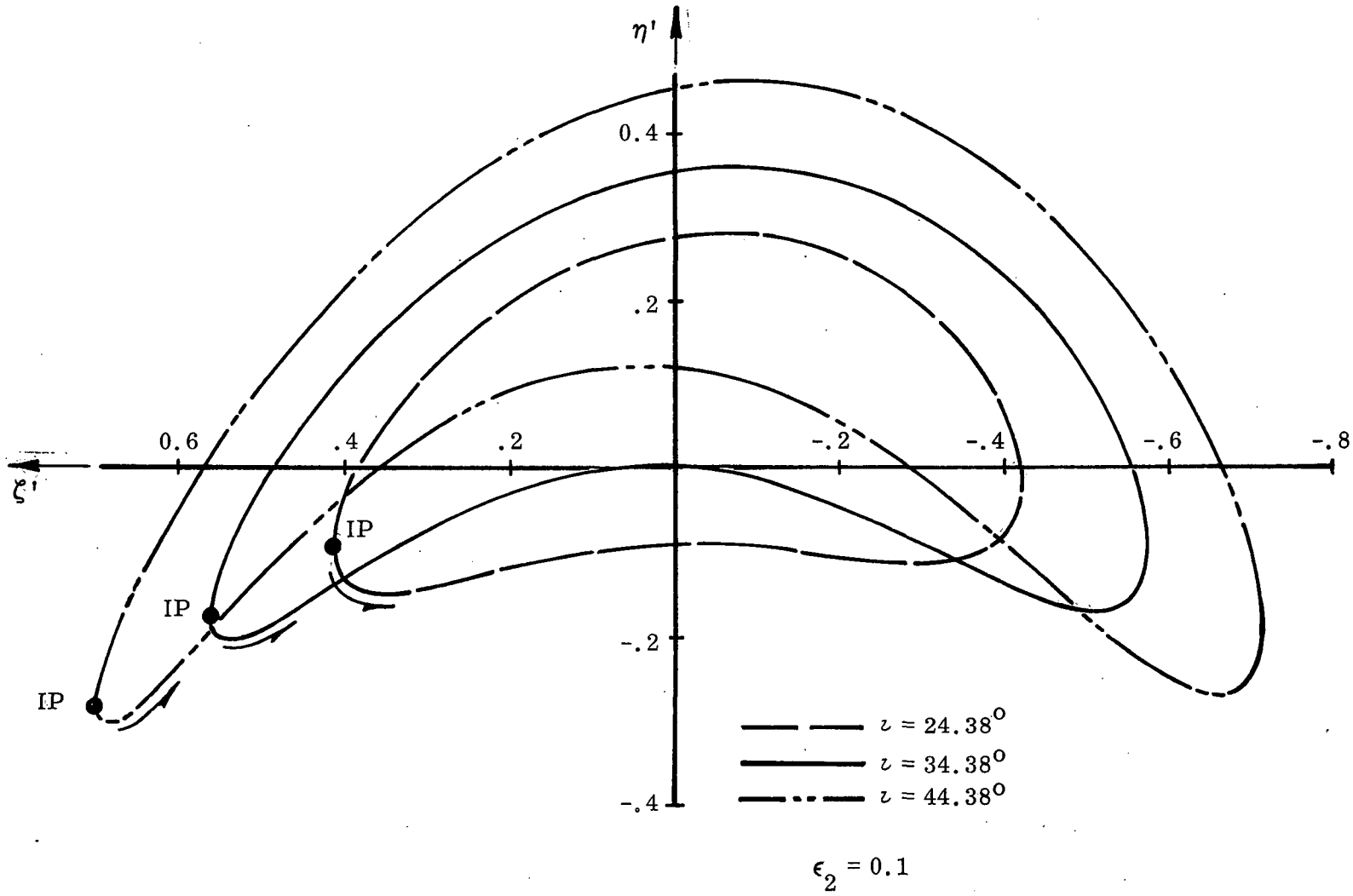

Fig. VII.7e. Hodograph Projections, onto the (η', ζ')-plane, for a cusp in the (η, ζ)-traces. (Note the curve for $\iota = 34.38^{\circ}$ passes through origin).

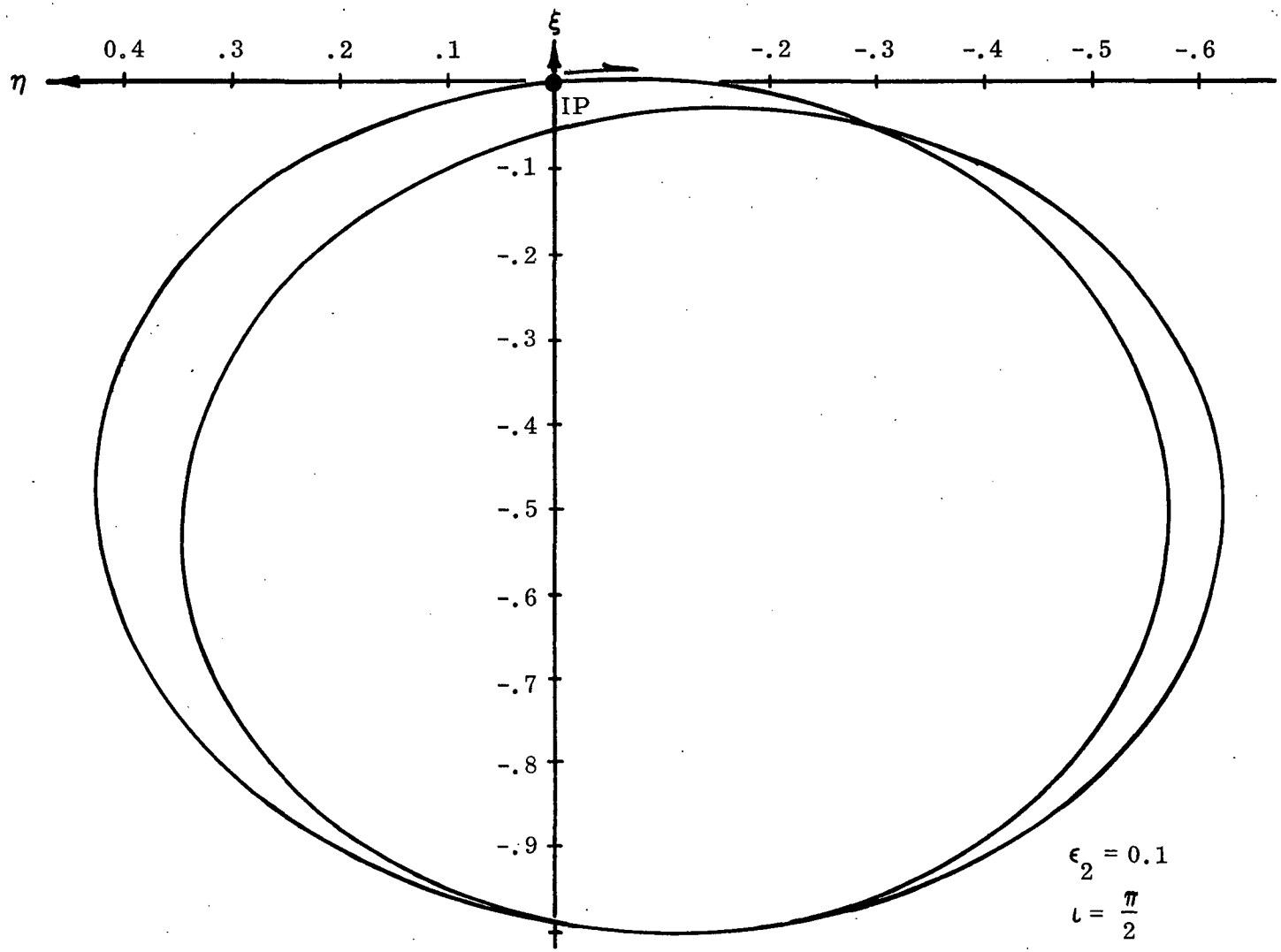

Fig. VII.8a. Relative Motion Trace, on the (ξ, η)-plane, at $\iota = \pi/2$, for an Orbit Eccentricity ($\epsilon_2 = 0.1$). Note: the trace produces two circuits per orbit, and tends to a circular orbit case (Fig. VII.6).

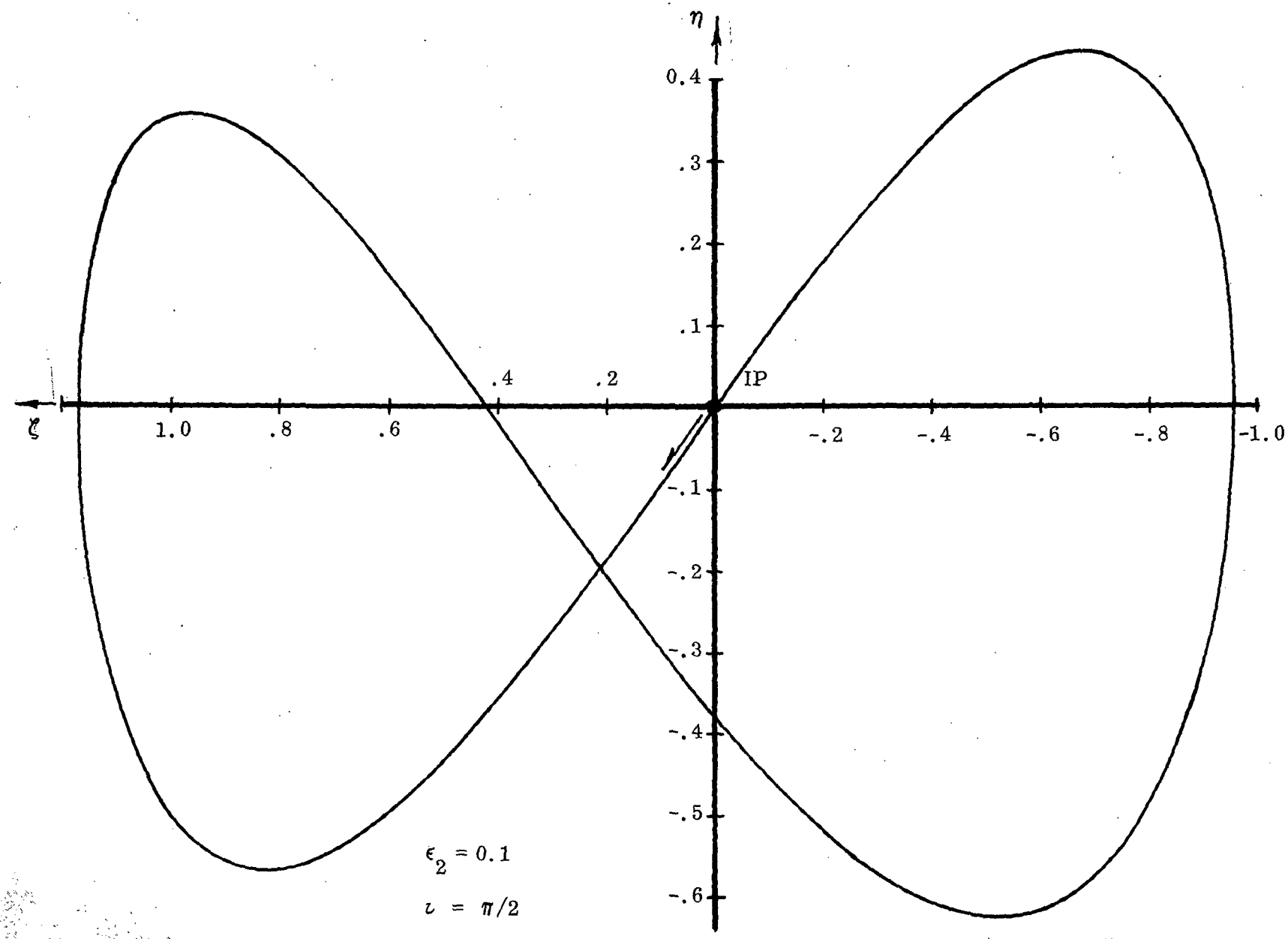

Fig. VII.8b. Relative Motion Traces, at $\iota = \pi/2$, on (η, ζ)-plane. Compare this graph with Fig. VII.6b ($\epsilon = 0$).

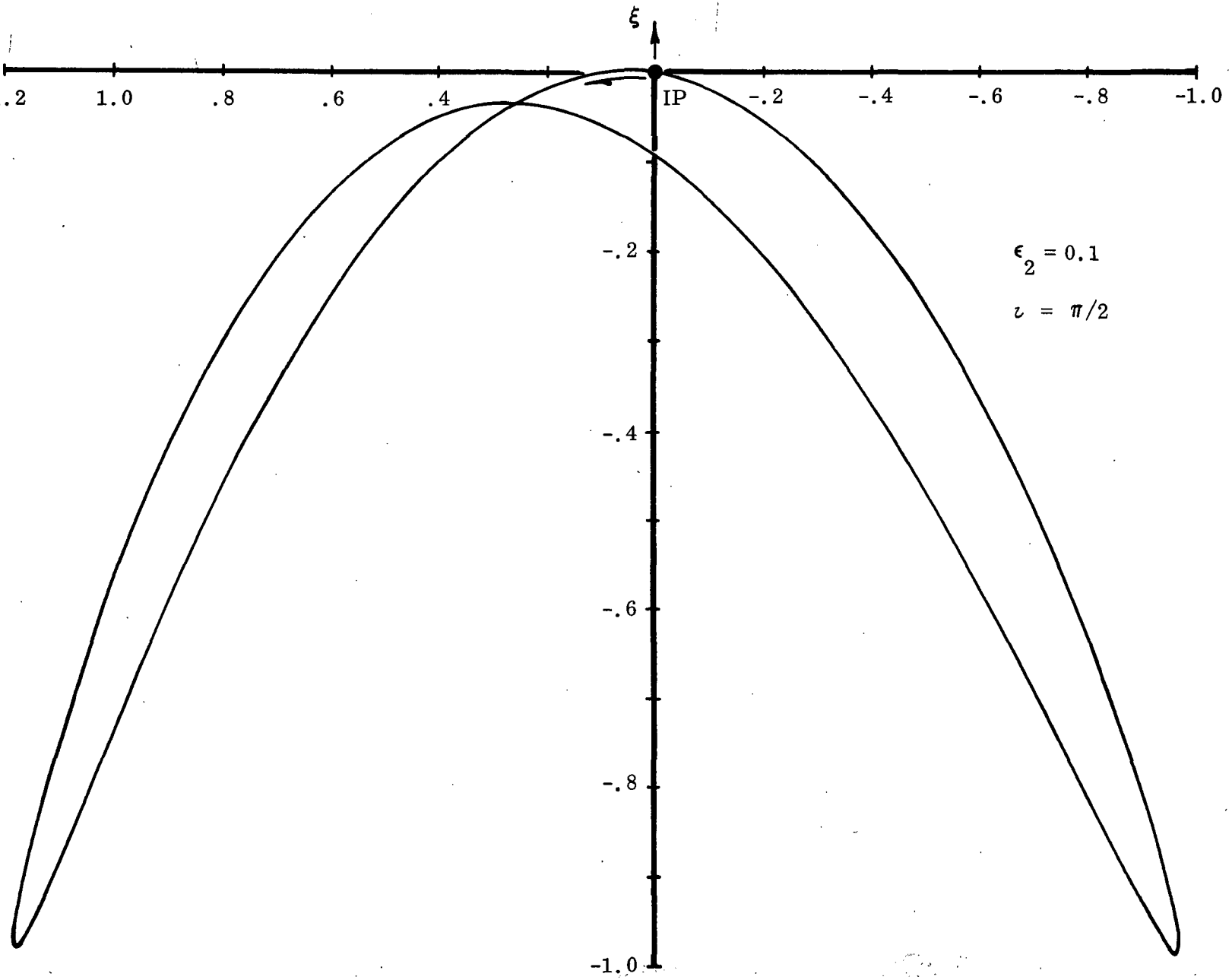

Fig. VII.8c. Continuation of Extreme Inclination Motion Traces. Compare this plot with Fig. VII.6c.

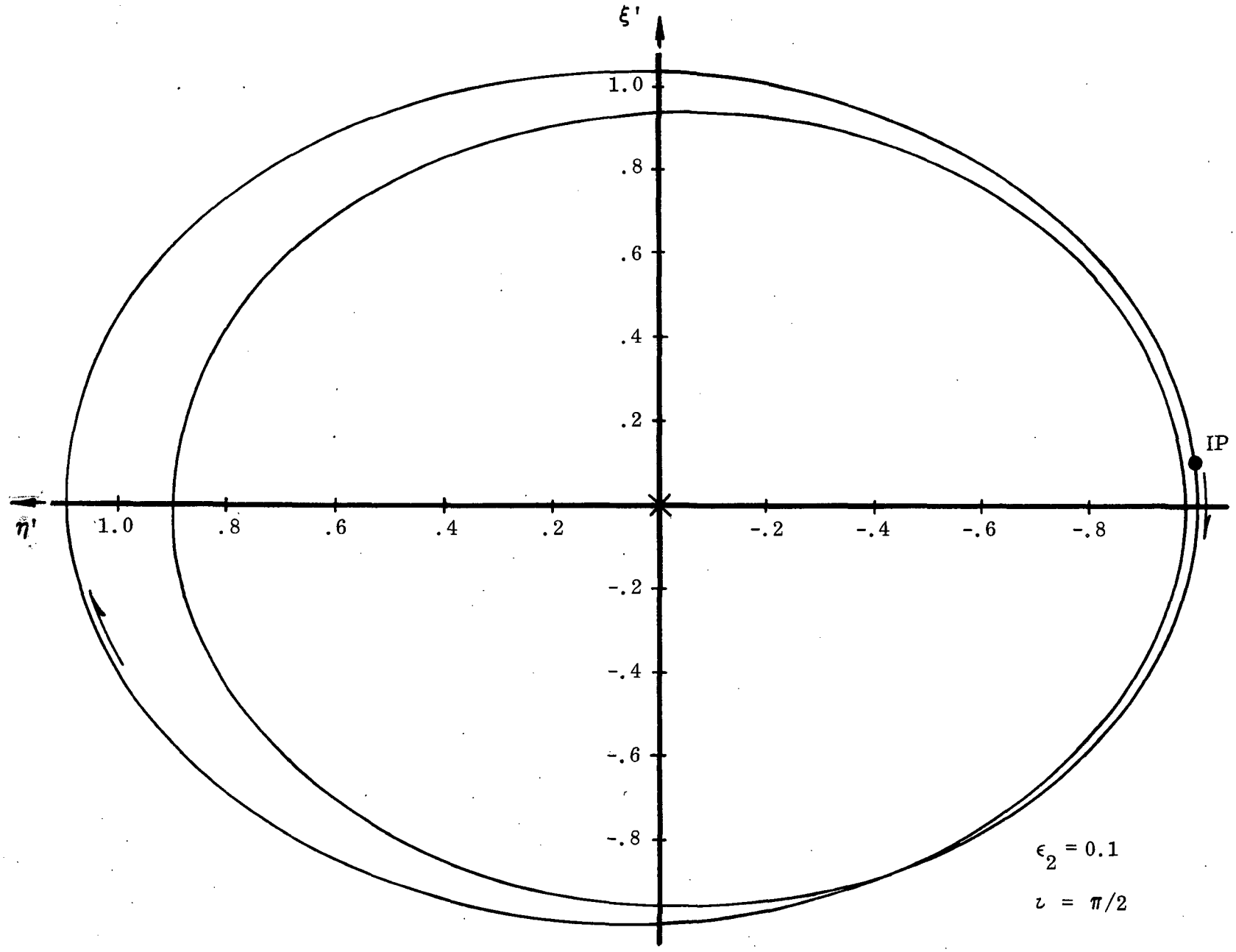

Fig. VII.8d. Hodograph Plot for the Extreme Inclination Relative Motion Case. Note this trace has two circuits per orbital period. Compare with Fig. VII.6a (circular orbit).

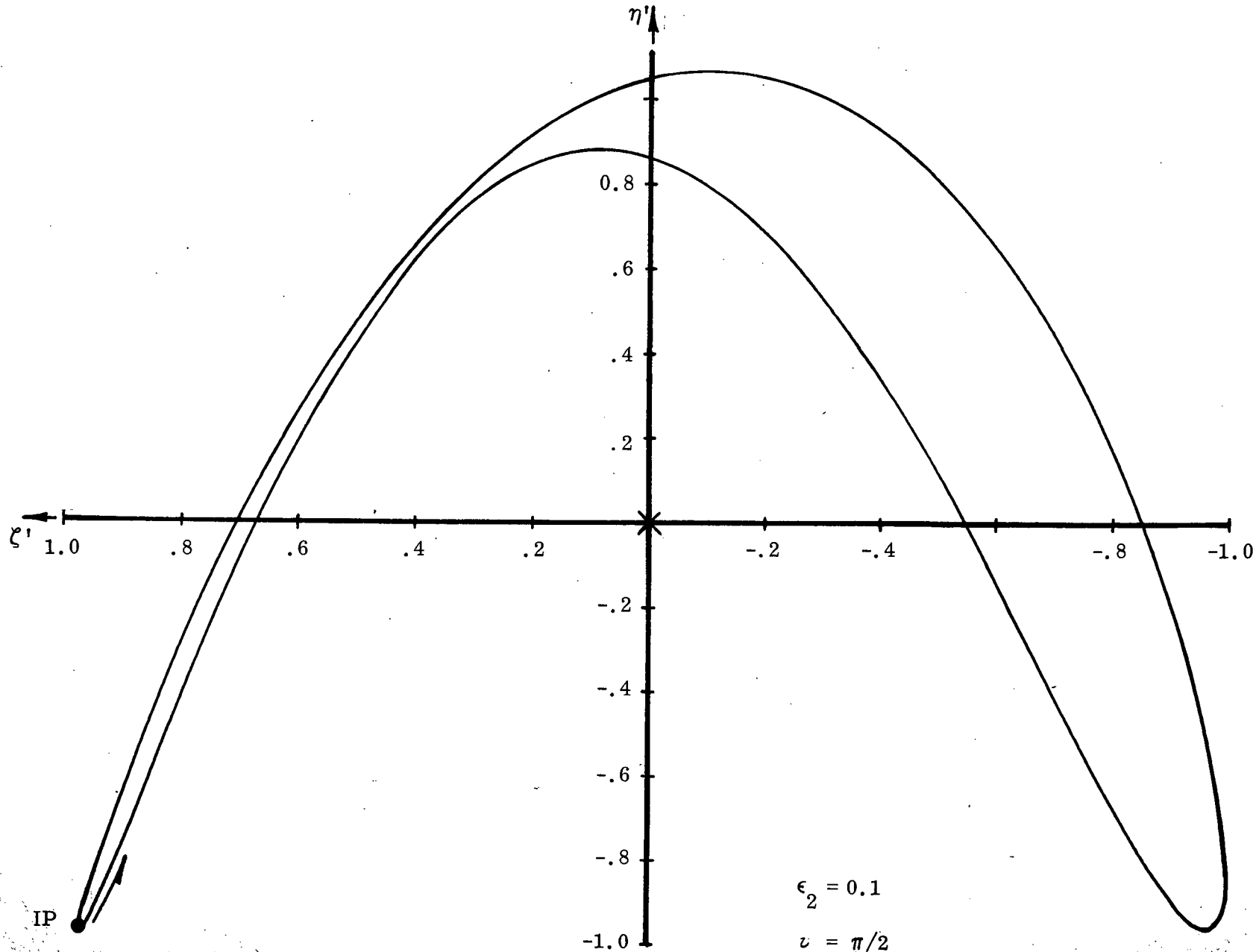

Fig. VII.8e. Hodographs for Extreme Inclination Problem (continued). Compare with Fig. VII.6c.

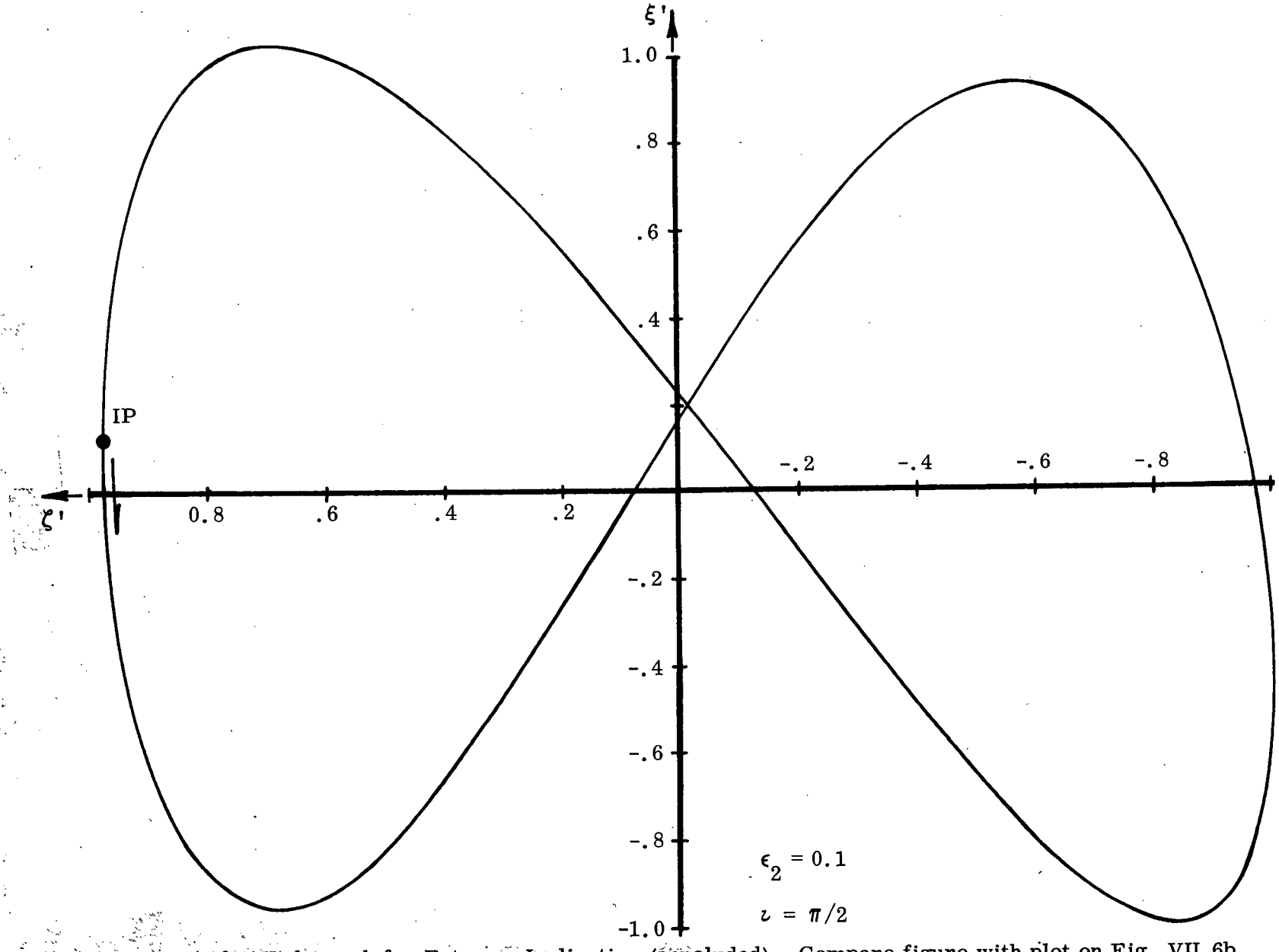

Fig. VII. 8f. Hodograph for Extreme Inclination (concluded). Compare figure with plot on Fig. VII. 6b.

It is clear, now, that range-rate does not vanish during the period of motion, even though it does diminish to a comparatively low level, in the neighborhood of the cusp. What is more interesting is that the range-rate curve is composed of two, nearly symmetric, segments - these segments having their local minima at about π radians apart. Though it is not immediately apparent, the interior maximum is the true maximum for the figure, in this case.

The range data, plotted here, shows that m_2 is cyclic in its relative distance from m_1, during the period of motion. It should be remembered that these body motions are of equal period; and, that these data would be repeated for each orbital excursion of the particles.

VII. 8 General comments. - In this section of the report general and specific relative motion expressions have been obtained, based on specific assumptions. To demonstrate the deterministic relative motion results an example was selected for study; and, in particular, the one chosen developed a "cusp" on one of the motion traces.

Other case studies were also included for comparison and illustrative purposes. These were a case considering zero eccentricity; and one for maximum inclination at a selected eccentricity. These examples were indicative of the degree of variation which could be expected for this type of relative motion problem.

The most revealing feature of the plotted traces was the "evolution of a cusp" on one of the coordinate planes. The graphs clearly show the change in geometry, associated with the cusp, as it is developed. It should be mentioned that this phenomenon was not found in the corresponding linearized solutions; apparently it was lost when higher ordered terms were deleted from the describing differential equations. It is significant to note, also, that the "cusp" was found by the deterministic solution, it was not a consequence of numerical evaluations.

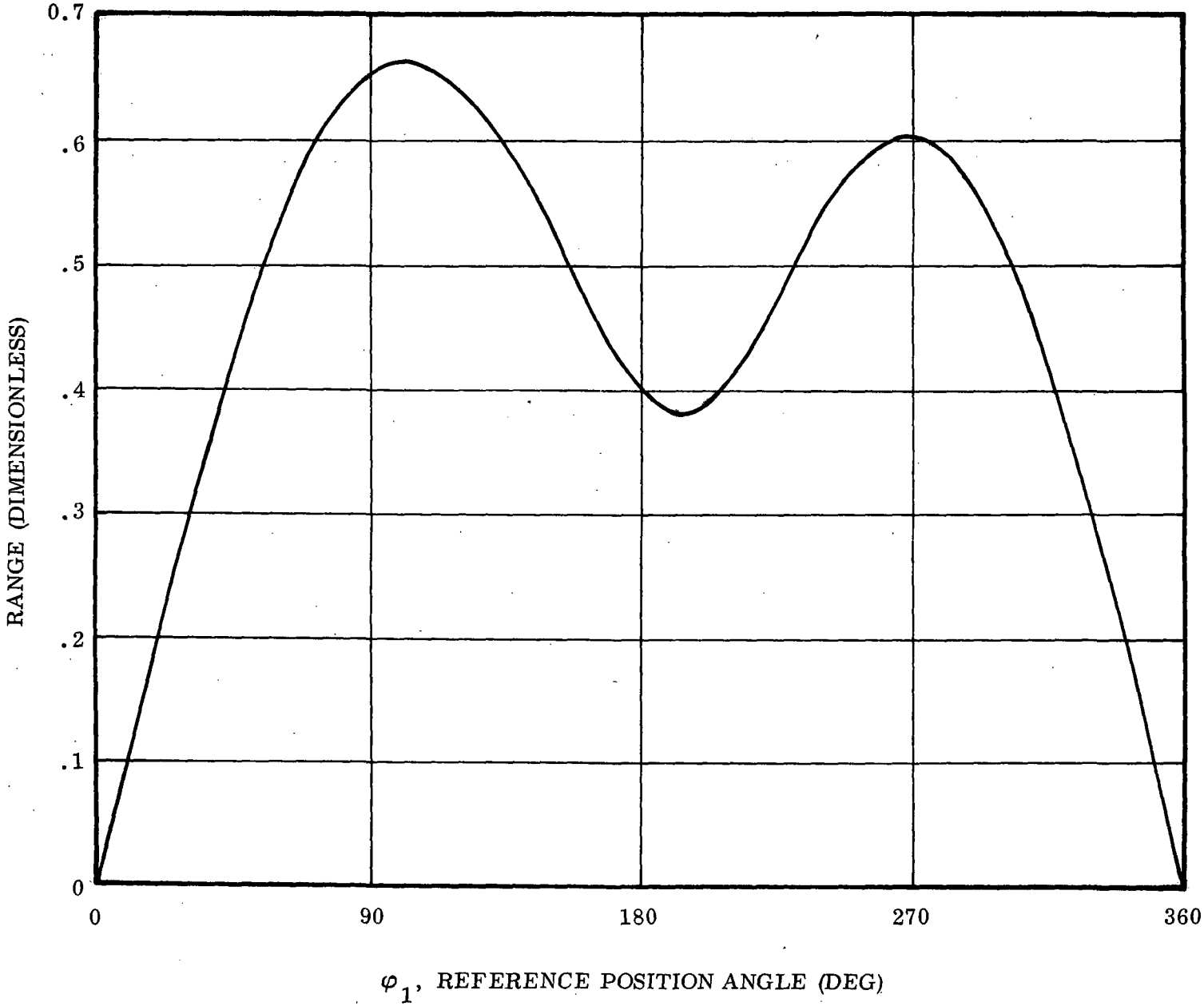

Fig. VII.9a. Dimensionless Relative Range Variation with Reference Position Angle (φ_1) for the critical inclination case ($\iota_{cr} = 34.38^{o}$, $\epsilon_2 = 0.1$).

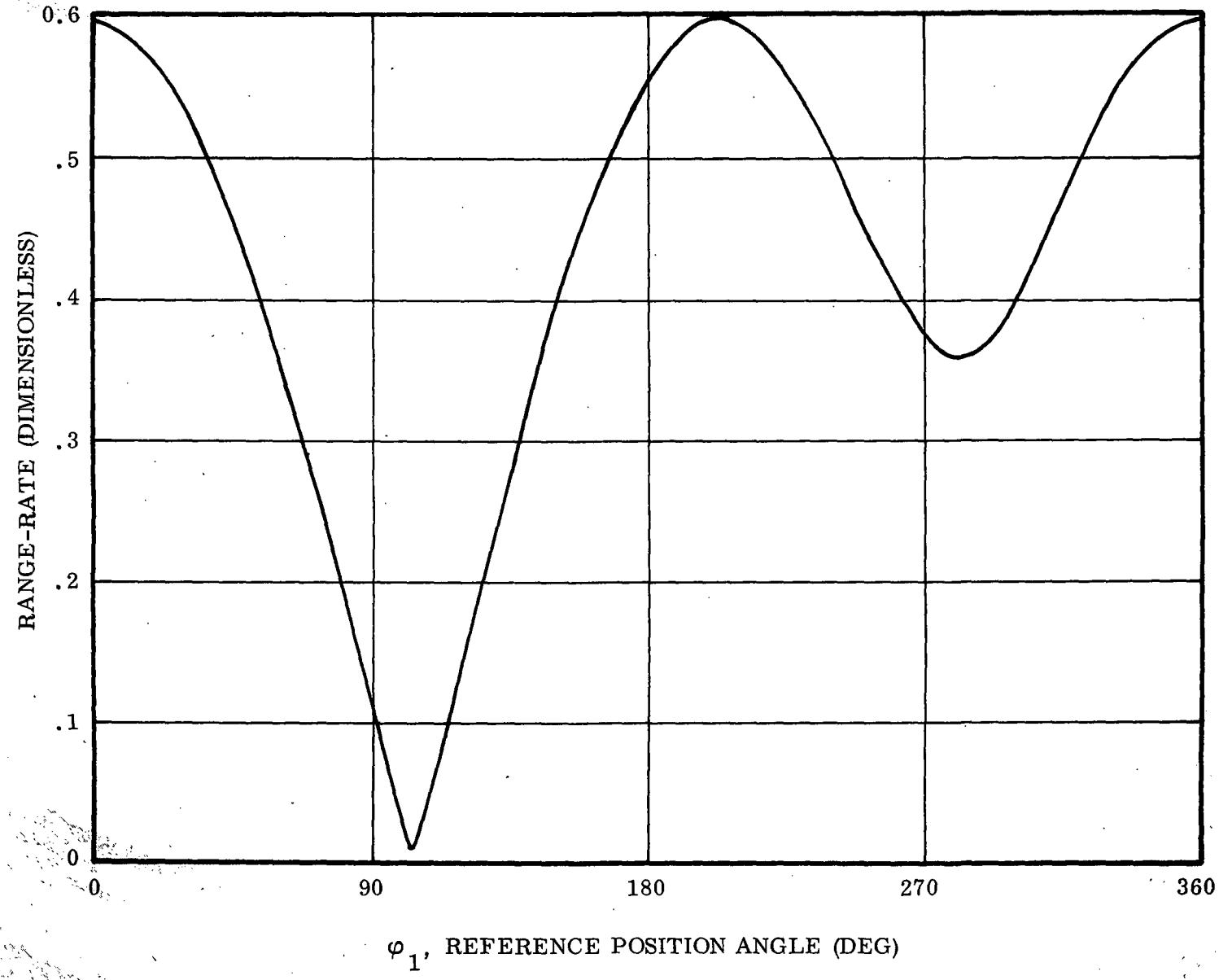

Fig. VII.9b. Dimensionless Relative Range-Rate versus Position Angle, for the Critical Inclination Problem ($\iota_{cr} = 34.38^{\circ}$, $\epsilon_2 = 0.1$).

Only limited results are included herein; the geometry associated with very small eccentricities, or that associated with an eccentricity near to the upper limit has not been presented. It would be informative and illuminating to study a larger number of cases and to acquire a more clear understanding of the described phenomenon.

Even though curves for "range" and "range-rate" have not been included here, for all of the study, it is fairly easy to visualize the general (geometry) trend for those traces not shown. For instance, it is evident now that neither of these curves will show a "cusp", but they may possess a shape which would closely represent this geometric property. Once again, the need for a variety of case studies, having different conditions imposed, would be useful for a best understanding of the parameter influences. An extended investigation would be valuable to more fully understand this problem.

CONCLUDING REMARKS

VIII.1 General. - The investigation which has been described in this report was concerned with various aspects of the relative motion problem as it applied to orbiting mass particles moving about a common primary on closed trajectories. The material presented herein has described these motions, for the bodies moving near to one another, by analytical formulae, and from the numerical integration of appropriate dynamical equations. Throughout this document, physical aspects of the many problems examined have been discussed and illustrated. Primarily these results have been presented in this manner, with the hope that such would enhance the reader's understanding of the relative motions exhibited by orbiting particles.

For this study the state of motion has been referred to a moving frame of reference having one specific orientation. It was felt that the scheme selected, here, was one which is generally accepted and well understood by those interested in this problem area. Having reached this point in the investigation, it has become apparent that there is at least one other particular orientation which is equally as important to the physical problem of relative motion as that one used. In this regard it is suggested that in a future study, of this type, the relative motions should be examined with respect to an inertially oriented, but moving, frame of reference. In some respects such a system of axes may be more compatible with vehicle reference alignment systems than is the scheme which has been employed herein. Without regard to "best" or "better" orientations, the situation studied and reported here has provided information leading to a much better grasp of the pecularities particular to the relative state of motion for orbiting bodies.

In a like manner, the limitations and accuracies which can be ascribed to linear theory, and to the approximations introduced here, are better understood now than before. The inclusion of second order corrections, and a direct comparison with numerically integrated results - as is available in the developed computer program - will lead to a quick and direct comparison for a variety of

sample cases.

The introduction of the relative motion hodograph, and the correlation of it with the displacements, leads to a more realistic representation and grasp of the total motion history than has been noted previously in the literature.

One unusual and interesting phenomenon, noted and reported here, is that of a cusp which was found to appear on certain of the relative motion traces. The fact that these geometric anomalies were discovered and described from a purely analytical examination should be indicative of the value which analyses such as these can provide. Also, it points to the worthwhile aspects of formulations which extend, in some depth, beyond those of a more basic nature - those for instance which arise from (say) the more familiar linear theory developments.

Hopefully the implications, which should have come through to the readers of this document, will suggest that the material contained herein has a much wider application than that to which it has been put here. Due to the obvious limitations of space and time, it has not been feasible to attempt to set down all likely situations which could be studied by the formulations developed and described. It is expected that the inquisitive, future investigators in this area will devise more unique and inventive problems to examine.

VIII.2 The J2 effect. - In the early stages of this study a question arose regarding the possibility that serious influences on the relative motion could be missed by having assumed, as a basis for the investigation, Keplerian type orbits. In order to ascertain whether or not this could be the case, it was decided that one or more of these physical anomalies should be studied to determine the subsequent variations produced. In the end, it was concluded that a most likely influence would be that attributed to the J2-term in the gravitational potential! It was felt that this quantity was as likely to affect the relative motions, for a large family of orbits, as any of the other perturbation parameters.

To test the influence of J2, on a relative motion, the following numerical experiment was devised, executed and analyzed.

A pair of orbiting particles would be placed on well defined trajectories, above the earth, having a selected orbital inclination, altitude and period. From the motions of these two mass particles, a relative displacement and velocity would be determined (by numerically integrating the descriptive equations of motion). For one case, the gravitational potential would describe a spherically homogeneous earth. In a second set of runs, the J2-term would be added to the potential. Both orbital problems were given the same initial conditions, etc.; and both were integrated to produce data for slightly more than one Keplerian orbital period. (The computer program used for this purpose is described in reference 15, it is the ITEM program. It should be noted that this program is quite versatile and inclusive in its capabilities. For this numerical experiment, all perturbative influences - such as other planets, the sun, moon, atmospheric effects, etc. - were nulled in the input and calling sequences. Consequently, the one remaining influence, included here, was the J2 term in an (otherwise) point mass, central field gravitational potential).

To define an influence for the J2-term, on a satellite's relative motion, the following sample problem is examined and discussed:

Initial (and Unperturbed) Values

Quantity	Body (1); Circular Orbit	Body (2); Elliptic Orbit
Geocentric Alt.	1000 km	963.10917 km
Orbit Inclination	45.0^{o}	45.0^{o}
Period of Motion	1.75198 hr.	1.75198 hr.
Eccentricity	$\cong 0$	0.005.
Semi-major axis (a)	1.15678	1.15678
Orbit Pericenter	7378.165 km	7341.274 km
Orbit Apocenter	7378.165 km	7415.056 km

This problem begins at pericenter (Body 2); correspondingly, the initial (relative) state is:

$$\Delta r_o = 36.890825 \text{ km}, \quad \Delta V_o = 0.036609 \text{ km/sec}.$$

Having examined results from the numerical integration of these cases, it was found that the maximum variations in state, for the two orbits (one with and one without J2), was less than one-quarter of one percent. The maximum variation in the relative state quantities was less than one-half of one percent. Consequently it was deemed that the J2 effect on the relative motion was not significant. Hence, the linear analysis (considering an idealized gravitational influence) was not likely to be affected by any J2 influence, per se. The errors which could arise from the linearization should not be adversely magnified if this latter influence had been included in the analysis.

As a matter of interest, the orbits were initiated at the equator of the planet; the subsequent influence of J2 was to reduce the orbital radii, as the orbit progressed, and (correspondingly) to raise the speed, slightly. The largest effect (noted for this example) was on the change in eccentricity for the Body 2 orbit. Of course the eccentricity was initially small (.005), and the apparent, extreme change was of the order of thirty percent.

The consequence of this numerical experiment can be summarized as follows: insofar as can be ascertained, from the data collected here, the neglecting of J2 (as a representative, physically evident, perturbative parameter) would not significantly affect the results of this investigation. The errors which have been noted, between the linearized results, and other more accurate methods, are truly indicative of this (the linearization) and should not be adversely influenced by other neglected parameters.

All in all, it is felt that the information provided from this investigation represents a significant contribution to the understanding of relative motions for orbiting bodies.

APPENDIX A

THE LINEARIZED SOLUTION FOR THE RELATIVE MOTION OF TWO ORBITING MASS PARTICLES, USING CARTESIAN COORDINATES

A.1 The equations of motion (cartesian coordinates). - Under the assumptions of a spherically homogeneous planetary mass, negligible perturbations and negligible attraction between particles, the equations of motion, for two distinct particles moving in a central force field, can be written as:

$$m_k \frac{d\bar{V}_k}{dt} = - m_k \frac{\mu}{r_k^2} \bar{e}_{r_k} \quad ; \tag{A.1}$$

for $k = T, I$; respectively. (Here "T" refers to the target particle, and "I" signifies the interceptor; these names are used to make a recognition of the particles more precise). In eq. (A.1) the m_k represents particle masses; $\bar{V}_k$ their inertial velocities, while $\bar{e}_{r_k}$ are unit vectors parallel to $\bar{r}_k$, their position vectors. In the expression, $\frac{\mu}{r_k^2}$ describes the specific gravitational attraction* of the central force field, on the masses, m_k.

In form, eqs. (A.1) treat each particle as a restricted two-body problem; in this regard these expressions are independent of one another. That is, there is no interaction between these mass particles and, especially, there are no mutual attraction forces present.

According to definition, the velocity $\bar{V}_I$ is

$$\bar{V}_I \equiv \frac{d\bar{r}_I}{dt} \quad , \tag{A.2}$$

* $\mu = GM = gr_k^2$; G is the universal gravitational constant, M is the primary (planetary) mass, and g is the "local gravity", at a radius r_k.

and consequently the interceptor's equation of motion becomes, for a fixed mass particle*,

$$\frac{d^2\bar{r}_I}{dt^2} = -\frac{\mu}{r_I^2}\,\bar{e}_{r_I} \quad . \tag{A.3}$$

From Fig. A.1 it is noted that, $\bar{r}_I = \bar{r}_T + \bar{r}_r$, where $\bar{r}_r$ is the relative position vector, which can be expressed as

$$\bar{r}_r = x\,\bar{e}_x + y\,\bar{e}_y + z\,\bar{e}_z \; ; \tag{A.4}$$

and, accordingly, eq. (A.3) can be written as

$$\frac{d^2\bar{r}_T}{dt^2} + \frac{d^2\bar{r}_r}{dt^2} = -\frac{\mu}{r_I^3}\,\bar{r}_I \, . \tag{A.5}$$

Recognizing, from the figure, that the position vector for the interceptor can be written as

$$\bar{r}_I = r_T\,\bar{e}_{r_T} + x\,\bar{e}_x + y\,\bar{e}_y + z\,\bar{e}_z \, ,$$

then

$$|\bar{r}_I|^3 = r_T^3\left[\left(1 + \frac{x}{r_T}\right)^2 + \frac{y^2 + z^2}{r_T^2}\right]^{3/2} .$$

Also, in agreement with Fig. A.1, it is apparent that

$$r_I^3 = r_T^3\left[\left(1 + \frac{x}{r_T}\right)^2 + \sin^2\theta\right]^{3/2} ,$$

which can be approximated, for relatively small $\bar{r}_r$ values, as

*The assumption of fixed mass bodies is employed here in order to retain the analytic nature of these developments. For small thrusting capabilities and small quantities of stored propellants, such an assumption is physically reasonable.

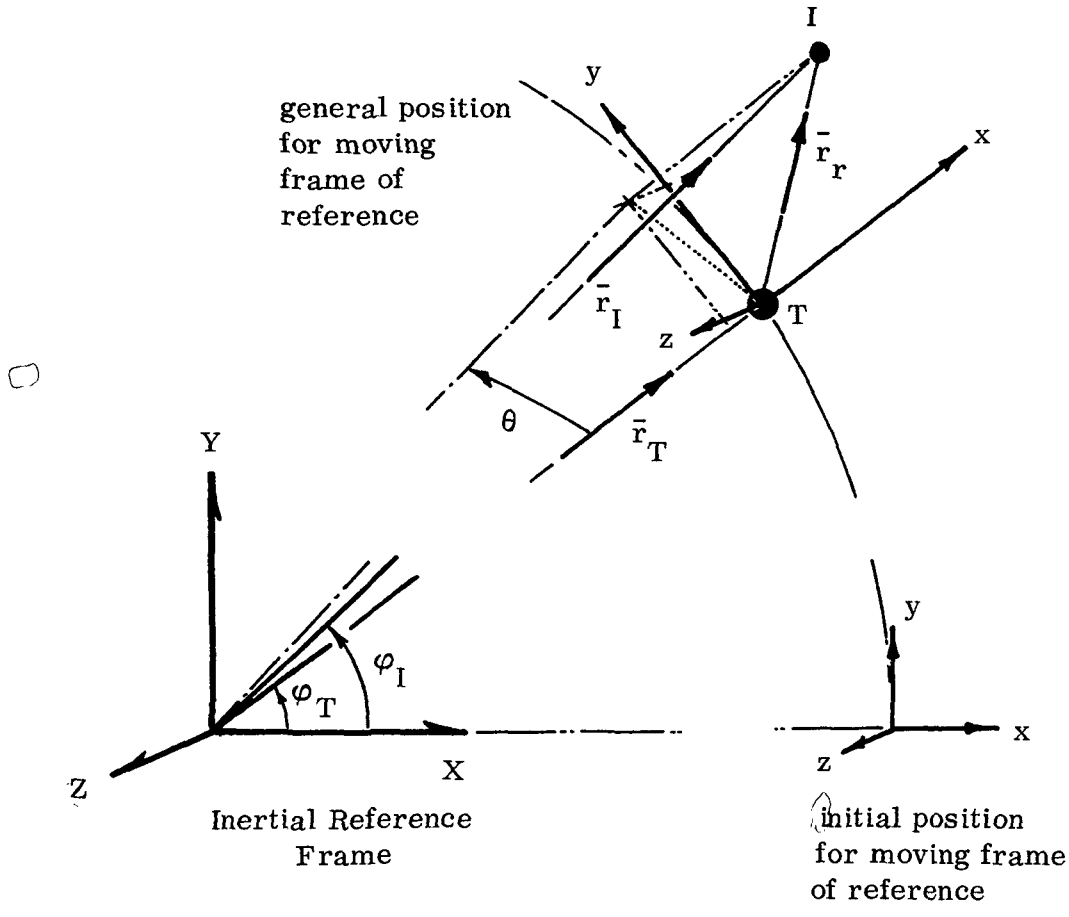

Fig. A.1. Geometry for the Relative Motion Problem expressed in Cartesian Coordinates.

$$r_I^3 \cong r_T^3 \left[\left(1 + \frac{2x}{r_T}\right)\right]^{3/2}, \tag{A.6}$$

retaining only linear quantities in (x, y, z).

Using this approximation, then

$$\frac{\bar{r}_I}{r_I^3} \cong \frac{\bar{r}_I}{r_T^3 \left[1 + \frac{2x}{r_T}\right]^{3/2}}, \tag{A.7a}$$

and after expanding the denominator, as a first estimate,

$$\frac{\bar{r}_I}{r_I^3} \cong \frac{\bar{r}_I}{r_T^3}\left[1 - 3\frac{x}{r_T} + \ldots\right], \tag{A.7b}$$

where the terms deleted are of order $\left(\frac{x^2}{r_T^2}\right)$ and greater. Next, expressing $\bar{r}_I$ in terms of the coordinates (x, y, z), and collecting terms (recognizing that $\bar{e}_{r_T} \equiv \bar{e}_x$), it is found that

$$\frac{\bar{r}_I}{r_I^3} \cong \left(\frac{1}{r_T^2} - 2\frac{x}{r_T^3}\right)\bar{e}_x + \frac{y}{r_T^3}\bar{e}_y + \frac{z}{r_T^3}\bar{e}_z \left\{\begin{array}{l}\text{terms of higher} \\ \text{order in x, y, z.}\end{array}\right\}. \tag{A.8}$$

Eq. (A.8) is the linearization to be used on the right side of eq. (A.5); this should be a valid approximation so long as $\left|\bar{r}_r\right| \ll \left|\bar{r}_T\right|$; that is, so long as the interceptor is not at too large a distance from the target particle. As a matter of practical interest distances up to a few hundred kilometers, between particles, have been found to satisfy this restriction reasonably well.

Now, using eq. (A.8) in the differential equation of motion, eq. (A.5) one can write

$$\frac{d^2\bar{r}_T}{dt^2} + \frac{d^2\bar{r}_r}{dt^2} \cong -\mu\left[\frac{\bar{e}_{r_T}}{r_T^2} - 2\frac{x}{r_T^3}\bar{e}_x + \frac{y}{r_T^3}\bar{e}_y + \frac{z}{r_T^3}\bar{e}_z\right], \tag{A.9}$$

as a first order representation.

In this expression, the lead terms on both sides of the equality are noted to constitute eq. (A.1) for a k = T - a statement which is assumed to be satisfied at all times - hence eq. (A.9) reduces to

$$\frac{d^2\bar{r}_r}{dt^2} \cong \mu\left[2\frac{x}{r_T^3}\bar{e}_x - \frac{y}{r_T^3}\bar{e}_y - \frac{z}{r_T^3}\bar{e}_z\right]. \tag{A.10}$$

This equation is presumed to describe the relative motion of the interceptor with respect to the target satellite (to the degree of approximation noted above).

A.2 Kinematic description of the acceleration. - Before eq. (A.10) can be solved it will be necessary to describe the relative acceleration,

$$\frac{d^2\bar{r}_r}{dt^2},$$

kinematically, for the problem. In evaluating the acceleration, it will be necessary to properly account for the fact that the coordinates (x, y, z) are relative values and thereby constitute a moving frame of reference. Thus, there is an added motion which must be accounted for in the formulation of the acceleration in this problem. In particular the coordinate frame moves with the particle ("T") and rotates in space, so that the unit vector $\bar{e}_x$ is parallel to $\bar{e}_{r_T}$ at all times.

To establish a kinematic expression for the acceleration one can begin with the definition of $\bar{r}_r$, and differentiate to obtain the velocity; that is, write the relative velocity vector as,

$$\bar{V}_r \equiv \frac{d\bar{r}_r}{dt} = \frac{dx}{dt}\,\bar{e}_x + \frac{dy}{dt}\,\bar{e}_y + \frac{dz}{dt}\,\bar{e}_z + x\frac{d\bar{e}_x}{dt} + y\frac{d\bar{e}_y}{dt} + z\frac{d\bar{e}_z}{dt}\ , \qquad (A.11)$$

where the unit vector derivatives arise as a consequence of their motion (with the moving frame of reference). Recalling that these vector derivatives are obtained from

$$\frac{d\bar{e}_i}{dt} = \bar{\omega} \times \bar{e}_i\ , \quad (i = x,\ y,\ z),$$

where $\bar{\omega}$ is the (instantaneous) angular velocity of this moving frame of reference $(\hat{x},\ \hat{y},\ \hat{z})$; then, for $\bar{\omega} \equiv \omega\,\bar{e}_z$ (which describes the present case),

$$\frac{d\bar{e}_i}{dt} = \omega(\bar{e}_z \times \bar{e}_i),\ \text{or} \quad \begin{cases} \dot{\bar{e}}_x = \omega(\bar{e}_z \times \bar{e}_x) = \omega\,\bar{e}_y\ , \\ \text{and} \\ \dot{\bar{e}}_y = \omega(\bar{e}_z \times \bar{e}_y) = -\,\omega\,\bar{e}_x. \end{cases} \qquad (A.12)$$

Using eqs. (A.12), in (A.11), it follows that the velocity vector is,

$$\frac{d\bar{r}_r}{dt} = (\dot{x} - \omega y)\,\bar{e}_x + (\dot{y} + \omega x)\,\bar{e}_y + \dot{z}\,\bar{e}_z\ , \qquad (A.13)$$

where the "dots" infer differentiation with respect to time. Correspondingly, the acceleration vector, formed by differentiating eq. (A.13), can be shown to be

$$\frac{d^2\bar{r}_r}{dt^2} = \left[\ddot{x} - y\,\dot{\omega} - \omega^2\left(\frac{2\dot{y}}{\omega} + x\right)\right]\bar{e}_x + \left[\ddot{y} + x\,\dot{\omega} + \omega^2\left(\frac{2\dot{x}}{\omega} - y\right)\right]\bar{e}_y + \ddot{z}\,\bar{e}_z\ . \qquad (A.14)$$

Eq. (A.14) includes the relative (coordinate) acceleration terms $(\ddot{x}, \ddot{y}, \ddot{z})$; the Coriolis terms $(2\,\omega\dot{y},\ 2\,\omega\dot{x})$; the Euler accelerations $(\dot{\omega}y,\ \dot{\omega}x)$, and the centripetal terms $(\propto \omega^2)$. These quantities properly describe the absolute acceleration, $\dfrac{d^2\bar{r}_r}{dt^2}$, kinematically. This result, eq. (A.14), will be introduced into eq. (A.10); and, as a consequence the equation of motion for the interceptor is expressed, then, in terms of its position coordinates relative to the target.

A.3 A formulation of the restricted equations of motion. - Introducing eq. (A.14) into (A.10), the motion of the interceptor (or rendezvous vehicle) is described by the differential expression,

$$(\ddot{x} - \dot{\omega}y - 2\,\omega\dot{y} - \omega^2 x)\,\bar{e}_x + (\ddot{y} + \dot{\omega}x + 2\,\omega\dot{x} - \omega^2 y)\,\bar{e}_y + \ddot{z}\,\bar{e}_z = -\frac{\mu}{r_T^3}\left[-2x\bar{e}_x + y\bar{e}_y + z\bar{e}_z\right]; \qquad \text{(A.15a)}$$

which is equivalent to the following set of scalar equations:

$$\ddot{x} - \dot{\omega}y - 2\,\omega\dot{y} - \omega^2 x = \frac{2\mu x}{r_T^3},$$

$$\ddot{y} + \dot{\omega}x + 2\,\omega\dot{x} - \omega^2 y = \frac{-\mu y}{r_T^3},$$

and

$$\ddot{z} = -\frac{\mu z}{r_T^3}. \qquad \text{(A.15b)}$$

Eqs. (A.15b) are the approximate differential equations of motion subject to the restrictions that: (1) the target and the interceptor particles are

not coupled through their mutual attraction; and, (2) the inequality for distances $(r_T + x) \gg y, z$ is retained. For terminal guidance and maneuvering the last restriction can certainly be retained; however, for large separation distances, between satellites, this approximation is weakened.

When attempting to solve the above scalar equations of motion, one should note that the first two are kinematically coupled and must be solved together. However, the last equation, being independent, is easily solved to obtain a description of the distance z as a function of time.

In order to facilitate an analytic solution to eqs. (A.15b) it is prudent to assume that the target moves on a circular orbit. Then, in accord with this last assumption, $\bar{\omega}$ $(= \dot{\varphi}_T \bar{e}_z)$ is a constant; and, consequently, eqs. (A.15b) may be reduced, further.

A.4 A special case, the target moving on a circular orbit. - The added restrictions imposed here are that ω $(= \dot{\varphi}_T)$ is constant, and that the radius vector $(\bar{r}_T)$ has a fixed magnitude. For these conditions eq. (A.1), for $k = T$, is manipulated as follows; Since

$$\frac{d^2\bar{r}_T}{dt^2} = -\frac{\mu}{r_T^2}\,\bar{e}_{r_T} \quad ; \tag{A.16a}$$

and, kinematically, it can be shown that

$$\frac{d^2\bar{r}_T}{dt^2} = (\ddot{r}_T - r_T \dot{\varphi}_T^2)\,\bar{e}_x + \frac{1}{r_T}\left[\frac{d}{dt}\,(r_T^2\,\dot{\varphi}_T)\right]\bar{e}_y \quad ; \tag{A.16b}$$

then, for a circular orbit (r_T, $\dot{\varphi}_T$ are constants), this last expression reduces to

$$\frac{d^2\bar{r}_T}{dt^2} = -(r_T \dot{\varphi}_T^2)\,\bar{e}_x + \frac{1}{r_T}\left[\frac{d}{dt}(r_T^2 \dot{\varphi}_T)\right]\bar{e}_y ,$$

where the quantities in the parentheses are noted to be constants. Consequently, from the scalar equations of motion (A.16a, A.16b) one finds that,

$$-r_T \dot{\varphi}_T^2 = -\frac{\mu}{r_T^2}$$ (expressing a balance between gravity and centrifugal force);

and

$$r_T^2 \dot{\varphi}_T = \text{constant}$$ (describing the specific moment of momentum for the motion). (A.16c)*

Introducing these two results into eqs. (A.15b) leads to a modification and specialization of the interceptor's equations of motion. That is, after making the appropriate substitutions one finds that eqs. (A.15b) become;

$$\ddot{x} - 2\dot{y}\dot{\varphi}_T - 3x\dot{\varphi}_T^2 = 0,$$

$$\ddot{y} + 2\dot{x}\dot{\varphi}_T = 0,$$

and

$$\ddot{z} + z\dot{\varphi}_T^2 = 0.$$ (A.17)

These last expressions govern the relative motion of the interceptor, with respect to a target which is flying on a circular path.

A.5 A solution for the relative motion of the interceptor. - The first two of eqs. (A.17) remain kinematically coupled through the Coriolis terms; hence they must be solved together.

*The first expression is a description of the circular satellite speed. That is, since $V_T = V_\varphi = V_{cir} \equiv \sqrt{\mu/r_T}$, then by a simple manipulation $(r_T \dot{\varphi}_T)^2 = \sqrt{\mu/r_T} \equiv V_{cir}$ (as expected). Thus, the balancing of gravity and centrifugal force implies a circular orbit.

A solution for the coupled expressions may be obtained by the following scheme: First, it should be noted that the second of eqs. (A.17) has a first integral; namely,

$$\dot{y} = K_1' - 2\dot{\varphi}_T x, \tag{A.18}$$

where K_1 is an integration constant. Now, when eq. (A.18) is inserted into the first expression of the set (eqs. (A.17)) one obtains

$$\ddot{x} = 3x\dot{\varphi}_T^2 + 2\dot{\varphi}_T (K_1 - 2x\dot{\varphi}_T), \tag{A.19a}$$

which reduces the expression to one involving only the dependent variable, x. Now, if this is rewritten in terms of a transformed coordinate q ($\equiv x - \frac{2K_1}{\dot{\varphi}_T}$), eq. (A.19) can be replaced by

$$\ddot{q} = -\dot{\varphi}_T^2 q, \text{ (where } \dot{\varphi}_T \text{ is a constant)}, \tag{A.19b}$$

which has a simple, elementary solution, such as

$$q = K_2 \cos(\dot{\varphi}_T t + K_3), \tag{A.20}$$

where K_2 and K_3 are constants of integration to be described from the initial conditions. As an alternate form of eq. (A.20), the displacement x can be written as

$$x = \frac{2K_1}{\dot{\varphi}_T} + K_2 \cos(\dot{\varphi}_T t + K_3), \tag{A.21}$$

accounting for the transformation q(x), introduced above.

Next, using the above resultant in eq. (A.18), and integrating, one finds that

$$y = K_4 - 3K_1 t - 2K_2 \sin(\dot{\varphi}_T t + K_3), \tag{A.22}$$

wherein K_4 is another of the constants of integration.

A.6 Evaluation of constants. - In order to retain the generality of this problem it will be assumed that the initial values are those specified below:

$$\begin{aligned} \text{at } t\ (= t_o) = 0: \qquad & x = x_o, \qquad \dot{x} = \dot{x}_o, \\ & y = y_o, \qquad \dot{y} = \dot{y}_o, \\ & z = z_o, \qquad \dot{z} = \dot{z}_o; \end{aligned} \tag{A.23}$$

which is equivalent to stating that at the initial time the relative motion state may be represented by the vectors,

$$\bar{r}_I = \bar{r}_{I_o}, \quad \bar{V}_I = \bar{V}_{I_o}.$$

Applying these general initial conditions to eqs. (A.18), (A.21) and (A.22), it is easy to show that the various constants may be expressed by,

$$K_1 = \dot{y}_o + 2x_o \dot{\varphi}_T,$$

$$K_2 = \sqrt{\left(\frac{\dot{x}_o}{\dot{\varphi}_T}\right)^2 + \left(2\frac{\dot{y}_o}{\dot{\varphi}_T} + 3x_o\right)^2},$$

$$K_3 = \tan^{-1}\left[\frac{-\dot{x}_o}{-(2\dot{y}_o + 3x_o\dot{\varphi}_T)}\right],$$

and

$$K_4 = y_o - 2\frac{\dot{x}_o}{\dot{\varphi}_T}.$$

After substituting for these constants the equations for the relative motion coordinates (x, y) are found to be;

$$x = 2\left(\frac{\dot{y}_o}{\dot{\varphi}_T} + 2x_o\right) + \sqrt{\left(\frac{\dot{x}_o}{\dot{\varphi}_T}\right)^2 + \left(2\frac{\dot{y}_o}{\dot{\varphi}_T} + 3x_o\right)^2}\cos\left(\dot{\varphi}_T t + K_3\right),$$

and

$$y = \left(y_o - 2\frac{\dot{x}_o}{\dot{\varphi}_T}\right) - 3\dot{\varphi}_T\left(\frac{\dot{y}_o}{\dot{\varphi}_T} + 2x_o\right)t - 2\sqrt{\left(\frac{\dot{x}_o}{\dot{\varphi}_T}\right)^2 + \left(2\frac{\dot{y}_o}{\dot{\varphi}_T} + 3x_o\right)^2}\sin\left(\dot{\varphi}_T t + K_3\right). \quad (A.24)$$

Before seeking a solution for the z-displacement, it would be constructive to rewrite eqs. (A.24) in another form. This will be accomplished by expanding the trigonometric terms, and re-grouping quantities. As a result of these manipulations, the following expressions for the relative displacements are obtained:

$$x = x_o + \left(3x_o + 2\frac{\dot{y}_o}{\dot{\varphi}_T}\right)(1-\cos\dot{\varphi}_T t) + \frac{\dot{x}_o}{\dot{\varphi}_T}\sin\dot{\varphi}_T t,$$

and

$$y = y_o - 3\left(\frac{\dot{y}_o}{\dot{\varphi}_T} + 2x_o\right)\dot{\varphi}_T t - 2\frac{\dot{x}_o}{\dot{\varphi}_T}(1-\cos\dot{\varphi}_T t) + 2\left(3x_o + 2\frac{\dot{y}_o}{\dot{\varphi}_T}\right)\sin\dot{\varphi}_T t; \quad (A.25)$$

wherein the $(\sim)_o$ quantities infer initial values, and $\dot{\varphi}_T$ is the constant angular speed of the target moving along its assumed circular orbit.

A.7 A solution for the z-displacement. - The differential equation of motion, in the z-coordinate is (from eqs. (A.17)),

$$\ddot{z} = -\dot{\varphi}_T^2 z. \quad (A.26)$$

This expression, being similar to eq. (A.19b), also has an elementary solution, such as,

$$z = K_5 \cos (\dot{\varphi}_T t + K_6), \tag{A.27a}$$

where K_5 and K_6 are integration constants. Analogous to the manipulations carried out above, an alternate form of this solution is

$$z = K_7 \cos \dot{\varphi}_T t + K_8 \sin \dot{\varphi}_T t, \tag{A.27b}$$

wherein the K_j are integration constants. Introducing the initial conditions, eqs. (A.23), one finds that these constants may be described by,

$$K_5 = \sqrt{z_o^2 + \left(\frac{\dot{z}_o}{\dot{\varphi}_T}\right)^2}, \text{ and } K_6 = \tan^{-1}\left[\frac{-\dot{z}_o/\dot{\varphi}_T}{z_o}\right];$$

with $K_7 = z_o$, and $K_8 = \dot{z}_o/\dot{\varphi}_T$. Making the necessary substitutions, the z-displacement expression(s) can be written as:

$$z = \sqrt{z_o^2 \left(\frac{\dot{z}_o}{\dot{\varphi}_T}\right)^2} \cos (\dot{\varphi}_T t + K_6), \tag{A.28a}$$

and/or

$$z = z_o \cos \dot{\varphi}_T t + \frac{\dot{z}_o}{\dot{\varphi}_T} \sin \dot{\varphi}_T t. \tag{A.28b}$$

A.8 The displacement expressions (summary). - The purpose of this appendix was to develop equations which would describe the displacement of the "interceptor" particle relative to the "target" (or "satellite") particle, as these moved along their independent paths. The desired equations, which are expressed in rectangular coordinates, and given by eqs. (A.24)(or eqs. (A.25)) and (A.28). For convenience, these are summarized here: From eqs. (A.24) and (A.28a):

$$x = 2\left(\frac{\dot{y}_o}{\dot{\varphi}_T} + 2x_o\right) + \sqrt{\left(\frac{\dot{x}_o}{\dot{\varphi}_T}\right)^2 + \left(2\frac{\dot{y}_o}{\dot{\varphi}_T} + 3x_o\right)^2}\cos(\dot{\varphi}_T t + K_3),$$

$$y = \left(y_o - 2\frac{\dot{x}_o}{\dot{\varphi}_T}\right) - 3\left(\frac{\dot{y}_o}{\dot{\varphi}_T} + 2x_o\right)\dot{\varphi}_T t - 2\sqrt{\left(\frac{\dot{x}_o}{\dot{\varphi}_T}\right)^2 + \left(2\frac{\dot{y}_o}{\dot{\varphi}_T} + 3x_o\right)^2}\sin(\dot{\varphi}_T t + K_3),$$

and

$$z = \sqrt{z_o^2 + \left(\frac{\dot{z}_o}{\dot{\varphi}_T}\right)^2}\cos(\dot{\varphi}_T t + K_6);$$

wherein

$$K_3 = \tan^{-1}\left[\frac{-\dot{x}_o}{-(2\dot{y}_o + 3x_o\dot{\varphi}_T)}\right], \text{ and } K_6 = \tan^{-1}\left[\frac{-\dot{z}_o}{z_o\dot{\varphi}_T}\right]. \qquad \text{(A.29a)}$$

Similarily, from eqs. (A.25) and (A.28b):

$$x = x_o + \left(3x_o + 2\frac{\dot{y}_o}{\dot{\varphi}_T}\right)(1-\cos\dot{\varphi}_T t) + \frac{\dot{x}_o}{\dot{\varphi}_T}\sin\dot{\varphi}_T t,$$

$$y = y_o - 3\left(\frac{\dot{y}_o}{\dot{\varphi}_T} + 2x_o\right)\dot{\varphi}_T t - 2\frac{\dot{x}_o}{\dot{\varphi}_T}(1-\cos\dot{\varphi}_T t) + 2\left(3x_o + 2\frac{\dot{y}_o}{\dot{\varphi}_T}\right)\sin\dot{\varphi}_T t,$$

and

$$z = z_o\cos\dot{\varphi}_T t + \frac{\dot{z}_o}{\dot{\varphi}_T}\sin\dot{\varphi}_T t. \qquad \text{(A.29b)}$$

A.9 The relative speed expressions. - Eqs. (A.29) may be differentiated to yield equations describing theiinterceptor's speed components. Recognizing that only the trigonometric, and secular, terms are those having time dependence, then the speed components are easily obtained.

On differentiating eqs. (A.29a), one can show that:

$$\dot{x} = -\left(\sqrt{\dot{x}_o^{\,2} + (2\dot{y}_o + 3x_o\dot{\varphi}_T)^2}\right) \sin(\dot{\varphi}_T t + K_3),$$

$$\dot{y} = \dot{y}_o - 2\left[(2\dot{y}_o + 3x_o\dot{\varphi}_T) + \left(\sqrt{\dot{x}_o^{\,2} + (2\dot{y}_o + 3x_o\dot{\varphi}_T)^2}\right)\cos(\dot{\varphi}_T t + K_3)\right],$$

and $$\dot{z} = -\left(\sqrt{\dot{z}_o^{\,2} + (z_o\dot{\varphi}_T)^2}\right) \sin(\dot{\varphi}_T t + K_6); \qquad \text{(A.30a)}$$

wherein

$$K_3 = \tan^{-1}\left[\frac{-\dot{x}_o}{-(2y_o + 3x_o\dot{\varphi}_T)}\right], \text{ and } K_6 = \tan^{-1}\left[\frac{-\dot{z}_o}{z_o\dot{\varphi}_T}\right], \text{ as before.}$$

In addition, the differentiation of eqs. (A.29b) leads to:

$$\dot{x} = \dot{x}_o \cos(\dot{\varphi}_T t) + \left[3x_o\dot{\varphi}_T + 2\dot{y}_o\right]\sin(\dot{\varphi}_T t),$$

$$\dot{y} = \dot{y}_o - 2\left\{\left[3x_o\dot{\varphi}_T + 2\dot{y}_o\right]\left[1-\cos(\dot{\varphi}_T t)\right] + \dot{x}_o \sin(\dot{\varphi}_T t)\right\},$$

and $$\dot{z} = \dot{z}_o \cos(\dot{\varphi}_T t) - z_o\dot{\varphi}_T \sin(\dot{\varphi}_T t). \qquad \text{(A.30b)}$$

A.10 Dimensionless representation for the relative displacements and speeds. - The problem being studied has the target (hence, the relative coordinates origin) moving along a circular path; therefore, r_T and $\dot{\varphi}_T$ are constants. A look at eqs. (A.29) and (A.30) suggests a transformation which will lead to a full set of dimensionless quantities. For this reduction the displacements will be normalized by r_T; the speeds will be referenced to the (target's) circular speed, $r_T\dot{\varphi}_T$; and, finally, the independent variable will be changed from "t" to "φ_T" by means of:

$\varphi_T \equiv \dot{\varphi}_T t$ (since $\dot{\varphi}_T$ = constant; note that t = 0 will nominally correspond to $\varphi_T = 0$).

Defining the dimensionless state variables as: displacement (ξ, η, ζ), and speeds (ξ', η', ζ'), wherein $(\sim)' \equiv \frac{d}{d\varphi_T} = \frac{d}{\dot{\varphi}_T dt} \equiv \frac{d}{d(\dot{\varphi}_T t)}$; then the two sets of quantities are related by:

$$\begin{bmatrix} \xi \\ \eta \\ \zeta \end{bmatrix} = \frac{1}{r_T} \begin{bmatrix} x \\ y \\ z \end{bmatrix} ; \quad \begin{bmatrix} \dot{\xi} \\ \dot{\eta} \\ \dot{\zeta} \end{bmatrix} = \frac{d}{dt} \begin{bmatrix} \xi \\ \eta \\ \zeta \end{bmatrix} ; \text{ and } \begin{bmatrix} \xi' \\ \eta' \\ \zeta' \end{bmatrix} = \frac{d}{d\varphi_T} \begin{bmatrix} \xi \\ \eta \\ \zeta \end{bmatrix} . \tag{A.31}$$

Conversely, to revert to dimensional variables, from dimensionless ones, it is apparent that one can do so by means of the following transforms:

$$\begin{bmatrix} x \\ y \\ z \end{bmatrix} = r_T \begin{bmatrix} \xi \\ \eta \\ \zeta \end{bmatrix} ; \text{ and, } \begin{bmatrix} \dot{x} \\ \dot{y} \\ \dot{z} \end{bmatrix} = (r_T \dot{\varphi}_T) \begin{bmatrix} \xi' \\ \eta' \\ \zeta' \end{bmatrix} . \tag{A.32}$$

Utilizing the transformations in eqs. (A.31), it is easy to replace eqs. (A.29) and (A.30) with the following sets of (dimensionless) displacements and speed relations. Thus,

(a) From eqs. (A.29a):-

$$\xi \left(\equiv \frac{x}{r_T} \right) = 2 (2\xi_o + \eta_o') + \left(\sqrt{(\xi_o')^2 + (3\xi_o + 2\eta_o')^2} \right) \cos (\varphi_T + K_3),$$

$$\eta \left(\equiv \frac{y}{r_T} \right) = (\eta_o - 2\xi_o') - 3(2\xi_o + \eta_o') \varphi_T - 2 \left(\sqrt{(\xi_o')^2 + (3\xi_o + 2\eta_o')^2} \right) \sin (\varphi_T + K_3),$$

and

$$\zeta \left(\equiv \frac{z}{r_T} \right) = \left(\sqrt{\zeta_o^2 + (\zeta_o')^2} \right) \cos (\varphi_T + K_6); \tag{A.33a}$$

wherein

$$K_3 = \tan^{-1} \left[\frac{-\xi_o'}{-(3\xi_o + 2\eta_o')} \right], \text{ and } K_6 = \tan^{-1} \left[\frac{-\zeta_o'}{\zeta_o} \right].$$

(b) From eqs. (A.29b): -

$$\xi = \xi_o + (3\xi_o + 2\eta_o') (1-\cos \varphi_T) + \xi_o' \sin \varphi_T,$$

$$\eta = \eta_o + \eta_o' \varphi_T - 2 \left[(3\xi_o + 2\eta_o') (\varphi_T - \sin \varphi_T) + \xi_o' (1-\cos \varphi_T) \right],$$

and $$\zeta = \zeta_o \cos \varphi_T + \zeta_o' \sin \varphi_T. \tag{A.33b}$$

(c) From eqs. (A.30a): -

$$\xi' \left(\equiv \frac{d\xi}{d\varphi_T} \right) = - \left(\sqrt{(\xi_o')^2 + (2\eta_o' + 3\xi_o)^2} \right) \sin (\varphi_T + K_3),$$

$$\eta' \left(\equiv \frac{d\eta}{d\varphi_T} \right) = \eta_o' - 2 \left[(2\eta_o' + 3\xi_o) + \left(\sqrt{(\xi_o')^2 + (2\eta_o' + 3\xi_o)^2} \right) \cos (\varphi_T + K_3) \right],$$

and

$$\zeta' \left(\equiv \frac{d\zeta}{d\varphi_T} \right) = - \left(\sqrt{\zeta_o^2 + (\zeta_o')^2} \right) \sin (\varphi_T + K_6). \tag{A.34a}$$

wherein

$$K_3 = \tan^{-1} \left[\frac{-\xi_o'}{-(2\eta_o' + 3\xi_o)} \right], \text{ and } K_6 = \tan^{-1} \left[\frac{-\zeta_o'}{\zeta_o} \right].$$

(d) From eqs. (A.30b): -

$$\xi' = \xi'_o \cos \varphi_T + (3\xi_o + 2\eta'_o) \sin \varphi_T,$$

$$\eta' = \eta'_o - 2\left[(3\xi_o + 2\eta'_o)(1-\cos \varphi_T) + \xi'_o \sin \varphi_T\right],$$

and $$\zeta' = \zeta'_o \cos \varphi_T - \zeta_o \sin \varphi_T . \qquad \text{(A.34b)}$$

In eqs. (A.33), (A.34) the independent variable (φ_T) has its origin at a preselected, arbitrary position for the target vehicle. Consequently, there is no need to define (or determine) a pericenter for these problems; in this regard the choice of a circular path for the target was fortituous. Any selected position along this base trajectory (the circle) will serve, adequately, to define an initial state (or value) for the problem.

There are two sets of relations--for displacement, and for speed - included in the above listing. These describe the relative state of motion for the interceptor with respect to the target. In principle these two sets are included here for comparison purposes; however, in some instances it is more informative to refer a motion to one type of these relations than it is the other.

APPENDIX B

DEVELOPMENT OF THE EQUATIONS OF MOTION (SHELL COORDINATES)

B.1 Shell coordinates, defined. - This system of relative motion coordinates has its origin at the "target" satellite. Here the displacement of the interceptor relative to the target will be described by (ρ, s, z). For this coordinate representation ρ is the radial separation distance, s is an arc distance, and z is the out-of-plane displacement. Since the present problem is primarily a planar one, the z-coordinate will not be included in the analysis.

Accordingly, it is evident that the shell coordinates (ρ, s) may be expressed by:

$$\rho = r_I - r_T, \text{ and } s = r_T (\varphi_I - \varphi_T). \tag{B.1}$$

(The z-coordinate would complete an orthogonal coordinate system, centered at T). See Fig. B.1.

B.2 Equations of motion (planar case). - Treating both vehicles as two-body problems (without mutual attraction) then the central field equations of motion are:

$$m_k \frac{d^2 \bar{r}_k}{dt^2} = - \frac{m_k \mu}{r_k^2} \bar{e}_{r_k} , \tag{B.2}$$

wherein $\bar{e}_{r_k} \equiv \frac{\bar{r}_k}{|\bar{r}_k|}$; $k = I, T,$ as before.

It should be recalled that for the kinematics of this problem (wherein a single simple rotation, $\dot{\varphi}$, is assumed for the triads) the acceleration is:

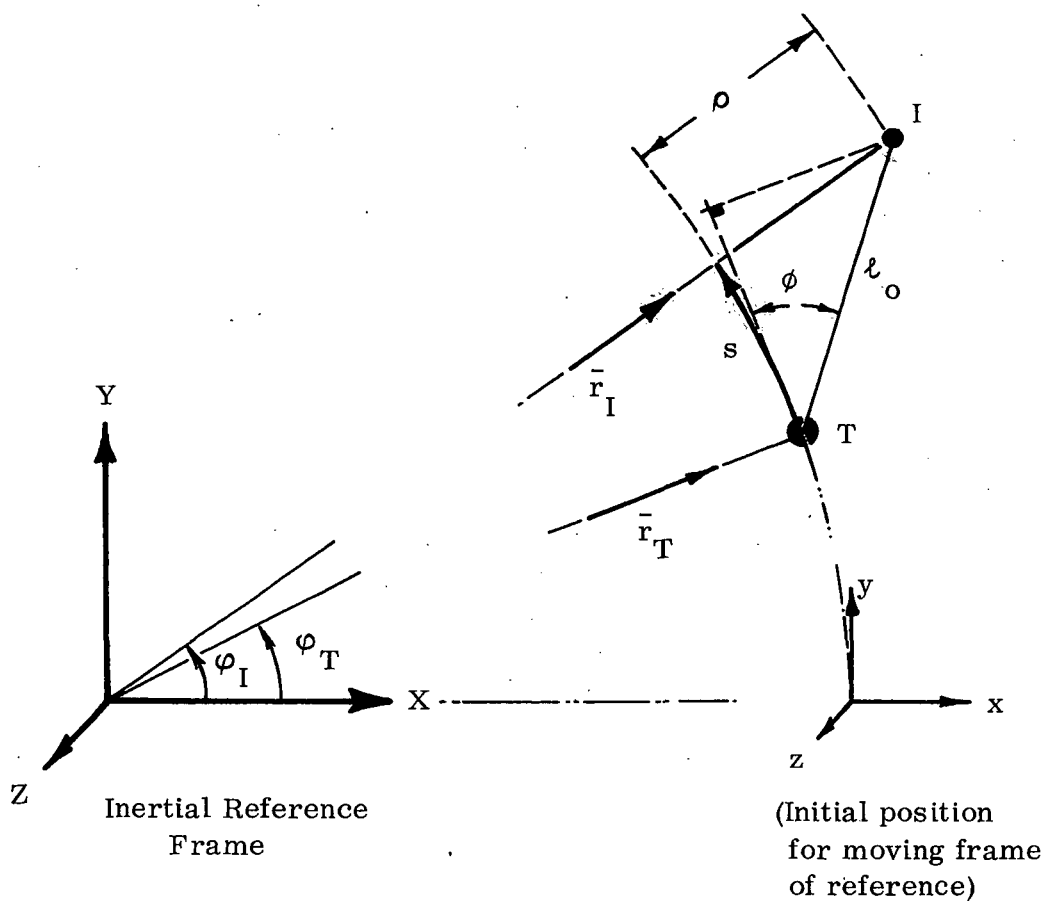

Fig. B.1. Geometry of the Relative Motion Problem expressed in Shell Coordinates.

$$\frac{d^2\bar{r}_k}{dt^2} = (\ddot{r}_k - r_k \dot{\varphi}_k^2)\, \bar{e}_{r_k} + (2\dot{r}_k \dot{\varphi}_k + r_k \ddot{\varphi}_k)\, \bar{e}_{\varphi_k}, \qquad \text{(B.3)}$$

where the unit vector $\bar{e}_{\varphi_k}$ is orthogonal to $\bar{e}_{r_k}$; k = I, T. Using the coordinate relations noted above, it is presumed that solutions for the displacement of both vehicles can be obtained by solving, independently, the following sets of equations:

for the TARGET VEHICLE

$$\ddot{r}_T - r_T \dot{\varphi}_T^2 = -\frac{\mu}{r_T^2},$$

and

$$2\dot{r}_T \dot{\varphi}_T + r_T \ddot{\varphi}_T \equiv \frac{1}{r_T}\frac{d}{dt}\left(r_T^2 \dot{\varphi}_T\right) = 0.$$

for the INTERCEPTOR VEHICLE

$$\ddot{r}_I - r_I \dot{\varphi}_I^2 = -\frac{\mu}{r_I^2},$$

and

$$2\dot{r}_I \dot{\varphi}_I + r_I \ddot{\varphi}_I \equiv \frac{1}{r_I}\frac{d}{dt}\left(r_I^2 \dot{\varphi}_I\right) = 0. \qquad \text{(B.4)}$$

In order to describe the relative motion of the interceptor, the shell coordinates defined above will be used. However, in order to obtain analytic results it is necessary, again, to assume that the target particle moves along a circular orbit. Also, the relative motion equations must be linearized so that the required mathematical manipulations can be performed.

Supposing the target vehicle flies a circular orbit; then necessarily:

$$r_T = \text{constant} \quad (\text{hence } \dot{r}_T = \ddot{r}_T = 0)$$

and

$$\dot{\varphi}_T = \text{constant} \ (\text{so, } \ddot{\varphi}_T = 0;\ \varphi_T = \dot{\varphi}_T t). \qquad \text{(B.5)}$$

As a consequence of these restrictions the equations of motion for the target vehicle reduce to:

$$r_T \dot{\varphi}_T^2 = \frac{\mu}{r_T^2} \quad \text{(describing a circular speed for this vehicle),}$$

and

$$r_T^2 \dot{\varphi}_T = \text{constant} \equiv h_T, \quad \text{(defining the specific angular momentum magnitude).} \tag{B.6}$$

Next, turning to the shell coordinates and using these to describe the problem, then the following kinematic relations are obtained:

With the position coordinates defined as,

$$\rho \equiv r_I - r_T, \text{ and } s \equiv r_T \left(\varphi_I - \varphi_T\right) = r_T \left(\varphi_I - \dot{\varphi}_T t\right); \text{ then,} \tag{B.7a}$$

(a) the speed relations become,

$$\dot{\rho} = \dot{r}_I, \text{ and } \dot{s} = r_T \left(\dot{\varphi}_I - \dot{\varphi}_T\right);$$

$$\text{wherein } \dot{\varphi}_I = \frac{h_I}{r_I^2}; \tag{B.7b}$$

(b) and, the scalar accelerations are,

$$\ddot{\rho} = \ddot{r}_I, \quad \text{and} \quad \ddot{s} = r_T \ddot{\varphi}_I,$$

B.3 The general case. - Generally, the planar motion of the interceptor about the target will be expressed in shell coordinates (ρ, s). These corresponding relative motion expressions will be developed from eqs. (B.4), utilizing eqs. (B.7)

As outlined below a transformation scheme, leading to the desired relative motion equations, expressed in shell coordinates is used; i.e.,

(a) From eq. (B.7a), note that: $r_I = r_T \left(1 + \frac{\rho}{r_T}\right)$;

and

(b) from eq. (B.7b): $\dot{\varphi}_I = \frac{\dot{s}}{r_T} + \dot{\varphi}_T$.

(c) If these results are substituted into the second of eqs. (B.4) one obtains:

$$\ddot{\varphi}_I = \frac{\ddot{s}}{r_T} = -\frac{2\rho}{r_I}\left(\dot{\varphi}_T + \frac{\dot{s}}{r_T}\right);$$

or, solving for $\ddot{s}$, find that:

$$\ddot{s} = -\frac{2\dot{\rho}\left(1 + \frac{\dot{s}}{r_T\dot{\varphi}_T}\right)\dot{\varphi}_T}{\left(1 + \frac{\rho}{r_T}\right)} . \qquad (B.8)$$

(d) In addition, from the first of eqs. (B.4) one can show that:

$$\ddot{\rho} = r_T\left\{\left(1 + \frac{\rho}{r_T}\right)\left(\frac{\dot{s}}{r_T\dot{\varphi}_T} + 1\right)^2 - \frac{1}{\left(1 + \frac{\rho}{r_T}\right)^2}\right\}\dot{\varphi}_T^{\,2} , \qquad (B.9)$$

after incorporating eq. (B.6).

Next, eqs. (B.8, B.9) may be expressed in dimensionless form, after the following transformations are introduced:

Letting $\lambda = \frac{\rho}{r_T}$, and $\sigma = \frac{s}{r_T}$;

then $\dot{\lambda} = \frac{\dot{\rho}}{r_T}$, $\dot{\sigma} = \frac{\dot{s}}{r_T}$; or, alternately: $\dot{\lambda}_d = \frac{\dot{\rho}}{r_T\dot{\varphi}_T}$, and $\dot{\sigma}_d = \frac{\dot{s}}{r_T\dot{\varphi}_T}$;

and, finally,

$$\ddot{\lambda} = \frac{\ddot{\rho}}{r_T} \text{ , and } \ddot{\sigma} = \frac{\ddot{s}}{r_T} \text{ ; or, alternately, } \ddot{\lambda}_d = \frac{\ddot{\rho}}{r_T \dot{\varphi}_T^2} \text{ , and } \ddot{\sigma}_d = \frac{\ddot{s}}{r_T \dot{\varphi}_T^2} \text{ ;} \qquad \text{(B.10)}$$

here, $(\tilde{\ })_d$ infers a fully dimensionless quantity. In a real sense these transforms suggest a normalization of distances, using the radius (r_T); the speeds are placed in ratio to the circular speed $(r_T \dot{\varphi}_T)$; and, the kinematic accelerations are normalized by the target's centrifugal acceleration component, $(r_T \dot{\varphi}_T^2)$.

Introducing these newly defined coordinates into the differential equations of motion one obtains, from eqs. (B.8, B.9):

$$\ddot{\sigma} = \frac{-2\dot{\lambda}\ (1 + \dot{\sigma})}{(1 + \lambda)} \text{ ,}$$

and

$$\ddot{\lambda} = (1 + \lambda)(1 + \dot{\sigma})^2 - (1 + \lambda)^{-2}. \qquad \text{(B.11)}$$

Note that identical equations would result if one used expressions for $\ddot{\sigma}_d$ and $\ddot{\lambda}_d$.

In the alternate form of eqs. (B.10), the powers of $\dot{\varphi}_T$ follow the order of differentiation; consequently, a convenient transform for the independent variable is suggested; namely, with

$$\varphi_T = \dot{\varphi}_T t,$$

then

$$\frac{d}{d\varphi_T} = \frac{d}{d(\dot{\varphi}_T t)} \text{ .} \qquad \text{(B.12)}$$

Taking advantage of this substitution, and recalling that (for instance)

$$\lambda = \frac{\rho}{r_T} \text{ ; then } \dot{\lambda}_d = \frac{\dot{\rho}}{r_T \dot{\varphi}_T} = \frac{1}{\dot{\varphi}_T} \frac{d\lambda}{dt} = \frac{d\lambda}{d\varphi_T} \equiv \lambda' \text{ , etc. ;}$$

then eqs. (B.11) may be alternately expressed as,

$$\sigma'' = \frac{-2\lambda' (1 + \sigma')}{(1 + \lambda)} ,$$

and

$$\lambda'' = (1 + \lambda) (1 + \sigma')^2 - (1 + \lambda)^{-2} , \tag{B.13}$$

where primes signify differentiation with respect to the angle, φ_T, used as the independent variable, now.

B.4 The linearized differential equations of motion. - Because eqs. (B.13) are nonlinear, and because there is coupling between these two expressions, it is evident that analytic results are not readily obtained. Hence, in order to proceed, it will be necessary to replace the general expressions with others more amenable to mathematical manipulation. To accomplish this task, it is suggested that the equation's denominator might be expanded in a binomial series. Thus, after expanding, and grouping on powers of the variables (λ, σ and λ', σ'), it is found that:

$$\sigma'' = -2[\lambda' + \lambda' \sigma' - \lambda \lambda' + \lambda^2 \lambda' - \lambda \lambda' \sigma' + 0 (\lambda^4)] ,$$

and

$$\lambda'' = 2\sigma' + 3\lambda + \sigma'^2 + 2\lambda \sigma' - 3\lambda^2 + \lambda \sigma'^2 + 4\lambda^3 + 0 (\lambda^4). \tag{B.14}$$

Eqs. (B.14) are "correct" through a third order combination of terms; however, a first order (linear) solution is developed in the next paragraphs. This should lead to a result which is valid for small (λ, σ) and their derivatives; such results are analogous to the linearization carried out in Appendix A.

B.5 A linear solution. - From eqs. (B.14) a first order solution is obtained from the "reduced" equations of motion. Thus, if only first order quantities are retained, the system of equations reduces to:

$$\sigma'' \cong -2\lambda',$$

and

$$\lambda'' \cong 2\sigma' + 3\lambda . \tag{B.15}$$

The first expression provides a first integral immediately:

$$\sigma' = -2\lambda + K_1, \tag{B.16}$$

where K_1 is a constant of integration.

Using this result in the second of eqs. (B.15), then:

$$\lambda'' + \lambda = 2K_1, \tag{B.17a}$$

which integrates to give:

$$\lambda = 2K_1 + K_2 \sin \varphi_T + K_3 \cos \varphi_T , \tag{B.17b}$$

wherein K_2 and K_3 are also integration constants.

Next, this relation can be used in eq. (B.16) in order to complete the general "linear solution"; from this substitution:

$$\sigma' = -3K_1 - 2(K_2 \sin \varphi_T + K_3 \cos \varphi_T),$$

which integrates to:

$$\sigma = -3K_1 \varphi_T + 2K_2 \cos \varphi_T - 2K_3 \sin \varphi_T + K_4, \tag{B.18}$$

with the K_i ($i = 1 \rightarrow 4$) being integration constants. One should remember that (here) $\varphi_T = \dot{\varphi}_T t$, since $\dot{\varphi}_T$ is a constant.

B.6 Evaluation of constants. - In order to retain the generality of this problem the following set of initial values are assumed:

$$\text{at } t = 0\text{: let } \rho = \rho_o,\ s = s_o\ ;$$

$$\text{and } \dot{\rho} = \dot{\rho}_o,\ \dot{s} = \dot{s}_o. \tag{B.19a}$$

This is equivalent to stating that, at $t = 0$:

$$\lambda = \lambda_o,\ \sigma = \sigma_o;\ \lambda' = \lambda'_o \text{ and } \sigma' = \sigma'_o\ ;$$

since

$$\lambda \equiv \frac{\rho}{r_T}\ ,\ \text{etc};\ \sigma' \equiv \frac{d\sigma}{d\varphi_T} \Leftrightarrow \frac{ds}{d(r_T\dot{\varphi}_T t)}\ ,\ \text{etc.} \tag{B.19b}$$

An evaluation of the constants (K_i), using eqs. (B.19), (B.16), (B.17b) and (B.18), allows one to write the "linear" solution as:

$$\lambda = \lambda_o + \lambda'_o \sin\varphi_T + (3\lambda_o + 2\sigma'_o)(1 - \cos\varphi_T),$$

and

$$\sigma = \sigma_o + \sigma'_o\,\varphi_T - 2[\lambda'_o(1 - \cos\varphi_T) + (3\lambda_o + 2\sigma'_o)(\varphi_T - \sin\varphi_T)]. \tag{B.20}**$$

It should be evident that time is implied here, as the independent variable, through $\varphi_T = \dot{\varphi}_T t$. Also, an inspection of eqs. (B.20) indicates that this predicted motion could be rather complicated in its geometric interpretation.

B.7 Speed components for the interceptor. - The relative motion of the interceptor is approximated by eqs. (B.20), the linearized solution. Associated with these coordinates is a set of relative speed quantities which may be obtained by differentiating the displacements. These quantities are also expressed as dimensionless variables (λ', σ'), which can be converted to dimensional speeds.

**It should be recognized that φ_T can be measured from any convenient origin on the circular orbit; then, selecting the origin at the initial point (corresponding to t=0), it follows that φ_T is a measure of the transfer (angle) for the target particle. In this regard it is not necessary to describe a pericenter location for the target.

by a multiplication, using the constant quantity, $(r_T \dot{\varphi}_T)$.

Consequently, the dimensionless speeds, corresponding to eqs. (B.20), are:

$$\lambda' = \lambda'_o \cos \varphi_T + (3\lambda_o + 2\sigma'_o) \sin \varphi_T,$$

and

$$\sigma' = \sigma'_o - 2[\lambda'_o \sin \varphi_T + (3\lambda_o + 2\sigma'_o)(1 - \cos \varphi_T)]. \qquad \text{(B.21)*}$$

B.8 Displacements and speeds (a summary). - The purpose of this appendix was to develop a second set of state variables representing a solution to the relative motion problem. For this representation the problem is defined in (planar) shell coordinates; subsequently these were expressed in dimensionless variables. For these expressions the position angle, referred to the "target" trajectory, serves as the independent variable; the appropriate dimensionless displacements and speeds are given by eqs. (B.20) and (B.21). For convenience these several relations are listed below:

(a) The dimensionless displacements, from eqs. (B.20) are:

$$\lambda = \lambda_o + \lambda'_o \sin \varphi_T + (3\lambda_o + 2\sigma'_o)(1 - \cos \varphi_T),$$

and

$$\sigma = \sigma_o + \sigma'_o \varphi_T - 2[\lambda'_o (1 - \cos \varphi_T) + (3\lambda_o + 2\sigma'_o)(\varphi_T - \sin \varphi_T)]. \qquad \text{(B.22a)}$$

(b) The dimensionless speeds, from eqs. (B.21), are:

$$\lambda' = \lambda'_o \cos \varphi_T + (3\lambda_o + 2\sigma'_o) \sin \varphi_T,$$

and

$$\sigma' = \sigma'_o - 2[\lambda'_o \sin \varphi_T + (3\lambda_o + 2\sigma'_o)(1 - \cos \varphi_T)], \qquad \text{(B.22b)}$$

wherein $\lambda \equiv \frac{\rho}{r_T}$, $\sigma \equiv \frac{s}{r_T}$, $\lambda' \equiv \frac{d\rho}{d\varphi_T}$, $\sigma' \equiv \frac{ds}{d\varphi_T}$; and $(\sim)_o$ indicates initial values.

B.9 Dimensionless variables. - Eqs. (B.22), having been expressed in dimensionless form are adequate for representing the linearized solution; but they do not describe the physical and dimensional (or size) aspects of a relative motion, as time progresses.

In order to convert to dimensional quantities, and to employ time as the independent parameter, one can perform the same transformation manipulations as noted in Appendix A. Thus, to convert from λ, σ, λ', σ' to ρ, s, $\dot{\rho}$, $\dot{s}$ the operations are, simply:

$$\begin{bmatrix} \rho \\ s \end{bmatrix} = r_T \begin{bmatrix} \lambda \\ \sigma \end{bmatrix} , \qquad \text{and} \qquad \begin{bmatrix} \dot{\rho} \\ \dot{s} \end{bmatrix} = r_T \dot{\varphi}_T \begin{bmatrix} \lambda' \\ \sigma' \end{bmatrix} ,$$

with the definitions for ρ, s being those given by eqs. (B.1), in agreement with Figure B.1. For clarity, it should be recalled that r_T, $\dot{\varphi}_T$ are the radius and angular rate for the target vehicle as it moves along its circular flight path.

APPENDIX C

LINE-OF-SIGHT ANGLES FOR THE RELATIVE MOTION OF TWO ORBITING MASS PARTICLES

C.1 Defining the angle for line-of-sight (LOS); in-plane. - In this appendix analytic expressions are derived which describe the "line-of-sight", or "look" direction, used to locate the target from the interceptor (or vice-versa). Two cases are considered; one for the relative motion described in cartesian coordinates; and, the second case, for a representation in shell coordinates. In both developments the motions will be restricted to a common plane, initially; the extension to three dimensions follows a same general pattern.

C.1.1 Cartesian coordinates (two dimensional case): The sketch, on Fig. C.1, indicates a typical situation as it might occur at some time, $t > t_o$. The interceptor (I) is assumed to be at a position (x, y) relative to the target (T).

The line of sight (angle), designated as $\measuredangle$ LOS, is measured from the interceptor's local forward horizon (i.e., from $\bar{e}_{\varphi_I}$) in a clockwise (or anti-motion) direction to the target.

Relative to a fixed origin (O) the target and interceptor are located by coordinates (r_T, φ_T) and (r_I, φ_I), respectively.

From the sketch, one notes that

$$r_I \cos \delta\varphi = r_T + x,$$

and

$$r_I \sin \delta\varphi = y, \tag{C.1}$$

where $\delta\varphi = \varphi_I - \varphi_T$ (the difference in position angle for the two vehicles). According to the geometry shown on the figure;

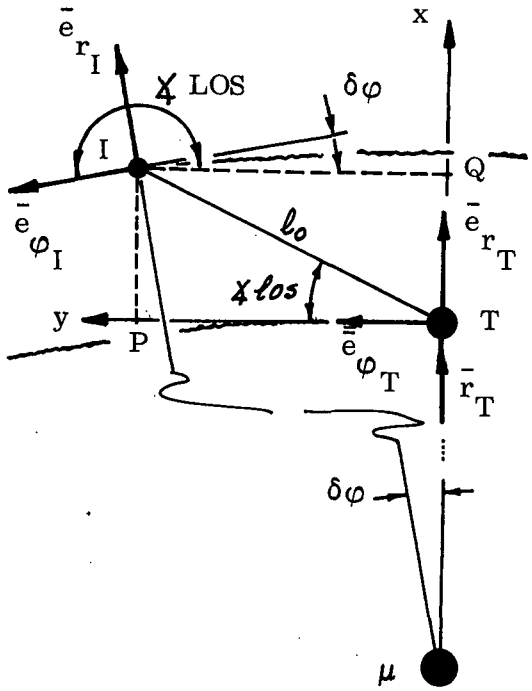

Fig. C.1. Line-of-Sight (or "look") Angles referred to Cartesian Frame of Reference.

χ_{los} , line of sight angle

ℓ_o , separation distance (I, T)

PQ , coordinates of I

$\delta\varphi = \varphi_I - \varphi_T$

(x, y), cartesian coordinates

(ρ, s), shell coordinates.

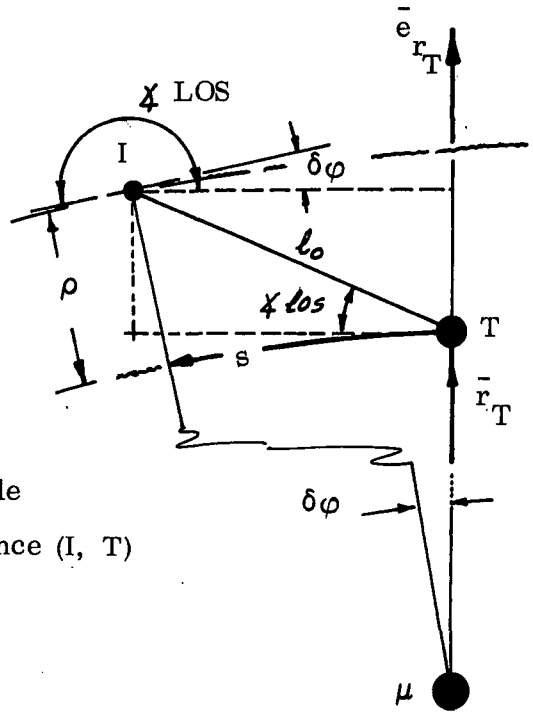

Fig. C.2. Line-of-Sight ("look") Angles described in Shell Coordinates.

$$\delta\varphi = \tan^{-1}\left(\frac{y}{r_T+x}\right) . \qquad (C.2)$$

It should be apparent that the target-to-interceptor line-of-sight angle ($\measuredangle$ los), locating the interceptor from the target, is described by

$$\measuredangle \text{ los} = \tan^{-1}\left(\frac{x}{y}\right). \qquad (C.3)$$

Using this last description, it is evident that the line-of-sight angle ($\measuredangle$ LOS) which locates the target vehicle <u>from</u> the interceptor, may be expressed as;

$$\measuredangle \text{ LOS} = \pi + \delta\varphi + \measuredangle \text{ los};$$

or, using eqs. (C.2) and (C.3);

$$\measuredangle \text{LOS} = \pi + \tan^{-1}\left(\frac{y/r_T}{1+x/r_T}\right) + \tan^{-1}\left(\frac{x/r_T}{y/r_T}\right). \qquad (C.4a)$$

Expressed in terms of the dimensionless quantities (ξ, η), it is easily shown that;

$$\measuredangle \text{ LOS} = \pi + \tan^{-1}\left(\frac{\eta}{1+\xi}\right) + \tan^{-1}\left(\frac{\xi}{\eta}\right), \qquad (C.4b)$$

wherein $\xi \equiv \frac{x}{r_T}$ and $\eta \equiv \frac{y}{r_T}$ (introduced in Appendix A).

One notes that so long as the <u>interceptor</u> is <u>above</u> the target, then the line-of-sight lies in the range

$$\pi < \measuredangle \text{ LOS} < 2\pi ,$$

generally. For the converse situation, when the <u>target</u> is <u>above</u> the interceptor, then the range for $\measuredangle$ LOS is,

$$0 < \measuredangle \text{ LOS} < \pi .$$

C.1.2 Shell coordinates: A definition for the line-of-sight (angle), when the motion is described in shell coordinates, follows here in agreement with the sketch shown above. Again the development considers the planar case only; that is, both vehicles are in a same plane of motion.

Here, the dimensional coordinates locating the interceptor (I), but measured from the target (T), are (ρ, s); where

$$\rho \equiv r_I - r_T,$$

and

$$s \equiv r_T \, \delta\varphi ; \; (\delta\varphi = \varphi_I - \varphi_T). \tag{C.5}$$

Correlating the two descriptive sets of relative coordinates, (x, y) and (ρ, s) one can see that;

$$y = (\rho + r_T) \sin \delta\varphi ,$$

and

$$x = (\rho + r_T) \cos \delta\varphi - r_T. \tag{C.6}$$

As a consequence the "look" angle ($\measuredangle$ los) is, by definition,

$$\measuredangle \text{ los} = \tan^{-1} \left(\frac{x}{y} \right) \equiv \tan^{-1} \left[\frac{(\rho + r_T) \cos \delta\varphi - r_T}{(\rho + r_T) \sin \delta\varphi} \right].$$

Next, recalling that

$$\measuredangle \text{ LOS} = \pi + \delta\varphi + \measuredangle \text{ los},$$

then it follows that;

$$\measuredangle \text{ LOS} = \pi + \delta\varphi + \tan^{-1}\left[\frac{(\rho + r_T)\cos\delta\varphi - r_T}{(\rho + r_T)\sin\delta\varphi}\right], \qquad (C.7)$$

where $\delta\varphi = s/r_T$ (by definition).

Expressed in dimensionless coordinates (λ, σ) this last relationship can be rewritten as;

$$\measuredangle \text{ LOS} = \pi + \sigma + \tan^{-1}\left[\frac{(1+\lambda)\cos\sigma - 1}{(1+\lambda)\sin\sigma}\right], \qquad (C.8)$$

with $\lambda \equiv \rho/r_T$, $\sigma \equiv \dfrac{s}{r_T}$.

APPENDIX D

A SOLUTION FOR THE RELATIVE MOTION OF ADJACENT ORBITING PARTICLES, WITH THRUSTING

D.1 Equations of motion. - In Appendix A, the general problem of two adjacent mass particles was examined. There the relative motion, for one particle with respect to another, was formulated and an analytic (linearized) solution was obtained.

In this Appendix the linearized problem is reexamined for that case where a thrusting capability, for one particle, is included. By suitably restricting the formulation, it is possible to obtain analytic solutions for the relative motion with this added influence included. It is expected that by including this additional influence the reader will have an even more complete grasp of this problem; but without the complexity of a myriad of mathematical statements.

D.2 Formulation of the problem. - The formal description of this problem is quite similar to that found in Appendix A; it does differ in that it has the added thrust (acceleration) term. This added capability, to alter the relative motion, is applied to the interceptor particle, hence its influence on the state variables is direct.

In the formulation, the general thrust is assumed to have components (F_x, F_y, F_z); thus, the fixed, specific thrust terms will be denoted as (T_x, T_y, T_z).

Since the linearization of the differential equations, describing the problem, would follow the same steps as outlined in Appendix A, they are not repeated here. Consequently, the linearized expressions to be solved for the relative displacements, including the specific thrust terms, are those noted below:

$$\ddot{x} - 2\dot{\varphi}_T\dot{y} - 3\dot{\varphi}_T^2 x = \frac{F_x}{m} \equiv T_x,$$

$$\ddot{y} + 2\dot{\varphi}_T\dot{x} = \frac{F_y}{m} \equiv T_y,$$

and

$$\ddot{z} + \dot{\varphi}_T^2 z = \frac{F_x}{m} \equiv T_z. \qquad \text{(D.1)*}$$

D.3 /Solutions to the equations of motion. - Once again the descriptive expressions, for the motion, are separated into two sets. The third equation in eqs. (D.1), is not influenced by the other two, hence it may be solved independently. Contrary to this, the remaining expressions are coupled and must be solved together. The scheme which has been employed here is the same as that noted in Appendix A. In this regard the second equation yields a first integral, which can be inserted into the first expression to obtain an equation in one dependent variable. The resulting expression provides a solution for (here) x; and, this resultant can be utilized, then, in the previously acquired first integral to obtain a solution for the remaining variable.

In an outlined form, the several steps involved are as follows:

A first integral of the second of eqs. (D.1) can be written as:

$$\dot{y} + 2\dot{\varphi}_T x = T_y t + \mathcal{C}_1, \qquad \text{(D.2)}$$

where $\mathcal{C}_1$ is a constant of integration. In terms of the general initial values for the problem, this constant can be expressed by:

$$\mathcal{C}_1 = \dot{y}_o + 2\dot{\varphi}_T x_o. \qquad \text{(D.3)}$$

*As in the previous analysis, it has been assumed here that the particle, m_T, travels along a circular orbit about the primary (μ).

When eq. (D.2) is inserted into the first of eqs. (D.1), one obtains

$$\ddot{x} + \dot{\varphi}_T^2 x = (T_x + 2\mathcal{C}_1\dot{\varphi}_T) + (2\dot{\varphi}T_y)\,t,$$

which has a standard solution form - a harmonic resultant for the homogeneous expression, plus the particular solution. It is not difficult to show that,

$$x = A \sin \dot{\varphi}_T t + B \cos \dot{\varphi}_T t + \left(\frac{T_x}{\dot{\varphi}_T^2} + \frac{2\mathcal{C}_1}{\dot{\varphi}_T}\right) + \frac{2T_y}{\dot{\varphi}_T^2}\,t\,, \tag{D.4}$$

where A, B are constants to be evaluated. Modifying eq. (D.2), using eq. (D.4), then the elementary integral, resulting, can be written down immediately;

$$y = \mathcal{C}_4 - \left[\left(3\mathcal{C}_1 + 2\,\frac{T_x}{\dot{\varphi}_T}\right)t + \frac{3T_y}{\dot{\varphi}_T^2}\,t^2 - 2(A\cos\dot{\varphi}_T t - B\sin\dot{\varphi}_T t)\right], \tag{D.5}$$

wherein $\mathcal{C}_4$ is a (second) constant of integration.

Since the last differential expression can be solved, independently, then by inspection it is apparent that its solution may be written as:

$$z = K_1 \sin \dot{\varphi}_T t + K_2 \cos \dot{\varphi}_T t + \frac{T_z}{\dot{\varphi}_T^2}\,, \tag{D.6}$$

where the K_j are (initial valued) constants.

D.3.1 Evaluation of constants: Expressing the initial values as parameters, designated by $(\sim)_o$, then the constants appearing in eqs. (D.4, D.5, D.6) may be described. These several quantities are found to be:

$$A = \frac{\dot{x}_o}{\dot{\varphi}_T} - 2\,\frac{T_y}{\dot{\varphi}_T^{\,2}}\,,\quad B = -\left[3x_o + 2\,\frac{\dot{y}_o}{\dot{\varphi}_T} + \frac{T_x}{\dot{\varphi}_T^{\,2}}\right],$$

$$\mathcal{C}_1 = 2x_o\dot{\varphi}_T + \dot{y}_o,\quad \mathcal{C}_4 = y_o - 2A = y_o - 2\left(\frac{\dot{x}_o}{\dot{\varphi}_T} - 2\,\frac{T_y}{\dot{\varphi}_T^{\,2}}\right),$$

and $$K_1 = \frac{\dot{z}_o}{\dot{\varphi}_T}\,,\quad K_2 = z_o - \frac{T_3}{\dot{\varphi}_T^{\,2}}\,. \qquad \text{(D.7)}$$

D.4 Summary of relative motion state equations. - The relative motion displacement equations may be written down, now, in terms for the (general) initial state parameters. Similarly, by differentiation, the relative motion speed components may (also) be obtained; hence, the full state of the relative motion is known from the prescribed linearized equations of motion. A set of these expressions is included here, below; however, it should be noted that the speed component expressions have been altered slightly in order to present them in a more concise and homogeneous form. (The manipulation has been involved in substitutions through the constants (A, B) above).

(a) Relative motion displacements:

$$x = x_o + \frac{\dot{x}_o}{\dot{\varphi}_T}(\dot{\varphi}_T t) - \left[A\,(\dot{\varphi}_T t - \sin\dot{\varphi}_T t) + B\,(1-\cos\dot{\varphi}_T t)\right],$$

$$y = y_o + \left[\frac{\dot{y}_o}{\dot{\varphi}_T} - \frac{3}{2}\,\frac{T_y}{\dot{\varphi}_T^{\,2}}\,(\dot{\varphi}_T t)\right]\dot{\varphi}_T t + 2\left[B\,(\dot{\varphi}_T t - \sin\dot{\varphi}_T t) - A\,(1-\cos\dot{\varphi}_T t)\right],$$

and $$z = z_o\cos\dot{\varphi}_T t + \frac{\dot{z}_o}{\dot{\varphi}_T}\sin\dot{\varphi}_T t + \frac{T_z}{\dot{\varphi}_T^{\,2}}\,(1-\cos\dot{\varphi}_T t). \qquad \text{(D.8a)}$$

(b) Relative motion speed components:

$$\frac{\dot{x}}{\dot{\varphi}_T} = \frac{\dot{x}_o}{\dot{\varphi}_T} - \left[A\,(1-\cos\dot{\varphi}_T t) + B\sin\dot{\varphi}_T t\right],$$

$$\frac{\dot{y}}{\dot{\varphi}_T} = \frac{\dot{y}_o}{\dot{\varphi}_T} - \left[2\,\frac{x_o}{\dot{\varphi}_T} - \frac{T_y}{\dot{\varphi}_T^{\,2}}\right]\dot{\varphi}_T t + 2\left[B\,(1-\cos\dot{\varphi}_T t) + A\,(\dot{\varphi}_T t - \sin\dot{\varphi}_T t)\right],$$

and $$\frac{\dot{z}}{\dot{\varphi}_T} = \frac{\dot{z}_o}{\dot{\varphi}_T}\cos\dot{\varphi}_T t + \left(\frac{T_z}{\dot{\varphi}_T^{\,2}} - z_o\right)\sin\dot{\varphi}_T t; \qquad \text{(D. 8b)}$$

wherein $A = \dfrac{\dot{x}_o}{\dot{\varphi}_T} - 2\,\dfrac{T_y}{\dot{\varphi}_T^{\,2}}$, and $B = -\left(3x_o + 2\,\dfrac{\dot{y}_o}{\dot{\varphi}_T} + \dfrac{T_x}{\dot{\varphi}_T^{\,2}}\right)$.

In these expressions the argument for all trigonometric terms is $\dot{\varphi}_T t$ ($=\varphi_T$, since $\dot{\varphi}_T$ = constant). Also, the speeds appear in ratio to $\dot{\varphi}_T$; the reason for this is in anticipation of the nondimensionalization which is to occur (below). As a matter of fact, in this next operation the independent variable is changed, from t, and the state variables, etc. are <u>all</u> recast as dimensionless variables (and constants).

D. 5 <u>Equations for the relative motion in dimensionless form.</u> - Here the state variables (dependent variables) and the forcing quantities (thrust components) are expressed in dimensionless form. Also, the independent variable (t) is transformed to the position angle, via ($\varphi_T = \dot{\varphi}_T t$), and the expressions above, eqs. (D. 8), are recast in this alternate form.

The nondimensionalization is identical to that used in Appendix A, hence it is obtained by the operations indicated in eqs. (A. 31). In addition, the specific

thrust terms are normalized by the quantity, $\dot{\varphi}_T^2 \, r_T$, the centripetal acceleration (term) for the circular orbit (of m_T). These last quantities will be written as follows:

$$\tau_k \equiv \frac{T_j}{r_T \dot{\varphi}_T^2} \, , \quad (k = \xi, \, \eta, \, \zeta \, ; \; j = x, \, y, \, z). \tag{D.9}$$

A summary (set) of these dimensionless expressions is noted below; they correspond to, and are drawn from, eqs. (D.8) above:

(a) Dimensionless relative motion displacements:

$$\xi = \xi_o + \xi'_o \varphi_T - \left[A_o \, (\varphi_T - \sin \varphi_T) + B_o \, (1 - \cos \varphi_T) \right] ,$$

$$\eta = \eta_o + (\eta'_o - \frac{3}{2} \, \tau_\eta \varphi_T) \, \varphi_T + 2 \left[B_o \, (\varphi_T - \sin \varphi_T) - A_o \, (1 - \cos \varphi_T) \right],$$

and $$\zeta = \zeta_o \cos \varphi_T + \zeta'_o \sin \varphi_T + \tau_\zeta \, (1 - \cos \varphi_T); \tag{D.10a}$$

with A_o and B_o defined below.

(b) Dimensionless relative motion speed components:

$$\xi' = \xi'_o - \left[A_o \, (1 - \cos \varphi_T) + B_o \sin \varphi_T \right],$$

$$\eta' = \eta'_o - (2\xi'_o - \tau_\eta) \, \varphi_T + 2 \left[B_o \, (1 - \cos \varphi_T) + A_o \, (\varphi_T - \sin \varphi_T) \right],$$

and $$\zeta' = \zeta'_o \cos \varphi_T + (\tau_\zeta - \zeta_o) \sin \varphi_T ; \tag{D.10b}$$

where $A_o \equiv \xi'_o - 2\tau_\eta$ and $B_o \equiv - (3\xi_o + 2\eta'_o + \tau_\xi)$.

$$x = x_o\,(4-3\cos\dot{\varphi}_T t) + \frac{\dot{x}_o}{\dot{\varphi}_T}\sin\dot{\varphi}_T t + 2\,\frac{\dot{y}_o}{\dot{\varphi}}\,(1-\cos\dot{\varphi}_T t) + \frac{T_x}{\dot{\varphi}_T^{\,2}}\,(1-\cos\dot{\varphi}_T t)$$

$$+ 2\,\frac{T_y}{\dot{\varphi}_T^{\,2}}\,(\dot{\varphi}_T t - \sin\dot{\varphi}_T t)\,,$$

$$y = y_o - 3\left(2x_o + \frac{\dot{y}_o}{\dot{\varphi}_T}\right)\left(\dot{\varphi}_T t - \sin\dot{\varphi}_T t\right) + \frac{\dot{y}_o}{\dot{\varphi}_T}\sin\dot{\varphi}_T t - 2\,\frac{\dot{x}_o}{\dot{\varphi}_T}\,(1-\cos\dot{\varphi}_T t)$$

$$+ \frac{T_y}{\dot{\varphi}_T^{\,2}}\left[4\,(1-\cos\dot{\varphi}_T t) - \frac{3}{2}\,(\dot{\varphi}_T t)^2\right] - 2\,\frac{T_x}{\dot{\varphi}_T^{\,2}}\,(\dot{\varphi}_T t - \sin\dot{\varphi}_T t),$$

and

$$z = z_o\cos\dot{\varphi}_T t + \frac{\dot{z}_o}{\dot{\varphi}_T}\sin\dot{\varphi}_T t + \frac{T_z}{\dot{\varphi}_T^{\,2}}\,(1-\cos\dot{\varphi}_T t). \tag{D.11}$$

Symbolically, these last equations can be represented as,

$$\begin{bmatrix} x \\ y \\ z \end{bmatrix} = \begin{bmatrix} J_x \\ J_y \\ J_z \end{bmatrix} + \begin{bmatrix} K_{xx} & K_{xy} & K_{xz} \\ K_{yx} & K_{yy} & K_{yz} \\ K_{zx} & K_{zy} & K_{zz} \end{bmatrix} \begin{bmatrix} T_x \\ T_y \\ T_z \end{bmatrix}, \tag{D.12a}$$

or

$$\{\varkappa\} = \{J\} + [K]\{T\}\,. \tag{D.12b}$$

Actually, in the scheme above there is no need to include the z-component since this is not coupled with the x, y components. Hence, in the determination to follow it will be presumed that the matrices are constructed without the $\dot{z}$-th elements being present.

Now, setting $\{\varkappa\} = 0$ as the requirement for intercept, it follows that the thrusts needed to null $\{\varkappa\}$ are obtained by the following method:

Since intercept infers

$$0 = \{J^*\} + [K^*]\{T^*\},$$

then

$$\{T^*\} = -[K^*]^{-1}\{J^*\}, \tag{D.13}$$

where $[K^*]^{-1}$ is the inverse of the matrix $[K^*]$; here $(\sim)^*$ infers those quantities particular to $t = t^*$, the intercept time.

When the operation in eq. (D.13) has been carried out, the following set of equations (plus the z-th component) is obtained:

$$\frac{T^*_x}{(\dot\varphi_T)^2}\Delta = x_o\left[24(\dot\varphi_T t^*)\sin\dot\varphi_T t^* - 3(\dot\varphi_T t^*)^2\left(2+\frac{3}{2}\cos\dot\varphi_T t^*\right) - 28(1-\cos\dot\varphi_T t^*)\right.$$

$$+ 2y_o\left[\dot\varphi_T t^* - \sin\dot\varphi_T t^*\right] + \frac{\dot x_o}{\dot\varphi_T}\left[\frac{3}{2}(\dot\varphi_T t^*)\sin\dot\varphi_T t^* - 4(1-\cos\dot\varphi_T t^*)\right]\dot\varphi_T t^*$$

$$\left. + \frac{\dot y_o}{\dot\varphi_T}\left[14(\dot\varphi_T t^*)\sin\dot\varphi_T t^* - 3(\dot\varphi_T t^*)^2(1-\cos\dot\varphi_T t^*) - 16(1-\cos\dot\varphi_T t^*)\right]\right],$$

$$\frac{T^*_y}{(\dot\varphi_T)^2}\Delta = \left[\left(4\frac{\dot x_o}{\dot\varphi_T} - \frac{\dot y_o}{\dot\varphi_T}(\dot\varphi_T t^*) - y_o\right)(1-\cos\dot\varphi_T t^*)\right] - 2\left[x_o(\dot\varphi_T t^* - \sin\dot\varphi_T t^*)\right.$$

$$\left. + \frac{\dot x_o}{\dot\varphi_T}(\dot\varphi_T t^*)\sin\dot\varphi_T t^*\right], \tag{D.14a}$$

wherein, the determinant,

$$\Delta = 8\left[1-\cos \dot{\varphi}_T t^* - (\dot{\varphi}_T t^*) \sin \dot{\varphi}_T t^*\right] + \frac{(\dot{\varphi}_T t^*)^2}{2}\left[5 + 3 \cos \dot{\varphi}_T t^*\right]. \qquad \text{(D.14b)}$$

Lastly, the z-th thrust component is found to be,

$$\frac{T^*_z}{(\dot{\varphi}_T)^2} = -\frac{\frac{\dot{z}_o}{\dot{\varphi}_T} \sin \dot{\varphi}_T t^* + z_o \cos \dot{\varphi}_T t^*}{1 - \cos \dot{\varphi}_T t^*}. \qquad \text{(D.14c)}$$

The expressions above, eqs. (D.14), specify the magnitude and direction of the (specific) thrust required to produce an intercept, with m_T, from a known (a priori) state. Of necessity, these quantities presume the intercept will occur in a predetermined time (t^*); or, after the target (m_T) has traversed a specified transfer angle ($\varphi^*_T = \dot{\varphi}_T t^*$). In the next sub-section, the above expressions will be rewritten, but (now) in dimensionless form.

D.6.2 Dimensionless thrusts, for intercept: The following equations are equivalent to eqs. (D.14),but are given in dimensionless quantities. Here, as before, the nondimensional parameters follow the scheme illustrated by eqs. (A.31), in Appendix A.

The desired expressions are:

$$\tau^*_\xi \Delta = \xi_o\left[24 (\varphi^*_T) \sin \varphi^*_T - 3 \varphi^{*2}_T (2 + \frac{3}{2} \cos \varphi^*_T) - 28 (1-\cos \varphi^*_T)\right]$$

$$+ 2\eta_o\left[\varphi^*_T - \sin \varphi^*_T\right] + (\xi'_o)\left[\frac{3}{2} \varphi^*_T \sin \varphi^*_T - 4 (1-\cos \varphi^*_T)\right] \varphi^*_T$$

$$+ (\eta'_o)\left[14 \varphi^*_T \sin \varphi^*_T - 3 (\varphi^*_T)^2 (1+\cos \varphi^*_T) - 16 (1-\cos \varphi^*_T)\right],$$

$$\tau^*_\eta \Delta = \left[(4\xi'_o - \eta'_o \varphi^*_T - \eta_o)(1-\cos \varphi^*_T)\right] - 2\left[\xi_o (\varphi^*_T - \sin\varphi^*_T) + \xi'_o \varphi^*_T \sin\varphi^*_T\right], \qquad \text{(D.15a)}$$

wherein

$$\Delta = 8\left[1-\cos\varphi^*_T - \varphi^*_T \sin\varphi^*_T\right] + \frac{(\varphi^*_T)^2}{2}\left[5 + 3\cos\varphi^*_T\right]. \qquad \text{(D.15b)}$$

Finally, the last intercept requirement (component) is,

$$\tau^*_\zeta = -\frac{\zeta'_o \sin\varphi^*_T + \zeta_o \cos\varphi^*_T}{1 - \cos\varphi^*_T}. \qquad \text{(D.15c)}$$

APPENDIX E

A SECOND ORDER CORRECTION FOR THE RELATIVE MOTION OF TWO ORBITING MASS PARTICLES

E.1 The equations of motion. - In Appendix A, equations governing the relative motion of one orbiting particle, with respect to another particle, were developed. These expressions were of particular use in providing general descriptions of the relative motion state; and, in explaining the geometrical traces of such motions. Of course, the applicability of those expressions is limited, due to the inherent inaccuracies arising from the attendant assumptions employed. In order to overcome some of this inadequacy, due to linearization, a second order correction (to be applied to the "linear solution") is developed, here. This development is an extension of the work presented in Appendix A; consequently, it will follow the same general procedures presented there. For conciseness of notation, the major portion of this work will be carried out in dimensionless variables; and, as before, the "target" particle is presumed to follow a circular orbit about the primary (μ).

E.2 Development of the governing equations. - Here, as in Appendix A, each of the two particles are assumed to have a Keplerian motion about the primary (μ), but without any mutual attraction force, or other perturbative influences. The geometry for this problem is described on Fig. A.1; there one sees the reference triad with origin at "T".

Since the particle m_I is located by the relative position vector, $\bar{r}_r$, where $\bar{r}_r = (x\bar{e}_x + y\bar{e}_y + z\bar{e}_z)$, then from eqs. (A.1) one can construct the expression

$$\ddot{\bar{r}}_I = -\frac{\mu}{r_I^3}(\bar{r}_T + \bar{r}_r) \tag{E.1}$$

recognizing that $\bar{r}_I = \bar{r}_T + \bar{r}_r$.

When eq. (A.1) is applied to the particle "T", on its assumed circular orbit, it is found that

$$r_T^3 \dot{\varphi}_T^2 = \mu ,$$

and

$$r_T^2 \dot{\varphi}_T = h_T \text{ (constant)}, \tag{E.2}$$

as shown by eq. (A.16). Making use of the equations above, and expressing $\ddot{\bar{r}}_I$, kinematically, as

$$\ddot{\bar{r}}_I = \left[\ddot{r}_T + \ddot{x} - 2\dot{\varphi}_T \dot{y} - y\ddot{\varphi}_T - (x + r_T)\dot{\varphi}_T^2\right]\bar{e}_x + \left[\ddot{y} + 2\dot{\varphi}_T (\dot{x} + \dot{r}_T) + (x + r_T)\ddot{\varphi}_T - y\dot{\varphi}_T^2\right]\bar{e}_y + \ddot{z}\,\bar{e}_z , \tag{E.3}$$

taking account of the fact that $\bar{\omega} = \dot{\varphi}_T \bar{e}_z$ and $\bar{r}_T = r_T \bar{e}_x$, as in eq. (A.14). Recognizing that r_T and $\dot{\varphi}_T$ are fixed quantities, here, then eq. (E.1) can be recast as

$$\left[\ddot{x} - 2\dot{\varphi}_T \dot{y} - (x + r_T)\dot{\varphi}_T^2\right]\bar{e}_x + \left[\ddot{y} + 2\dot{\varphi}_T \dot{x} - y\dot{\varphi}_T^2\right]\bar{e}_y + \ddot{z}\, e_z =$$

$$- \frac{\dot{\varphi}_T^2 r_T^3}{r_I^3}\left[(x + r_T)\bar{e}_x + y\bar{e}_y + z\bar{e}_z\right], \tag{E.4}$$

accounting for eqs. (E.2) and (E.3).

For eq. (E.4), the term $(r_T/r_I)^3$ can be expressed by

$$\left(\frac{r_I}{r_T}\right)^3 = \left[\left(1 + \frac{x}{r_T}\right)^2 + \frac{y^2 + z^2}{r_T^2}\right]^{3/2} ; \tag{E.5}$$

then the scalar equations describing the problem follow directly.

E.3 Dimensionless variables. - For the conciseness of notation, mentioned earlier, a change of the independent variable, and dimensionless dependent variables are introduced. The scheme which is used here is that indicated by eq. (A.31), Appendix A.

Also, in this formulation, the quantities in eq. (E.5) are expanded (binomially) - up to third order - so that the dimensionless scalar expressions for the relative motion are:

$$\xi'' - 2\eta' - 3\xi \simeq -3\xi^2 + \frac{3}{2}(\eta^2 + \zeta^2),$$

$$\eta'' + 2\xi' \simeq 3\xi\eta,$$

and

$$\zeta'' + \zeta \simeq 3\xi\zeta. \qquad \text{(E.6)}$$

It is immediately apparent that a linearized solution can be obtained from this "reduced" set of expressions if one deletes the higher order terms in the dependent variables.

E.4 First and second order equations. - A scheme which is most direct in describing the second order corrections is indicated below:

Here, each of the dependent variables is assumed to be composed of a first and second order element, with the second order elements assumed to be of an order of magnitude "smaller" than the first order elements. That is, the second order components are "negligibly small" when they are compared, directly, with the first order terms. However, any multiplicity of first order terms is assumed to constitute second, third, etc. order quantities depending on the order of the multiplicity.

For this purpose, then, write the dependent variables as

$$\xi = \xi_1 + \xi_2 + \ldots ; \quad \eta = \eta_1 + \eta_2 + \ldots ; \quad \zeta = \zeta_1 + \zeta_2 + \ldots \tag{E.7}$$

where the subscripts indicate the order for the terms. For orders of magnitude, for instance, write

$$O(\xi_2) \sim O(\xi_1^{\,2}) \sim O(\xi_1 \, \eta_1), \text{ etc;}$$

and, correspondingly, the order of magnitude for the derivative terms is assumed to follow this same argument.

When terms like those shown in eq. (E.7) are substituted into eq. (E.6), and grouped according to orders of magnitude, one finds that the first and second order equations are:

(a) first order (linearized) differential equations;

$$\xi_1'' - 2\,\eta_1' - 3\,\xi_1 = 0 ,$$

$$\eta_1'' + 2\,\xi_1' = 0,$$

and

$$\zeta_1'' + \zeta_1 = 0. \tag{E.8}$$

(b) second order differential equations;

$$\xi_2'' - 2\,\eta_2' - 3\,\xi_2 = -3\left(\xi_1^{\,2} - \frac{\eta_1^{\,2} + \zeta_1^{\,2}}{2}\right),$$

$$\eta_2'' + 2\,\xi_2' = 3\,\xi_1\,\eta_1 ,$$

and

$$\zeta_2'' + \zeta_2 = 3\,\xi_1\,\zeta_1 . \tag{E.9}$$

Equations (E.8) are seen to have the form of eqs. (A.17), in Appendix A. Hence the solution to these expressions would be identical to eqs. (A.33). Of course, the dimensionless relative speed components (shown in the previous Appendix) can be obtained by direct differentiation; these results would match those given as eqs. (A.34), Appendix A. (In Appendix A the variables bearing the subscript "O", $(\ )_o$, are initial values; these would be assigned according to conditions for an initial value problem being studied).

When eqs. (E.9) are being solved, analytically, one should note that these expressions (in ξ_2, η_2, ζ_2, etc) depend explicitly on the linearized results. For reference purposes the linearized solutions, to solve eqs. (E.9) are, from Appendix A:

$$\xi_1 = \xi_o + (3\,\xi_o + 2\,\eta'_o)(1-\cos\varphi_T) + \xi'_o \sin\varphi_T,$$

$$\eta_1 = \eta_o - 3(\eta'_o + 2\,\xi_o)\varphi_T - 2\,\xi'_o(1-\cos\varphi_T) + 2(3\,\xi_o + 2\,\eta'_o)\sin\varphi_T,$$

and $$\zeta_1 = \zeta_o \cos\varphi_T + \zeta'_o \sin\varphi_T. \qquad \text{(E.10)}$$

In a formal sense, eqs. (E.10) will serve as "driving functions" for eqs. (E.9). One should recognize that when using eqs. (E.9), the initial state has been accounted for, already, consequently the initial values (needed to describe constants arising in the analytic solutions to eqs. (E.9)), for the second order results, will be set to zero.

In the following paragraphs a method for solving for the $(\ )_2$-terms will be outlined; no attempt is made here to present the work in detail since the procedure is one used frequently and is well understood.

E.5 A solution for the second-order correction terms. - Even though the solution is straight forward, some comments may be appropriate. For this reason the statements, below, are given as an aid in following the procedure.

On looking at eqs. (E.9) it is apparent that the first two are coupled (in the second order terms) and, consequently, they must be solved together. The third expression, however, is independent of the first two and can be solved directly. (The fact that the driving functions are not uncoupled is of no concern since these are known; they are eqs. (E.10)).

When solving the first two differential equations, one should recognize an immediate first integral is obtained from the second expression. With this in hand, a substitution into the first equation can be made, yielding a differential equation for $\xi_2'' = \xi_2''(\varphi_T)$ which can be solved, analytically. Then, with an expression for ξ_2, the first integral of the second equation is solved, for η_2. This completes the solution for the second order correction terms (ξ_2, η_2, ζ_2).

The second order corrections for the speed components $(\xi_2', \eta_2', \zeta_2')$ may be obtained by direct differentiation; or, these could be obtained (in part) during the solution procedure outlined above. It should be kept in mind that the initial values for the second order corrections are all zero-as mentioned earlier.

For convenience some notes on the mathematical operations, leading to the second-order corrections, are included below. These will serve as a guide for obtaining the final results.

E.6 Notes on the second-order solution manipulations.

(a) A solution procedure leading to ζ_2. - The third expression in eqs. (E.9) is the simplest in form and the easiest to manipulate. For this reason it is examined, first, and the steps leading to its solution will be described here.

For convenience, the following quantities, in the driving functions, are renamed as shown below:

$$A \equiv 3\,\xi_o + 2\,\eta_o' \;;\; B \equiv \eta_o' + 2\,\xi_o. \tag{E.11}$$

Using eqs. (E.10), the driving function appropriate to this step in the procedure can be written as:

$$3\,\xi_1\,\zeta_1 = 3(A+\xi_o)(\zeta_o \cos\varphi_T + \zeta_o' \sin\varphi_T) + \frac{3}{2}\left[(\xi_o'\,\zeta_o - A\,\zeta_o')\sin 2\varphi_T\right.$$

$$\left. -(A\,\zeta_o + \zeta_o'\,\xi_o')\cos 2\varphi_T + (\xi_o'\,\zeta_o' - A\,\zeta_o)\right], \tag{E.12}$$

A solution to the homogeneous differential expression (for ζ_2) leads directly to a harmonic resultant, while the particular solution is assumed to be of the form:

$$(\zeta_2)_p = K_1 + K_2 \sin 2\varphi_T + K_3 \cos 2\varphi_T + K_4\varphi_T \sin\varphi_T + K_5\varphi_T \cos\varphi_T. \tag{E.13a}$$

Here the (K_j) are constants to be evaluated by matching like terms in the independent variable, φ_T.

Symbolically, the full solution for ζ_2 is expected to be in the form:

$$\zeta_2 = \phi_3 \sin\varphi_T + \phi_4 \cos\varphi_T + K_1 + K_2 \sin 2\varphi_T + K_3 \cos 2\varphi_T + K_4\varphi_T \sin\varphi_T$$

$$+ K_5\varphi_T \cos\varphi_T\,. \tag{E.13b}$$

E.6.1 Evaluation of the constants (ϕ_i, K_j). - As mentioned above, the constants in eq. (E.13) are obtained by matching coefficients of like terms in the variable, φ_T. When the assumed solution (E.13a) is substituted into the last of eqs. (E.9), and due account of eq. (E.12) is taken, one finds that the K_j are described as:

$$K_1 = \frac{3}{2}\left[\xi_o' \zeta_o' - \zeta_o (3\xi_o + 2\eta_o')\right],$$

$$K_2 = \frac{1}{2}\left[\zeta_o' (3\xi_o + 2\eta_o') - \zeta_o \xi_o'\right],$$

$$K_3 = \frac{1}{2}\left[\zeta_o (3\xi_o + 2\eta_o') + \xi_o' \zeta_o'\right],$$

$$K_4 = 3\zeta_o \left[2\xi_o + \eta_o'\right],$$

and

$$K_5 = -3\zeta_o' \left[2\xi_o + \eta_o'\right]. \qquad \text{(E.14)}$$

Recalling that $\zeta_2(0) = \zeta_2'(0) = 0$, it can be shown that the remaining constants (ϕ_i) are:

$$\phi_3 = 3\xi_o \zeta_o' + \eta_o' \zeta_o' + \xi_o' \zeta_o ,$$

and

$$\phi_4 = 3\zeta_o \xi_o + 2(\zeta_o \eta_o' - \xi_o' \zeta_o'). \qquad \text{(E.15)}$$

This should complete the (analytic) solution for ζ_2, when the various constants are inserted into eq. (E.13b).

E.6.2 An expression for the state component ζ_2'. - Having obtained the analytic expression for ζ_2, it is a simple matter to define the relative speed component (ζ_2'). That is, differentiating eq. (E.13b), one obtains the symbolic expressions:

$$\zeta_2' = (K_4 - \phi_4)\sin\varphi_T + (K_5 + \phi_3)\cos\varphi_T + 2(K_2 \cos 2\varphi_T - K_3 \sin 2\varphi_T)$$

$$+ (K_4 \cos\varphi_T - K_5 \sin\varphi_T)\varphi_T . \qquad \text{(E.16)}$$

The constants (K_j, ϕ_i) appearing here are described in eqs. (E.14, E.15).

E.6.3 A solution for the component ξ_2. - Due to the coupling which exists between the differential equations for ξ_2 and η_2, it is necessary to manipulate these expressions simultaneously. The direct method of solving for ξ_2 is to, first, obtain an expression for η_2' and then to solve explicitly for ξ_2.

(a) A first integral, for η_2'. - The "driving function" appearing in the second of eqs. (E.9) can be written as:

$$3\xi_1\eta_1 = 3\Big[\mathcal{C}_o\mathcal{C}_1 + (2A\mathcal{C}_1 + \xi_o'\mathcal{C}_o)\sin\varphi_T + (2\xi_o'\mathcal{C}_1 - A\mathcal{C}_o)\cos\varphi_T - 2A\xi_o'\cos 2\varphi_T + (\xi_o'^2 - A^2)\sin 2\varphi_T + 3B\varphi_T(A\cos\varphi_T - \xi_o'\sin\varphi_T - \mathcal{C}_1)\Big], \quad (E.17)$$

wherein

$$\mathcal{C}_o \equiv \eta_o - 2\xi_o', \quad \mathcal{C}_1 \equiv \xi_o + A, \quad (E.18)$$

with A, B as given in eq. (E.11). An appropriate first integral, of the differential equation, is readily shown to be:

$$\eta_2' = -2\xi_2 + K_\eta + 3\Big\{\mathcal{C}_o\mathcal{C}_1\varphi_T - (2A\mathcal{C}_1 + \xi_o'\mathcal{C}_o)\cos\varphi_T + (2\xi_o'\mathcal{C}_1 - A\mathcal{C}_o)\sin\varphi_T - A\xi_o'\sin 2\varphi_T - \frac{(\xi_o'^2 - A^2)}{2}\cos 2\varphi_T - \frac{3}{2}B\mathcal{C}_1\varphi_T^2 + 3B\Big[A(\cos\varphi_T + \varphi_T\sin\varphi_T) - \xi_o'(\sin\varphi_T - \varphi_T\cos\varphi_T)\Big]\Big\}, \quad (E.19)$$

with K_η being a constant of integration. Necessarily K_η is obtained from the initial condition, $\eta_2'(0) = \xi_2(0) = 0$; thus,

$$K_\eta = 3(2A\mathcal{C}_1 + \xi_o'\mathcal{C}_o) - 9AB + \frac{3}{2}(\xi_o'^2 - A^2). \quad (E.20)$$

(b) A solution for ξ_2. - The solution for ξ_2 follows from the first of eqs. (E.9), after one substitues for η_2' and the "driving function" appearing on the right side of that expression. Using eqs. (E.10), the driving function is found to be:

$$3\left\{\tfrac{1}{2}(\eta_1^2+\zeta_1^2) - \xi_1^2\right\} = 3\left\{\left[\frac{\mathcal{C}_o^2}{2} - \mathcal{C}_1^2 + \frac{\xi_o'^2 + A^2}{2} + \frac{\zeta_o^2 + \zeta_o'^2}{4}\right] + 2\mathcal{C}_o(\xi_o' \cos\varphi_T + A\sin\varphi_T) + 2\mathcal{C}_1(A\cos\varphi_T - \xi_o'\sin\varphi_T) + \left(3A\xi_o' + \frac{\zeta_o\zeta_o'}{2}\right)\sin 2\varphi_T + \left[\frac{3}{2}(\xi_o'^2 - A^2) + \frac{\zeta_o^2 - \zeta_o'^2}{4}\right]\cos 2\varphi_T + \left(\frac{9B^2}{2}\varphi_T^2 - 3B\mathcal{C}_o\varphi_T\right) - 6B(\xi_o'\cos\varphi_T + A\sin\varphi_T)\varphi_T\right\}. \quad (E.21)$$

After making the necessary substitutions it is apparent that the solution for ξ_2 involves a harmonic part (for the homogeneous expression) and the particular integral corresponding to eq. (E.21). Symbolically the inhomogeneous solution takes on the form:

$$(\xi_2)_p = K_6 + K_7\varphi_T + K_8\varphi_T^2 + K_9\varphi_T\sin\varphi_T + K_{10}\varphi_T\cos\varphi_T + K_{11}\sin 2\varphi_T + K_{12}\cos 2\varphi_T. \quad (E.22)$$

Incidentally, the complementary solution to this ordinary differential equation has the simple form:

$$(\xi_2)_c = \mathcal{C}_5\sin\varphi_T + \mathcal{C}_6\cos\varphi_T. \quad (E.23)$$

The constants (K_j) are obtained by matching coefficients of like terms in φ_T, while the $(\mathcal{C}_i)$ are defined from the conditions: $\xi_2(0) = \xi_2'(0) = 0$.

E.6.4 Evaluation of constants. - In the subsection above, the means for evaluating the constants was noted. All that needs to be done, now, is to set down the values ascertained from that procedure. After matching coefficients in the differential equation, for ξ_2, it was found that:

$$K_6 = 3\left\{\frac{\zeta_o^2 + \zeta_o'^2}{2} + \frac{\xi_o'^2 - A^2}{2} - \frac{\phi_o^2}{2} + 2B\,(A-B) + (\xi_o' + \phi_o)^2\right\}$$

$$K_7 = 3\,\phi_o B,$$

$$K_8 = -\frac{9}{2}\,B^2,$$

$$K_9 = 3AB,$$

$$K_{10} = 3\xi_o' B,$$

$$K_{11} = -\left[A\,\xi_o' + \frac{\zeta_o\,\zeta_o'}{2}\right]$$

and $$K_{12} = -\frac{1}{2}\left[\xi_o'^2 - A^2 + \frac{\zeta_o^2 - \zeta_o'^2}{2}\right], \qquad \text{(E.24)}$$

where the various quantities (A, B, ϕ_j) have been described earlier. Next, the ϕ_i (i = 5, 6) are obtained from the prescribed initial state (for ξ_2, ξ_2'); these are found to be,

$$\phi_5 = -(K_7 + K_{10} + 2K_{11}),$$

and $$\phi_6 = -(K_6 + K_{12}). \qquad \text{(E.25)}$$

E.6.5 The solution for ξ'_2, ξ_2. - Having determined the constants for ξ_2, one can write the solution (form) for this state component immediately. Similar to what was indicated earlier, the solution for ξ'_2 follows directly by differentiating ξ_2. For convenience, a symbolic form for these variables is noted below:

$$\xi_2 = \mathcal{C}_5 \sin\varphi_T + \mathcal{C}_6 \cos\varphi_T + K_6 + K_7\varphi_T + K_8\varphi_T^2 + (K_9 \sin\varphi_T + K_{10} \cos\varphi_T)\,\varphi_T$$

$$+K_{11} \sin\varphi_T + K_{12} \cos 2\varphi_T \ ,$$

and

$$\xi'_2 = K_7 + (K_9 - \mathcal{C}_6) \sin\varphi_T + (K_{10} + \mathcal{C}_5) \cos\varphi_T + 2(K_{11} \cos 2\varphi_T - K_{12} \sin 2\varphi_T)$$

$$+ (K_9 \cos\varphi_T - K_{10} \sin\varphi_T + 2K_8)\,\varphi_T. \qquad \text{(E.26)}$$

In the next section a solution for the components η_2, η'_2 is presented; this will complete the development of the second-order corrections being sought.

E.6.6 A solution for the components η_2, η'_2. - The remaining second-order components to be evaluated are η_2 and η'_2. These could be readily obtained from the first integral described in Section E.6.3 since, there, a solution for η'_2 was acquired. The solution for η_2 could, of course, be had by means of one more integration procedure.

Actually, the scheme followed here was to integrate for η_2, and then obtain η'_2 by direct differentiation. This procedure was adopted in order to follow a common method of approach throughout the evaluations.

It is easy to show that a symbolic form for η_2 can be given as:

$$\eta_2 = K_{\eta\eta} + K_{13}\,\varphi_T + K_{14} \sin\varphi_T + K_{15} \cos\varphi_T + K_{16} \sin 2\varphi_T + K_{17} \cos 2\varphi_T$$

$$+ (K_{18} \sin\varphi_T + K_{19} \cos\varphi_T)\,\varphi_T \ , \qquad \text{(E.27)}$$

with $K_{\eta\eta}$ being a constant of integration, evaluated from the condition $\eta_2(0) = 0$.

Differentiating eq. (E.27) one finds that the second-order component, η_2' is:

$$\eta_2' = K_{13} + (K_{18} - K_{15}) \sin\varphi_T + (K_{19} + K_{14}) \cos\varphi_T + 2\,(K_{16} \cos 2\varphi_T - K_{17} \sin 2\varphi_T)$$

$$+ (K_{18} \cos\varphi_T - K_{19} \sin\varphi_T)\,\varphi_T \quad . \quad (E.28)$$

As before, the constants (K_j) included here are obtained by matching coefficients in appropriate expressions. For reasons of conciseness these are not listed here, but will be noted in the summary section which follows.

E.7 Summary. - In the foregoing sections of this Appendix a method used to determine the set of second-order correction variables has been outlined. In this section the results are summarized, and briefly discussed, in regard to their use and application.

Throughout this development the manipulations have been made in terms of dimensionless variables $(\xi, \eta, \zeta, \xi', \eta', \zeta')$, using the position angle (φ_T) as an independent variable. Since the path for "T" is a circular orbit the value of φ_T is arbitrarily set to "zero" when the problem is at its initial state. Hence, there is no need to be concerned about initial angles, arguments of pericenter and the like.

If one wishes to convert the dimensionless quantities to dimensional variables, he may do so according to the scheme noted in eqs. (A.32), Appendix A.

The second order quantities, obtained here, will be described in terms of constants (defined by initial values) and terms involving the independent variable, φ_T.

When one wishes to describe a problem's solution, including the second-order correction terms, he may do so as follows:

Having the linearized (first-order) solution, the second-order corrections are added, algebraically, to the linear results to complete the solution form. That is, for any of the variables (ξ, η, ζ), the (symbolic) solution is given as,

$$\varkappa = \varkappa_1 + \varkappa_2 ,$$

$$\varkappa' = \varkappa'_1 + \varkappa'_2 ;$$

the subscripts representing the solution order.

For convenience, and immediate reference, the formal solutions for the $(\sim)_1$ and $(\sim)_2$ variables are listed below; and, for the second-order correction terms, the constants are tabulated following the symbolic expressions.

E.7.1 Linear (first-order) results.

(a) Dimensionless relative motion position coordinates.

$$\xi_1 = \xi_o + (3\xi_o + 2\eta'_o)(1-\cos\varphi_T) + \xi'_o \sin\varphi_T,$$

$$\eta_1 = \eta_o - 3(\eta'_o + 2\xi_o)\varphi_T - 2\xi'_o(1-\cos\varphi_T) + 2(3\xi_o + 2\eta'_o)\sin\varphi_T$$

and $$\zeta_1 = \zeta_o \cos\varphi_T + \zeta'_o \sin\varphi_T . \qquad \text{(E.29)}$$

(b) Dimensionless relative motion speed components.

$$\xi'_1 = \xi'_o \cos\varphi_T + (3\xi_o + 2\eta'_o)\sin\varphi_T,$$

$$\eta'_1 = 2(3\xi_o + 2\eta'_o)\cos\varphi_T - \left[3(\eta'_o + 2\xi_o) + 2\xi'_o \sin\varphi_T\right],$$

and $$\zeta'_1 = \zeta'_o \cos\varphi_T - \zeta_o \sin\varphi_T . \qquad \text{(E.30)}$$

E.7.2 Second-order corrections.

(a) Dimensionless relative motion coordinates.

$$\xi_2 = \mathcal{C}_5 \sin\varphi_T + \mathcal{C}_6 \cos\varphi_T + K_6 + K_7\varphi_T + K_8\varphi_T^2 + (K_9 \sin\varphi_T + K_{10}\cos\varphi_T)\varphi_T + K_{11}\sin 2\varphi_T + K_{12}\cos 2\varphi_T,$$

$$\eta_2 = K_{\eta\eta} + K_{13}\varphi_T + K_{14}\sin\varphi_T + K_{15}\cos\varphi_T + K_{16}\sin 2\varphi_T + K_{17}\cos 2\varphi_T + (K_{18}\sin\varphi_T + K_{19}\cos\varphi_T)\varphi_T,$$

and $$\zeta_2 = \mathcal{C}_3 \sin\varphi_T + \mathcal{C}_4\cos\varphi_T + K_1 + K_2\sin 2\varphi_T + K_3\cos 2\varphi_T + (K_4\sin\varphi_T + K_5\cos\varphi_T)\varphi_T . \quad (E.31)$$

(b) Dimensionless relative motion speed components.

$$\xi_2' = K_7 + (K_9 - \mathcal{C}_6)\sin\varphi_T + (K_{10} + \mathcal{C}_5)\cos\varphi_T + 2(K_{11}\cos 2\varphi_T - K_{12}\sin 2\varphi_T) + (K_9\cos\varphi_T - K_{10}\sin\varphi_T + 2K_8)\varphi_T,$$

$$\eta_2' = K_{13} + (K_{18} - K_{15})\sin\varphi_T + (K_{19} + K_{14})\cos\varphi_T + 2(K_{16}\cos 2\varphi_T - K_{17}\sin 2\varphi_T) + (K_{18}\cos\varphi_T - K_{19}\sin\varphi_T)\varphi_T,$$

and $$\zeta_2' = (K_4 - \mathcal{C}_4)\sin\varphi_T + (K_5 + \mathcal{C}_3)\cos\varphi_T + 2\left[K_2\cos 2\varphi_T - K_3\sin 2\varphi_T\right] + (K_4\cos\varphi_T - K_5\sin\varphi_T)\varphi_T. \quad (E.32)$$

The constant coefficients used in the above second-order correction terms are tabulated below; these are expressed in terms of the general initial values for the problem.

(a) The K_j ($j = 1, \ldots, 19, \eta\eta$).

$$K_1 = \frac{3}{2}\left[\xi'_o\,\zeta'_o - \zeta_o\,(3\xi_o + 2\eta'_o)\right]$$

$$K_2 = \frac{1}{2}\left[\zeta'_o\,(3\xi_o + 2\eta'_o) - \zeta_o\,\xi'_o\right]$$

$$K_3 = \frac{1}{2}\left[\zeta_o\,(3\xi_o + 2\eta'_o) + \xi'_o\,\zeta'_o\right]$$

$$K_4 = 3\zeta_o\,(2\xi_o + \eta'_o)$$

$$K_5 = -3\zeta'_o\,(2\xi_o + \eta'_o) \qquad \text{(E.33a)}$$

$$K_6 = \frac{3}{2}\left[7\xi_o^2 + \eta_o^2 + \frac{1}{2}\zeta_o^2 - \xi_o'^2 + \frac{1}{2}\zeta_o'^2\right] + 12\xi_o\,\eta'_o + 3\eta_o'^2$$

$$K_7 = 3(\eta_o\,\eta'_o - 4\xi_o\,\xi'_o + 2\xi_o\,\eta_o - 2\xi'_o\,\eta'_o)$$

$$K_8 = -\frac{9}{2}\,(\eta_o'^2 + 4\xi_o\,\eta'_o + 4\xi_o^2)$$

$$K_9 = 3(6\xi_o^2 + 7\xi_o\,\eta'_o + 2\eta_o'^2)$$

$$K_{10} = 3\,(2\xi_o\,\xi'_o + \xi'_o\,\eta'_o) \qquad \text{(E.33b)}$$

$$K_{11} = -(3\xi_o \xi'_o + 2\xi'_o \eta'_o + \frac{1}{2}\zeta_o \zeta'_o)$$

$$K_{12} = +\frac{1}{2}\left[-\xi'^2_o + (9\xi^2_o + 12\xi_o \eta'_o + 4\eta'^2_o) - \frac{1}{2}(\zeta^2_o - \zeta'^2_o)\right]$$

$$K_{13} = 3\left[-\frac{11}{2}\xi^2_o - \eta^2_o - \frac{1}{2}\zeta^2_o - \frac{1}{2}\xi'^2_o - \frac{1}{2}\zeta'^2_o + \eta_o \xi'_o - 7\xi_o \eta'_o - 2\eta'^2_o\right]$$

$$K_{14} = 30\xi^2_o + 3\eta^2_o + \zeta^2_o + 2\xi'^2_o + 10\eta'^2_o + 2\zeta'^2_o + 36\xi_o \eta'_o - 3\xi'_o \eta_o$$

$$K_{15} = 6\xi_o \xi'_o + 2\zeta_o \zeta'_o - 3\xi_o \eta'_o + 2\xi'_o \eta'_o \qquad \text{(E.33c)}$$

$$K_{16} = \frac{1}{4}(9\xi^2_o + \zeta^2_o - \xi'^2_o + 4\eta'^2_o - \zeta'^2_o + 12\xi_o \eta'_o)$$

$$K_{17} = \frac{1}{2}(3\xi_o \xi'_o + 2\xi'_o \eta'_o - \zeta_o \zeta'_o)$$

$$K_{18} = 6\xi_o \xi'_o + 3\xi'_o \eta'_o$$

$$K_{19} = -3(6\xi^2_o + 7\xi_o \eta'_o + 2\eta'^2_o)$$

$$K_{\eta\eta} = 3\left(-\frac{5}{2}\xi_o \xi'_o - \frac{1}{2}\zeta_o \zeta'_o + \xi_o \eta'_o - \xi'_o \eta'_o\right)$$

(b) The $\mathcal{C}_i$ $(i = 3, \ldots, 6)$. (E.33d)

$$\mathcal{C}_3 = 3\xi_o \zeta'_o + \eta'_o \zeta'_o + \xi'_o \zeta_o$$

$$\mathcal{C}_4 = 3\xi_o \zeta_o + 2\zeta_o \eta'_o - 2\xi'_o \zeta'_o$$

$$\mathcal{C}_5 = -\left(3\eta_o \eta_o' + 6\xi_o \eta_o - 7\xi_o' \eta_o' - 12\xi_o \xi_o' - \zeta_o \zeta_o'\right)$$

$$\mathcal{C}_6 = -15\xi_o^2 - \frac{3}{2}\eta_o^2 - \frac{1}{2}\zeta_o^2 + 2\xi_o'^2 - 5\eta_o'^2 - \zeta_o'^2 - 18\xi_o \eta_o' \qquad \text{(E.33e)*}$$

In the preceding list of equations the independent variable has been φ_T, the position angle of the target particle ("T"). This angle is measured from an initial position on the target's circular orbit; it is the primary variable in this problem's formulation.

One should recognize that the second-order (corrective) solution differs from the first-order (linear) solution, in one main respect; namely, that the corrections involve terms in both φ_T and $2\varphi_T$; however, both solution forms do incorporate secular terms. Even so, the corrective expressions are more heavily dependent on the secular terms. Because of the more formidable expressions involved in the second-order equations, it would be most difficult to describe the geometry of the state displacement figures generated by these resultants, in general. For this reason no attempt at this has been made, here.

*Generally, the procedure used here to determine the second-order corrections is similar to that carried out by Anthony and Sasaki (see reference [1]). An exception in these results is that the constants obtained here are different, for some values, from those given in this article.

APPENDIX F

A GENERAL DESCRIPTION OF RELATIVE MOTION

F.1.1 The relative motion displacement. - In this appendix the general description of a relative motion is described, in terms of the natural geometry for the problem.

Results in the following paragraphs describe a means for obtaining deterministic relative motion solutions which, in principle, do not suffer the consequence of linearization imposed on others of the methods.

Consider the motion of two particles (m_1, m_2) about a common primary (μ). It is assumed that the two orbits are closed curves, produced by a central field attraction, with no other forces present. In particular, there is no mutual attraction between the bodies. Consistent with this constraint the particles are located by the bounded radius vectors $(\bar{r}_1, \bar{r}_2)$, measured from μ.

The position of m_2, relative to m_1, is

$$\bar{r}_r \equiv \bar{r}_r\ (x,\ y,\ z) = \bar{r}_2 - r_1\ , \tag{F.1}$$

see Fig. F.1.

From the notation on the figure, the relative position coordinates (x, y, z) are obtained by means of;

$$x = \bar{r}_r \cdot \hat{x}_1,\quad y = \bar{r}_r \cdot \hat{y}_1,\quad z = \bar{r}_r \cdot \hat{z}_1, \tag{F.2}$$

where $\hat{x}_1$, etc., are unit vectors.

On Fig. F.1 the unit triad $(\hat{x}_1, \hat{y}_1, \hat{z}_1)$ is presumed to move with m_1. Now, in representing a particle's motion, in a moving frame of reference, relative to (say) a fixed frame of reference, such as $(\hat{x}_o, \hat{y}_o, \hat{z}_o)$, it is necessary

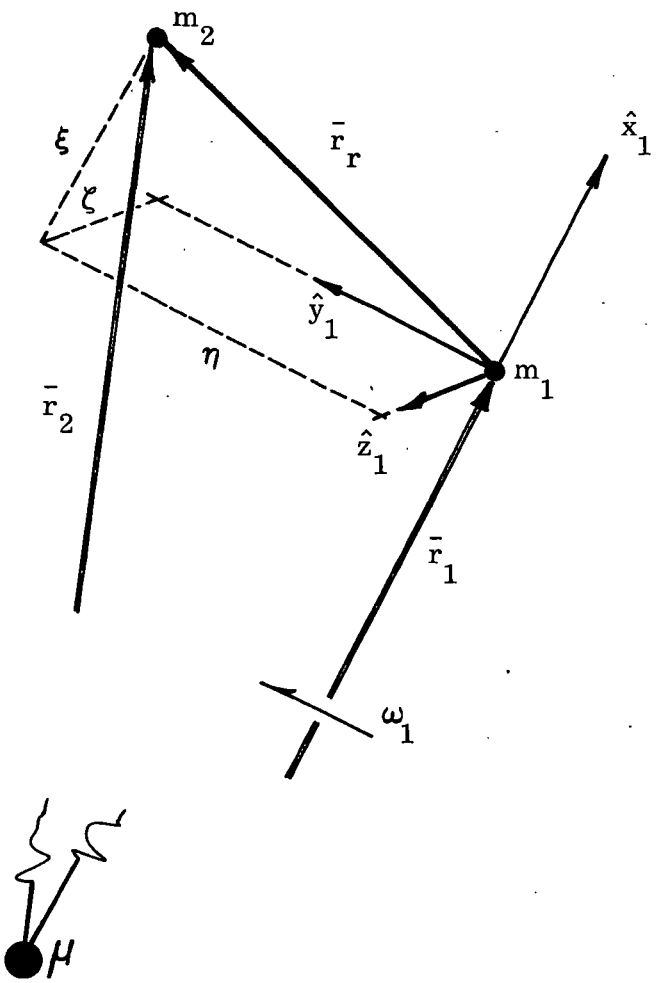

Fig. F.1. Geometry Descriptions of a Relative Motion, m_2, with respect to m_1.

to provide suitable "transformation matrices", relating the orientation of one frame relative to the other. (A proper set of matrices has been developed; these are found in Appendix G).

When using the transformation matrices, it should be noted that the triad fixed to m_1 in Appendix G is denoted as $(\hat{x}_1, \hat{y}_1, \hat{z}_1)$, while the one attached to m_2 is designated as $(\hat{x}_b, \hat{y}_b, \hat{z}_b)$, there. Also, it is important to recognize that the unit vectors $(\hat{x}_j)$ are directed radially (away from μ), while the $(\hat{z}_j)$ are normal to the (two) planes of motion. Finally, the unit vectors $(\hat{y}_j)$ complete each orthogonal triad; these are described by

$$\hat{y}_j = \hat{z}_j \times \hat{x}_j, \qquad (j = 1, 2). \tag{F.3}$$

Lastly, it should be apparent that the (two) position vectors may be written as

$$\bar{r}_j = r_j \hat{x}_j,$$

where $$r_j = |\bar{r}_j|, \quad (j = 1, 2). \tag{F.4}$$

F.1.2 Scalar equations for the relative position. - The relative position coordinate, x, is described by eq. (F.2) as,

$$x = \bar{r}_r \cdot \hat{x}_1 = \bar{r}_2 \cdot \hat{x}_1 - \bar{r}_1 \cdot \hat{x}_1 ;$$

or, making use of eqs. (F.4), (G.3), (G.4), then

$$x = r_2 (\cos\theta\, \hat{x}_o + \sin\theta \cos\iota\, \hat{y}_o + \sin\theta \sin\iota\, \hat{z}_o) \cdot (\cos\psi\, \hat{x}_o + \sin\psi\, \hat{y}_o) - r_1,$$

(accounting for $\hat{x}_1 \cdot \hat{x}_1 = 1$). Carrying out the required multiplications one finds that

$$x = r_2 (\cos\theta \cos\psi + \sin\theta \cos\iota \sin\psi) - r_1. \tag{F.5a}$$

Likewise, the other two relative coordinates are obtained as;

$$y = \bar{r}_2 \cdot \hat{y}_1 - \bar{r}_1 \cdot \hat{y}_1 = r_2 \,(-\cos\,\theta \sin\,\psi + \sin\,\theta \sin\,\iota \cos\,\psi), \tag{F.5b}$$

and

$$z = \bar{r}_2 \cdot \hat{z}_1 - \bar{r}_1 \cdot \hat{z}_1 = r_2 \,(\sin\,\theta \sin\,\iota). \tag{F.5c}$$

The description of a position for m_2 is not yet complete since each of the r_j depends on its true anomaly, φ_j. In the expressions above, the angles, θ and ψ, are particular position angles, measured <u>from</u> the line of nodes (see Appendix G). In fact, these angles are related to the true anomalies, but in a manner not yet described.

F.2.1 <u>The relative speeds.</u> - Since the relative velocity of m_2 can be written as

$$\dot{\bar{r}}_r = \dot{\bar{r}}_2 - \dot{\bar{r}}_1 , \tag{F.6}$$

then the relative speeds may be obtained by differentiating eq. (F.2). That is, for instance, since $x = \bar{r}_r \cdot \hat{x}_1$, then

$$\dot{x} = \frac{d}{dt}\,(\bar{r}_r \cdot \hat{x}_1) = \dot{\bar{r}}_r \cdot \hat{x}_1 + \bar{r}_r \cdot \dot{\hat{x}}_1 , \tag{F.7}$$

the derivative $\dot{\hat{x}}_1$ arises because the triad, $(\sim)_1$, moves relative to the 'fixed' frame of reference. Here, derivatives like $(\dot{\hat{x}}_1)$ may be obtained by the operation

$$\dot{\hat{x}}_1 = \bar{\omega}_1 \times \hat{x}_1, \tag{F.8}$$

where $\bar{\omega}_1$ is the angular velocity for m_1; which is the angular velocity of the triad.

In order to complete the description for $\dot{\bar{r}}_r$, one needs to obtain expressions for $\dot{\bar{r}}_j$ $(j = 1, 2)$ in order to satisfy eq. (F.6). For this purpose define these derivatives as,

$$\dot{\bar{r}}_j = \frac{d}{dt}\,(r_j\,\hat{x}_j) = \dot{r}_j\,\hat{x}_j + r_j\,\dot{\hat{x}}_j\,, \tag{F.9}$$

where the $\dot{\hat{x}}_j$ are acquired from eq. (F.8) above.

Since the plane of motion for a particle is described by both $\bar{r}_j$ and $\dot{\bar{r}}_j$, then, necessarily, the angular velocities $(\bar{\omega}_j)$ are normal to these planes; and $\bar{\omega}_j$ may be defined as,

$$\bar{\omega}_j = \dot{\varphi}_j\,\hat{z}_j, \quad (j = 1, 2). \tag{F.10}$$

Here $\dot{\varphi}$ is the "local" angular speed for each of the (j) orbits.

Taking account of eqs. (F.8), (F.9) and (F.10), then

$$\dot{\bar{r}}_j = \dot{r}_j\,\hat{x}_j + r_j\,\dot{\varphi}_j\,\hat{y}_j\,; \tag{F.11}$$

thus, eq. (F.7) is found to reduce to

$$\dot{x} = \dot{r}_2\,(\hat{x}_2 \cdot \hat{x}_1) + r_2\,\dot{\varphi}_2\,(\hat{y}_2 \cdot \hat{x}_1) - \dot{r}_1 + r_2\,\dot{\varphi}_1\,(\hat{x}_2 \cdot \hat{y}_1). \tag{F.12a}$$

(The scalar multiplications in eqs. (12) are carried out using the matrices developed in Appendix G). Similar to the above, expressions for $\dot{y}$, $\dot{z}$ are readily shown to be:

$$\dot{y} = \dot{r}_2\,(\hat{x}_2 \cdot \hat{y}_1) + r_2\left[\dot{\varphi}_2\,(\hat{y}_2 \cdot \hat{y}_1) - \dot{\varphi}_1\,(\hat{x}_2 \cdot \hat{y}_1)\right], \tag{F.12b}$$

and

$$\dot{z} = \dot{r}_2\,(\hat{x}_2 \cdot \hat{z}_1) + r_2\,\dot{\varphi}_2\,(\hat{y}_2 \cdot \hat{z}_1). \tag{F.12c}$$

F.2.2 Scalar speed equations. - Having performed the multiplications indicated in eq. (F.12a); then, after some reduction one finds that

$$\dot{x} = \dot{r}_2 (\cos\theta \cos\psi + \sin\theta \cos\iota \sin\psi) + r_2 \dot{\varphi}_2 (-\sin\theta \cos\psi + \cos\theta \cos\iota \sin\psi)$$

$$- \dot{r}_1 + r_2 \dot{\varphi}_1 (-\cos\theta \sin\psi + \sin\theta \cos\iota \cos\psi) . \qquad \text{(F.13a)}$$

Similar operations are carried out for $\dot{y}$ and $\dot{z}$; and, as a consequence, it is found that these relative speed components reduce to;

$$\dot{y} = \dot{r}_2 (-\cos\theta \sin\psi + \sin\theta \cos\iota \cos\psi) + r_2 \dot{\varphi}_2 (\sin\theta \sin\psi + \cos\theta \cos\iota \cos\psi)$$

$$- r_2 \dot{\varphi}_1 (\cos\theta \cos\psi + \sin\theta \cos\iota \sin\psi), \qquad \text{(F.13b)}$$

and

$$\dot{z} = (\dot{r}_2 \sin\theta + r_2 \dot{\varphi}_2 \cos\theta) \sin\iota . \qquad \text{(F.13c)}$$

In the above expressions the angles (ψ, θ) are measured from the line of nodes (see Fig. G.1, Appendix G), in the planes of motion for m_1 and m_2, respectively. The angle, ι, the dihedral angle between these orbital planes, is a constant for the present formulation.

It should be evident that in eqs. (F.13) the speed components $(\dot{r}_j, r_j \dot{\varphi}_j)$ are particular to the motion of each particle (m_j). Consequently, these quantities must properly account for associated initial conditions imposed on the problem.

F.2.3 Local speed components. - General expressions for the radial and transverse speed components; describing a central field, inverse square motion are:

$$V_r \equiv \dot{r} = \frac{d}{dt} \left(\frac{p}{1 + \epsilon \cos\varphi} \right) = \frac{\mu}{h} \epsilon \sin\varphi , \qquad \text{(F.14a)}$$

and

$$V_\varphi \equiv r \dot{\varphi} = \frac{h}{r} = \frac{\mu}{h} (1 + \epsilon \cos\varphi), \qquad \text{(F.14b)}$$

recognizing that $p = h^2/\mu$. Here, the position angle, φ, is the true anomaly measured from the periapsis position.

On combining the expressions above, one finds that the local speed ($|V|$) can be expressed by,

$$V = \frac{\mu}{h} (1 + \epsilon^2 + 2\epsilon \cos \varphi)^{\frac{1}{2}} . \qquad \text{(F.14c)}$$

F.3 Angle relations. - To make a proper use of the Euler angles introduced in Appendix G, it is necessary to relate the particular position angles (θ, ψ) to the true anomalies (φ_j).

For the polar conic equations, true anomalies (φ) are measured from the periapse positions; however, the Euler angles introduced here, (θ, ψ), are measured from the line of nodes (NN').* Generally, the line of nodes does not coincide with the line of apsides; consequently, the nodal axis is at a position (say φ_{j_o}) relative to the apsidal line at pericenter.

Taking these conditions into account, then the angular position for a particle on the two trajectories will be described by,

$$\varphi_j = \varphi_{j_o} + \begin{Bmatrix} \psi \\ \theta \end{Bmatrix}, \quad (j = 1, 2), \qquad \text{(F.15)}$$

depending on the orbit considered.

The angles (φ_{j_o}), above, locate the nodal line (hence the intersection) for the two planes of motion. For the two-body, central field studies conducted herein these angles are constants.

The last angle description needed for this problem is that for the elevation angle (γ). This is used in describing the local speed components and can be expressed from

*See Fig. G-1 in Appendix G.

$$\tan \gamma = \frac{\dot{r}}{r\dot{\varphi}} = \frac{\epsilon \sin \varphi}{1 + \epsilon \cos \varphi} \, . \qquad \text{(F.16)}$$

This completes the formal developments for the deterministic relative motion problem. Applications of these formulas will be made in the main body of this report. There, an example will be used to illustrate the geometry of a relative motion, and to describe the character of the resulting motion traces.

APPENDIX G

AN EULER ANGLE DEVELOPMENT

G.1 Euler angles used to describe orbit positions. - Here a set of Euler angles is defined to locate a particle, on an orbit, referred to a pre-selected frame of reference. This development is carried out to provide transformation matrices for the rotations used to connect the triads of interest for a particular type of motion.

Fig. G.1 shows the geometry which is to be considered: First, a reference plane, and a reference triad $(\hat{x}_o, \hat{y}_o, \hat{z}_o)$ are assumed. Beginning with axes parallel to this triad, the Euler angles (ι, θ) are used to: (1) define an inclined plane, and to locate a "transformed" triad $(\hat{x}_a, \hat{y}_a, \hat{z}_a)$; and, (2) to describe a rotation (θ) in this inclined plane, thereby locating a second triad $(\hat{x}_b, \hat{y}_b, \hat{z}_b)$. This two-angle sequence is employed to define positions on the inclined plane; and, to refer these positions back to the initial (reference) triad.

The line of intersection (NN'), for the two principal planes, plays the role of a line of nodes. Note that the nodal axis coincides with the initial unit vector, $\hat{x}_o$, as shown on the figure.

In order to provide for the positioning of a moving triad in the reference plane, a third rotation (ψ) is introduced; this angle locates the triad $(\hat{x}_1, \hat{y}_1, \hat{z}_1)$ relative to the reference triad $(\hat{x}_o, \hat{y}_o, \hat{z}_o)$.

G.2 The Euler rotations. - The first angle (ι) is a displacement about the line of nodes (NN'); it is used to locate the triad $(\hat{x}_a, \hat{y}_a, \hat{z}_a)$. In matrix notation the transformation corresponding to this rotation is:

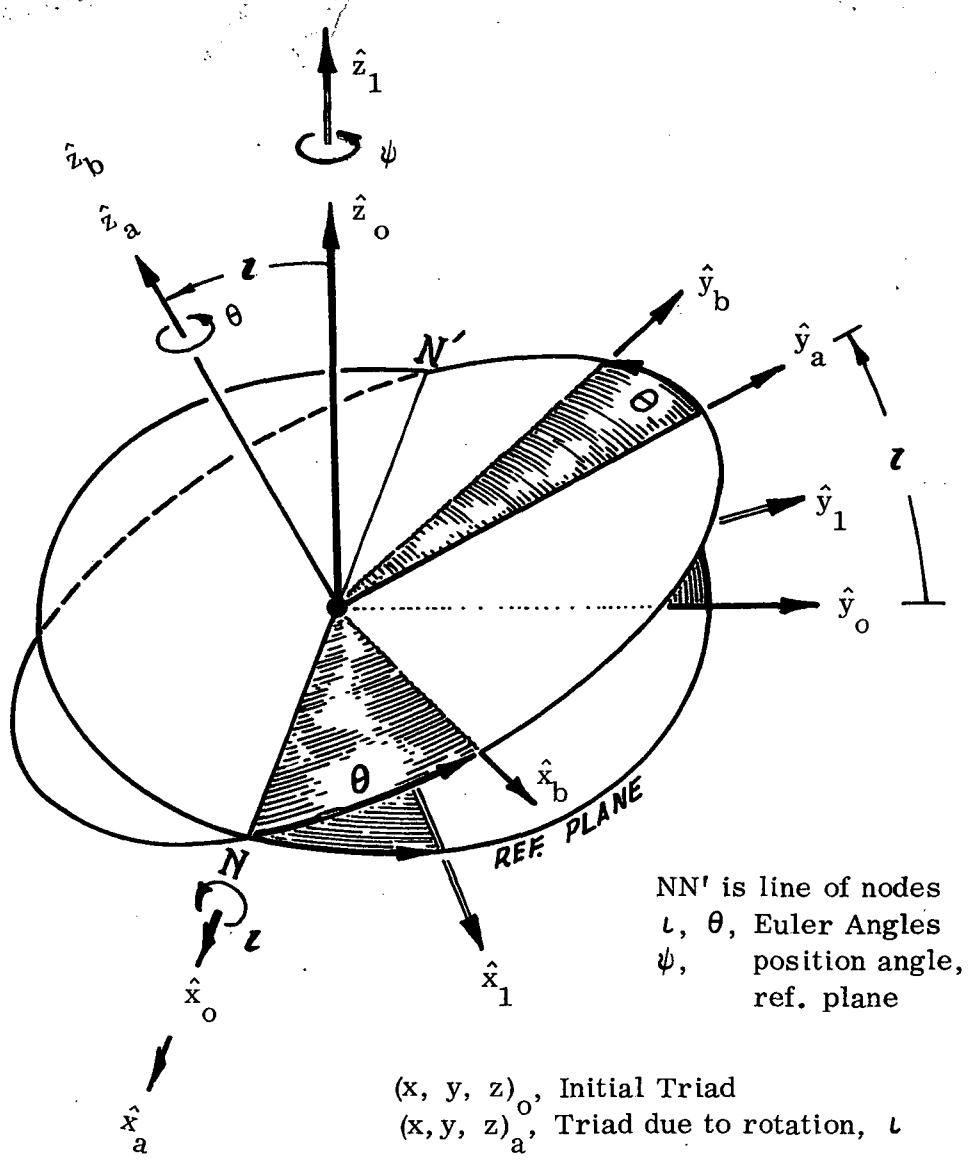

Fig. G.1. Sketch describing Euler Angles, and Reference Position Angles, used with Triad Transformations.

$$\begin{bmatrix} \hat{x}_a \\ \hat{y}_a \\ \hat{z}_a \end{bmatrix} = \begin{bmatrix} 1 & 0 & 0 \\ 0 & \cos \iota & \sin \iota \\ 0 & -\sin \iota & \cos \iota \end{bmatrix} \begin{bmatrix} \hat{x}_o \\ \hat{y}_o \\ \hat{z}_o \end{bmatrix} . \tag{G.1}$$

The second angle (θ) occurs about the z_a-axis; it locates a new triad, denoted as $(\hat{x}_b, \hat{y}_b, \hat{z}_b)$. The transformation matrix for this displacement is:

$$\begin{bmatrix} \hat{x}_b \\ \hat{y}_b \\ \hat{z}_b \end{bmatrix} = \begin{bmatrix} \cos \theta & \sin \theta & 0 \\ -\sin \theta & \cos \theta & 0 \\ 0 & 0 & 1 \end{bmatrix} \begin{bmatrix} \hat{x}_a \\ \hat{y}_a \\ \hat{z}_a \end{bmatrix} . \tag{G.2}$$

Combining eqs. (G.1) and (G.2), the transformation matrix connecting the triad $(\sim)_b$, to the initial one, $(\sim)_o$, is:

$$\begin{bmatrix} \hat{x}_b \\ \hat{y}_b \\ \hat{z}_b \end{bmatrix} = \begin{bmatrix} \cos \theta & \sin \theta \cos \iota & \sin \theta \sin \iota \\ -\sin \theta & \cos \theta \cos \iota & \cos \theta \sin \iota \\ 0 & -\sin \iota & \cos \iota \end{bmatrix} \begin{bmatrix} \hat{x}_o \\ \hat{y}_o \\ \hat{z}_o \end{bmatrix} . \tag{G.3}$$

In order to position a moving triad in the reference plane the angle, ψ, is introduced. The axis of rotation is chosen, here, to be the z_o-axis; this rotational displacement locates the triad $(\hat{x}_1, \hat{y}_1, \hat{z}_1)$. This resulting triad is related to the initial, or $(\sim)_o$ triad, by the transformation matrix:

$$\begin{bmatrix} \hat{x}_1 \\ \hat{y}_1 \\ \hat{z}_1 \end{bmatrix} = \begin{bmatrix} \cos \psi & \sin \psi & 0 \\ -\sin \psi & \cos \psi & 0 \\ 0 & 0 & 1 \end{bmatrix} \begin{bmatrix} \hat{x}_o \\ \hat{y}_o \\ \hat{z}_o \end{bmatrix} . \tag{G.4}$$

Eqs. (G.3) and (G.4) will be used to describe positions for the $(\sim)_b$ and $(\sim)_1$-triads, respectively, in the $(\sim)_o$ frame of reference. Such matrices are employed to refer quantities of interest, in a moving triad, back to the base frame of reference.

APPENDIX H

RELMOT, A RELATIVE MOTION COMPUTER PROGRAM

H.1 Introduction. - RELMOT is a computer program to calculate the relative motion of two bodies under the influence of a fixed initial thrust or a fixed initial impulse, or both. The program has several options which permit it to calculate an integrated solution, a linear approximation to the solution, and the corresponding second order corrections thereto. It can, in addition, iterate for an optimum solution with respect to the initial thrust or impulse which will generate a fixed, final position.

The equations to be integrated are:

$\ddot{R} = f(R, \dot{R}, Th, t)$ where R, $\dot{R}$ are the position and velocity vectors, Th is the specific thrust vector, and t is the time.

Letting

$$\ddot{R} = (\ddot{x}, \ddot{y}, \ddot{z});$$

and

$$x1 \equiv x + 1,$$

then the scalar equations may be expressed by:

$$w = (x1^2 + y^2 + z^2)^{3/2}$$

$$x'' = 2y' + x1 - \frac{x1}{w} + Th_x$$

$$y'' = -2x' + y - \frac{y}{w} - Th_y$$

$$z'' = -\frac{z}{w} - Th_z$$

where the x, y, z are now dimensionless variables and $(\sim)'$ denotes differentiation.

A development leading to the equations for the linear solution and second order corrections are found in Appendix A and E, respectively.

H.2 Inputs. - The inputs are in dimensional units; however, the program performs all calculations and yields outputs in dimensionless units. The program is written in the FORTRAN IV language under the H compiler for the IBM 360 Operating System. A description of the inputs, program operations, and outputs follows below.

Inputs to RELMOT are given through the namelist feature of the IBM Fortran IV programming language. The input namelist is named NML; every input required or used in the program is declared by name in the list. The general form for assigning an input value to a quantity is, simply:

NAME = VALUE,

where NAME is the name assigned to the variable and is included in the namelist. VALUE is a numerical or logical quantity, consistent in form (i.e., logical, integer, or real) with NAME. Unless otherwise specified, all NML names commencing with the letters I-N represent integers, whereas all names commencing with the letters A-H or O-Z are double precision floating point numbers.

Each namelist case must begin with the characters

&NML,

commencing in card column 2 and followed by at least one blank. Each case must end with the characters,

&END,

preceded by at least one blank if data is specified on the same line.

Card column 1 is ignored on all input cards.

Multiple data assignments on a single card are permissible if separated by commas. Blanks in the variable field, VALUE, are taken as zeroes. A comma following the last specified VALUE on a card is optional.

The order of the input data assignments is arbitrary; i.e., they need not be in the same order as listed in the namelist. In fact, it is not a requirement that any specific input parameter be represented in the input data set. If no value is included in input set, for a particular parameter, the default value is used, if defined. (See Default Values).

For other details regarding the namelist feature, the reader is referred to the IBM System/360 Fortran IV Language manual. Namelist cases may be stacked in sequence; a single namelist error could wipe-out the remaining namelist inputs.

Definition of input parameters.

NAME	DIMENSION	DESCRIPTION	DEFAULT
RIN	3	initial input position vector (nominally in miles (km))	
RDIN	3	initial input velocity vector (nominally in feet/sec. (m/sec))	
THRIN	3	initial input thrust vector (nominally in feet/sec^2 (m/sec^2))	
BBB	3	step size for computing partial derivative matrix, for iterations	3*1.D-7
TO		initial time, in sec.	
TFIN		final time, in sec.	

NAME	DIMENSION	DESCRIPTION	DEFAULT
EMU		Earth's gravitational constant (feet^3/sec^2 (m^3/sec^2))	1.40771289D16
RCNV		conversion factor, to convert input position vector. (nominally into feet (meters))	5280D0 (1.D3)
VCNV		conversion factor to convert input velocity vector (nominally into feet/sec. (m/sec))	1.
R		input circular orbital radius (nominally in miles (km))	
HS		integration step size	0.1325D0
ICASE		case number, to determine which option to run	
12D		trigger to indicate if problem should be treated as two-dimensional or three dimensional: (I2D=1, 2-dimensional case) (I2D≠1, 3-dimensional case)	1
IPLLNR		trigger to indicate if plots of a solution, resulting from linear equations, should be generated: (=1, generate plots) (≠1, do not generate plots)	1
IPLINT		trigger to indicate if plots of solution, resulting from integrated equations, should be generated: (=1, generate plots) (≠1, do not generate plots)	1

NAME	DIMENSION	DESCRIPTION	DEFAULT
ISHELL		trigger to print solutions in shell coordinates. Applicable to cases 1, 4 and 5: (ISHELL=1, convert to shell coordinates) (ISHELL≠1, nominal printout)	0

H.3 Program capabilities. - There are five different options in the program, these are specified by case number, ICASE. The options, and a description of what they solve, are noted below:

ICASE=1 Linearized and Integrated Solutions for a Thrusting Particle

inputs: R, V, Th

computes: Linear solution, using subroutines STB and STC.
Integrated solution, using subroutines RKFOR and DERIV.

output: Time history printout of R, V, A; linear and integrated solution plots.

ICASE=2 Linearized and Integrated Solutions for Intercept by a Thrusting Particle.

inputs: R, V

computes: Th, using subroutine STA.
Linear intercept solution, using subroutines STB and STC.
Integrated solution, using subroutine RKFOR and DERIV.

output: Time history printout of R, V, A; linear and integrated solution plots.

ICASE=3 Linearized, Integrated, and Second Order Correction Solutions for a Non-Thrusting Particle.

inputs: R, V

computes: (for computations set Th=0)
Linear solution, using subroutines STB and STC.
Second order corrections, using subroutine SNDCR.
Integrated solution, using subroutines RKFOR and DERIV.

output: Time history printout of R, V, A; for linear, linear + second order correction, and integrated solutions; also, plots of linear, linear + second order, and integrated solutions.

ICASE=4 Intercept Problem for a Thrusting Particle (Iterated "exact" Solution).

inputs: R, V

computes: Iterates for correct thrust, Th, so that R (t_f) = 0; i.e., final R goes to 0. Uses subroutines STA (for initial guess of thrust), MINMX3 (iterator package), and TRAJ, RKFOR and DERIV (to generate trajectories).

outputs: Th, final converged thrust vector.
Time history of R, V, A from the integrated solution.
Plots of the integrated solution.

ICASE=5 Intercept Problem using an Initial Impulse.

inputs: R, Th (usually = 0)

computes: Iterated value of initial impulse (V_0^*), such that R (t_f)=0.
Uses subroutine VINIT (for initial guess of the impulse); MINMX3 (iterator package), and TRAJ, RKFOR and DERIV (to generate trajectories).

output: V*, converged value of initial velocity vector.
Time history of R, V, A from integrated solution.
Plots of integrated solutions.

Additional output. - Whenever two ICASE=5 cases are run, in sequence, the difference of R and V, at each time step, is calculated. These differences are then printed out and plotted. Note that data defined from the first input are substracted from data developed from the second input, describing the relative values, of R, V of the first with respect to the second.

SAMPLE INPUTS

&NML RIN=-50.,50.,0.,RDIN=3*0., TO=0.,TFIN=1200., 12D=1,IPLLNR=1,IPLINT=1,	values needed for each case in addition to default values
ICASE=1,THRIN=3*2.05D-2 &END	case 1
&NML ICASE=2,THRIN=3*0.,&END	case 2
&NML ICASE=3,&END	case 3
&NML ICASE=4,BBB=6*1.D-7 &END	case 4
&NML ICASE=5,&END	case 5
&NML ICASE=5,RIN=50.,-50.,&END	second case 5

The above are cases to be run in sequence. The two successive case 5's will generate plots of their differences.

The iterator. - The iterator is the software module (MINMX3) which drives the two-boundary-value problem to a solution. The following discussion is taken from a previous report*.

Correction Scheme. - The iterator's underlying mathematical operation is formulated as follows: Let X denote the vector of independent variables and Y denote the vector of dependent variables. The relationship between these two vectors is assumed to be given by

$$Y = F(X).$$

The vector function, F, is evaluated by integrating a trajectory; that is, given a complete set of control parameters and initial conditions, the corresponding values of the end conditions (Y) can be determined. Subroutine TRAJ maps X onto Y and is, therefore, the software package which corresponds to the function

*Horsewood, J. L., et al: HILTOP, Heliocentric Interplanetary Low Thrust Trajectory Optimization Program; Report No. 71-38, Contract NAS5-11364, Nov. 1971; Analytical Mechanics Associates, Inc., Seabrook, Md.

F. The problem becomes one of finding the vector X^* which will lead to the specified values of the dependent variables, Y^*; that is, a set of values leading to

$$Y^* = F\ (X^*),$$

where Y^* is known.

This procedure is treated as a minimization problem. The weighted sum of the residuals (q_i) is given by;

$$q_i = \left[Y^* - F\ (X_i)\right]^T W_y \left[Y^* - F\ (X_i)\right],$$

where X_i is the "current estimate" of the independent variables, and W_y is a diagonal, positive definite weighting matrix.

The situation becomes one of choosing a new value, X_{i+1}, which will minimize, q_{i+1}. If X_{i+1} is close to x_i, then

$$F\ (X_{i+1}) \cong F\ (X_i) + P\ \Delta X,$$

where $\Delta X \equiv X_{i+1} - X_i$; and, the partial derivative matrix, P, is

$$P \equiv \frac{\partial Y}{\partial X}\ .$$

Evaluating q_{i+1} with the approximation leads to an expression

$$q_{i+1} = (\Delta Y - P\Delta X)^T W_y\ (\Delta Y - P\Delta X)$$

where ΔY, the residual vector, is obtained from

$$\Delta Y = Y^* - F\ (X_i).$$

Finally, the problem is to choose a ΔX which will minimize q.

Inhibitor Control. - For nonlinear functions, F, linear approximations will work only if ΔX is small. Therefore, the following constraint is imposed on this variant;

$$\Delta X^T W_x \Delta X \leq \ell ,$$

where W_x is the input diagonal, positive definite weighting matrix associated with the independent parameters.

Attaching to the constraint a scalar inhibitor, λ, the vector to be minimized is given by;

$$Q = (\Delta Y - P \Delta X)^T W_y (\Delta Y - P \Delta X) + \lambda (\Delta X^T W_x \Delta X).$$

Finding the minimum of the vector function yields a solution,

$$\Delta X = (P^T W_y P + \lambda W_x)^{-1} P^T W_y \Delta Y.$$

It has been shown (see HILTOP reference) that as λ increases, ℓ decreases, monotonically. Therefore λ can always be chosen large enough to satisfy the above inequality. Moreover, if λ is sufficiently large, the condition is, approximately,

$$\Delta X \cong \frac{1}{\lambda} W_x^{-1} (P^T W_y) \Delta Y.$$

For ΔX small enough, or λ large enough, one can guarantee that

$$q_{i+1} \leq q_i .$$

It is advantageous to take as large a step as possible toward satisfying $Y^* = F(X^*)$. The procedure is initiated with a relatively small value of λ. The idea is: make a correction, determine if any improvement can be made; and, if not, reduce the correction.

The following iteration scheme is utilized. Given an X_i, the trajectory is integrated (again) to produce Y_{i+1}, starting with the values $X_{i+1} = X_i + \Delta X$; and, then, q_{i+1} is calculated. This value, q_{i+1} is compared with q_i. If there is no improvement, λ is increased; then ΔX is recalculated and a new trajectory is integrated. This procedure is repeated until an improvement does result. When this happens, the trajectory is integrated, again, and a partial derivative matrix is computed. Next, λ is reset to its original value and the iteration continues until q is less than the prescribed tolerance, or no further improvement can be made, or the maximum number of iterations is exceeded.

Constraints (dependent variables). - The constraints, Y, are divided into two types: parameters that are driven to a given value (point constraints), and parameters to be maximized or minimized (performance indices).

For a well-posed problem, there is only one performance index. For each dependent variable, y_i, two values must be specified; y_{min} and y_{max}. If a dependent variable is a point constraint, y_{min} and y_{max} are chosen close together; i.e.,

$$y_{min} = y^* - \delta ; \; y_{max} = y^* + \delta ,$$

where y^* is the desired value and δ is a tolerance utilized for weighting purposes. For the performance index, the interval is chosen so that it cannot possibly be attained if the other constraints are satisfied. For instance, if y is to be minimized, y_{min} and y_{max} are taken larger than attainable. In this way the iteration procedure drives the variable (to be optimized) in the correct direction until no further improvement is possible or the input maximum number of iterations is exceeded.

Modes. - Two modes of solution are available, the indirect (select) mode and the direct (optimize) mode. In the indirect mode, a solution which satisfies the end

conditions is attempted. Indirect optimization is performed in this mode. The direct mode computes a series of trajectories, each of which satisfies the specified end conditions while successively minimizing the performance index residual. The specified end conditions are first satisfied, using the indirect mode, ignoring the performance index.

Weighting. - The scale matrices, W_x and W_y, are used to insure that elements of the vectors X and Y are compatible for the iteration procedure. The relative importance of the variables is represented in this way. Differing magnitudes are compensated for through the weighting matrices. W_x is input to the program, while W_y is computed (internally) using input tolerances and importance factors. For point constraint variables, the elements of W_y are given by the following relation:

$$W_y = \frac{2^{-38}}{\delta_y^2} ,$$

where δ_y is the corresponding tolerance.

The weighting factor for a performance index is computed from,

$$W_y = \frac{n}{r^2} 2^{-38} ,$$

when n is the number of dependent variables and r is the performance index residual. This balances the residual for the parameter being optimized against the weighted residuals in the other variables, in order to satisfy constraints as the optimization proceeds.

REFERENCES AND BIBLIOGRAPHY

[1] Anthony, M. L. and Sasaki, F. T., "Rendezvous Problems for Nearly Circular Orbits", AIAA J., 3, 1666-1673 (1965).

[2] Barbieri, R. W., "An Analytical Development of the Relative Motion of Two Close Satellites of an Oblate Planet", NASA X-551-70-313, Goddard Space Flight Center, (1970).

[3] Clohessey, W. H. and Wiltshire, R. S., "Terminal Guidance System for Satellite Rendezvous", J. Aero. Sci, 27, 653-658 and 674 (1960.

[4] Darby, W. G., "Correction for the Effect of Finite Thrusting Times in Orbit Changing Maneuvers", IAS preprint 61-154-1848 (1961).

[5] Eades, J. B. and Wyatt, G. H., "A Study from Kinematics - The Problems of Intercept and Pursuit", NASA X-643-69-106, Goddard Space Flight Center (1969).

[6] Eades, J. B. and Drewry, J. W., "Relative Motion of Near Orbiting Satellites", Cel. Mech. (to be published).

[7] Eggleston, J. M. and Beck, H. D., "A Study of the Positions and Velocities of a Space Station and a Ferry Vehicle during Rendezvous and Return", NASA TR-87 (1961).

[8] Englar, T. S., "A Lagrangian Derivative of the Clohessy-Wiltshire Equations and Some Remarks Concerning their Application", TR 66-310-3, Bell Com, Inc. (1966).

[9] Hord, R. A., "Relative Motion in the Terminal Phase of Intercept of a Satellite or a Ballistic Missile", NASA TN 4399 (1958).

[10] Knollman, G. O. and Pyron, B. O., "Relative Trajectories of Objects Ejected from a Near Satellite", AIAA J, 1, 424-429 (1963).

[11] London, H. S., "Second Approximation to the Solution of Rendezvous Equations", AIAA J., 1, 1691-1693 (1963).

[12] Meirovitch, L., Methods of Analytical Dynamics, pp. 428-430, McGraw-Hill (1970).

[13] Ruppe, H.O., Introduction to Astronautics, Vol. 2, pp. 70-80, Academic Press (1967).

[14] Szebehely, V.G., Theory of Orbits, Art 10.4, Academic Press (1967).

[15] Whitlock, F.H., Wolf, H., et al, "Interplanetary Trajectory Encke Method Fortran Program Manual for the I.B.M. System/360", NASA X-643-70-330, Goddard Space Flight Center (1970).